



National Library
of Canada

Bibliothèque nationale
du Canada

Canadian Theses Service

Services des thèses canadiennes

Ottawa, Canada
K1A 0N4

CANADIAN THESES

THÈSES CANADIENNES

NOTICE

The quality of this microfiche is heavily dependent upon the quality of the original thesis submitted for microfilming. Every effort has been made to ensure the highest quality of reproduction possible.

If pages are missing, contact the university which granted the degree.

Some pages may have indistinct print especially if the original pages were typed with a poor typewriter ribbon or if the university sent us an inferior photocopy.

Previously copyrighted materials (journal articles, published tests, etc.) are not filmed.

Reproduction in full or in part of this film is governed by the Canadian Copyright Act, R.S.C. 1970; c. C-30.

**THIS DISSERTATION
HAS BEEN MICROFILMED
EXACTLY AS RECEIVED**

AVIS

La qualité de cette microfiche dépend grandement de la qualité de la thèse soumise au microfilmage. Nous avons tout fait pour assurer une qualité supérieure de reproduction.

S'il manque des pages, veuillez communiquer avec l'université qui a conféré le grade.

La qualité d'impression de certaines pages peut laisser à désirer, surtout si les pages originales ont été dactylographiées à l'aide d'un ruban usé ou si l'université nous a fait parvenir une photocopie de qualité inférieure.

Les documents qui font déjà l'objet d'un droit d'auteur (articles de revue, examens publiés, etc.) ne sont pas microfilmés.

La reproduction, même partielle, de ce microfilm est soumise à la Loi canadienne sur le droit d'auteur, SRC 1970, c. C-30.

**LA THÈSE A ÉTÉ
MICROFILMÉE TELLE QUE
NOUS L'AVONS REÇUE**

Canada

ON SPECTRALLY EFFICIENT DIGITAL TRANSMISSION SYSTEMS

by

Kuang-Tsan Wu

A thesis
presented to the University of Ottawa
in fulfillment of the
thesis requirement for the degree of
Doctor of Philosophy
in
Electrical Engineering

OTTAWA, Ontario, 1986

Permission has been granted to the National Library of Canada to microfilm this thesis and to lend or sell copies of the film.

The author (copyright owner) has reserved other publication rights, and neither the thesis nor extensive extracts from it may be printed or otherwise reproduced without his/her written permission.

L'autorisation a été accordée à la Bibliothèque nationale du Canada de microfilmer cette thèse et de prêter ou de vendre des exemplaires du film.

L'auteur (titulaire du droit d'auteur) se réserve les autres droits de publication; ni la thèse ni de longs extraits de celle-ci ne doivent être imprimés ou autrement reproduits sans son autorisation écrite.

ISBN 0-315-33257-3



UNIVERSITÉ D'OTTAWA
UNIVERSITY OF OTTAWA

The University of Ottawa requires the signatures of all persons using or photocopying this thesis. Please sign below, and give address and date.

ABSTRACT

Two candidate modulation techniques, i.e., 256-QAM (Quadrature Amplitude Modulation) and 225-QPRS (Quadrature Partial-Response Signalling) are investigated in order to achieve a spectral efficiency of more than 6 b/s/Hz which is required for the transmission of a T1 carrier in a standard analog supergroup band and for many other applications.

A new data filtering strategy (chopping technique) for PRS/QPRS above the Nyquist rate, which enables a higher transmission rate than feasible with the conventional method, is introduced. It is demonstrated that, with the use of our technique for class-I 225-QPRS, an efficiency of 6.3 b/s/Hz can be achieved. The advantages of combining our technique with class-IV PRS are that a small bandwidth around dc can be used for a service channel and that a higher increase in spectral efficiency can be obtained in an FDM-SSB system. However, to achieve an efficiency of more than 6.3 b/s/Hz, 256-QAM is recommended.

To investigate the hardware feasibility of the concept of our new chopping technique, a 7-level class-IV PRS system operated above the Nyquist rate is designed and implemented. Measured results are shown to agree well with the simulated ones.

A quantitative evaluation of the effect of linear channel distortions on 256-QAM and 225-QPRS is presented to compare the sensitivities of these schemes and the numerical results could show modem designers and researchers how flat and how linear the filters' amplitude and phase responses should be.

To enable a rigorous comparison of the conventional method and our new method for PRS above the Nyquist rate, a truncated peak distortion is defined and a new method is presented to evaluate the error floors of these systems. This method is more general and could be applied also to the study of other transmission systems.

Since co-channel interference (CCI) is one of the major sources of performance impairments, its impact on the performance of 225-QPRS and 256-QAM is evaluated so that their potential for radio systems could be assessed.

Finally, in order to improve the performance of 256-QAM systems degraded by channel distortions, the use of an adaptive complex base-band equalizer is described and simulated.

ACKNOWLEDGMENTS

I wish to express my sincere gratitude to Dr. K. Feher for the many forms of support, guidance, and helpful criticisms he provided in supervising this work. The financial support of the Natural Sciences and Engineering Research Council of Canada (NSERC) and of Karkar Electronics, Inc., San Francisco is acknowledged. I am grateful to the Department of Electrical Engineering, University of Ottawa, for providing the facilities to carry out this thesis. I would like to thank the advisory committee, consisting of Dr. W. Steenaert, Dr. P. Galiko, and Dr. I. Sasase for their constructive suggestions and criticisms.

I have benefited during the past 3 years from a close collaboration with all the members of Digital Communications Research Group at the University of Ottawa, including valuable discussions, comments and the limited but precious leisure time we spent together. They are Messrs. M.X. Chen, J. Coll, M. Hamze, D. Hatzinakos, A. Kucar, Z.Z. Lei, J.X. Li, D. Makrakis, T. Mathiopoulos, K. Nagaraj, H. Ohnishi, D. Prendergast, R.V. Scott, J.S. Seo, K. Sreenath, I. Tezcan, A. Yonogoglu, and Drs. M. Sato, M.S. Murthy, I. Sasase, R. Zakaravicius.

My special thank goes to Dr. J. C. Y. Huang. From him and the one-month work he arranged for me at Karkar Electronics, Inc., during November and December, 1984, I learned how to simulate adaptive tran-

versal equalizers and decision feedback equalizers employed for high-level QAM and QPRS systems to combat channel distortions. I am thankful to Dr. D.D. Falconer, for the helpful discussion on equalization and for his introducing me the adaptive filtering theory.

I am indeed indebted to my family, especially my elder brother, Mr. Kuang-Hui Wu, for fostering my career.

Finally, I wish to thank my parents-in-law for their timely support and encouragement and my wife, Ling-Ling for typing the entire manuscript and for her patience and constant encouragement during my Ph.D. study. Our lovely daughter, Tsai-Yu (or Tati) has been contributing many to our daily life. At the age of three, she was so cooperative, patient and understanding during weekends and long evening hours while I was writing this thesis.

In addition, I acknowledge the examiners of the thesis defence - Dr. S. Mahmoud, Dr. E. Petriu, Dr. H. Sinnreich, Dr. W. Steenaart, and Dr. K. Feher for their comments and contributions to the final version of the thesis.

LIST OF FIGURES

	<u>Page</u>
Fig.1.1 Illustrative power spectrum of a T1/SG DIV signal in a standard CCITT mastergroup.	4
Fig.1.2 Spectral efficiency (b/s/Hz) and C/N requirement at $P_e = 10^{-8}$ of various modulation systems.	6
Fig.2.1(a) Block diagram of a conceptual duobinary PRS base-band system.	13
Fig.2.1(b) QPRS modem block diagram.	14
Fig.2.2 Model-A : Conventional system model for duobinary PRS above the Nyquist rate and cascaded transfer function.	16
Fig.2.3 Model-B : New system model for duobinary PRS above the Nyquist rate and corresponding cascaded transfer function.	17
Fig.2.4 A frequency-domain comparison for the two models for duobinary PRS above the Nyquist rate. (a) Conventional Model-A, (b) Our new Model-B.	19
Fig.2.5 Discrete-time impulse response of duobinary (class-I) PRS with a 5% increase above the Nyquist rate. (a) Conventional Model-A, (b) Our new Model-B.	22
Fig.2.6 Discrete-time impulse response of duobinary (class-I) PRS with a 10% increase above the Nyquist rate. (a) Conventional Model-A, (b) Our new Model-B.	23
Fig.2.7 Eye diagrams of 3-level PRS/9-QPRS with a 20% increase above the Nyquist rate. (a) Using the conventional Model-A, (b) Using our new Model-B.	25
Fig.2.8 Eye diagrams of 7-level PRS/49-QPRS with a 10% increase above the Nyquist rate. (a) Using the conventional Model-A, (b) Using our new Model-B.	26
Fig.2.9 Eye diagrams of 15-level PRS/225-QPRS with a 4.2% increase above the Nyquist rate. (a) Using the conventional Model-A, (b) Using our new Model-B.	27
Fig.2.10 Hardware implementation of 15-level duobinary PRS above the Nyquist rate using our new "Model-B".	29

- Fig.2.11 Measured baseband eye diagram and corresponding power spectral density of a 15-level duobinary PRS signal using our new Model-B. This eye diagram corresponds to the I (or Q) channel of a 225-QPRS modem operated at $f_b=1.6$ Mb/s. The spectral efficiency of the baseband system and of the quadrature modem is $800 \text{ kb/s} : 128 \text{ kHz} = 6.25 \text{ b/s/Hz}$. 31
- Fig.2.12 Probability of error performance of 225-QPRS above the Nyquist rate versus C/N, using Model-A or Model-B. 33
- Fig.3.1 Conventional system model: Model-A for class-IV (modified duobinary) PRS above the Nyquist rate and the cascaded transfer function. 37
- Fig.3.2 New system model: Model-B for class-IV (modified duobinary) PRS above the Nyquist rate with m-ary inputs and the corresponding transfer function. 41
- Fig.3.3 Eye diagram of an ideal 15-level class-IV (modified duobinary) PRS signal. 43
- Fig.3.4 Eye diagram of an improved efficiency class-IV 15-level PRS/225-QPRS with a 4% increase above the Nyquist rate. 44
- Fig.3.5 Eye diagram of a conventional class-IV 15-level PRS/225-QPRS with a 4% increase above the Nyquist rate. 44
- Fig.3.6 Probability of error of our improved efficiency class-IV 15-level PRS/225-QPRS above the Nyquist rate versus carrier-to-noise ratio (C/N). 46
- Fig.3.7 System model for an improved efficiency class-IV PRS above the Nyquist rate and for service channel transmission. 49
- Fig.3.8 Performance of an improved efficiency class-IV 15-level PRS/225-QPRS with a 4% increase above the Nyquist rate and with various bandwidths carved out for a service channel. 51
- Fig.4.1 System model for an experimental 7-level class-IV PRS above the Nyquist rate using our new Model-B. 54
- Fig.4.2 System block diagram of the experimental 7-level Class-IV PRS above the Nyquist rate using our new Model-B. 56
- Fig.4.3(a) Circuit diagram of a 7-level class-IV PRS encoder. 58
- Fig.4.3(b) Output stage of the encoder and the sampling clock. 59
- Fig.4.4 Measured amplitude characteristic of an $\alpha=0.08$ raised-cosine filter. 63
- Fig.4.5 Measured amplitude characteristic of an $\alpha=0.08$ raised-cosine filter with $x/\sin(x)$ equalization. 63

	<u>Page</u>
Fig.4.6 Circuit diagram of a 7-level class-IV PRS decoder.	67
Fig.4.7 Measured eye diagram of a 7-level class-IV PRS signal and the sampling clock.	69
Fig.4.8 Close-up of the inner two eyes of a 7-level class-IV PRS signal.	69
Fig.4.9 Illustrative transmitted and decoded data for a PRBS pattern of 1110010.	70
Fig.4.10 Illustrative transmitted and decoded data for a PRBS pattern of 100110101111000.	70
Fig.4.11 Measured BER performance of improved efficiency 7-level class-IV PRS above the Nyquist rate.	72
Fig.4.12 Measured PSD's and corresponding eye diagram of a 7-level class-IV PRS signal with $f_b=470.3$ kb/s.	74
Fig.4.13 Measured PSD's and corresponding eye diagram of a 7-level class-IV PRS signal with $f_b=506.2$ kb/s.	75
Fig.4.14 Measured PSD's and corresponding eye diagram of a 7-level class-IV PRS signal with $f_b=524$ kb/s.	76
Fig.4.15 Photograph of the experimental set-up in the Digital Communications Laboratory, Department of Electrical Engineering, University of Ottawa.	77
Fig.5.1 256 and/or 64-QAM system block diagram.	80
Fig.5.2 Computer simulation model.	82
Fig.5.3(a) Eye diagram of 256-QAM with $\alpha=0.1$.	84
Fig.5.3(b) Eye diagram of 256-QAM with $\alpha=0.4$.	85
Fig.5.3(c) Eye diagram of 256-QAM ($\alpha=0.2$) with a sinusoidal group delay distortion, $D(f)=S_D \sin(2\pi Kf/2f_{BW})$, $S_D=12$ ns and $K=4$. Bit rate $f_b=120$ Mb/s.	86
Fig.5.4 Measured 16-level and 8-level PAM eye diagrams. (a) and (b) for 16-level PAM, (c) for 8-level PAM.	87
Fig.5.5 P_s^k versus C/N for linear, parabolic, and sinusoidal group delay distortions for 256-QAM with a bit rate of 120 Mb/s and $\alpha=0.4$.	90
Fig.5.6 Degradation of C/N versus T_m for linear, parabolic, and sinusoidal group delay distortions for 256-QAM and 64-QAM with a symbol rate of 15 Mbaud and $\alpha=0.4$ raised-cosine filters.	91

	<u>Page</u>
Fig.5.7 P versus C/N for linear, parabolic, and sinusoidal amplitude distortions for 256-QAM with a bit rate of 120 Mb/s, i.e., 15 MBaud and $\alpha=0.4$.	93
Fig.5.8 Degradation of C/N versus A for linear, parabolic, and sinusoidal amplitude distortions for 256-QAM and 64-QAM with a symbol rate of 15 MBaud and $\alpha=0.4$ raised-cosine filters.	94
Fig.6.1 Probability of error of 256-QAM, conventional 225-QPRS, and improved efficiency 225-QPRS versus C/N.	102
Fig.6.2 Probability of error of 225-QPRS above the Nyquist rate and 256-QAM for linear group delay distortions versus C/N.	105
Fig.6.3 Probability of error of 225-QPRS above the Nyquist rate and 256-QAM for parabolic group delay distortions versus C/N.	106
Fig.6.4 Probability of error of 225-QPRS above the Nyquist rate and 256-QAM for sinusoidal group delay distortions versus C/N.	107
Fig.6.5 Probability of error of 225-QPRS above the Nyquist rate and 256-QAM for linear amplitude distortions versus C/N.	108
Fig.6.6 Probability of error of 225-QPRS above the Nyquist rate and 256-QAM for parabolic amplitude distortions versus C/N.	109
Fig.6.7 Probability of error of 225-QPRS above the Nyquist rate and 256-QAM for sinusoidal amplitude distortions versus C/N.	110
Fig.6.8 Frequency-domain comparison of 256-QAM ($\alpha=0.27$) and 225-QPRS (5% increase) with a parabolic amplitude distortion.	113
Fig.6.9 Frequency-domain comparison of 256-QAM ($\alpha=0.27$) and 225-QPRS (5% increase) with a sinusoidal amplitude distortion.	113
Fig.6.10 Frequency-domain comparison of 256-QAM ($\alpha=0.27$) and 225-QPRS (5% increase) with a linear amplitude distortion.	113
Fig.7.1 Illustrative P_e curves with error floors.	120
Fig.7.2 A PAM system model.	123
Fig.8.1 Block diagram of a conceptual co-channel system.	127
Fig.8.2 Error probability of 64-QAM ($\alpha=0.2$) with a single sinusoidal CCI	131
Fig.8.3 Error probability of 225-QPRS with a single sinusoidal CCI.	132
Fig.8.4 Error probability of 256-QAM ($\alpha=0.2$) with a single sinusoidal CCI.	133

	<u>Page</u>
Fig.8.5 Degradation in C/N for 64-, 256-QAM ($\alpha=0.2$), and 225-QPRS with a single sinusoidal CCI.	134
Fig.8.6 Error probability of 64-QAM ($\alpha=0.2$) with a 64-QAM ($\alpha=0.2$) CCI.	136
Fig.8.7 Error probability of 225-QPRS with a 225-QPRS CCI.	137
Fig.8.8 Error probability of 256-QAM ($\alpha=0.2$) with a 256-QAM ($\alpha=0.2$) CCI.	138
Fig.8.9 Degradation in C/N for 64-, 256-QAM ($\alpha=0.2$), and 225-QPRS with an amplitude-modulated CCI which has the same format as the desired signal; e.g., 64-QAM with a 64-QAM CCI.	139
Fig.8.10 Measured performance of a 256-QAM modem in the presence of co-channel interference.	140
Fig.9.1 Block diagram of a 256-QAM system with a complex baseband equalizer.	144
Fig.9.2 Complex transversal equalizer for QAM modems.	145
Fig.9.3 An illustrative structure of a 5-tap complex baseband adaptive equalizer for QAM systems.	147
Fig.9.4 Eye diagrams of 256-QAM ($\alpha=0.2$) with a parabolic group delay distortion, $P_D=0.81$ ns/MHz. Bit rate=120 Mb/s. (a) Before equalization, (b) After equalization.	150
Fig.9.5 Eye diagrams of 256-QAM ($\alpha=0.2$) with a sinusoidal group delay distortion $D(f)=S_D \sin(2\pi Kf/2f_{BW})$, $S_D=12$ ns and $K=4$. Bit rate $f_b=120$ Mb/s. (a) Before equalization, (b) After equalization.	151
Fig.9.6 Simulated probability of error performance of 256-QAM ($\alpha=0.2$) with a parabolic group delay channel distortion ($P_D=0.81$ ns/MHz ²).	152
Fig.9.7 Simulated probability of error performance of 256-QAM ($\alpha=0.2$) with a sinusoidal group delay distortion ($S_D=12$ ns and $K=4$).	153
Fig.A.1 Block diagram of PRS systems.	160

LIST OF TABLES

	<u>Page</u>
TABLE 2.1 Required C/N (dB) at $P_e = 10^{-9}$ for 225-QPRS above the Nyquist rate.	34
TABLE 3.1 Speed tolerance of class-IV (modified duobinary) PRS for multi-level inputs.	39
TABLE 3.2 Required C/N at $P_e = 10^{-9}$ for 225-QPRS above the Nyquist rate using our new method.	47
TABLE 4.1 Gray-code operation with reference to Fig.4.3(a).	61
TABLE 4.2 The number mapping with reference to Fig.4.3(a) & (b).	61
TABLE 4.3 Four-level signal transmission with class-IV PRS.	66
TABLE 4.4 Decoding table with reference to Fig.4.6.	66
TABLE 5.1 Relationship between distortion parameters and bit rates for two systems having the same modulation format and performance but different bit rates.	98
TABLE 6.1 C/N degradation of 225-QPRS above the Nyquist rate and 256-QAM for group delay and amplitude distortions at $P_e = 10^{-4}$.	111
TABLE 7.1 Comparison of the shortest length of the worst data sequence and the corresponding error floors for Model-A and Model-B with 8-level inputs (15-level outputs).	122

LIST OF ABBREVIATIONS

ACI - adjacent channel interference
BER - bit error rate
CCI - co-channel interference
CCITT - international telegraphy & telephone consultative committee
C/N - carrier to noise power ratio
DAV - data above voice/video
DFE - decision feedback equalizer
DIV - data in voice
DUV - data under voice
FFT - fast Fourier transform
ISI - intersymbol interference
MLSD - maximum likelihood sequence detection
PRBS - pseudo random binary sequence
PRS - partial-response signalling
PSD - power spectral density
PSK - phase shift keying
QAM - quadrature amplitude modulation
QPRS - quadrature partial-response signalling
SG - supergroup
SSB - single side band
S/N - signal to noise power ratio
TWT - travelling wave tube

LIST OF SYMBOLS

$\{I_n\}$	i-channel data symbols	
$\{Q_n\}$	q-channel data symbols	
E	expectation operator	
$\operatorname{erfc}(x)$	$= \frac{2}{\sqrt{\pi}} \int_x^{\infty} e^{-t^2} dt$	
F	Fourier transform operator	
F^{-1}	inverse Fourier transform operator	
f_b	bit rate	
f_o	carrier frequency	
f_s	symbol rate	
N_o	one-sided power spectral density of the AWGN (additive white Gaussian noise)	
Pr	Probability	
P_e	the probability of error	
$Q(x)$	$= \frac{1}{\sqrt{2\pi}} \int_x^{\infty} e^{-t^2/2} dt$	$\operatorname{erfc}(x) = 2Q(\sqrt{2}x)$
T_s	symbol interval	
T_b	bit interval	
$\operatorname{sgn}(x)$	$= 1$, if $x \geq 0$ $= -1$ if $x < 0$	
$\delta(t)$	Dirac delta function, $\int_{-\infty}^{\infty} \delta(t) dt = 1$, $\delta(t) = 0$ for $t \neq 0$.	

CONTENTS

ABSTRACT	iv
ACKNOWLEDGMENTS	vi
LIST OF FIGURES	viii
LIST OF TABLES	xiii
LIST OF ABBREVIATIONS	xiv
LIST OF SYMBOLS	xv

<u>Chapter</u>	<u>page</u>
I. INTRODUCTION	1
1.1 THE DEMAND FOR HIGHLY SPECTRUM-EFFICIENT MODULATION SCHEMES	1
1.1.1 The Need for Hybrid Systems	1
1.1.2 T1/SG : The Required Spectral Efficiency and its Advantages	3
1.1.3 Candidate Modulation Techniques	5
1.1.4 Signalling Above the Nyquist Rate	8
1.2 THESIS ORGANIZATION	9
II. MULTI-LEVEL PRS/QPRS ABOVE THE NYQUIST RATE	11
2.1 SYSTEM MODELS	12
2.2 WHY IS OUR NEW MODEL-B BETTER THAN THE CONVENTIONAL MODEL-A?	18
2.2.1 Frequency-Domain Comparison	18
2.2.2 Time-Domain Comparison	20
2.3 COMPARISON OF EYE DIAGRAMS	24
2.4 EXPERIMENTAL RESULTS FOR A 15-LEVEL-PRS USING OUR NEW MODEL-B	28
2.5 PROBABILITY OF ERROR OF 225-QPRS ABOVE THE NYQUIST RATE	32
2.6 CONCLUSIONS	35
III. IMPROVED EFFICIENCY 15-LEVEL MODIFIED DUOBINARY PRS ABOVE THE NYQUIST RATE	36
3.1 SPEED TOLERANCE OF CLASS-IV PRS WITH MULTI-LEVEL INPUTS	36

3.2	A NEW TECHNIQUE FOR CLASS-IV PRS ABOVE THE NYQUIST RATE	40
3.3	PERFORMANCE OF IMPROVED EFFICIENCY CLASS-IV 15-LEVEL PRS/225-QPRS ABOVE THE NYQUIST RATE	45
3.4	AN EFFICIENT METHOD FOR SERVICE CHANNEL TRANSMISSION	48
3.5	CONCLUSIONS	52
IV.	IMPLEMENTATION AND PERFORMANCE EVALUATION OF AN IMPROVED EFFICIENCY 7-LEVEL CLASS-IV PRS SYSTEM	53
4.1	SYSTEM MODEL	53
4.2	DESCRIPTION OF HARDWARE IMPLEMENTATION	55
4.2.1	Encoder Operation	55
4.2.2	Detailed Description of the Encoder Circuit	57
4.2.3	Filter Characteristics and Signalling Above the Nyquist Rate	62
4.2.4	Decoder Operation	64
4.2.5	Detailed Description of the Decoder Circuit	65
4.3	EXPERIMENTAL RESULTS AND DISCUSSIONS	68
4.4	CONCLUSIONS	78
V.	256-QAM MODEM PERFORMANCE IN DISTORTED CHANNELS	79
5.1	DESCRIPTION OF COMPUTER SIMULATIONS	81
5.2	GROUP DELAY DISTORTIONS	88
5.3	AMPLITUDE DISTORTIONS	92
5.4	APPLYING THE SIMULATED RESULTS TO SYSTEMS WITH DIFFERENT BIT RATES	95
5.5	CONCLUSIONS	99
VI.	COMPARISON OF 256-QAM AND IMPROVED EFFICIENCY 225-QPRS IN DISTORTED CHANNELS	100
6.1	BACKGROUND FOR THE COMPARISON OF 256-QAM AND 225-QPRS	101
6.2	COMPUTER SIMULATION DESCRIPTIONS	101
6.3	256-QAM AND IMPROVED EFFICIENCY 225-QPRS WITH GROUP DELAY AND AMPLITUDE DISTORTIONS	104
6.4	PHYSICAL INTERPRETATION OF THE RESULTS	112
6.5	CONCLUSIONS	115
VII.	ERROR FLOORS IN DIGITAL TRANSMISSION SYSTEMS	116
7.1	ERROR FLOORS IN MULTI-LEVEL PRS/QPRS SYSTEMS OPERATED ABOVE THE NYQUIST RATE	116
7.2	ERROR FLOORS IN PAM SYSTEMS UNDER SEVERE IMPAIRMENTS	121
7.3	CONCLUSIONS	125

VIII.	THE PERFORMANCE OF 64-QAM AND 225-QPRS AND 256-QAM IN A CO-CHANNEL INTERFERENCE ENVIRONMENT	126
8.1	SYSTEM PARAMETERS AND DESCRIPTION OF THE SIMULATION METHOD	126
8.2	SIMULATED RESULTS AND DISCUSSIONS	130
	EXPERIMENTAL RESULTS	135
8.3	CONCLUSIONS	141
IX.	AN ADAPTIVE BASEBAND EQUALIZER FOR 256-QAM OVER DISTORTED CHANNELS	142
9.1	FUNCTIONAL DESCRIPTION OF THE EQUALIZER	143
9.2	EQUALIZER PERFORMANCE	148
9.3	CONCLUSIONS	154
X.	CONCLUSION AND RECOMMENDED FURTHER RESEARCH	155
10.1	SUMMARY	155
10.2	SUGGESTIONS FOR FURTHER RESEARCH	157
10.2.1	Carrier and Symbol Timing Recovery for 256-QAM and 225-QPRS	158
10.2.2	Effects of Nonlinear Amplifiers on the Performance of 256-QAM and 225-QPRS	158
10.2.3	The Performance of 256-QAM and 225-QPRS in an Adjacent Channel Interference (ACI) Environment	158
10.2.4	Tailing Off BER Curves in QAM and QPRS Systems	159
10.2.5	The Performance of 256-QAM and 225-QPRS in a Multipath Fading Environment	159
<u>Appendix</u>		<u>page</u>
A.	DERIVATION OF THE P_e PERFORMANCE OF CLASS-I AND CLASS-IV PRS SYSTEMS	160
A.1	OPTIMALLY SPLIT FILTERS	164
A.2	SUBOPTIMUM DISTRIBUTION OF FILTERS	165
B.	SIMULATION PROGRAMS FOR QAM AND QPRS SYSTEMS	169
	REFERENCES	207

Chapter I
INTRODUCTION

1.1 THE DEMAND FOR HIGHLY SPECTRUM-EFFICIENT MODULATION SCHEMES

The need to increase digital channel capacity over the past few years has led to the development of spectrally efficient modulation systems, such as 8-PSK, 9-QPRS, 16-QAM, 49-QPRS, and 64-QAM [1]-[14]. Due to the increasing need for more efficient utilization of spectrum in the digital radio world and especially in hybrid analog and digital channels, such as Data-In-Voice (DIV), Data-Under-Voice (DUV), and Data-Above-Voice/Video (DAV) [15], digital modulation schemes which achieve an even higher spectral efficiency are required. Before going any further, let us briefly mention the need for hybrid systems.

1.1.1 The Need for Hybrid Systems

It is well known that, on all continents, there were high investments in operational analog multiplex and radio systems, which were originally designed to carry only frequency-division multiplexed (FDM) voice signals. During the last two decades, data traffic has been growing rapidly. However, installation of a new digital transcontinental system would cost enormously in research, development, design, and installa-

tion efforts. Consequently, there is an increasing tendency to make use of existing analog FDM microwave systems as digital carriers.

The primary objectives of hybrid transmission techniques include minimal or no modification to existing hardware, minimal degradation to existing analog performance, and of course, efficient data transmission with a low probability of error.

With the recent developments of high capacity SSB analog microwave systems, the interest in hybrid microwave systems, particularly in DIV systems increases significantly [17]. SSB analog microwave systems have a capacity of up to 6000 toll-grade telephone voice channels in a 30 MHz radio frequency (RF) bandwidth. These SSB systems improve the efficiency of FDM FM microwave systems from 2400 voice channels to 6000 channels in the same bandwidth. There is a strong demand in addition to telephony voice transmission for data transmission on these long distance systems.

In [17], the following conclusion has been reached. For a number of applications, if it is required to carry data at a rate from 56 kb/s up to 8.448 Mb/s, it is more economical to modify an FDM FM, FDM SSB, or FDM baseband cable system into a hybrid system than to install a completely new, dedicated digital system. One specific DIV application for the transmission of a T1 carrier in a standard analog supergroup (SG), call it T1/SG, is described in the following section.

1.1.2 . T1/SG : The Required Spectral Efficiency and its Advantages

According to the International Telegraphy & Telephone Consultative Committee (CCITT) modulation plan [16], a supergroup (SG) contains five standard CCITT groups, equivalent to 60 voice channels. Each voice channel is a nominal 4-kHz voice channel occupying the 300-to-3400 Hz spectrum. The standard SG before translation occupies the frequency band 312 to 552 kHz. Consider the transmission of a T1 carrier (1.544 Mb/s rate data) in a standard SG band (T1/SG) [17]. In Fig.1.1, the power spectrum of a T1/SG DIV system is illustrated as an example, where one of the SG voice signals has been replaced by a digitally modulated T1 signal. It may be required to add bits for forward error correction (FEC), system control/monitoring and synchronization purposes. In this case, the transmission rate is 1.6 Mb/s. In order to transmit 1.6 Mb/s data in a 256 kHz SG band (including guard bands) a spectral efficiency of $1.6 \text{ Mb/s} : 256 \text{ kHz} = 6.25 \text{ b/s/Hz}$ is required. Moreover, to transmit 1.6 Mb/s data over CCITT standard SG through-connect 240 kHz filters requires a spectral efficiency of $1.6 \text{ Mb/s} : 240 \text{ kHz} = 6.67 \text{ b/s/Hz}$. Thus it is apparent that a digital modem having a spectral efficiency of more than 6 b/s/Hz is needed for DIV applications.

The description of DIV approach would not be complete without a comment on its advantages. Major advantages of the T1/SG DIV approach include [17]:

- 1) An economical means to transmit one or more T1 rate data streams over a single FM or SSB radio system. Up to 100 separate T1

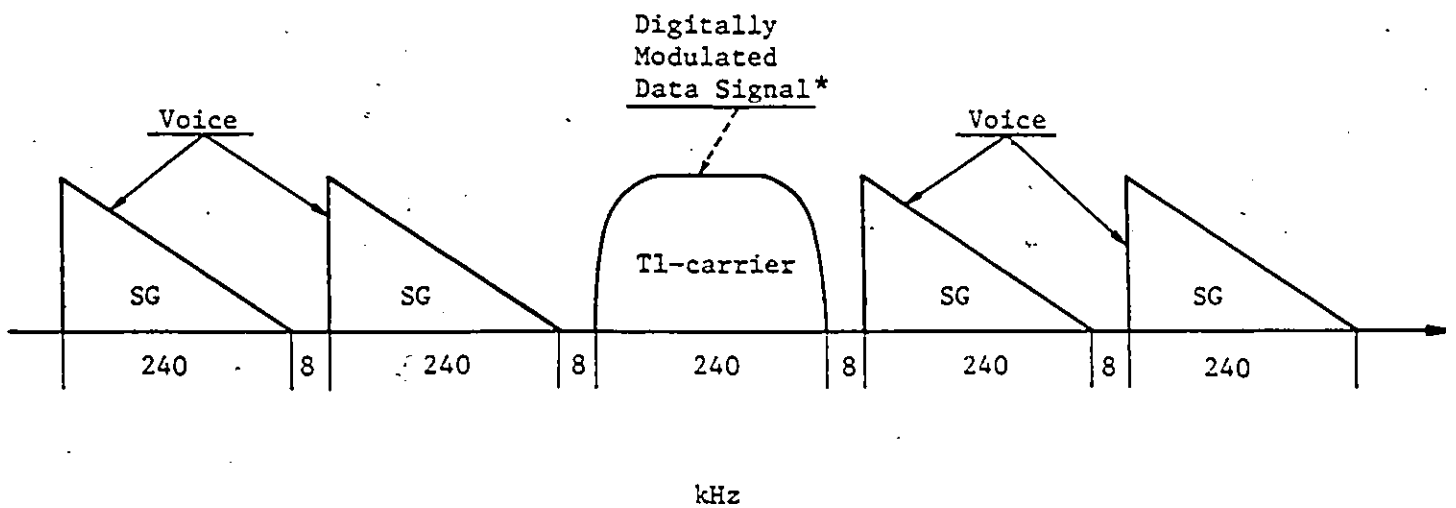


Fig.1.1 Illustrative power spectrum of a T1/SG DIV signal in a standard CCITT mastergroup. A standard supergroup (SG) before translation occupies the frequency band 312 to 552 kHz.

* e.g., 256-QAM.

signals, having a total capacity of 154.44 Mb/s (100 times T1) could be transmitted over a 30 MHz SSB system.

- ii) Flexible operational requirements - with this technique, it is simple to make changes. Data traffic capacity can be added to existing analog routes.
- iii) BER performance of less than 10^{-8} can be achieved.
- iv) Regenerative span over 1000 km - there is no need for regenerative modems for more than 1000 km. This is in sharp contrast with dedicated digital radio systems which require regenerative modems typically spaced at every 60 km.
- v) 50% more efficient than 64-QAM digital radio - a spectral efficiency which is about 50% higher than currently attainable with 4.5 b/s/Hz 64-QAM radio systems is achieved.
- vi) No selective fade problems - due to the narrow (240kHz) bandwidth of DIV modems, the selective fade caused problems are virtually non-existent. Adaptive equalizers easily compensate for transmission impairments.

1.1.3 Candidate Modulation Techniques

The spectral efficiency in terms of b/s/Hz and required carrier-to-noise ratio (C/N) at $P_e = 10^{-8}$ of various modulated systems are summarized in Fig.1.2 [14], [15]. A glance at Fig.1.2 has made M-ary PSK out of consideration for the aforementioned application since it requires a higher C/N as compared to QAM and QPRS systems in order to achieve a spectral efficiency of more than 3 b/s/Hz.

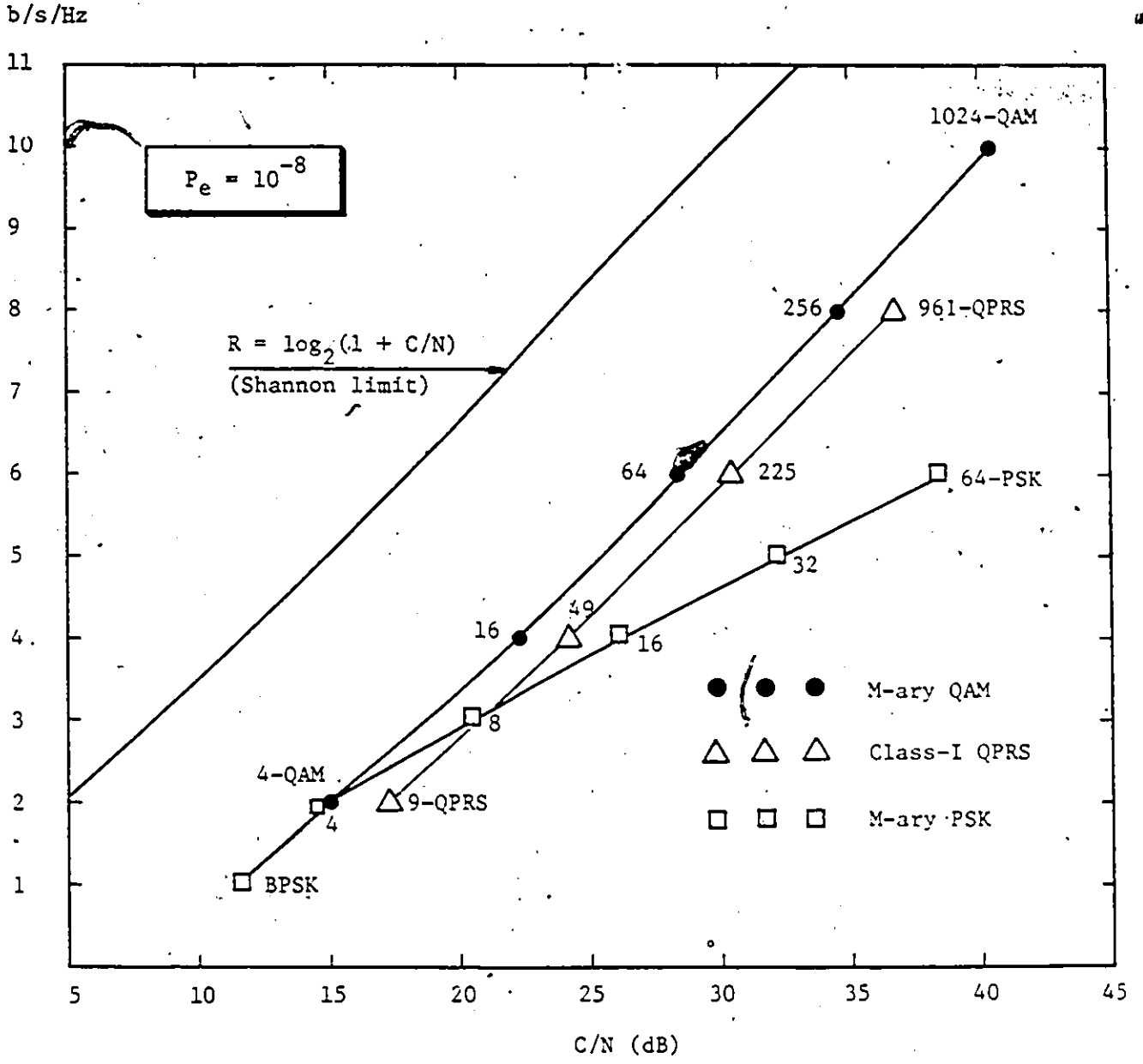


Fig.1.2 Spectral efficiency (b/s/Hz) and C/N requirement at $P_e = 10^{-8}$ of various modulation systems.

The average C/N is specified in the double-sided Nyquist bandwidth which equals the symbol rate. Ideal $\alpha = 0$ filtering has been assumed. (Adopted from Ref. [14], [15], and [17])

From Fig.1.2, we note that the theoretical spectral efficiency of 256-QAM modems is 8 b/s/Hz. An $\alpha=0.2$ raised-cosine filtered 256-QAM could achieve a practical efficiency of $8 \text{ b/s/Hz} : 1.2=6.67 \text{ b/s/Hz}$, which is required for the above-mentioned T1/SG DIV application.

An alternative modulation technique 225-QPRS achieves a spectral efficiency of 6 b/s/Hz assuming transmission at the Nyquist rate. It is well known that partial-response signalling (PRS) systems are speed tolerant [18]-[21], i.e., that it is possible to transmit data at a rate which is higher than the Nyquist rate. It should be noted that speed tolerance of PRS systems, reported in the literature [18]-[21], was evaluated for binary inputs, e.g., class-I PRS has a speed tolerance of 43%. In the above 1.6 Mb/s application example, can we use 225-QPRS to meet the efficiency requirement? To achieve 6.25 b/s/Hz by means of 225-QPRS requires an increased transmission rate of $6.25 : 6=1.042$ that is 4.2% higher than the Nyquist rate.

From Fig.1.2, we see that the required carrier-to-noise ratio (C/N) for 225-QPRS at $P_e=10^{-8}$ is 30.5 dB, whereas 34.5 dB for 256-QAM. Thus, a potential advantage of 225-QPRS above the Nyquist rate is that an increase in carrier-to-noise ratio (C/N) immunity might be obtained as compared to 256-QAM. The performance of PRS/QPRS above the Nyquist rate with m-ary inputs rather than binary was not available before our investigation [22]. These led to the motivation of investigating the performance of multi-level PRS/QPRS above the Nyquist rate.

1.1.4 Signalling Above the Nyquist Rate

Signalling above the Nyquist rate was originally discussed for PRS systems for binary inputs [18]-[21]. Recently, a few schemes concerning faster-than-Nyquist signalling were addressed [23]-[25]. These schemes exploit other pulse shapes also, such as Nyquist pulses, not limited only to PRS pulses. However, there is a common feature in all the schemes mentioned so far. That is, signalling above the Nyquist rate is achieved by simply increasing the signalling rate with the originally designed transmission characteristic being kept fixed. As such, it introduces too much "undesired" intersymbol interference (ISI) which causes significant performance degradation by simple symbol-by-symbol detection. Maximum Likelihood Sequence Detection (MLSD) may be employed to overcome the consequent ISI in the best way possible [27]. However, the difficulty lies in the fact that the complexity of implementation may be beyond the capability of the present technology. For example, a number like 10^8 has been chosen as the number of states required by the Viterbi algorithm for decoding the Faster Binary Signalling (FBS) signal [24].

In this thesis, we do not insist on optimum receivers [26], and other advanced nonlinear receivers, such as MLSD and decision feedback equalizers (DFE) [27]-[32] for PRS/QPRS above the Nyquist rate because of the complexity involved in implementation. Instead, a symbol-by-symbol detection procedure is assumed because of easy implementation. We introduce a new method for PRS/QPRS above the Nyquist rate which allows the use of symbol-by-symbol detection and achieves a better performance than the conventional method.

1.2 THESIS ORGANIZATION

Following this introductory chapter, in Chapter 2 we discuss multi-level PRS/QPRS above the Nyquist rate. It is shown that the conventional method is not practical for 225-QPRS systems operated above the Nyquist rate. An improved efficiency PRS/QPRS data filtering strategy, which enables a higher transmission rate (more symbols/s/Hz in a normalized bandwidth) than feasible with conventional PRS/QPRS systems, is then introduced. Though the discussion in Chapter 2 emphasizes class-I (duobinary) PRS, it preserves sufficient generality to accommodate other classes of PRS.

In some systems, such as transformer coupled circuits, SSB modems, and carrier systems with carrier pilot tones, where reduced low-frequency components in the spectrum are required, class-IV (modified duobinary) PRS is more suitable than class-I. Thus, the study on the possibility of increasing the spectral efficiency above the Nyquist rate using class-IV PRS with multi-level inputs is presented in Chapter 3. We show that, by using our new technique, the performance of a class-IV 225-QPRS above the Nyquist rate is nearly as good as that of using class-I PRS. Additional advantages of class-IV PRS above the Nyquist rate using our new technique are that a service channel can be inserted and that a higher percentage increase in spectral efficiency can be obtained in an FDM SSB system.

In Chapter 4, we present the implementation of an experimental 7-level class-IV PRS system operated above the Nyquist rate using our new method. The performance is measured to confirm the concept and simulation accuracy.

The effect of channel and/or hardware imperfections on a 256-QAM modem is investigated in Chapter 5. The next chapter, Chapter 6, compares the performance of 256-QAM and improved efficiency 225-QPRS in distorted channels, based on the same spectral efficiency of 6.3 b/s/Hz. The effects of group delay and amplitude distortions with linear, parabolic, and sinusoidal characteristics on these two schemes are evaluated and compared.

In Chapter 7 we introduce and study error floors in digital transmission systems. Error floors are known in industry as one of the most severe problems of transmission systems. We first describe a new method to evaluate and compare the error floors of PRS systems operated above the Nyquist rate using the conventional and our new models. The concept is extended to evaluate error floors of PAM systems under severe distortions.

The discussion of co-channel interference (CCI) caused performance degradations on 64-QAM, 225-QPRS and 256-QAM is presented in Chapter 8.

Chapter 9 discusses the use of an adaptive baseband transversal equalizer for 256-QAM to combat channel distortions. Finally, Chapter 10 summarizes the results of the thesis and suggestions for further research.

Chapter II

MULTI-LEVEL PRS/QPRS ABOVE THE NYQUIST RATE

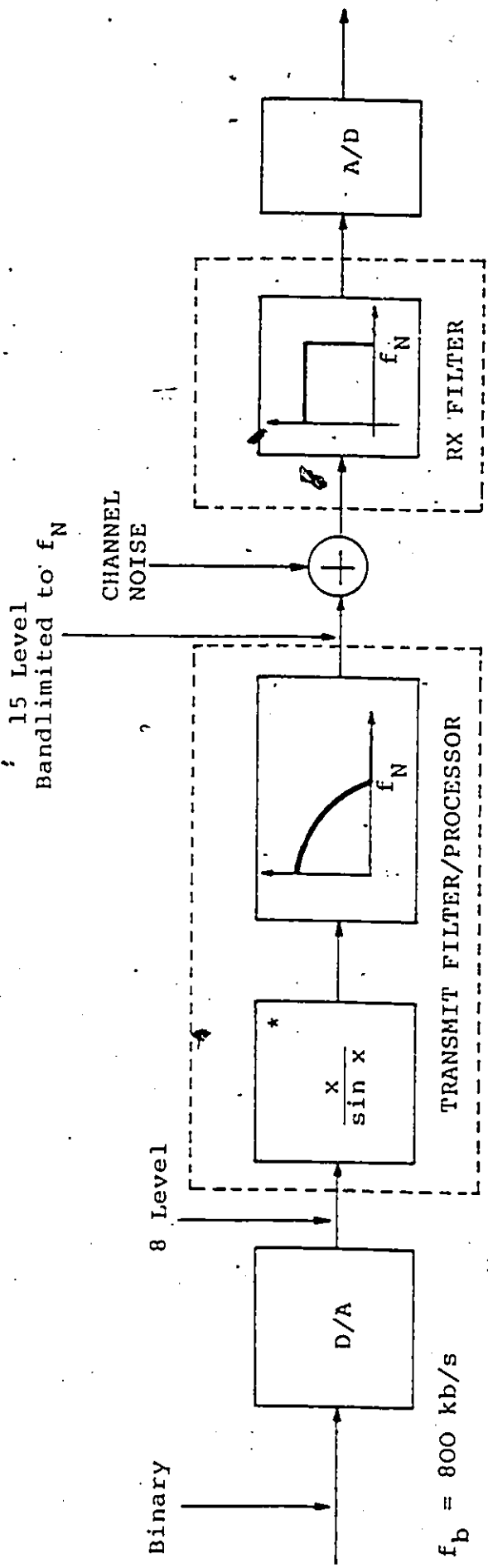
It is well known that partial-response signalling (PRS) systems are speed tolerant [18]-[21], i.e., that it is possible to transmit data at a rate which is higher than the Nyquist rate. Speed tolerance was defined [18]-[20] as the percentage increase over the Nyquist rate at which the smallest eye opening is zero with the transmission characteristic being kept fixed for binary inputs. Due to inherently higher intersymbol-interference (ISI) in multi-level systems, speed tolerance is expected to decrease as the number of input levels increases. However, it is not clear yet from the literature how speed tolerance would be changed for PRS systems with m-ary inputs rather than binary. And, as mentioned in Chapter 1, there is a need for highly spectrum-efficient modulation schemes. Therefore, it is important to study the performance of PRS/QPRS above the Nyquist rate in order that the feasibility of increasing the spectral efficiency for PRS/QPRS systems can be assessed. Since duobinary (class-I) PRS with binary inputs has a speed tolerance of 43% [18]-[20], which is the largest among various classes, it is logical to choose it as a starting point for studying PRS systems signalling above the Nyquist rate with m-ary inputs.

In Section 2.1 two models for duobinary PRS systems above the Nyquist rate with m-ary inputs are described, with Model-A represent-

ing the conventional method as speed tolerance was discussed [18]-[20] and Model-B standing for the new chopping method we propose. Based on a comparison from both the frequency and time domains, we show that Model-B is superior to Model-A. A few selected eye diagrams presented in Section 2.2, manifest the superiority of our new technique over the conventional method. In Section 2.3 experimental results are demonstrated to confirm that predicted by computer simulations. Evaluation of the probability of error for 225-QPRS above the Nyquist rate is given in Section 2.4. Results show that, by symbol-by-symbol detection, it is not practical to use the conventional method for 225-QPRS above Nyquist rate. However, with the use of our new technique (Model-B) for 225-QPRS, an increase of 5% above the Nyquist rate can be achieved with a small degradation. This increase is significant in some applications.

2.1 SYSTEM MODELS

Multi-level PRS and QPRS system block diagrams are shown in Fig.2.1(a) and (b). An illustrative example would be the transmission of an $f_b = 800$ kb/s rate data with a 15-level PRS system filtered at the Nyquist frequency of 133 kHz that is 6 b/s/Hz. In the QPRS Modem case the source rate at 1600 kb/s is serial-to-parallel converted and fed into the "inphase" and "quadrature" 800 kb/s channels of the modulator. In Fig.2.1(b), the transmit filter/processors and receive filters are identical with the ones illustrated in Fig. 2.1(a).



Also known as Duobinary encoder

* The $\frac{x}{\sin x}$ aperture equalizer is employed to convert the multi-level pulse stream into an "impulse stream".

Fig.2.1(a) Block diagram of a conceptual duobinary PRS baseband system. Illustrative example : Source rate $f_b = 800$ kb/s; Symbol rate of D/A output, assuming an 8-level output is used, is $f_s = 266$ k symbol/s. In this case $f_N = 133$ kHz. Thus, the spectral efficiency of the 8-level PAM signal, which gets converted to 15-level PRS is 800 kb/s : 133 kHz = 6 b/s/Hz.

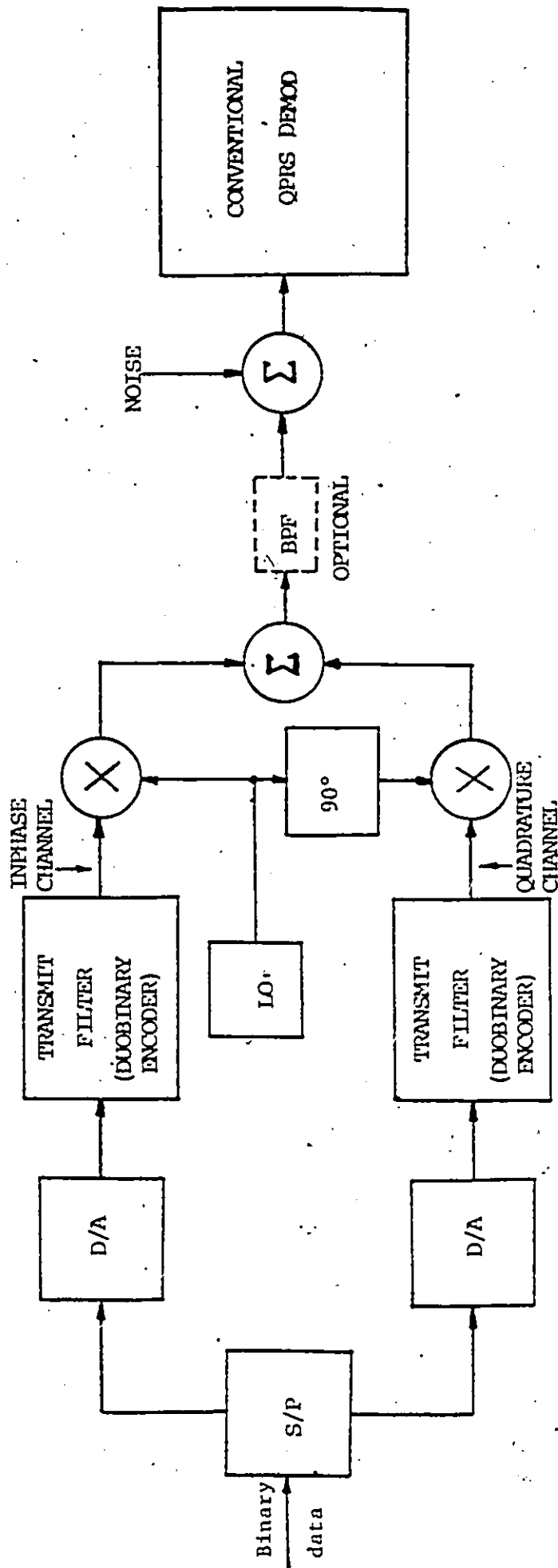


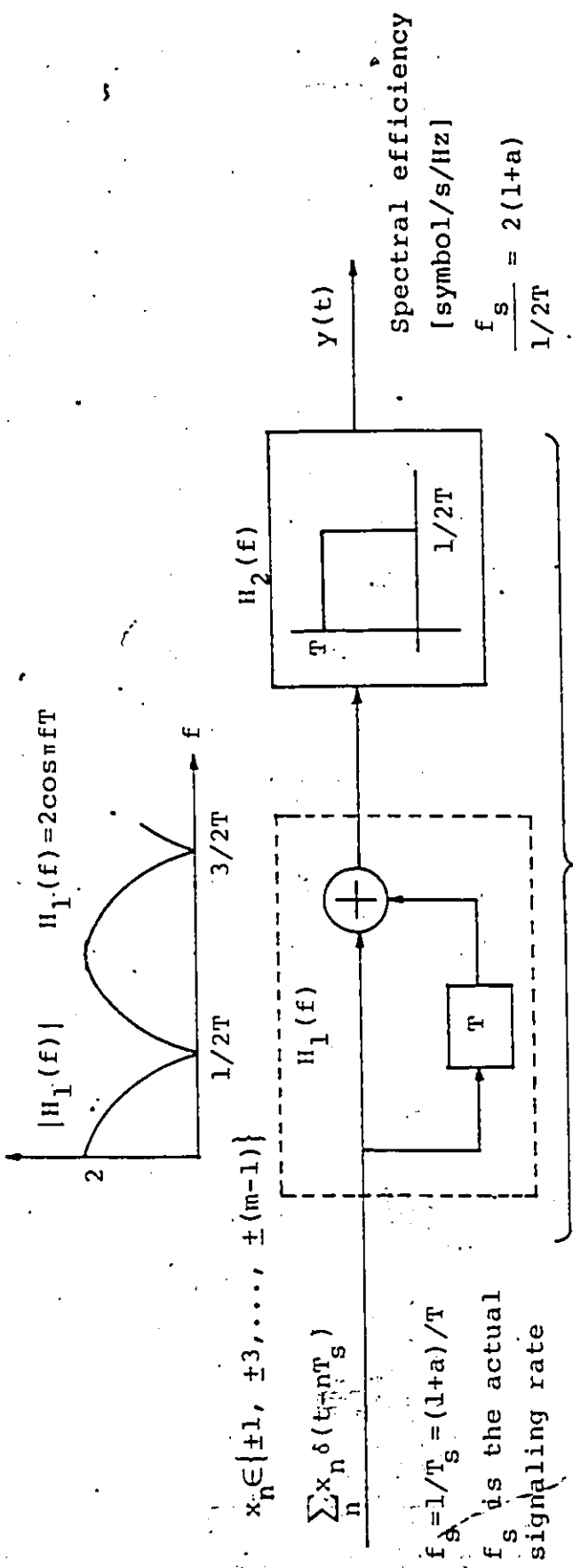
Fig.2.1(b) QPRS modem block diagram.
 The duobinary encoders in the in-phase and quadrature channels are identical to the ones in Fig.2.1(a).

Transmission above the Nyquist rate by PRS can be achieved by increasing the signalling rate with the transmission characteristic being kept fixed, as is the case in which speed tolerance was evaluated in the published literature [18]-[20]. This conventional method will be called Model-A, as depicted in Fig.2.2. With Model-A, one transmits data at a rate of $f_s=(1+a)/T$ symbols/s over a bandwidth of $1/2T$ Hz, resulting in an efficiency of $2(1+a)$ symbols/s/Hz where $100a$ represents the percentage increase above the Nyquist rate. In fact, Model-A consists of forcing a symbol rate through a duobinary filter that is higher than the rate for which the filter is designed. As such, it will introduce serious "undesired" ISI and result in very significant performance degradations.

It will soon be clear that Model-A does not give good results concerning the probability of error, especially when multi-level inputs are used. Hence, we propose a new scheme called Model-B, as illustrated in Fig.2.3. Our Model-B consists essentially of defining a new (infinite) partial-response system in the following manner:

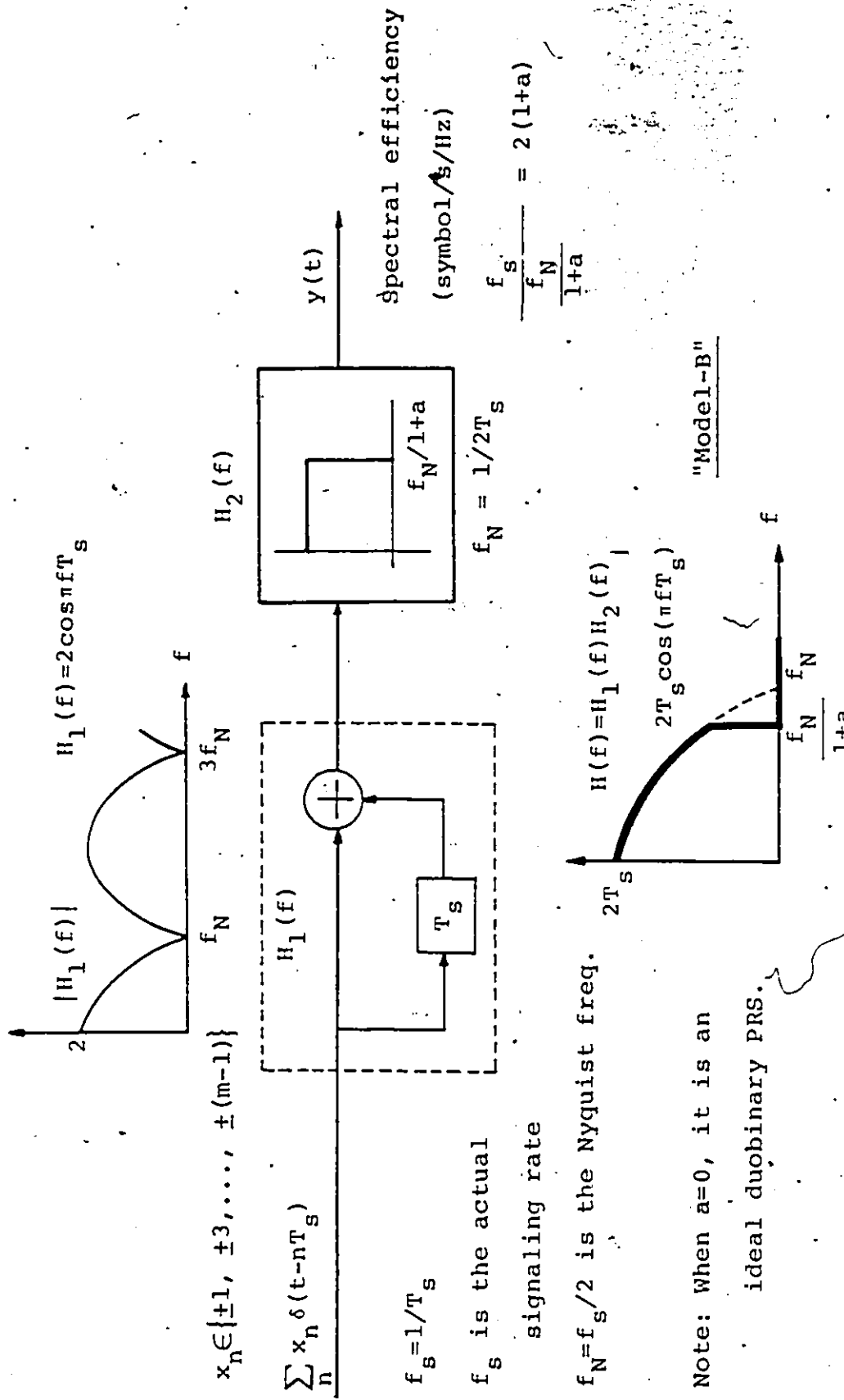
- i) Define an ideal duobinary response for the new higher symbol rate.
- ii) Truncate this response to achieve the desired spectral efficiency using an ideal brickwall filter ("chopping") which has a cutoff frequency at $f_N/(1+a)$ below the Nyquist frequency.

In Figs.2.1-2.3, we did not include the digital processing parts, such as precoding to avoid error propagation, Gray coding, etc. These pro-



Note: When $a=0$, i.e., $T_s = T$, it is an ideal duobinary PRS.

Fig.2.2 Model-A : Conventional system model for duobinary PRS above the Nyquist rate and cascaded transfer function. The spectral efficiency of this system is $2(1+a)$ symbol/s/Hz, i.e., 100% higher than the so-called Nyquist rate of 2 symbol/s/Hz.



$$x_n \in \{\pm 1, \pm 3, \dots, \pm(m-1)\}$$

$$\sum_n x_n \delta(t-nT_s)$$

$$f_s = 1/T_s$$

f_s is the actual signaling rate

$f_N = f_s/2$ is the Nyquist freq.

Note: When $a=0$, it is an ideal duobinary PRS.

Spectral efficiency (symbol/s/Hz)

$$\frac{f_s}{f_N} \frac{1}{1+a} = 2(1+a)$$

"Model-B"

Fig.2.3 Model-B : New system model for duobinary PRS above the Nyquist rate and corresponding cascaded transfer function. The spectral efficiency of this system is $2(1+a)$ symbol/s/Hz, i.e., 100% higher than the Nyquist rate of 2 symbol/s/Hz.

cessors were described in sufficient detail in [19]-[21], [53]. We shall first compare these two models from the frequency and time domains.

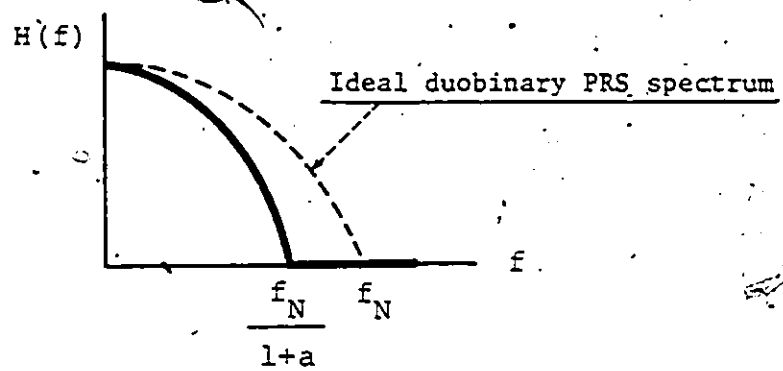
2.2 WHY IS OUR NEW MODEL-B BETTER THAN THE CONVENTIONAL MODEL-A?

In this section, we investigate the reason why our new Model-B is better than the conventional model-A for multi-level PRS/QPRS above the Nyquist rate.

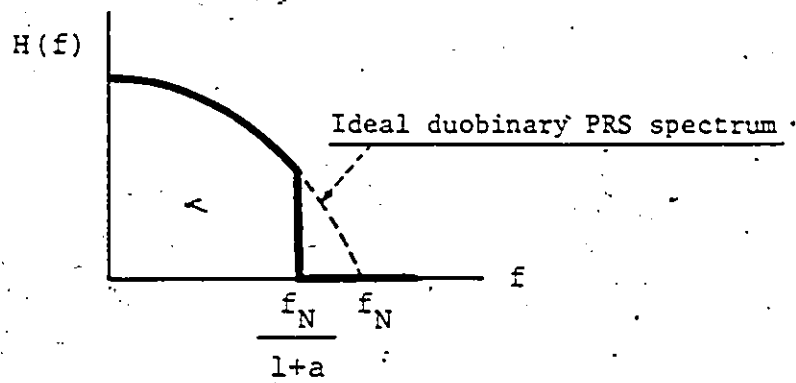
2.2.1 Frequency-Domain Comparison

An equivalent way of comparing operation above the Nyquist rate by PRS for the two models is to keep the signalling rate, f_s , the same but to reduce the bandwidth to less than f_N . Using this viewpoint, operation above the Nyquist rate in the Model-A scheme is illustrated in Fig.2.4(a) in which a scaled cosine shape is retained. Thus, only the frequency scale is changed, resulting in that all the frequency components suffer distortion. On the other hand, in our Model-B scheme shown in Fig.2.4(b), the old frequency response is simply "chopped off" at $f_N/(1+a)$. Most of the original frequency components are thus retained and the only frequency components that suffer distortion are the ones that have been cut off.

From this frequency-domain comparison, we would expect Model-B performs better, especially for multi-level inputs. The superiority of Model-B over Model-A can also be observed in the time domain.



(a) Conventional Model-A



(b) Our new Model-B

Fig.2.4 A frequency-domain comparison for the two models for duobinary PRS above the Nyquist rate.

2.2.2 Time-Domain Comparison

PRS systems operate by introducing a "controlled" or "desired" amount of ISI. When operated above the Nyquist rate, in addition to the "desired" ISI, there is introduced "undesired" ISI, which is responsible for the eventual deterioration of performance to below an acceptable level. We would expect Model-B to have less "undesired" ISI simply due to the fact that in Model-B most of the original frequency components are retained, as discussed earlier. To examine this ISI more rigorously, we shall consider the time domain behavior.

As a first step, expressions for impulse responses of Model-A and Model-B will be derived. Referring to Fig.2.2, the overall frequency response $H(f)$ of conventional Model-A is expressed as follows.

$$H(f) = \begin{cases} 2T \cos(\pi fT), & |f| \leq 1/2T \\ 0 & \text{elsewhere.} \end{cases} \quad (2.1)$$

The signaling rate f_s is related to T by (2.2).

$$f_s = 1/T_s = (1+a)/T \quad (2.2)$$

The corresponding impulse response $h(t)$ can be obtained by taking the inverse Fourier transform of (2.1), i.e.,

$$\begin{aligned} h(t) &= \int_{-\infty}^{\infty} H(f) e^{j2\pi ft} df \\ &= 4T \int_0^{1/2T} \cos(\pi fT) \cos(2\pi ft) df \\ &= \text{sinc}\left(\frac{t}{T} + \frac{1}{2}\right) + \text{sinc}\left(\frac{t}{T} - \frac{1}{2}\right) \end{aligned} \quad (2.3)$$

where

$$\text{sinc}(x) = \frac{\sin(\pi x)}{\pi x}$$

For our Model-B case (see Fig.2.3) the overall frequency response $H(f)$ can be written as (2.4).

$$H(f) = \begin{cases} 2T_s \cos(\pi f T_s), & |f| \leq f_N/(1+a) \\ 0 & \text{elsewhere.} \end{cases} \quad (2.4)$$

where

$f_N = 1/T_s$ is the Nyquist frequency of the signal.

Following the similar steps, the impulse response $h(t)$ of Model-B can be derived as follows.

$$\begin{aligned} h(t) &= \int_{-\infty}^{\infty} H(f) e^{j2\pi f t} df \\ &= 4T_s \int_0^{f_N/(1+a)} \cos(\pi f T_s) \cos(2\pi f t) df \\ &= \frac{1}{1+a} \left\{ \text{sinc} \left[\frac{1}{1+a} \left(\frac{t}{T} + \frac{1}{2} \right) \right] + \text{sinc} \left[\frac{1}{1+a} \left(\frac{t}{T} - \frac{1}{2} \right) \right] \right\} \quad (2.5) \end{aligned}$$

Note that in the above derivations, the center of the impulse response has been chosen as the time origin. Thus for the ideal duobinary PRS, i.e., $a = 0$ for either Model-A or Model-B, the only two nonzero samples are at $t = \pm T_s/2$, respectively.

The discrete-time impulse response $|h(t)|_{t=nT_s}$ is of interest since it provides insight into the behavior of the undesired ISI. We computed $|h(t)|_{t=nT_s}$ by using the equations (2.3) and (2.5) for the two models. For illustrative purposes, we plot $|h(t)|_{t=nT_s}$ of Model-A and Model-B in Figs.2.5 and 2.6 for the same percentage increases of 5% and 10% respectively. It is easily seen that, the undesired ISI's in our new Model-B case are much smaller than those of Model-A, especially

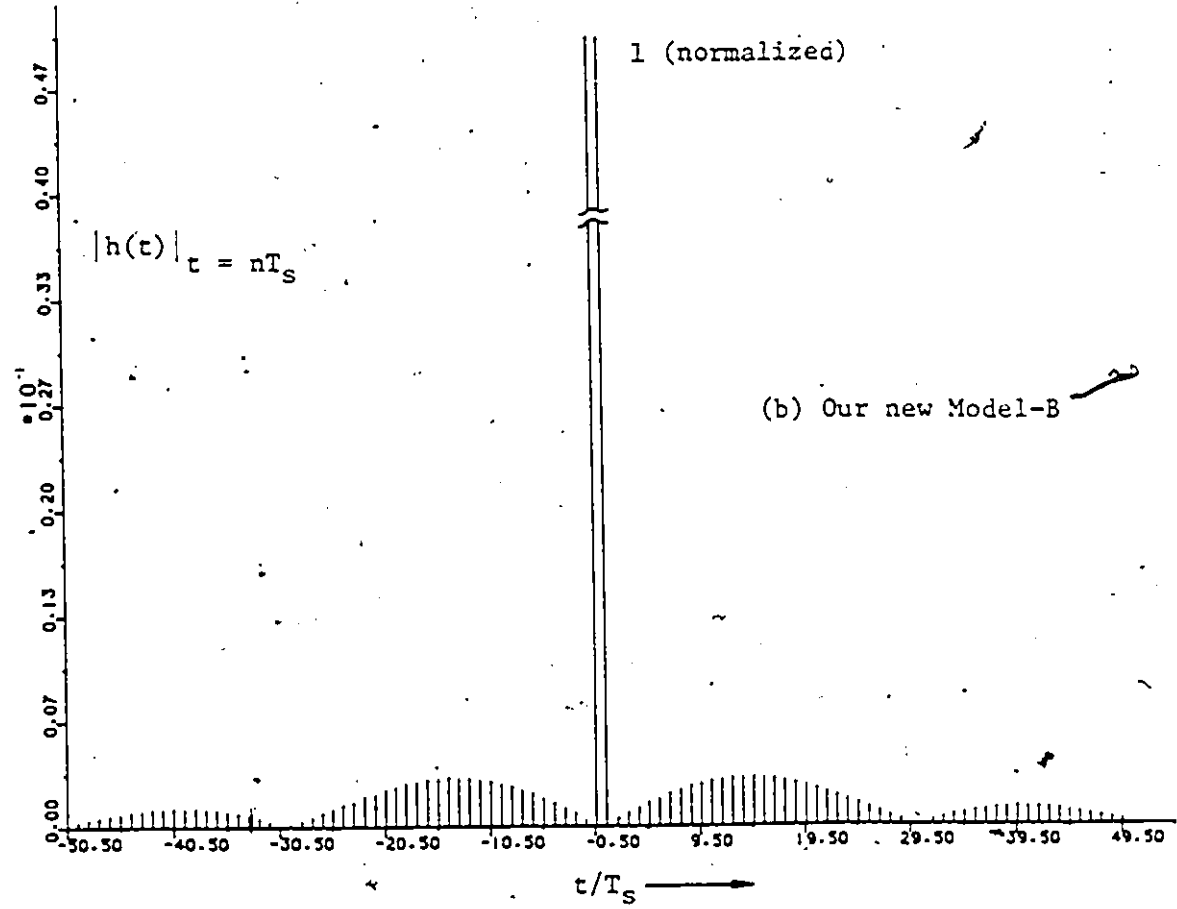
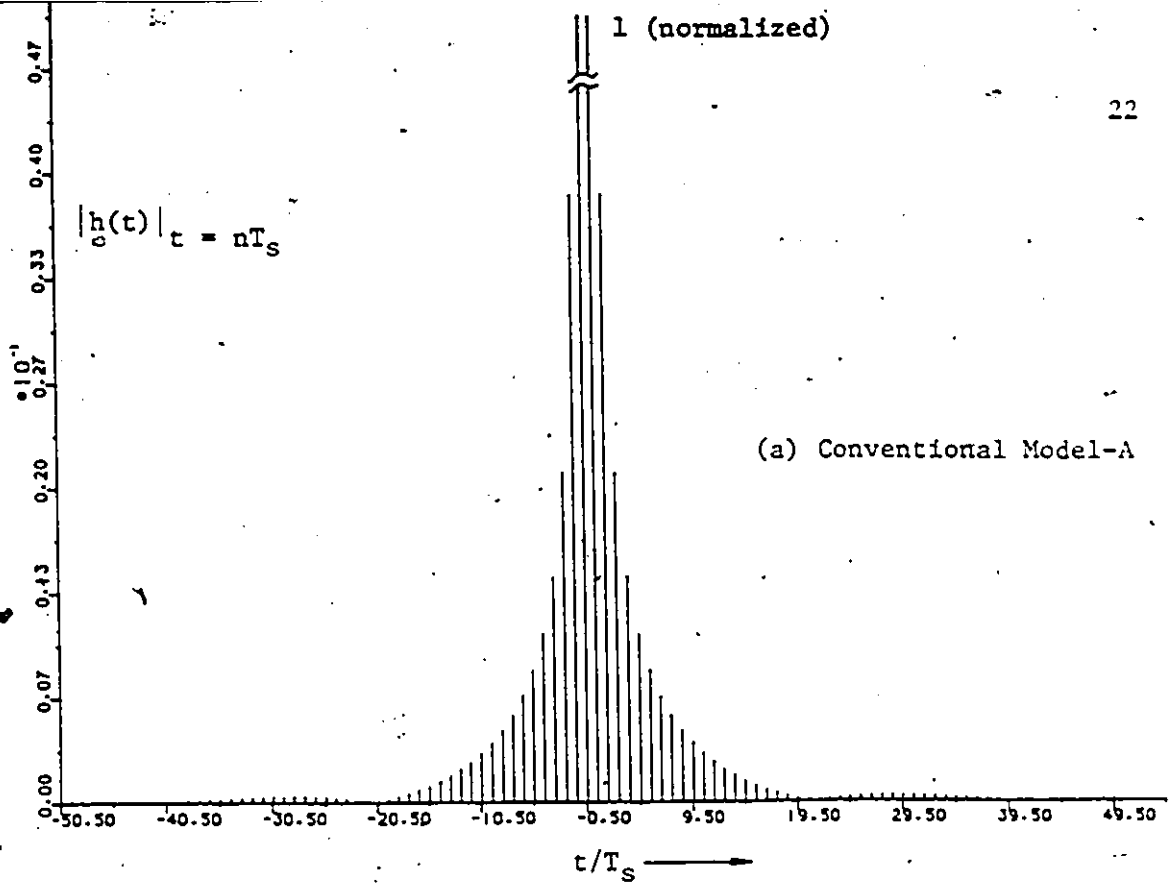


Fig.2.5 Discrete-time impulse response of duobinary (class-I) PRS with a 5% increase above the Nyquist rate. (a) Conventional Model-A, (b) Our new Model-B.

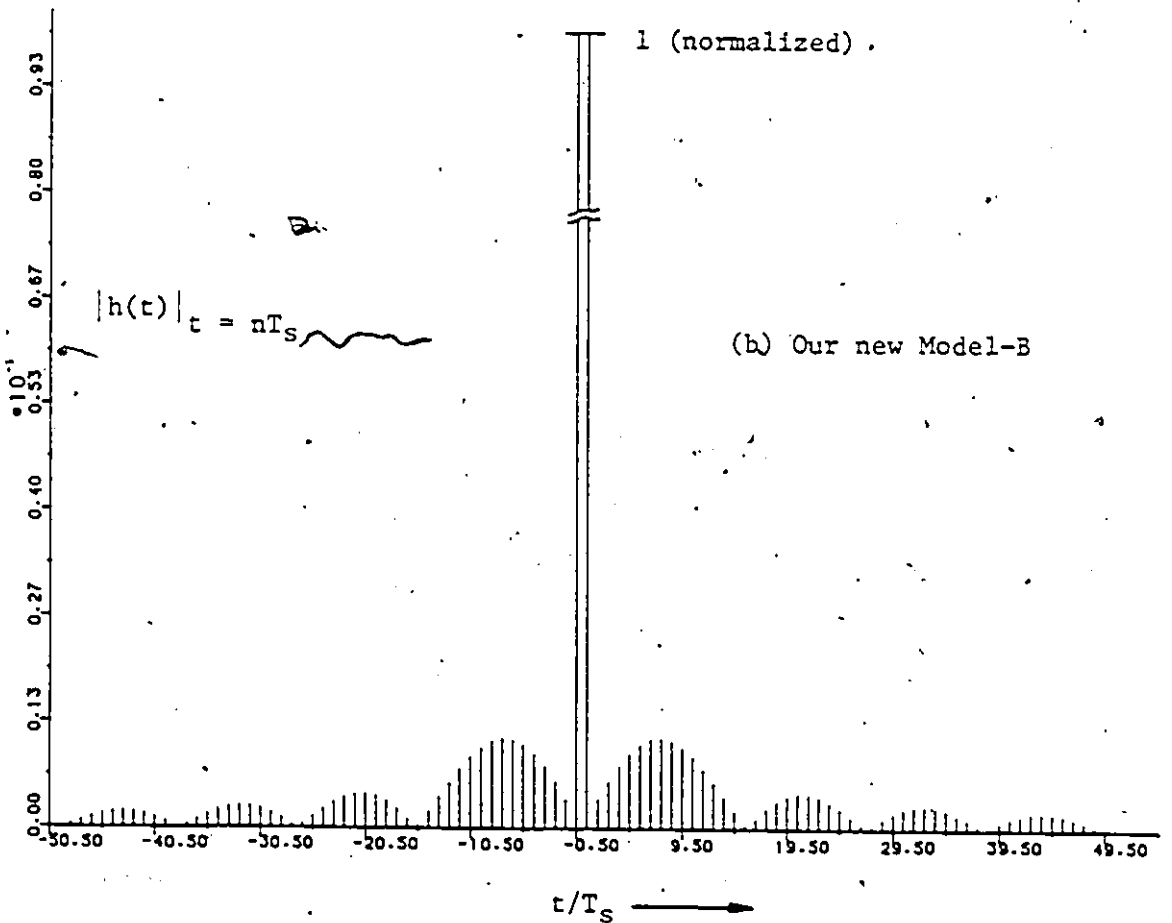
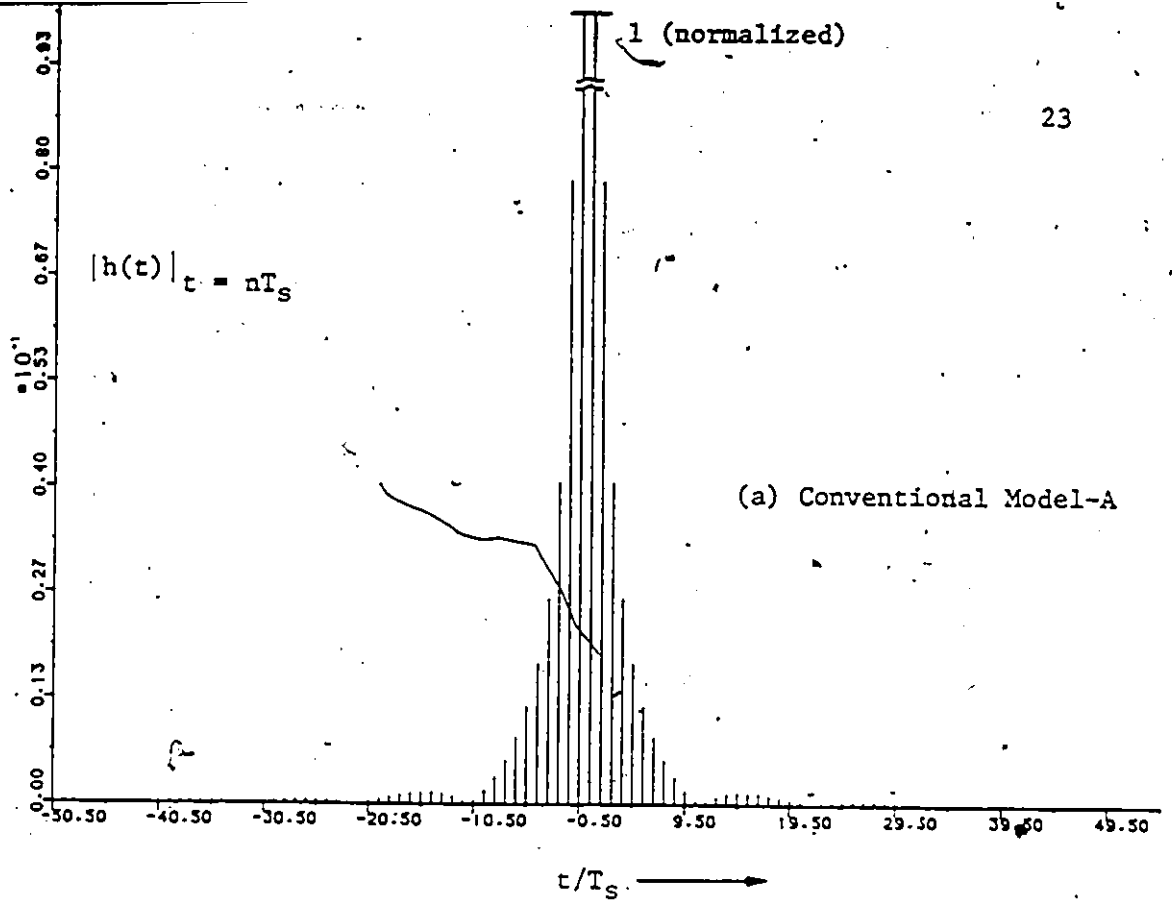


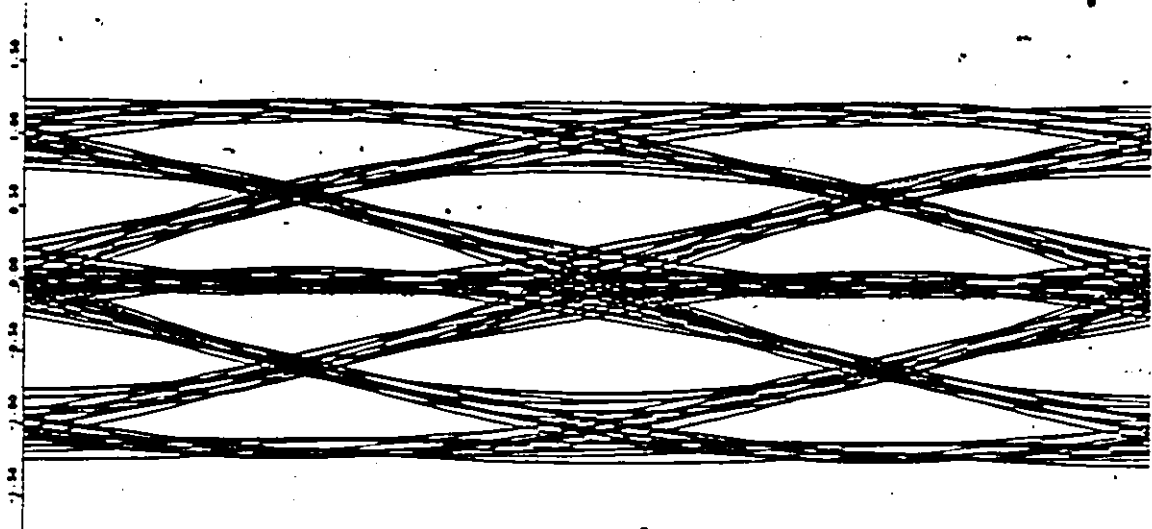
Fig.2.6 Discrete-time impulse response of duobinary (class-I) PRS with a 10% increase above the Nyquist rate. (a) Conventional Model-A, (b) Our new Model-B.

for those near the two desired ISI samples. This confirms our conjecture from the frequency-domain comparison. A more rigorous comparison of the two models which leads to concepts, such as truncated peak distortion and system error floor [22], will be treated in Chapter 7.

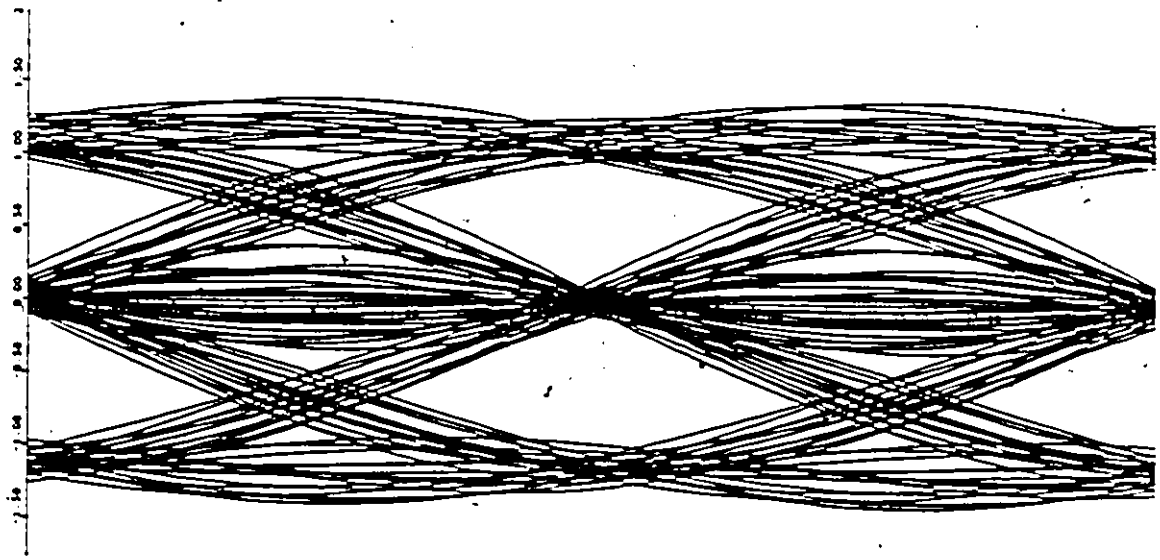
2.3 COMPARISON OF EYE DIAGRAMS

Since eye diagrams show a good indication of system performance, we shall first compare a few typical eye diagrams, generated by computer simulations. The attention will be focused on the vertical eye opening because it gives the noise margin at the optimum sampling instants. The eye diagrams, displayed in Figs.2.7-2.9, represent 9-, 49-, and 225-QPRS, which consist of modulating in quadrature two baseband 3-, 7-, and 15-level PRS systems, respectively, using Model-A or Model-B. The choice of these eye diagrams is, of course, arbitrary but proper for comparison. Fig.2.7(a) and(b) show the eye diagrams of 9-QPRS for Model-A and Model-B with an increase of 20% above the Nyquist rate. Both show that the eye is open. However, the eye opening in Fig.2.7(b) is much larger than that of Fig.2.7(a), indicating clearly that a larger noise margin exists by using our Model-B.

In the case of 49-QPRS with an increase of 10% above the Nyquist rate, Fig.2.8(b) (Model-B) gives a robust eye opening whereas in Fig.2.8(a) the eye is seen about to close. It shows that Model-B is better than Model-A as the number of input levels increases. This trend becomes clearer as we look into 225-QPRS with an increase of 4.2% above the Nyquist rate. While Fig.2.9(b) shows a reasonably good eye

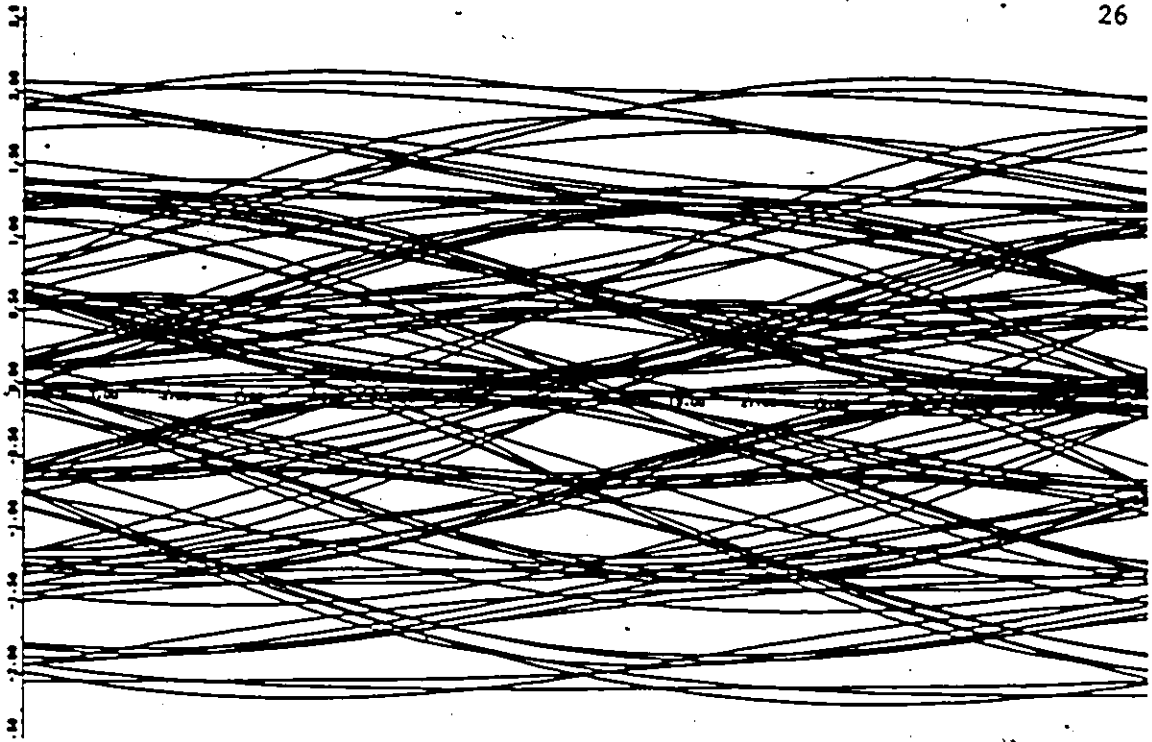


(a) Using the conventional Model-A.

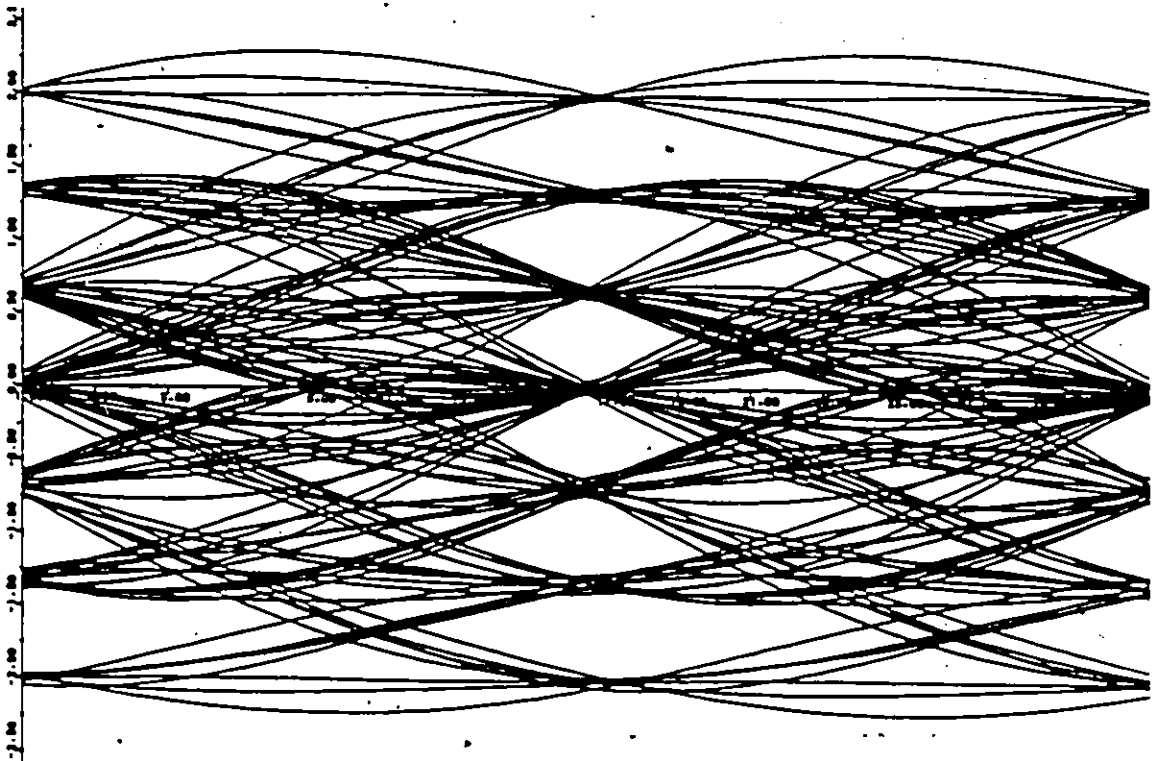


(b) Using our new Model-B.

Fig.2.7 Eye diagrams of 3-level PRS/9-QPRS with a 20% increase above the Nyquist rate. Spectral efficiency: 2.4 b/s/Hz.

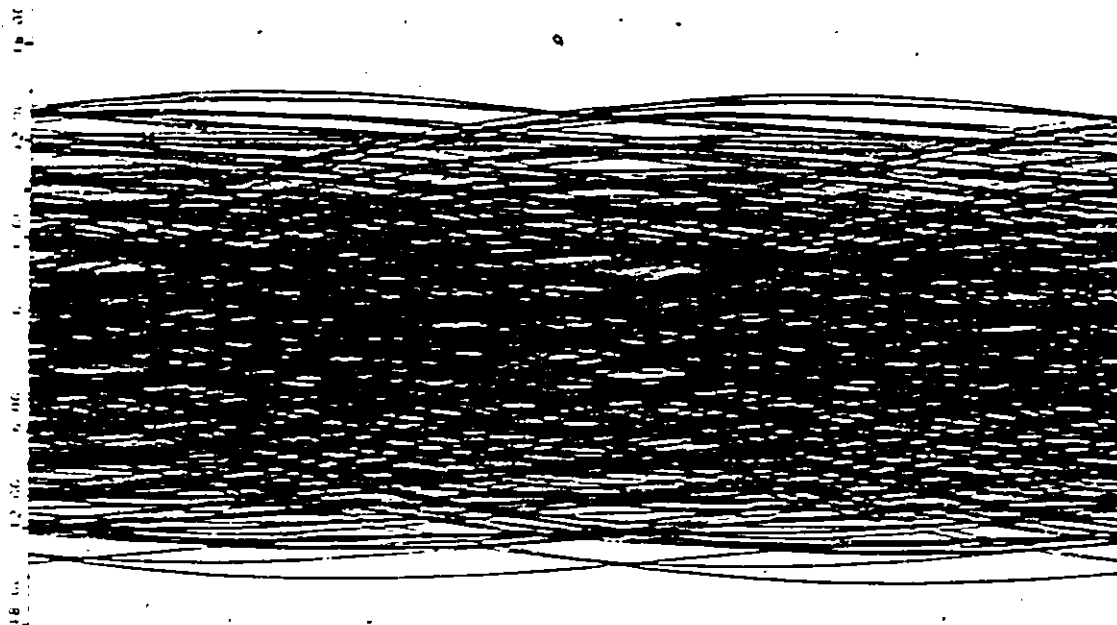


(a) Using the conventional Model-A.

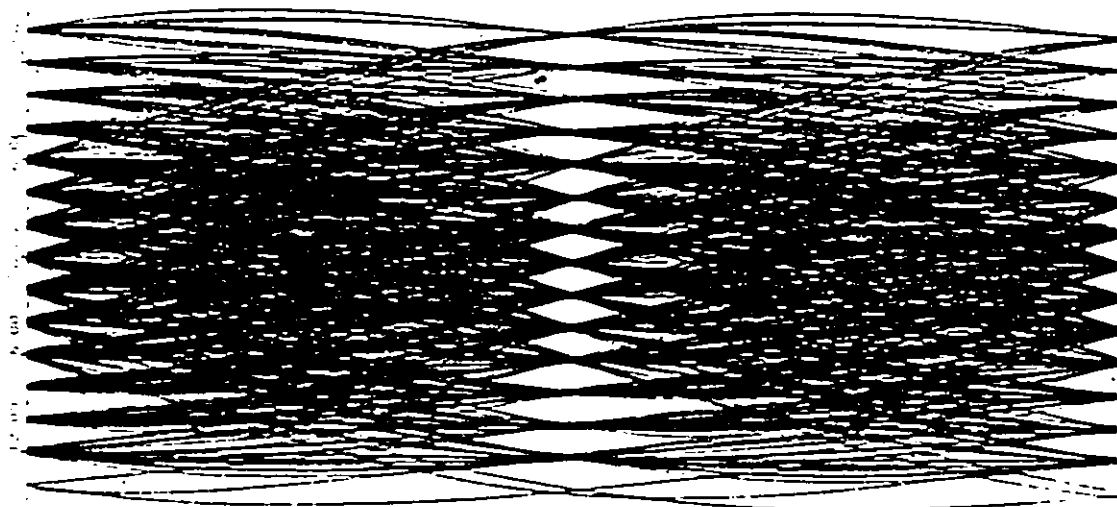


(b) Using our new Model-B.

Fig.2.8 Eye diagrams of 7-level PRS/49-QPRS with a 10% increase above the Nyquist rate. Spectral efficiency: 4.4 b/s/Hz.



(a) Using the conventional Model-A.



(b) Using our new Model-B.

Fig.2.9 Eye diagrams of 15-level PRS/225-QPRS with a 4.2% increase above the Nyquist rate. Spectral efficiency: 6.25 b/s/Hz.

opening, in Fig.2.9(a) the eye is completely closed, meaning that in this case symbol-by-symbol detection fails to decode the signal for the conventional Model-A.

From the study of eye diagrams, we found that speed tolerance of duobinary PRS has reduced from 43% for binary inputs to about 4% for 8-level inputs by using the conventional Model-A. On the other hand, with the use of our new Model-B it is possible to achieve a higher spectral efficiency for PRS/QPRS systems.

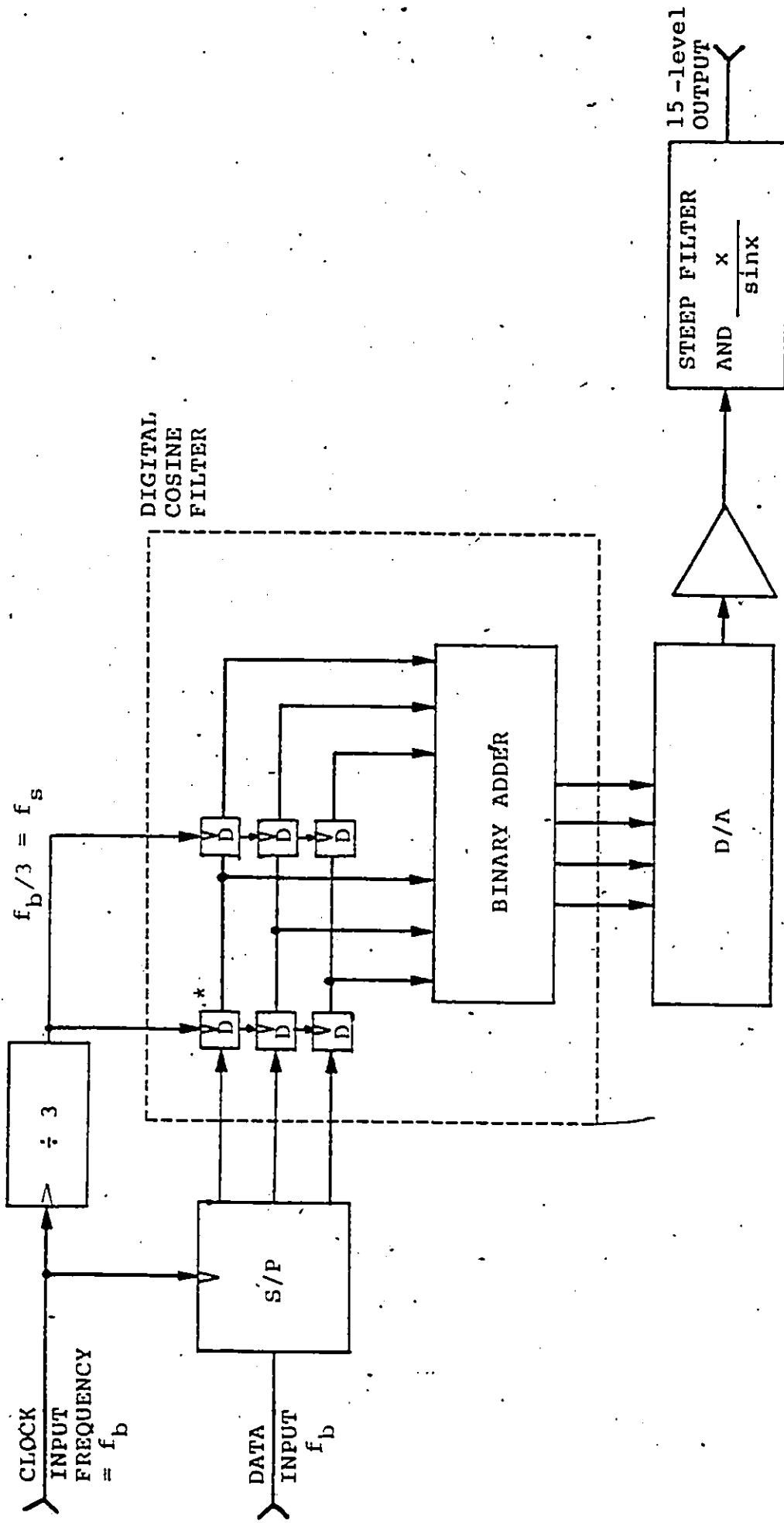
2.4 EXPERIMENTAL RESULTS FOR A 15-LEVEL PRS USING OUR NEW MODEL-B

We implemented an above-the-Nyquist-rate transmission system using our Model-B for a 15-level PRS system [33] according to Fig.2.10. The circuit of Fig.2.10 operates as follows. The incoming binary data, at a bit rate of $f_b = 800$ kb/s, is converted into an eight state symbol at a symbol rate of $f_s = f_b/3 = 266.66$ kBaud by the serial-to-parallel (S/P) converter. The symbol is time aligned by the first set of three "D" type flip-flops. The second set of three "D" type flip-flops provides a unit symbol delay between two successive symbols. These two successive 8 state symbols are then added to provide one 15-state PRS symbol at the symbol rate. Note that the "D" type flip-flops and the binary adder form a digital cosine filter as $H_1(f)$ in Fig.2.3, which can be expressed explicitly as (2.5).

$$|H_1(f)| = 2 \left| \cos(\pi f T_s) \right| \quad |f| < \infty \quad (2.6)$$

where

$T_s = 1/f_s$ is the signaling symbol interval.



50 dB
 Attenuation at
 $f_{\text{cutoff}} = f_N/(1+a)$
 $f_N = f_s/2$

* "D" represents a symbol interval delay element
 which is a D-type flip flop in practice.

Fig.2.10 Hardware implementation of 15-level duobinary PRS above the Nyquist rate using our new "Model-B".

The 15-state digital symbol is then converted into a 15-level analog symbol by the D/A converter. The amplifier serves as a buffer for the filter and voltage offset for the D/A converter.

The wideband 15-level PRS signal is then sent through a steep filter which has a 50 dB attenuation at $f_c = f_N/(1+a) = 128\text{kHz}$, where $f_N = f_s/2 = 133.33\text{ kHz}$. It is to be noted that, in practice, non-return to zero (NRZ) rectangular pulses are used instead of impulses. And for a rectangular pulse $p(t)$ defined by

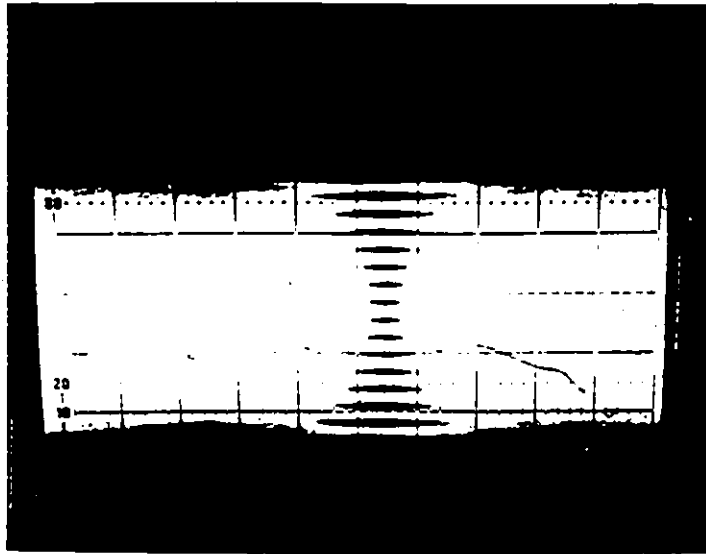
$$p(\tau) = \begin{cases} A & |\tau| \leq T_s/2, \\ 0 & \text{elsewhere.} \end{cases} \quad (2.7)$$

The Fourier transform of $p(t)$ is

$$P(f) = F\{p(\tau)\} = AT_s \frac{\sin(\pi f T_s)}{\pi f T_s} \quad (2.8)$$

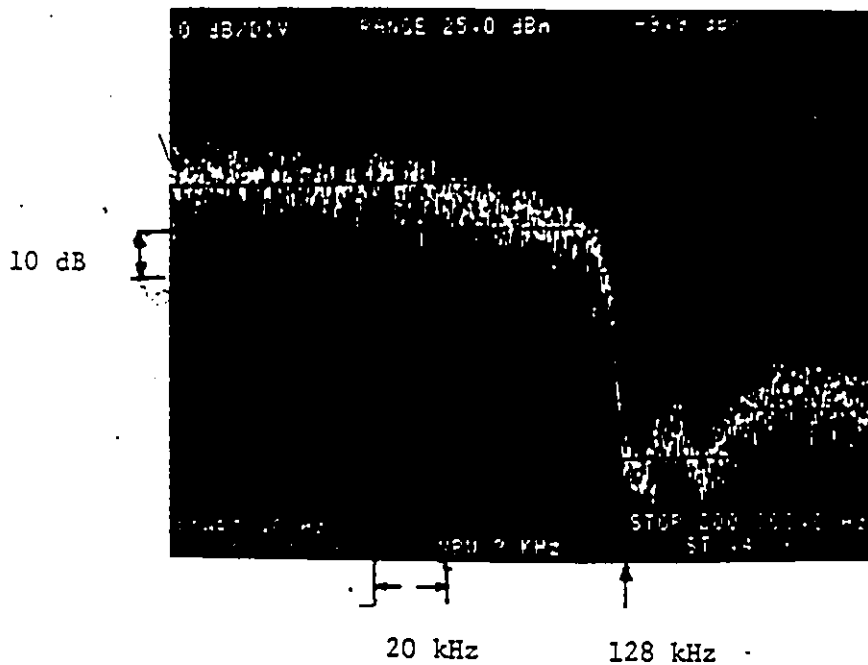
where $T_s = 1/f_s$ is the symbol interval.

Thus, the final transmit filter contains a compensating factor of $x/\sin(x)$ to account for the nonreturn-to-zero (NRZ) rectangular pulse (instead of impulse) induced $\sin(x)/x$ shaping of the spectrum. The measured eye diagram and corresponding power spectral density for $f_b = 800\text{ kb/s}$ and $f_c = 128\text{ kHz}$ are shown in Fig.2.11. In this case the spectral efficiency is $800:128 = 6.25\text{ b/s/Hz}$, i.e., an increase of 4.2% above the Nyquist rate. We note that the measured eye diagram is open as predicted in the simulation result of Fig.2.9(b).



H: 500 ns/div

V: 100 mV/div



H: 20 kHz/div

V: 10 dB/div

Fig.2.11 Measured baseband eye diagram and corresponding power spectral density of a 15-level PRS signal using our new Model-B. This eye diagram corresponds to that of the I (or Q) channel of a 225-QPRS modem operated at $f_b = 1.6$ Mb/s. The spectral efficiency of the baseband system and of the quadrature modem is $800 \text{ kb/s} \div 128 \text{ kHz} = 6.25 \text{ b/s/Hz}$, i.e., a 4.2% increase above the Nyquist rate of 6 b/s/Hz . This efficiency is defined at the 50 dB attenuation point. In this measurement, a Karkar Electronics, Inc. patented $\alpha = .01$ filter was used (Ref. U.S. Patent 3271705).

2.5 PROBABILITY OF ERROR OF 225-QPRS ABOVE THE NYQUIST RATE

Essentially 225-QPRS above the Nyquist rate can be generated by modulating in quadrature two baseband 15-level PRS systems using Model-A or Model-B. A FORTRAN program was written to evaluate the performance. The simulation method is very similar to that used in evaluating the performance of high-level QAM systems [8], [36].

Two baseband 15-level PRS signals are represented in a complex form. We assume the duobinary PRS filter shaping is fully at the transmitter whereas the receive filter merely bandlimits the channel noise which is assumed to be additive, white and Gaussian. In Appendix A, we show that this results in about a 1 dB degradation in C/N with respect to the case in which the filter shaping is optimally divided between the transmitter and the receiver. The well-known method for precoding [19]-[21] has been used to prevent error propagation. A perfect synchronization is assumed and symbol-by-symbol decision is used in the simulation.

Results are plotted in Fig.2.11. The ideal curve in Fig.2.11 represents the P_e performance corresponding to the optimum distribution of filters and is plotted according to the following equation.

$$P_e = \frac{63}{64} \operatorname{erfc} \left(\sqrt{\frac{1}{42} \left(\frac{\pi}{4} \right)^2 \frac{C}{N}} \right) \quad (2.9)$$

Eq. (2.9) is obtained by substituting $M = 8$ into (A.22) and replacing S/N by C/N, since 225-QPRS is equivalent to a 15-level PRS signal in

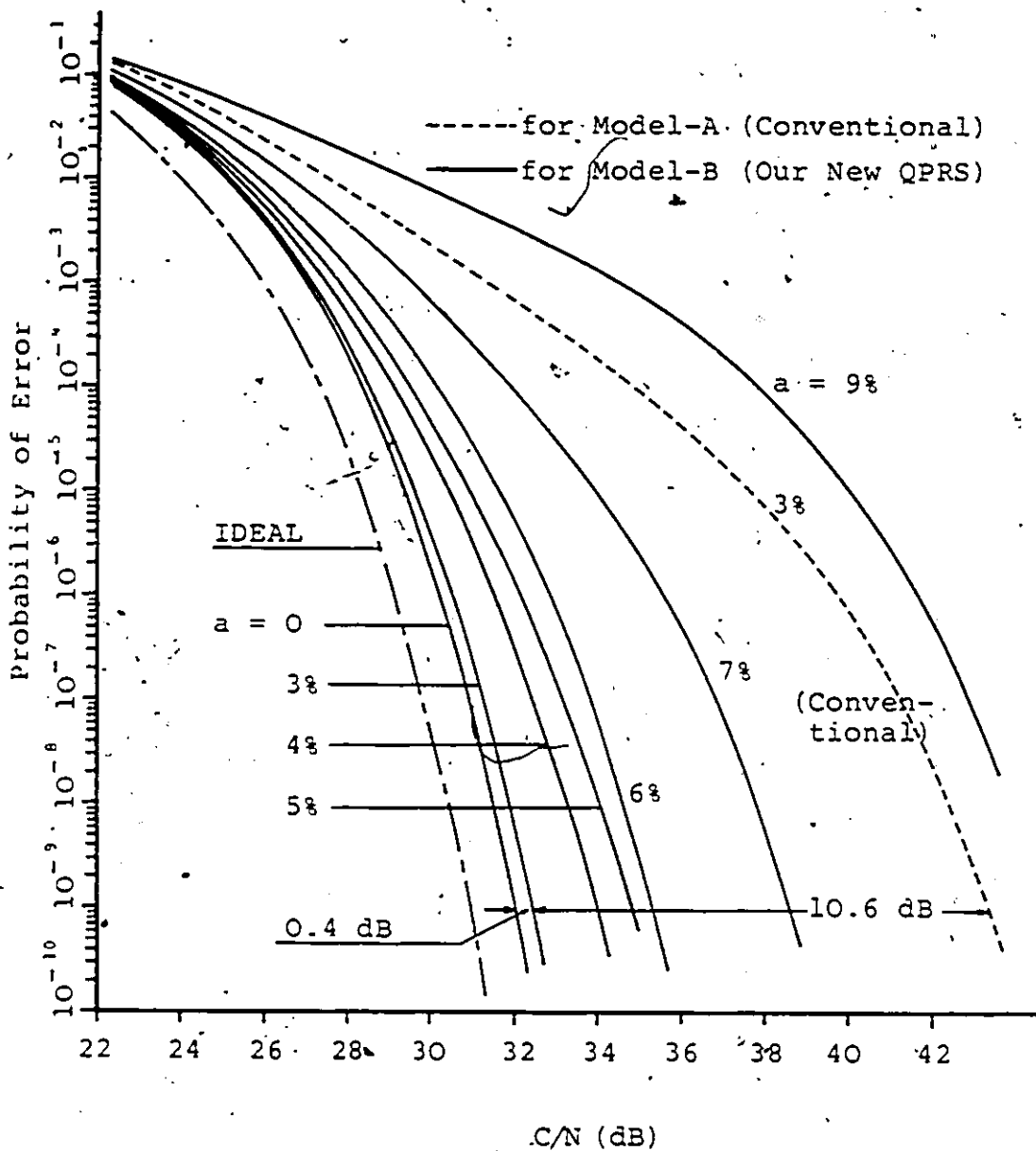


Fig.2.12 Probability of error performance of 225-QPRS above the Nyquist rate versus C/N , using Model-A or Model-B.

TABLE 2.1 Required C/N (dB) at $P_e = 10^{-9}$
for 225-QPRS above the Nyquist
rate.

% above Nyquist rate	Spectral efficiency (b/s/Hz)	Model-A (conventional) C/N (dB)	Model-B (new scheme) C/N (dB)
0	6	32	32
3	6.18	43.3	32.4
4	6.24	Not possible	34.
5	6.3	Not possible	34.9
6	6.36	Not possible	35.3

baseband. Table 2.2 summarizes the required C/N at $P_e = 10^{-9}$ for 225-QPRS for various percentage increases above the Nyquist rate using Model-A, or Model-B. The significant advantage of our Model-B is evident from Fig.2.11 and Table 2.2. For example, for 225-QPRS transmission, 3% above the Nyquist rate with conventional Model-A 11 dB degradation, while with our new Model-B only a 0.4 dB degradation is observed.

2.6 CONCLUSIONS

We conclude that, by simple symbol-by-symbol receiver structures without MLSD or other advanced nonlinear equalizers, the conventional Model-A is inappropriate for multi-level PRS/QPRS systems, such as 225-QPRS, operated above the Nyquist rate. However, with our new Model-B for 225-QPRS, an increase of up to 5% above the Nyquist rate can be achieved by simple symbol-by-symbol detection with a small degradation. This increase has very significant applications, such as the transmission of a T1 carrier in one standard analog supergroup band, as previously mentioned in Chapter 1.

Chapter III

IMPROVED EFFICIENCY 15-LEVEL MODIFIED DUOBINARY
PRS ABOVE THE NYQUIST RATE

An improved efficiency technique for duobinary (class-I) PRS above the Nyquist rate with multi-level inputs has been described in Chapter 2 and [22], [33]. However, duobinary PRS is not suitable for use in some systems, such as transformer coupled circuits, SSB modems, and carrier systems with carrier pilot tones, where reduced low-frequency components in the spectrum are required. On the other hand, modified duobinary (class-IV) PRS is ideally suited for the above-mentioned applications [34], since it has no energy at dc and a small amount at low frequencies. Thus, the objective of this chapter is to study the possibility of increasing the spectral efficiency above the Nyquist rate using class-IV PRS with multi-level inputs.

3.1 SPEED TOLERANCE OF CLASS-IV PRS WITH MULTI-LEVEL
INPUTS

The conventional method for class-IV PRS above the Nyquist rate transmission is illustrated in Fig.3.1 and will be called Model-A. Referring to Fig.3.1, the original system is designed to transmit $1/T$ symbols/s over a bandwidth of $1/2T$ Hz, resulting in a spectral efficiency of 2 symbols/s/Hz, i.e., the so-called Nyquist rate. Transmission above the Nyquist rate is conventionally achieved by simply increasing the

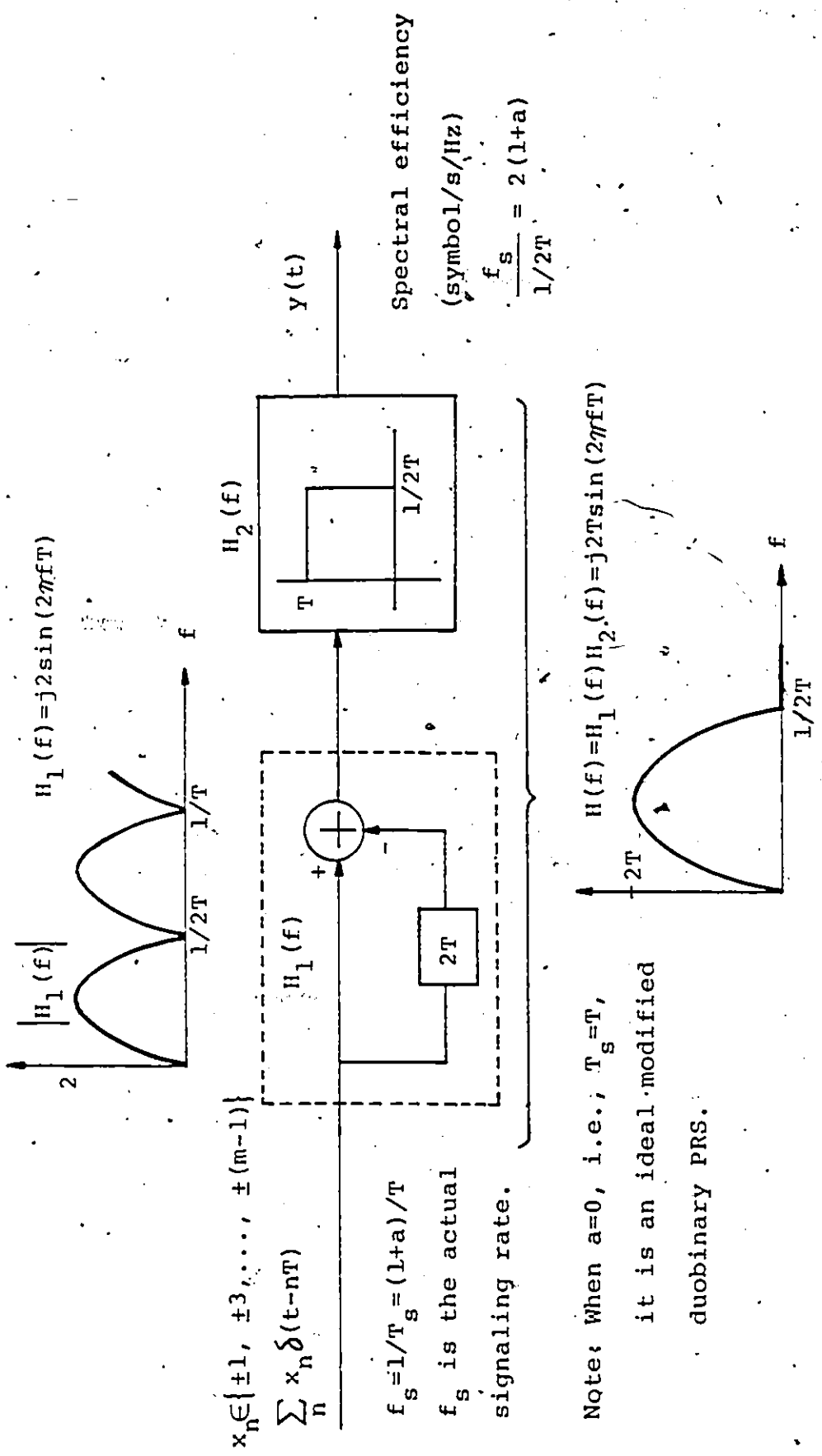


Fig.3.1 Conventional system Model: Model-A for class-IV (modified duobinary) PRS above the Nyquist rate and the cascaded transfer function. The spectral efficiency of this system is $2(1+a)$ symbol/s/Hz, i.e., 100% higher than the so-called Nyquist rate of 2 symbol/s/Hz.

signalling rate to $(1+a)/T$ symbols/s while keeping the transmission characteristic fixed, as is the case in which speed tolerance was evaluated [18]-[20]. Thus, the spectral efficiency of Model-A is $(1+a)/T : 1/2T=2(1+a)$ symbol/s/Hz, where the parameter, "a" represents the percentage increase above the Nyquist rate.

The speed tolerance for binary inputs is defined as the percentage increase over the Nyquist rate which will just cause overlap between adjacent levels ("eye closure") [19]. In the case of m-ary inputs, the speed tolerance can be defined as the percentage increase over the Nyquist rate which will just cause at least one of the multi-level eyes to be closed. Based on this definition, we evaluated the speed tolerance of class-IV PRS with m-ary inputs by computer simulation using "worst possible" data sequences [18],[19]. The results are summarized in Table 3.1 where the well-known 16% speed tolerance of class-IV PRS for binary inputs is confirmed and the results for 4- and 8- level inputs are new.

We notice that the speed tolerance of class-IV PRS has dramatically reduced to about 1% for 8-level inputs. This is mainly due to inherently higher ISI in multi-level systems. Hence, by simple symbol-by-symbol receiver structures, it is nearly impossible for using class-IV PRS to increase the spectral efficiency above the Nyquist rate by the conventional method.

TABLE 3.1. SPEED TOLERANCE OF CLASS-IV (MODIFIED
DUOBINARY) PRS FOR MULTI-LEVEL INPUTS.

Number of input levels	Speed tolerance
2	16%
4	3%
8	1%

Note: The speed tolerance of 16% for binary inputs is confirmed to agree with that in the published literature [19], [20].

Speed tolerances for 4- and 8-level inputs are our new results.

3.2 A NEW TECHNIQUE FOR CLASS-IV PRS ABOVE THE NYQUIST RATE

An improved efficiency technique for multi-level duobinary (class-I) PRS above the Nyquist rate has been proposed in Chapter 2. The merit of this technique lies in the following fact. For the duobinary system, there is only a small amount of energy at frequencies near the Nyquist frequency (which is defined as half the signaling symbol rate) so that part of it can be chopped off without causing too much performance degradation. Since the class-IV PRS system has a spectral characteristic near the Nyquist frequency very similar to that of duobinary, we expect the chopping technique can be applied.

Fig.3.2 shows a new system model [35], called Model-B, using the chopping technique for class-IV PRS above the Nyquist rate. It represents a scheme in which the original class-IV PRS filter is followed by an ideal brickwall filter with a cutoff frequency at $f_N/(1+a)$, where $f_N=1/2T_s$ is the Nyquist frequency of the signal. The spectral efficiency of this new model is $1/T_s : f_N/(1+a)=2(1+a)$ symbols/s/Hz, i.e., the same as that of the conventional Model-A. We shall concentrate on a 15-level system, i.e., with 8-level inputs since it has a potential to achieve a spectral efficiency of more than 6 b/s/Hz.

From Fig.3.2, the overall frequency response of the new Model-B for class-IV PRS above the Nyquist rate can be expressed as follows.

$$H(f) = \begin{cases} j2T_s \sin(2\pi f T_s) & |f| < f_N/(1+a), \\ 0 & \text{elsewhere.} \end{cases} \quad (3.1)$$

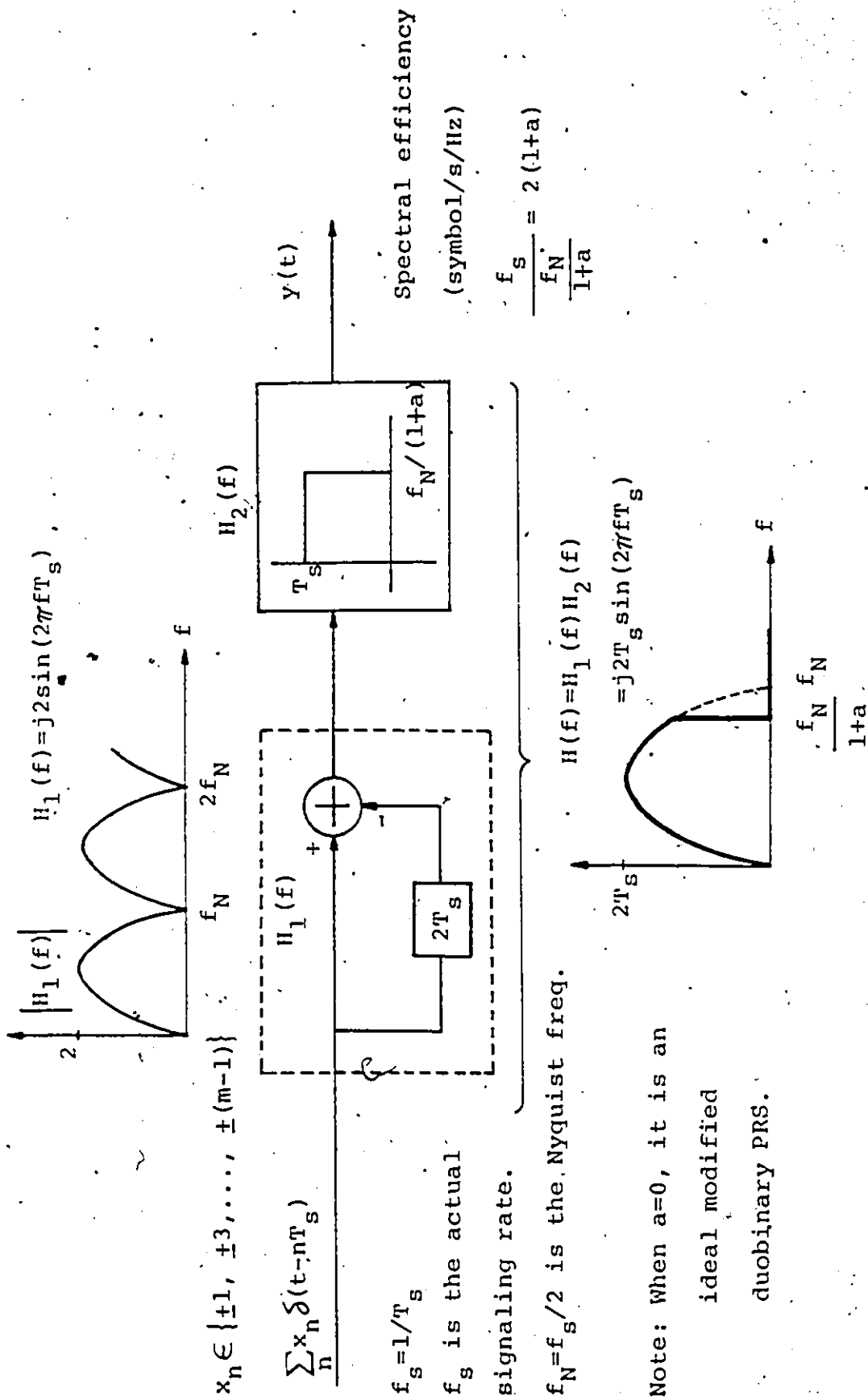


Fig.3.2 New system model: Model-B for class-IV (modified duobinary) PRS above the Nyquist rate with m-ary inputs and the corresponding transfer function. This also corresponds to the system model of the equivalent baseband in-phase or quadrature channel of a quadrature-modulated system.

And the corresponding impulse response can be easily obtained by a straightforward manipulation, i.e.,

$$\begin{aligned}
 h(t) &= \int_{-\infty}^{\infty} H(f) e^{j2\pi ft} df \\
 &= - \int_{-f_N/(1+a)}^{f_N/(1+a)} 2T_s \sin(2\pi f T_s) \sin(2\pi ft) df \quad (3.2) \\
 &= \frac{1}{1+a} \left\{ \text{sinc}\left(\left(\frac{t}{T_s} + 1\right)/(1+a)\right) - \text{sinc}\left(\left(\frac{t}{T_s} - 1\right)/(1+a)\right) \right\}
 \end{aligned}$$

Before proceeding to deal with the probability of error, we shall present a few typical eye diagrams, plotted by computer simulations. An ideal eye diagram of a 15-level class-IV PRS signal at the Nyquist rate is shown in Fig.3.3 for reference. The eye diagram for the new Model-B with 8-level inputs and $a=4\%$, i.e., with a spectral efficiency of 6.24 b/s/Hz is demonstrated in Fig.3.4. Though ISI exists at the optimum sampling instants, the quality of this eye pattern is excellent. For comparison, the eye diagram presented in Fig.3.5, with the same efficiency of 6.24 b/s/Hz using the conventional Model-A, is completely closed.

It is also important, at this moment, to compare the eye diagram shown in Fig.3.4 for class-IV PRS with that in Fig.2.9 (b) for class-I PRS. We observe that the vertical eye openings in both cases are quite comparable. This implies that, when signalling above the Nyquist rate using our new chopping technique, class-I and class-IV PRS will have similar performance in terms of the probability of error.

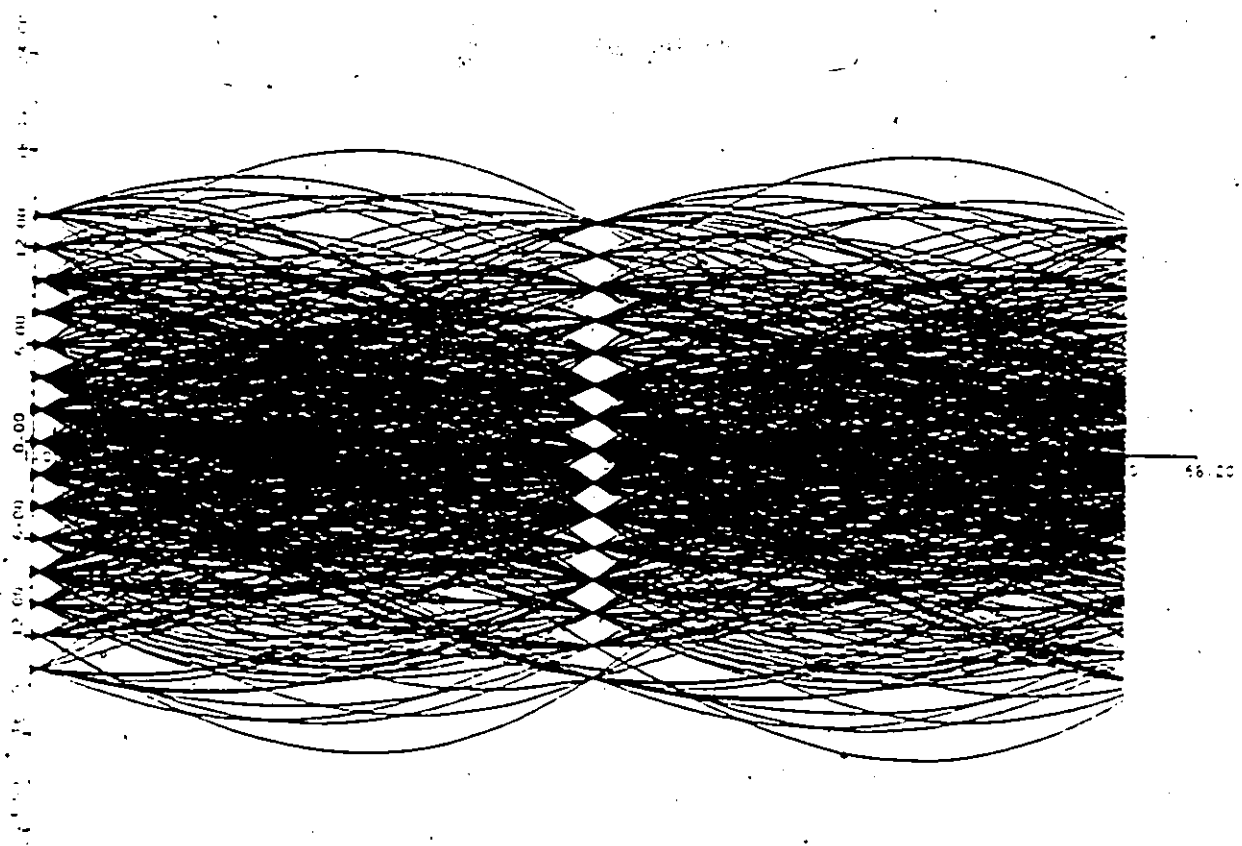


Fig.3-3 Eye diagram of an ideal 15-level class-IV (modified duobinary) PRS signal. Spectral efficiency : 6 b/s/Hz.

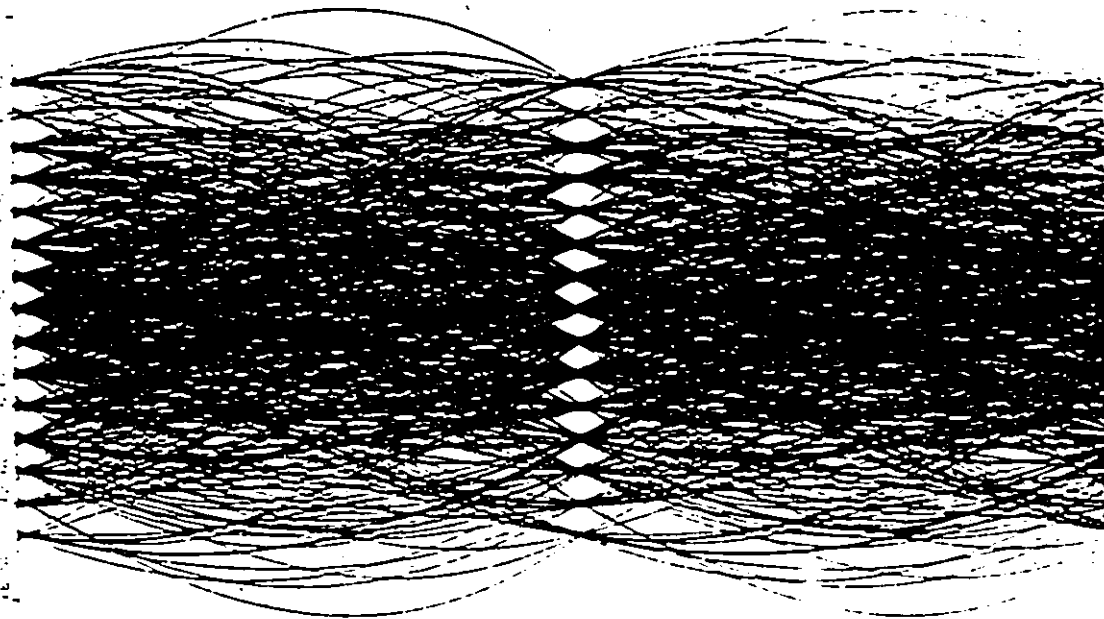


Fig.3.4 Eye diagram of an improved efficiency class-IV 15-level PRS/225-QPRS with a 4% increase above the Nyquist rate.
Spectral efficiency : 6.24 b/s/Hz.

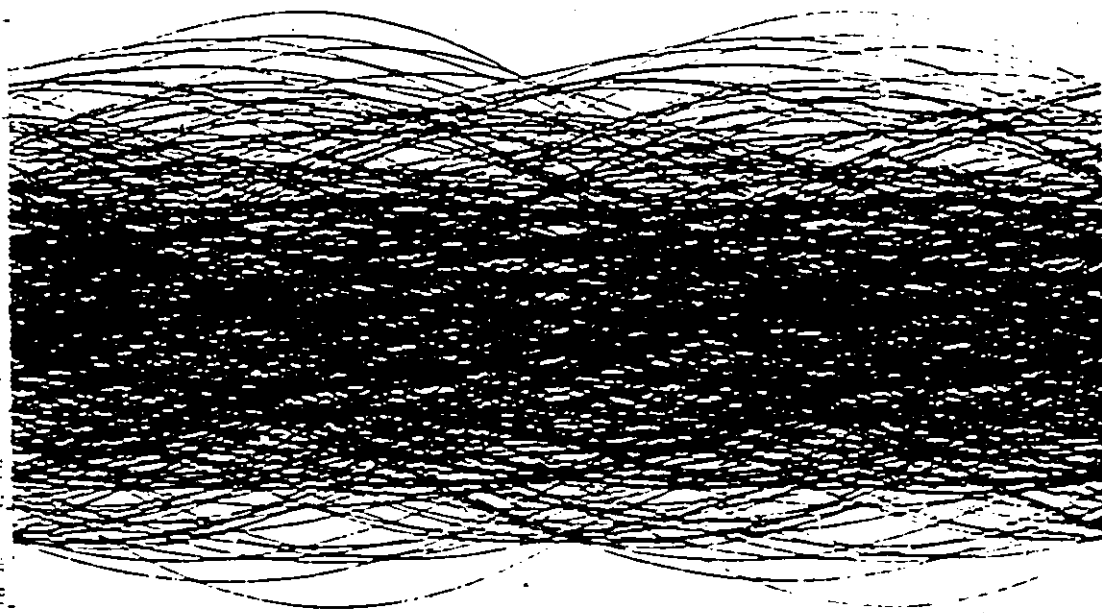


Fig.3.5 Eye diagram of a conventional class-IV 15-level PRS/225-QPRS with a 4% increase above the Nyquist rate.
Spectral efficiency : 6.24 b/s/Hz.

3.3 PERFORMANCE OF IMPROVED EFFICIENCY CLASS-IV 15-LEVEL PRS/225-QPRS ABOVE THE NYQUIST RATE

In this section, we evaluate the performance of an improved efficiency class-IV 15-level baseband and of modulated 225-QPRS using the new technique described in Section 3.2. Essentially, a class-IV 225-QPRS above the Nyquist rate can be generated by modulating in quadrature two baseband 15-level systems using Model-B in Fig.3.2. A FORTRAN program was written to evaluate the probability of error. As an illustrative example, a bit rate of 1.6 Mb/s is used in the simulation, i.e., with 800 kb/s in both in-phase and quadrature channels. The simulation is performed in a way very similar to that described in Chapters 2 and 5. Again, a perfect synchronization is assumed and symbol-by-symbol detection is used. Results are plotted in Fig.3.6. Table 3.2 summarizes the required C/N at $P_e=10^{-9}$ for various percentage increases above the Nyquist rate using the improved efficiency class-IV PRS.

The significant advantage of the new technique is evident from Table 3.2. For example, for class-IV 225-QPRS with a 3% increase above the Nyquist rate using our new Model-B, only a 0.6 dB degradation is observed. Also listed in Table 3.2 is the corresponding result of improved class-I 225-QPRS in Chapter 2 for comparison.

We notice that, with our new Model-B for 225-QPRS above the Nyquist rate for an increase of up to 5%, the performance of using class-IV PRS is nearly as good as that of using class-I PRS. For example, for the same 4% increase using class-IV PRS, there is only a 0.2 dB loss in

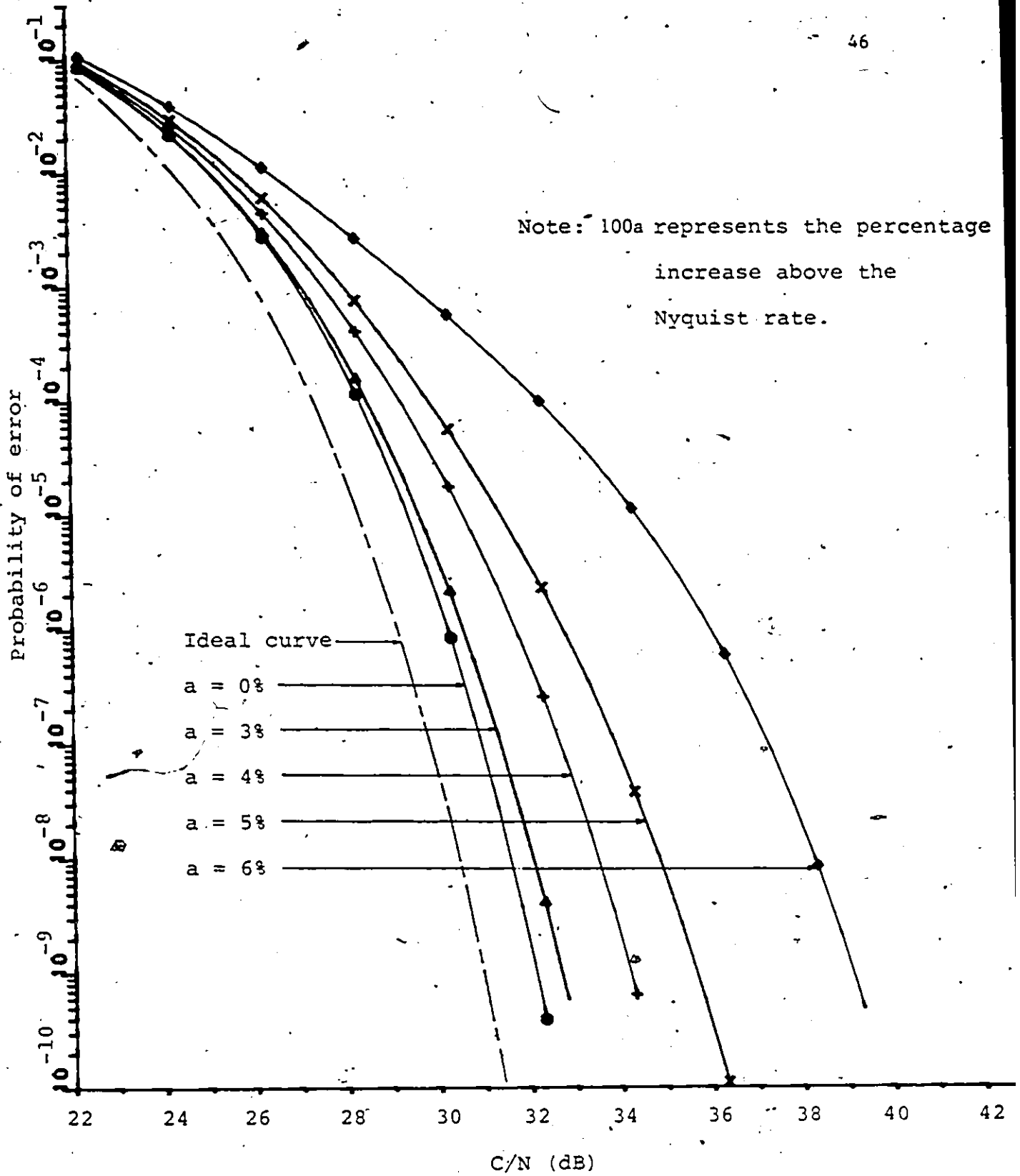


Fig.3.6 Probability of error of our improved efficiency class-IV 15-level PRS/225-QPRS above the Nyquist rate versus carrier-to-noise ratio (C/N), using our Model-B.

TABLE 3.2 REQUIRED C/N AT $P_e = 10^{-9}$ for 225-QPRS ABOVE THE NYQUIST RATE USING OUR NEW METHOD.

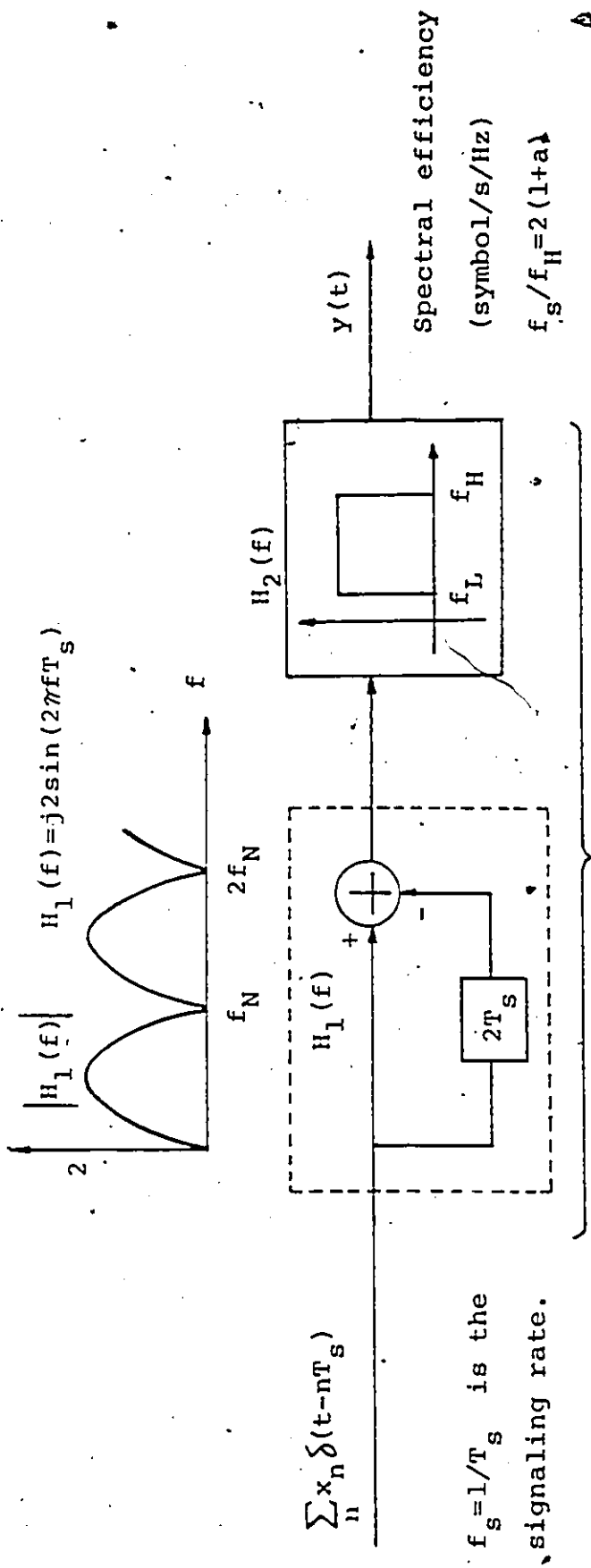
% above the Nyquist rate	Spectral Efficiency (b/s/Hz)	Class-IV 225-QPRS C/N (dB)	Class-I * 225-QPRS C/N (dB)
0	6	32	32
3	6.18	32.6	32.4
4	6.24	34.2	34
5	6.3	35.6	34.9
6	6.36	39.1	35.3

* From Table 2.1.

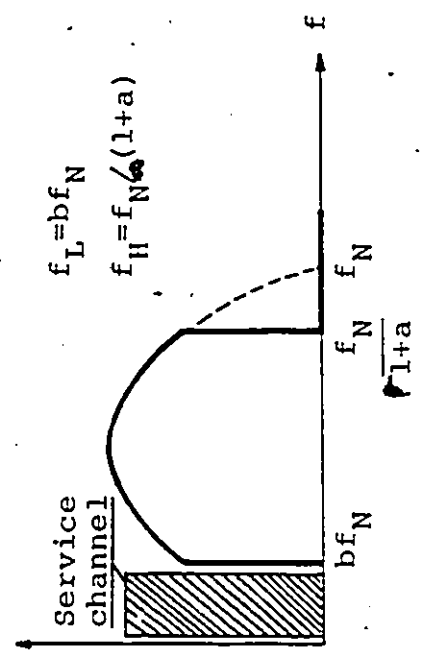
C/N at $P_e = 10^{-9}$ with respect to that of using class-I PRS. This is surprising since it might be tempting to say that, for transmission above the Nyquist rate, duobinary is better than modified duobinary for the following fact. The speed tolerance of duobinary is 43% for binary inputs whereas it is only 16% for modified duobinary. It is true when the conventional method is used. However, it is not true, especially for many inputs, by using the chopping technique described in section 3.2. In addition, modified duobinary has some other advantages. For example, it has no energy at dc, thus a carrier pilot can be inserted for easy carrier synchronization. Also, it has a very small amount of energy at low frequencies near dc so that a service channel can be added; this will be described in the next section.

3.4 AN EFFICIENT METHOD FOR SERVICE CHANNEL TRANSMISSION

An unusual and interesting aspect of class-IV PRS is that there is no energy at dc and a relatively small amount at low frequencies. Thus, in addition to increasing the spectral efficiency by chopping at the high-frequency end, a small bandwidth at the low-frequency end of the modified duobinary spectrum can be carved out for accommodating a service channel [21]. In this case, the advantage is having a service channel completely independent of the main traffic bit stream. That is, should the data stream be lost, the service (order) channel may still exist. It should be mentioned that a service channel is very important in control, supervision and servicing of a system.



$f_s = 1/T_s$ is the signaling rate.



$f_N = f_s/2$ is the Nyquist freq.

Fig.3.7 System model for an improved efficiency class-IV PRS above the Nyquist rate and for service channel transmission.

This particular application is illustrated in Fig.3.7, in which the modified duobinary filter is followed by an ideal bandpass filter with $f_L (=bf_N)$ and $f_H (=f_N/(1+a))$ representing the cutoff frequencies at the low end and at the high-frequency end, respectively. A service channel can then be inserted between dc and f_L .

We studied the effect of the location of f_L on the performance of a 15-level PRS/225-QPRS with $f_H = f_N/(1+a)$, $a=0.04$, i.e., with a 4% increase above the Nyquist rate. The simulation result is shown in Fig.3.8. It is seen that, as long as $b < 0.03$, the degradation is in fact negligible. This indicates that, under the condition of a 4% increase above the Nyquist rate for the improved efficiency class-IV 225-QPRS, a bandwidth of 3% f_N at the low-frequency end can be used for service channel transmission, which is not achievable by duobinary PRS.

It should be particularly noted that at the low-frequency end of the class-IV PRS spectrum not only a service channel can be used by using our chopping technique but also an increase in spectral efficiency is obtained in an FDM SSB system. For example, from the results shown in Fig.3.8, a 7% (i.e., with 3% of f_N cut at the low-frequency end and 4% at the high-frequency end) increase in spectral efficiency with respect to the Nyquist rate can be obtained by SSB modulation with a small degradation.

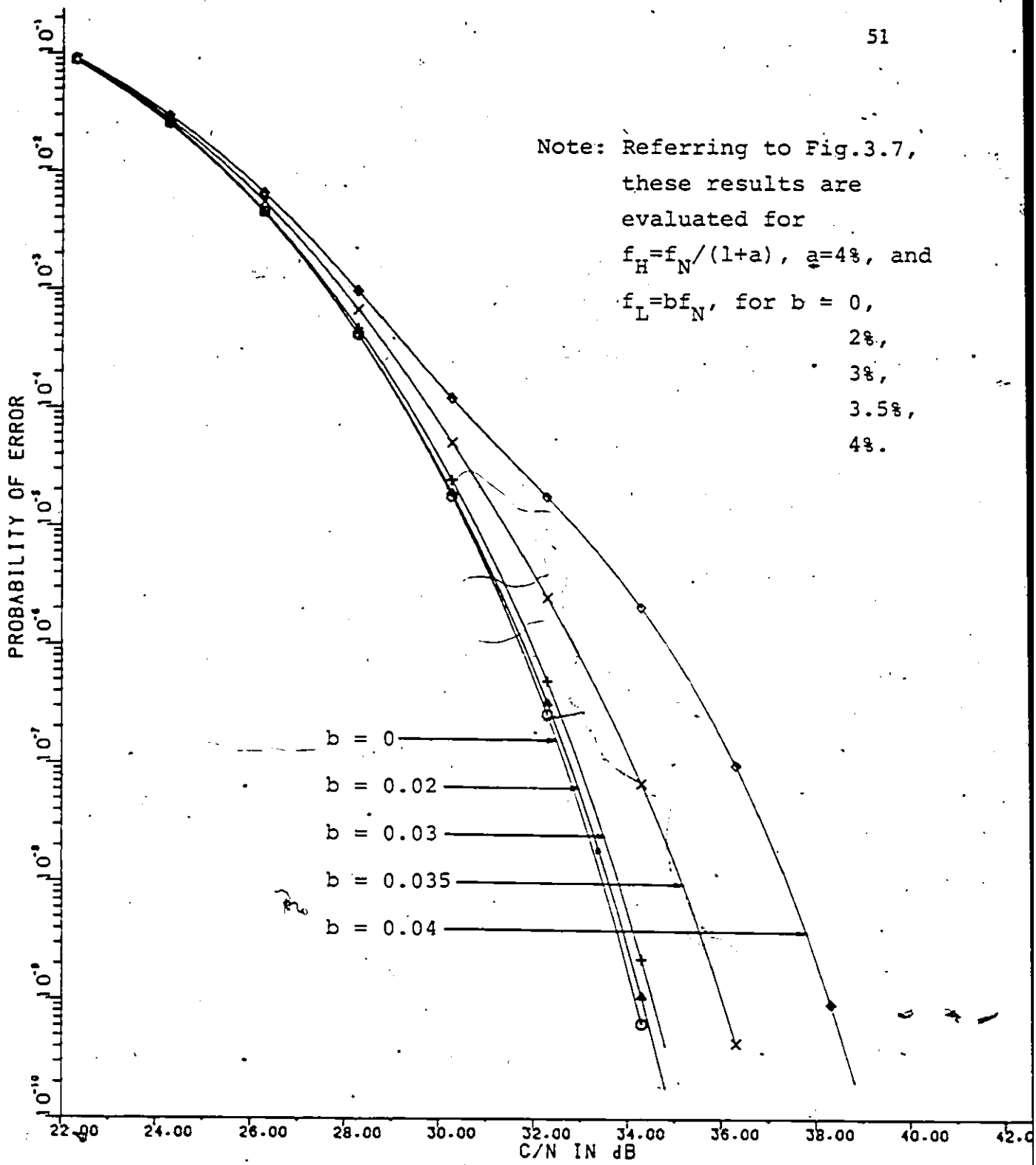


Fig.3.8 Performance of an improved efficiency class-IV 15-level PRS/225-QPRS with a 4% increase above the Nyquist rate and with various bandwidths carved out for a service channel.

3.5 CONCLUSIONS

An improved efficiency technique for modified duobinary (class-IV) PRS above the Nyquist rate transmission has been described. By using this technique, an increase of 4% or more above the Nyquist rate with class-IV 225-QPRS, i.e., a spectral efficiency of 6.24 b/s/Hz or more can be achieved by simple symbol-by-symbol detection and the performance is nearly comparable to that of duobinary (class-I) PRS. Furthermore, it is shown that with a 4% increase above the Nyquist rate for the improved class-IV 225-QPRS, an additional 3% of the Nyquist bandwidth can be carved out for service channel transmission with a negligible degradation. In particular, a 7% increase in spectral efficiency can be obtained by SSB-modulated class-IV 15-level PRS using our technique.

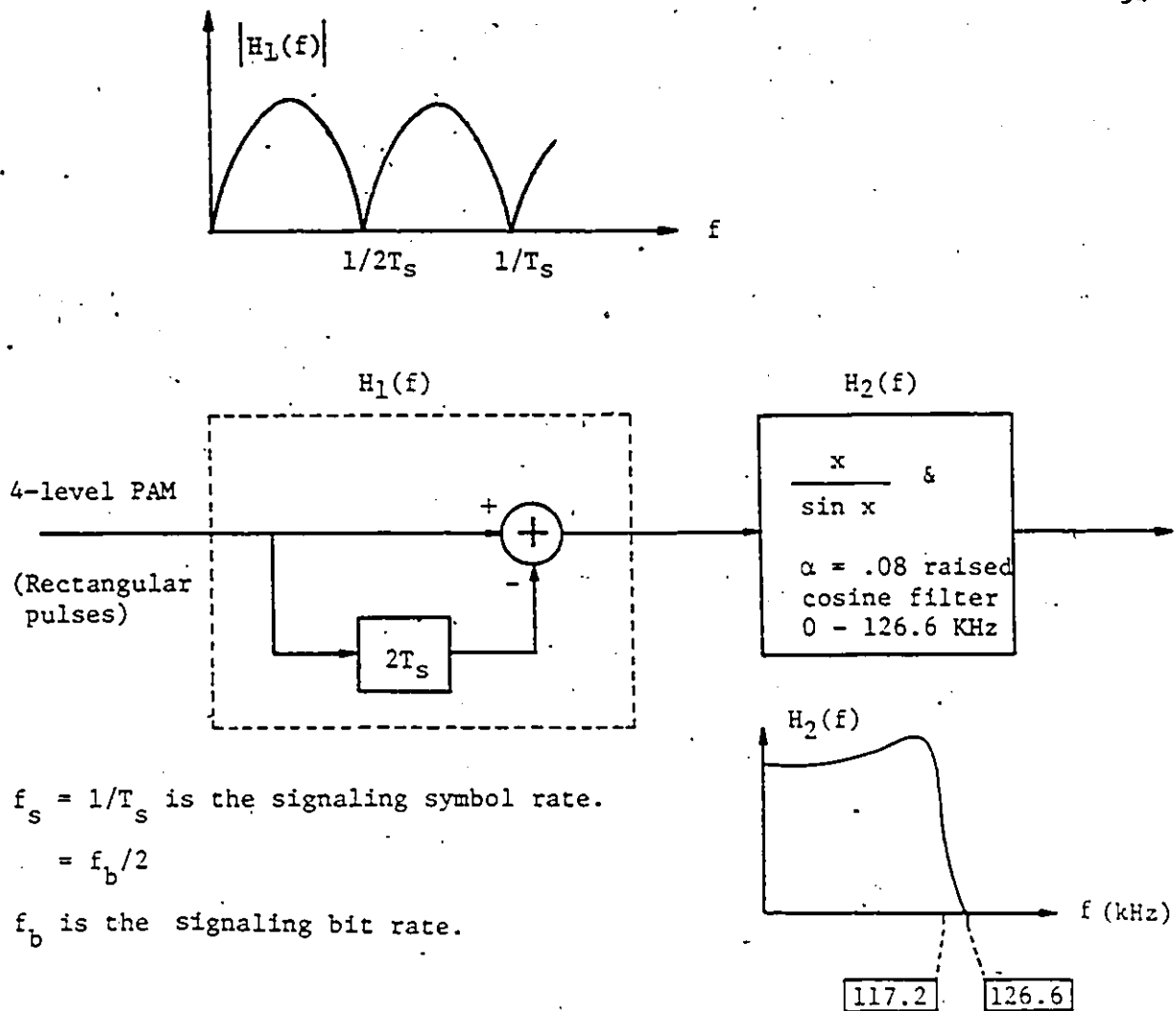
Chapter IV

IMPLEMENTATION AND PERFORMANCE EVALUATION OF AN IMPROVED EFFICIENCY 7-LEVEL CLASS-IV PRS SYSTEM

In order to perform practical research and investigate practical hardware feasibility of the new concept previously presented for PRS/QPRS above the Nyquist rate, we designed, by using our new Model-B, a 7-level class-IV PRS system which is the equivalent baseband of a 49-QPRS modem. Detailed description of the hardware design is presented. Several measured eye diagrams and corresponding power spectral densities are compared for various percentage increases of signalling rate above the Nyquist rate. Measured bit error rate (BER) performance versus signal-to-noise ratio (S/N) shows a good agreement with that predicted by computer simulations.

4.1 SYSTEM MODEL

Referring to Fig.4.1, which is redrawn here from Fig.3.2 for convenience, it is easy to see that the function of increasing the signalling rate while keeping the bandlimiting filter $H_2(f)$ unchanged is equivalent to that of keeping the signalling rate fixed while changing the cutoff frequency of $H_2(f)$. We adopted the former approach because of hardware simplicity. It should be noted that the ideal brickwall filter $H_2(f)$ in Fig.3.2 is practically replaced by a steep filter which approximates



Illustrative bit rates relative to the nominal one:

- $f_b = 468.8$ kHz --- the nominal bit rate for which the filter $H_2(f)$ is designed.
- $= 468.8 \times 1.05 = 492.2$ kHz --- a 5% increase relative to the nominal bit rate.
- $= 468.8 \times 1.1 = 515.7$ kHz --- a 10% increase relative to the nominal bit rate.

Fig.4.1 System model for the experimental 7-level class-IV PRS system operated above the Nyquist rate using our Model-B.

an $\alpha = 0.08$ raised-cosine filter in Fig.4.1. The choice of this practical filter will be explained in section 4.2.3, where the measured filter characteristics will be presented as well.

4.2 DESCRIPTION OF HARDWARE IMPLEMENTATION

A system block diagram of our experimental 7-level class-IV PRS above the Nyquist rate using our new Model-B is depicted in Fig.4.2. We elaborate the system operation in the following paragraphs.

4.2.1 Encoder Operation

Referring to Fig.4.2, the input to the system with a bit rate f_b is a usual serial binary data stream consisting of 1 and 0. A serial-to-parallel (S/P) converter is used to group every two serial bits into a four-state symbol (i.e., one of the numbers 0, 1, 2, 3) represented by two parallel bits at a symbol rate $f_s = f_b/2$. In order to ensure that an error in an adjacent level of the received signal results in only a bit error, the output of the S/P converter is Gray-coded. The precoding operation for preventing error propagation [21], [53] is then performed on the Gray-coded data stream, x_i , which consists of elements from the four numbers 0, 1, 2, 3. Let y_i denote the output data sequence of the precoder. The relationship between y_i and x_i is described by (4.1).

$$y_i = (x_i + y_{i-2}) \text{ Mod } 4 \quad (4.1)$$

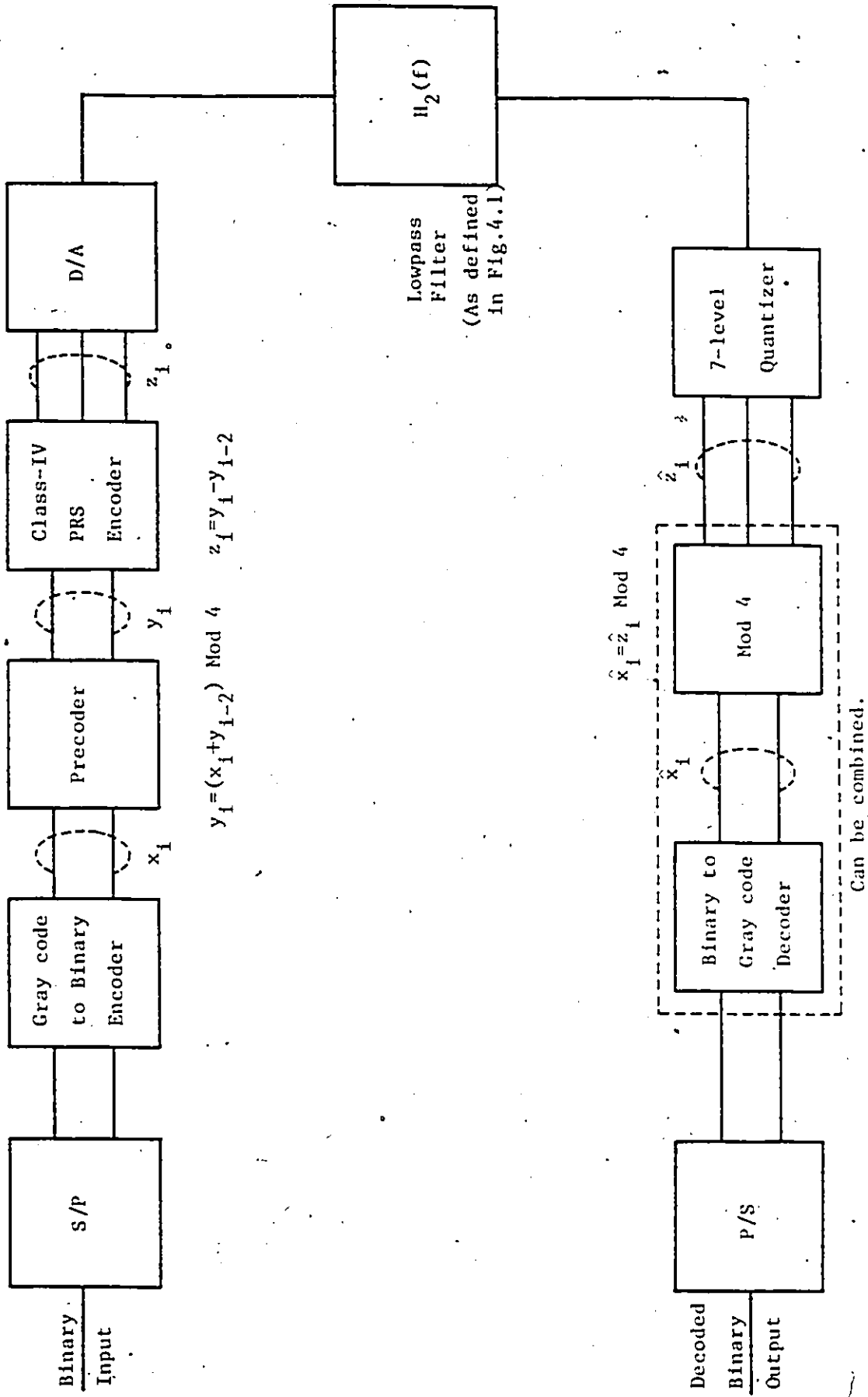


Fig.4.2 System block diagram of the experimental Class-IV PRS above the Nyquist rate using our new Model-B.

The next two blocks labelled class-IV PRS encoder and D/A converter convert the binary form (y_i) into a 7-level waveform in a digital manner. The function of the class-IV PRS encoder is to process the parallel binary signals as follows.

$$z_i = y_i - y_{i-2} \quad (4.2)$$

where y_{i-2} indicates a 2-symbol-interval-delayed version of y_i .

In effect, this is a combinational logic type digital filter that can conceptually be represented in the frequency domain as

$$|H_1(f)| = 2 \left| \sin(2\pi f T_s) \right| \quad \text{for } -\infty < f < \infty \quad (4.3)$$

To limit the bandwidth of the digital filter, a steep filter was employed as $H_2(f)$ in Fig.4.1. The filter characteristics will be described in Sec.4.2.3. In the next section, we describe in detail the operation of the encoder circuit.

4.2.2 Detailed Description of the Encoder Circuit

The following description refers to the circuit diagram of a 7-level class-IV PRS encoder depicted in Fig.4.3(a) and (b). The symbol-rate clock is derived through U5 by dividing the bit-rate clock by 2. The incoming binary data stream consisting of 1 and 0 which are represented by +5V and 0V, respectively, is S/P converted by U1 and the first two D flip-flops of U2 which are time aligned by the symbol-rate clock.

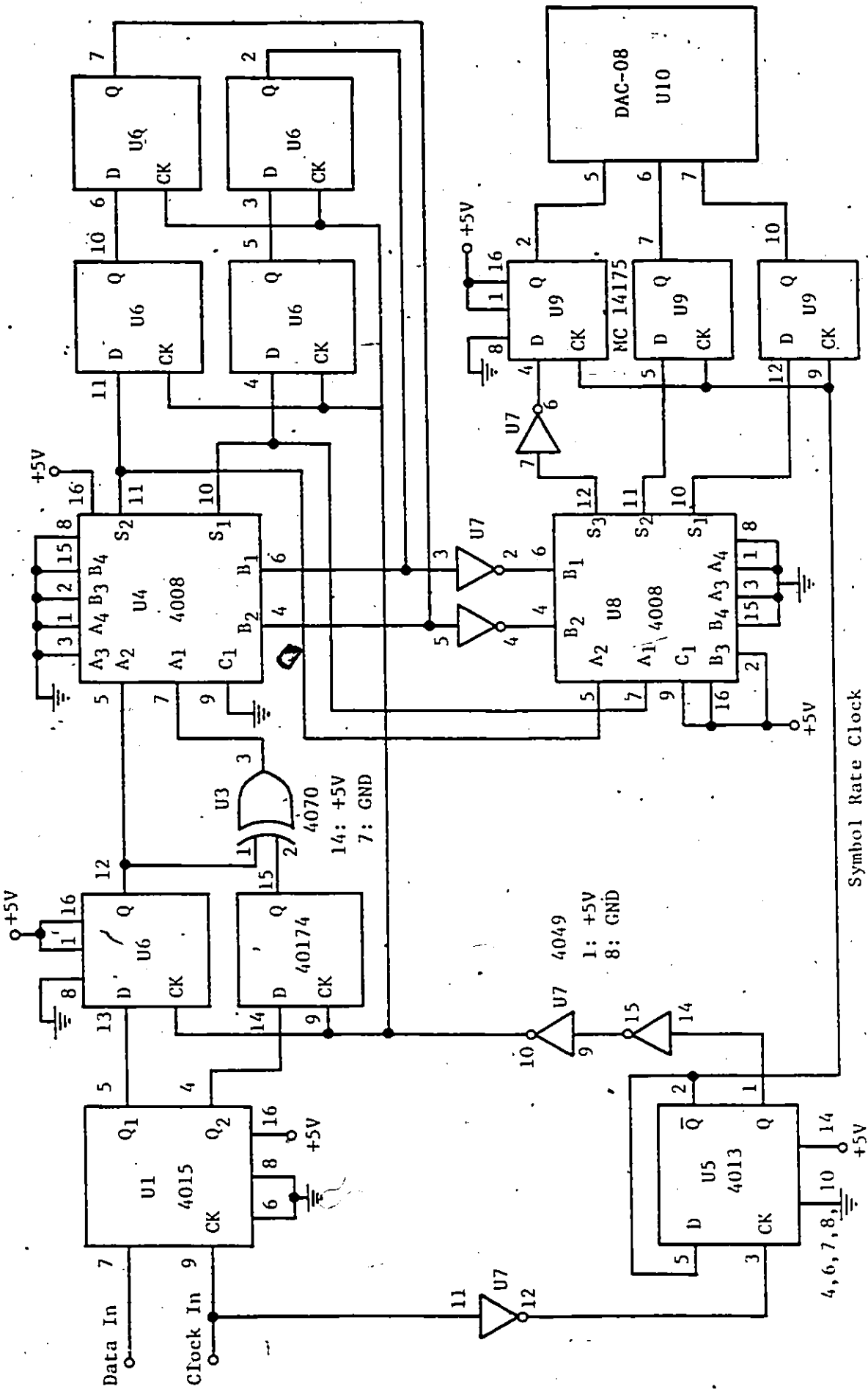


Fig.4.3(a) Circuit diagram of a 7-level class-IV PRS encoder.

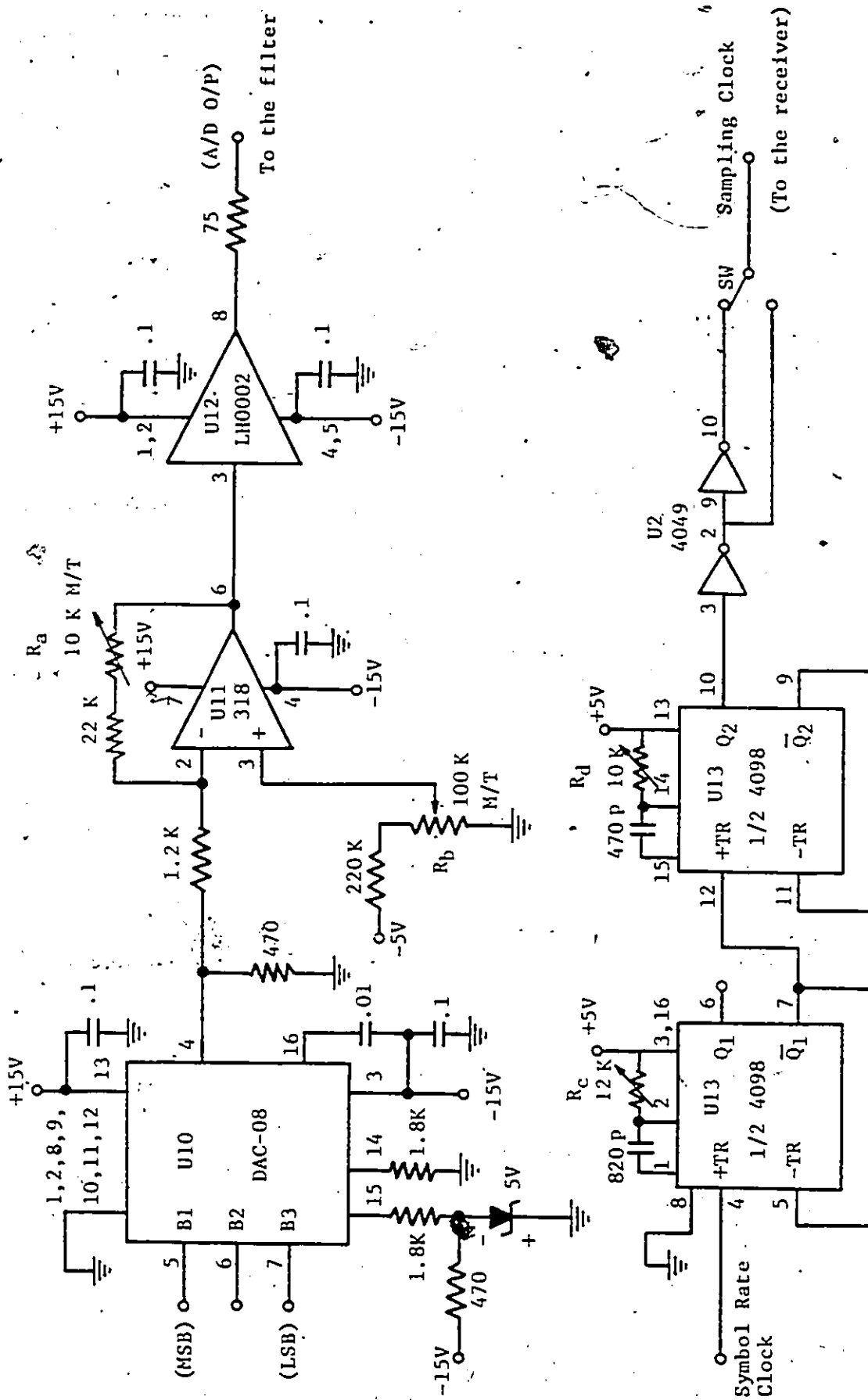


Fig. 4.3(b) Output stage of the encoder and the sampling clock.
(Continuation of Fig. 4.3(a))

U3 performs the gray-code operation on the aligned 2 parallel bits. Table 4.1 illustrates the gray-coding in detail.

After the gray coding, U4 and the remaining four D flip-flops of U2 carry out the precoding operation to prevent error propagation (see also Fig.4.2). In this case U4 is used as a 2-bit adder and because of the Mod 4 operation we simply discard the MSB of the result, i.e., the output is still 2 bits.

The class-IV PRS encoder is digitally fulfilled by U8, where the 2's complement subtraction is used. Due to different delays introduced in digital logic circuits, the output of U8 may have glitches. Therefore, three D flip-flops of U9 have been used to clock the output of U8 in order to ensure a glitch-free signal. Note that due to the specific correlation introduced by class-IV PRS, the 3 parallel bits at the output of U8, and of course U9, have only 7 different combinations. As a result, Table 4.2 summarizes the number mapping.

Due to the inherent structure, U10 maps a largest binary number (i.e., 111 in the present case) at its input into a most negative level. However, with the aid of the inverted amplifier (U11), finally a most positive level corresponds to the largest binary number, which is also illustrated in Table 4.2.

A dc balancing adjustment is provided by a 100 k multi-turn (M/T) potentiometer located at pin 3 of U11. A current amplifier (U12) is required to drive a 75 Ω load, which is the input impedance of the $\alpha = 0.08$ raised-cosine filter with $x/\sin(x)$ equalization. Thus the wideband

TABLE 4.1 GRAY-CODE OPERATION WITH REFERENCE TO Fig.4.3(a).

U1		U4	
Q ₁	Q ₂	A ₂	A ₁
0	0	0	0
0	1	0	1
1	1	1	0
1	0	1	1

TABLE 4.2 THE NUMBER MAPPING WITH REFERENCE TO Fig.4.3(a) & (b).

	U8			U10			U11
	S ₃	S ₂	S ₁	B ₁	B ₂	B ₃	pin 6
3	0	1	1	1	1	1	-----
2	0	1	0	1	1	0	-----
1	0	0	1	1	0	1	-----
0	0	0	0	1	0	0	----- 0
-1	1	1	1	0	1	1	-----
-2	1	1	0	0	1	0	-----
-3	1	0	1	0	0	1	-----

{ 2's complement
representation }

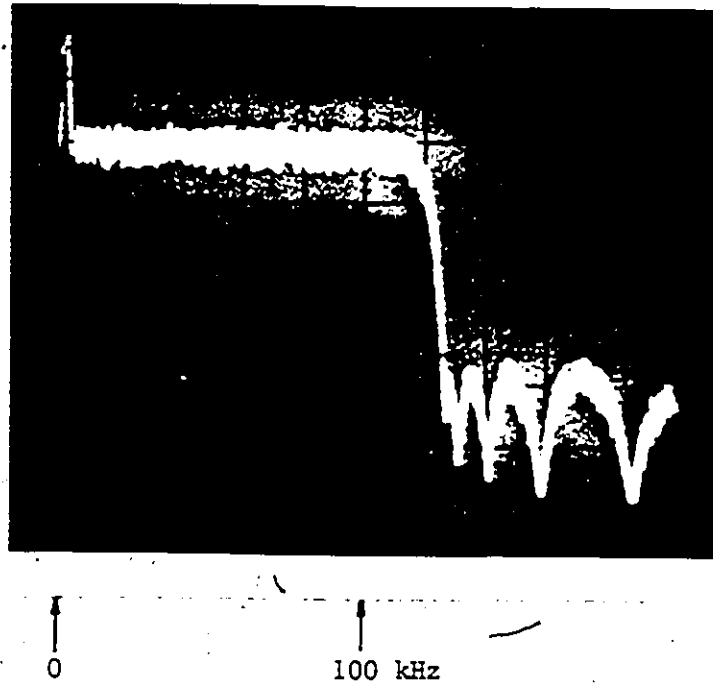
signal will be bandlimited by the steep filter to achieve the desired spectral efficiency.

The symbol-rate clock triggers a set of two one-shots to generate the required sampling clock, which will be hard-wired to the decoder. The first one-shot provides a delay which can be adjusted by the 5 k M/T potentiometer.

4.2.3 Filter Characteristics and Signalling Above the Nyquist Rate

In the analysis of our new Model-B for PRS above the Nyquist rate (see Figs.2.3 and 3.2), a brickwall filter (i.e., $\alpha = 0$) was used. A question may arise as to how an ideal brickwall filter can be realized. This can be solved by noting that the idea of using a brickwall filter is to cut off part of the energy below the Nyquist frequency of the signal so as to achieve a higher spectral efficiency. Thus, what we really need is a steep filter which has a cutoff frequency below the Nyquist frequency. In our experiment, a practical steep filter was employed, which approximates an $\alpha = 0.08$ raised-cosine filter and was designed by Karkar Electronics, Inc., San Francisco. First, let us clarify some parameters which are related to the filter characteristics. The measured amplitude characteristics of the $\alpha = .08$ raised-cosine filter without and with $x/\sin(x)$ equalization are shown in Figs.4.4 and 4.5, respectively. The $x/\sin(x)$ equalizer is to compensate for the rectangular input pulse induced $\sin(x)/x$ shaping of the spectrum. This filter has at least 35 dB attenuation at and beyond 126.6 kHz. The 3 dB cutoff frequency is

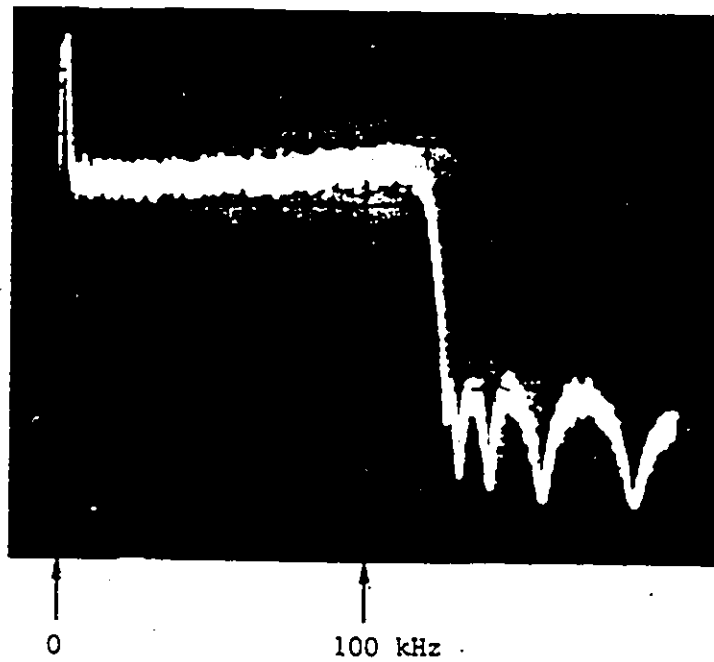
$$f_{3dB} = 126.6/(1+\alpha) = 126.6/1.08 = 117 \text{ kHz.} \quad (4.4)$$



V: 10 dB/div

H: 20 kHz/div

Fig.4.4 Measured amplitude characteristic of an approximate $\alpha = .08$ raised-cosine filter.



V: 10 dB/div

H: 20 kHz/div

Fig.4.5 Measured amplitude characteristic of an approximate $\alpha = .08$ raised-cosine filter with $x/\sin^2(x)$ equalization.

Thus, the filter was originally designed for transmitting data at a nominal symbol rate of

$$f_{sn} = 2f_{3dB} = 234.4 \text{ kBaud.} \quad (4.5)$$

For 4-level PAM signalling (or equivalently 7-level PRS), the nominal bit rate is

$$f_{bn} = 2f_{sn} = 468.8 \text{ kb/s.} \quad (4.6)$$

To investigate the performance of signalling above the Nyquist rate, we simply increase the input signalling rate higher than the nominal rate. Due to the nature of our hardware design, the delay elements (i.e., U4 in Fig.4.3(a)) yield a delay which is exactly equal to the symbol interval of the new signalling rate. Since the filter is fixed, as we increase the input signalling rate, the frequency components near the Nyquist frequency of the signal will be cut. Higher the increase in signalling rate, the more frequency components below the Nyquist frequency will be cut, resulting in a higher spectral efficiency. This explains that the function of the experimental system is equivalent to that of Fig.4.1.

4.2.4 Decoder Operation

With reference to Fig.4.2, the receiver employs, in a straightforward manner, 6 slicers (threshold detectors) to quantize the received signal into one of the 7 levels, \hat{z}_1 . In the absence of noise, \hat{z}_1 is identical to z_1 . The parallel binary outputs of the slicers are combined by

using standard logic gates which perform the modulo-4 operation and Gray code decoding to yield the original parallel bits. Finally, a parallel-to-serial (P/S) conversion takes place at the last stage to generate a replica of the transmitted binary input data.

An example of the precoding and decoding operations for class-IV PRS is illustrated in Table 4.1 for 4-level signalling. Detailed description of the decoder circuit follows.

4.2.5 Detailed Description of the Decoder Circuit

Referring to Fig.4.6, the received signal, $r(t)$, is passed through a 7-level quantizer consisting of six voltage comparators and six D flip-flops. The threshold voltages V_1, V_2, \dots, V_6 are set properly in the middle of each eye of the eye diagram. Denote by r_k the sampled value of $r(t)$ at $t = kT_s + \tau$, i.e.,

$$r_k = r(t) \Big|_{t = kT_s + \tau} \quad (4.7)$$

where

k is an integer,

τ is the sampler's phase, which is to be adjusted to the optimum sampling instants.

The output of 74174 depends on the location of r_k , as illustrated by Table 4.4.

TABLE 4.3 Four-level signal transmission with class-IV PRS.

i	1	2	3	4	5	6	7	8	9	10	11	12, 13	...	
x_i	0	2	1	2	3	0	3	3	2	1	1	2	1	...
y_i	0	2	1	0	0	0	3	3	1	0	2	2	3	...
z_i	0	2	1	2	-1	0	3	3	-2	-3	1	2	1	...
\hat{x}_i	0	2	1	2	3	0	3	3	2	1	1	2	1	...

$$y_i = (x_i + y_{i-2}) \text{ Mod } 4, \quad z_i = y_i - y_{i-2}$$

$$\hat{x}_i = \hat{z}_i \text{ Mod } 4 = z_i \text{ Mod } 4 = x_i \text{ (assume no noise)}$$

TABLE 4.4 DECODING TABLE WITH REFERENCE TO Fig.4.6.

	74174						Decoded symbol \hat{r}_k	$\hat{r}_k \text{ Mod } 4$	7420	
	Q_1	Q_2	Q_3	Q_4	Q_5	Q_6			\hat{Q}_1	\hat{Q}_2
$V_1 < r_k$	1	1	1	1	1	1	3	3 (1 1)	1	0
$V_2 < r_k < V_1$	0	1	1	1	1	1	2	2 (1 0)	1	1
$V_3 < r_k < V_2$	0	0	1	1	1	1	1	1 (0 1)	0	1
$V_4 < r_k < V_3$	0	0	0	1	1	1	0	0 (0 0)	0	0
$V_5 < r_k < V_4$	0	0	0	0	1	1	-1	3 (1 1)	1	0
$V_6 < r_k < V_5$	0	0	0	0	0	1	-2	2 (1 0)	1	1
$r_k < V_6$	0	0	0	0	0	0	-3	1 (0 1)	0	1

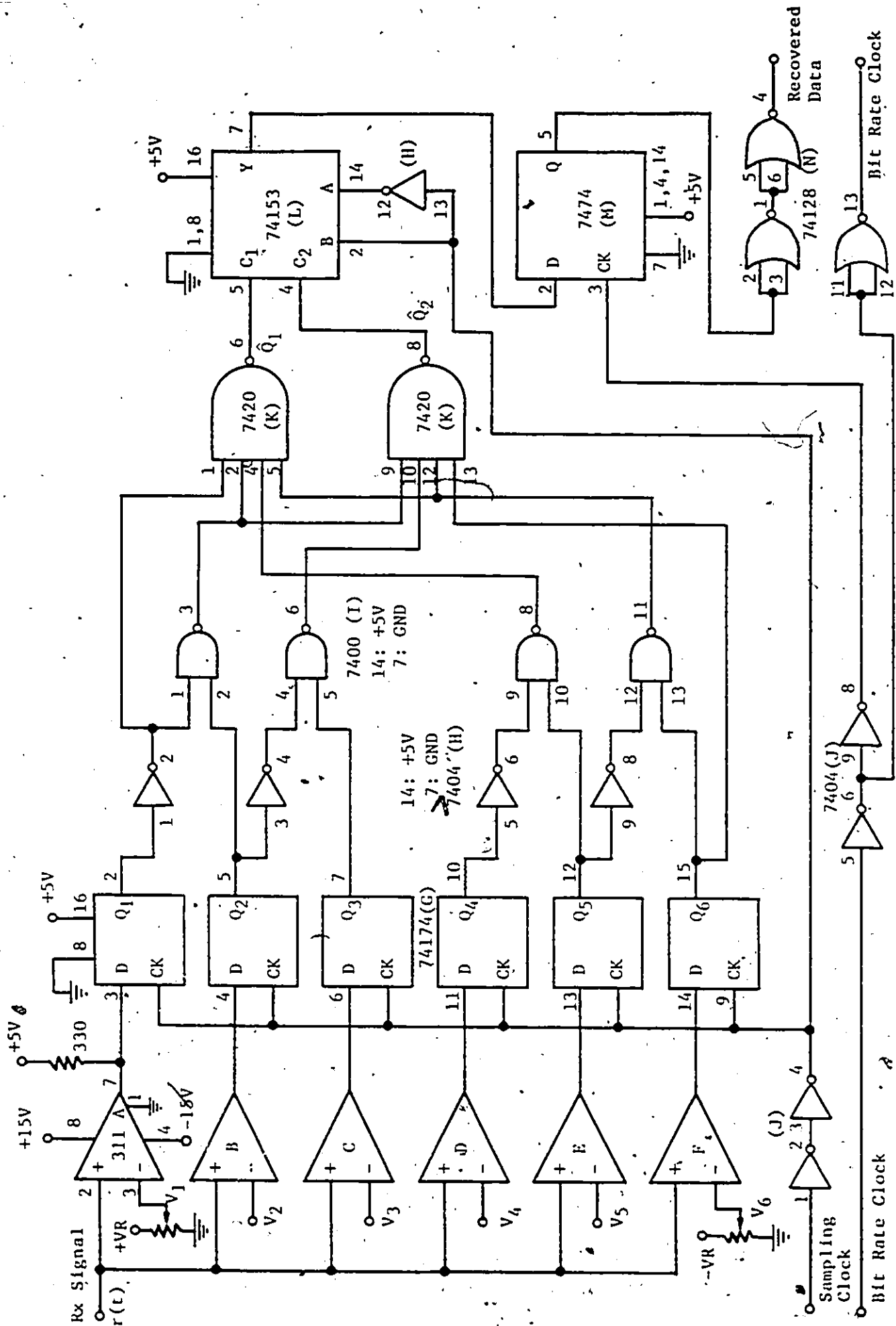


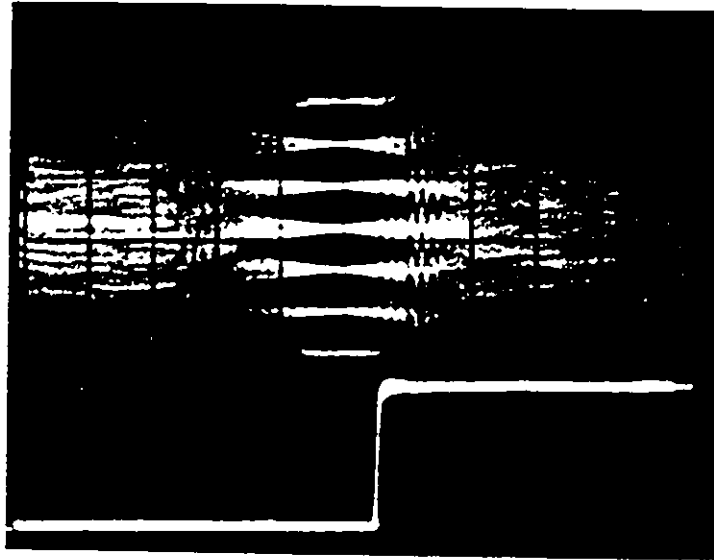
Fig.4.6 Circuit diagram of a 7-level class-IV PRS decoder.

Following 74174, the combinational logic gates 7404, 7400, and 7420 are combined to yield the desired output \hat{Q}_1 and \hat{Q}_2 by performing the decoding procedure which includes Mod 4 operation and gray-code decoding (see also Fig.4.2). With the aid of Table 4.4, the circuit connections among 7420, 7400, and 74174 are very straightforward.

Finally, 74153 converts the 2 parallel bits into a serial bit stream through the correct timing provided by the sampling clock. Again 7474 is employed to yield a clean recovered data stream and 74128 is used to drive a 50 Ω load, which may be the input impedance of an error analyzer. This completes the description of the circuit operation.

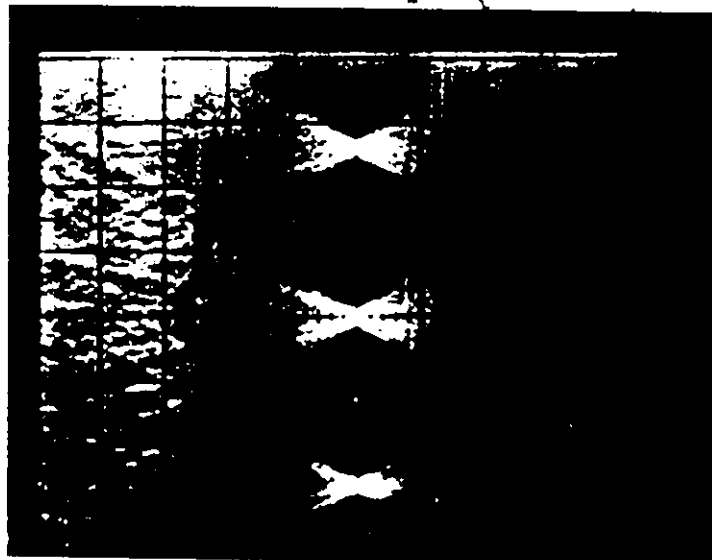
4.3 EXPERIMENTAL RESULTS AND DISCUSSIONS

A typical measured eye diagram and the sampling clock are shown in Fig.4.7 for the 7-level class-IV PRS at the Nyquist rate. It is worth noting that the optimum sampling instant seems not to be at the middle of the eye, as observed from Fig.4.7. According to our experience from the experimental evaluation of the BER performance, we found that the optimum sampling instant which results in minimum BER is indeed located at a point which is to the right of where the maximum eye opening is. This is because that the commercially available comparator IC's which are used in our circuit (311 in Fig.4.6) have a certain amount of response time (typically 300 ns from the data manual) which causes a delay for a stable output. The precise position of the optimum sampling instant can be located by adjusting the sampling clock while looking at an error analyzer until it gives a minimum reading of BER.



V:
 Upper trace:
 200 mV/div
 Lower trace:
 2 V/div
 H: 283 ns/div

Fig.4.7 Measured eye diagram of the 7-level class-IV PRS signal and the sampling clock.



V: 50 mV/div
 H: 283 ns/div
 $f_b = 473.6 \text{ kb/s.}$

Fig.4.8 Close-up of the inner two eyes of the 7-level class-IV PRS signal.

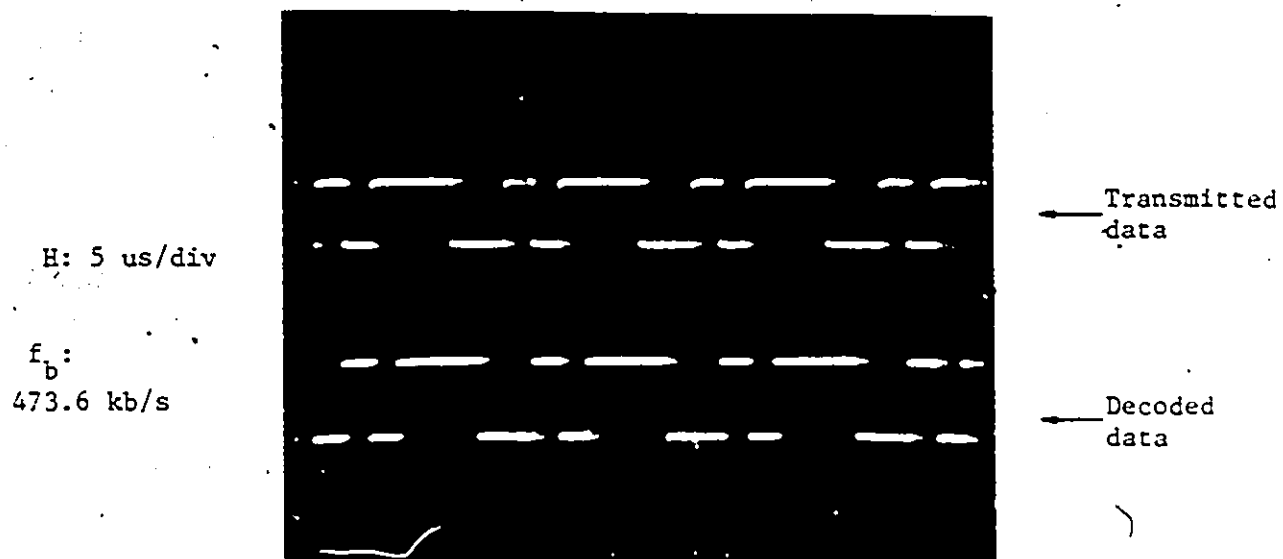


Fig.4.9 Illustrative transmitted and decoded data for a PRBS pattern of 1110010.

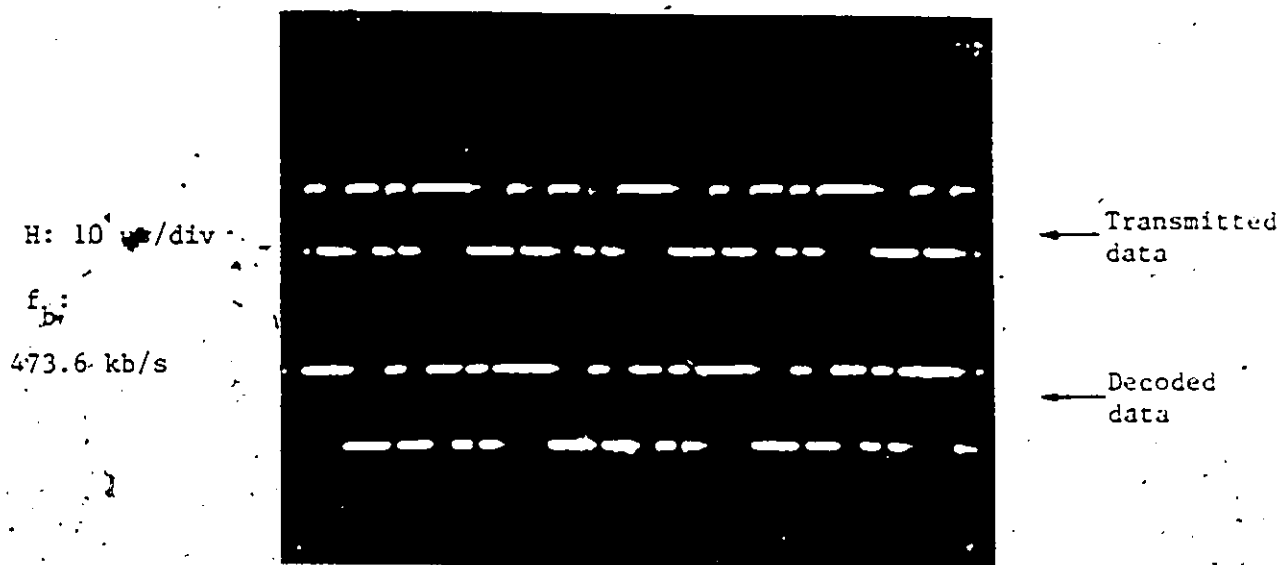


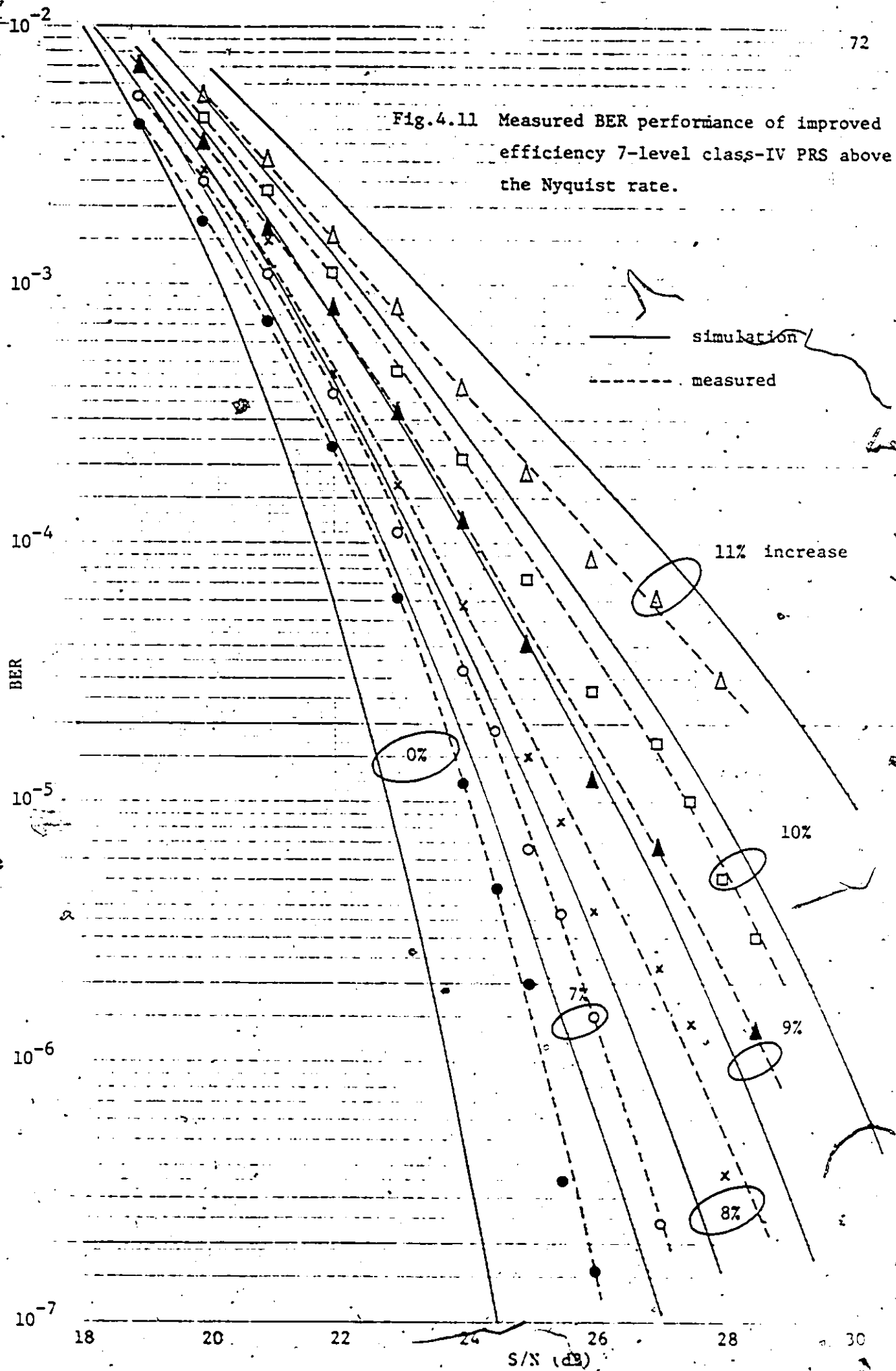
Fig.4.10 Illustrative transmitted and decoded data for a PRBS pattern of 100110101111000.

Fig.4.8 shows the close-up of the inner two eyes. Two decoded data patterns are illustrated in Fig.4.9 and 4.10 for PRBS lengths of 7 and 15 bits, respectively.

The BER performances versus S/N were measured for various percentage increases above the Nyquist rate. The signal and noise powers were measured at the output of the lowpass filter just before the threshold detectors. The measured results are shown in dotted curves in Fig.4.11. To confirm the accuracy of our simulation method, we simulated the experimental 7-level class-IV PRS system and the simulated results are also given in Fig.4.11 by the solid curves for comparison. We found that the measured results are basically in good agreement with the simulated ones.

A comparison at the 10^{-6} error rate indicates the experimental result is 1.5 dB away from the theory for the 7-level class-IV PRS at the Nyquist rate. The 1.5 dB degradation is mainly due to practical imperfections in filters and circuit layout since the experimental hardware is in breadboard rather than printed circuit form. As observed from Fig.4.11, for the increase of up to 9% above the Nyquist rate, the measured results are slightly worse than those by simulation. This is in general due to hardware imperfections. However, the situation is reverse when the increase is higher than 9%. This can be explained as follows. In the hardware measurements, the threshold voltages were always adjusted to the middle of each corresponding eye, whereas they were fixed and evenly spaced in the simulation. As the signaling rate is increased higher, the 6 eyes become uneven as can be seen from the

Fig.4.11 Measured BER performance of improved efficiency 7-level class-IV PRS above the Nyquist rate.



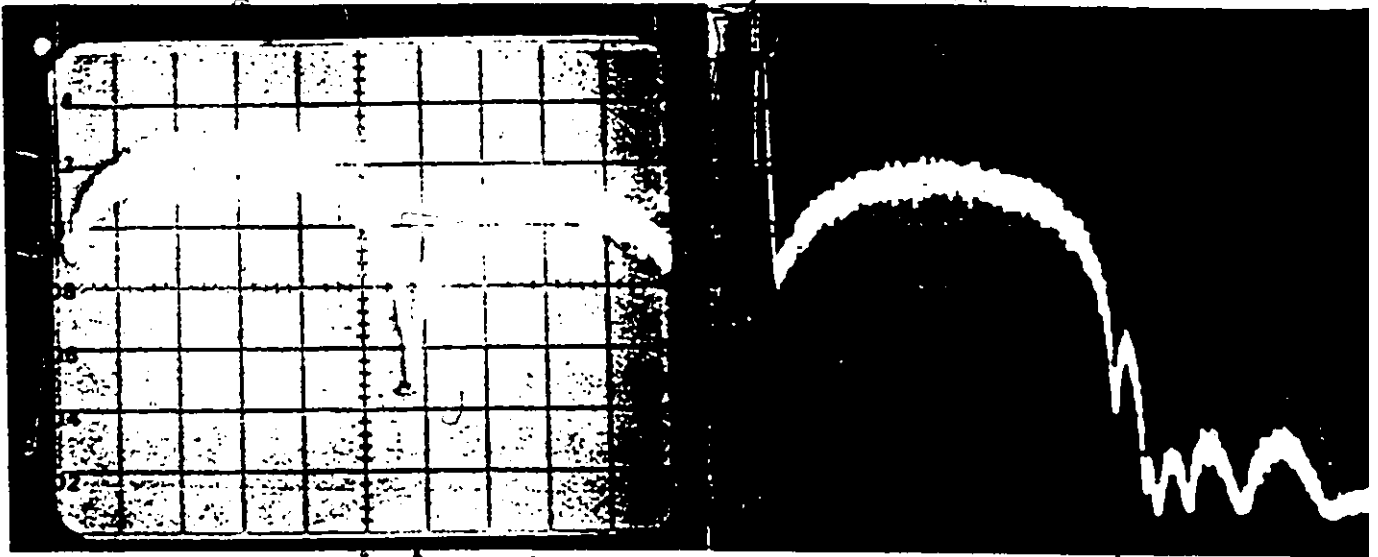
eye diagrams. The original threshold voltages are no longer at the optimum positions. Thus the measured results are found better than the simulated ones when the increase is higher than 9%.

We also notice from Fig.4.11 that for an increase of up to 9% above the Nyquist rate for the 7-level class-IV PRS using our new chopping technique, the degradation is reasonably small. Illustrative examples of the measured eye diagrams and corresponding PSD's are presented in Figs.4.12-4.14 for 0%, 8%, and 12% increases above the Nyquist rate, respectively. Note that all of the PSD's measured before the lowpass filter show nulls at dc and the Nyquist frequency of the signal. This confirms the frequency-domain behavior of the class-IV PRS.

As pointed out previously, the wideband spectrum of the signal is bandlimited by the lowpass filter whose characteristics are fixed. As the signalling rate is increased higher, the more frequency components below the Nyquist frequency will be cut. This can be observed from the PSD's measured after the LPF in Figs.4.12-14. As seen from the measured eye diagrams in Figs.4.12-4.14, the "undesired" ISI increases as the percentage increase above the Nyquist rate increases, which eventually causes performance degradation to an unacceptable level.

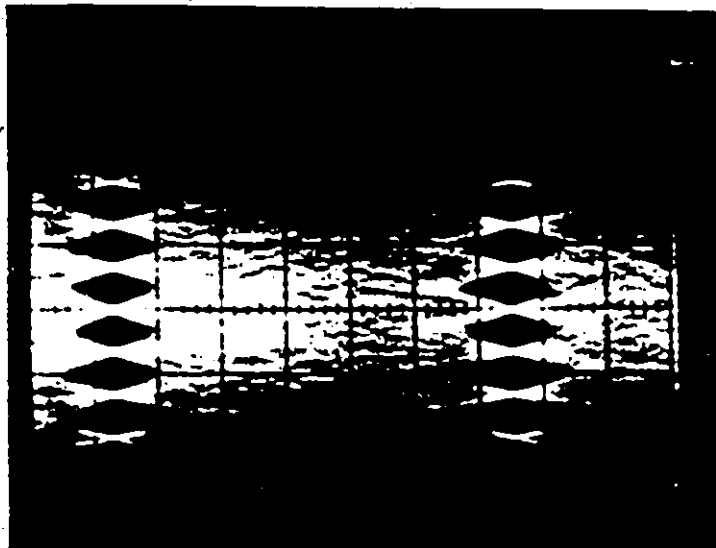
Fig.4.15 shows the photo of the experimental set-up in the Digital Communications Laboratory, Department of Electrical Engineering, University of Ottawa.

H: 20 kHz/div
V: 10 dB/div



117.6 kHz
(a) PSD before the lowpass filter.

117.6 kHz
(b) PSD after the lowpass filter.



V: 200 mV/div
H: 679 ns/div

(c) The received eye diagram.

Fig.4.12 Measured PSD's and corresponding eye diagram of our 7-level class-IV PRS signal with $f_b = 470.3$ kb/s.

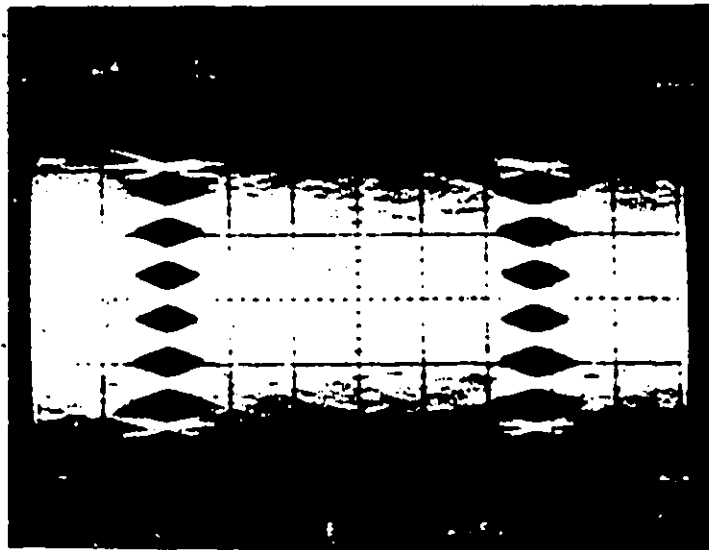
V: 10 dB/div
H: 20 kHz/div



126.5 kHz

(a) PSD before the lowpass filter.

(b) PSD after the lowpass filter.



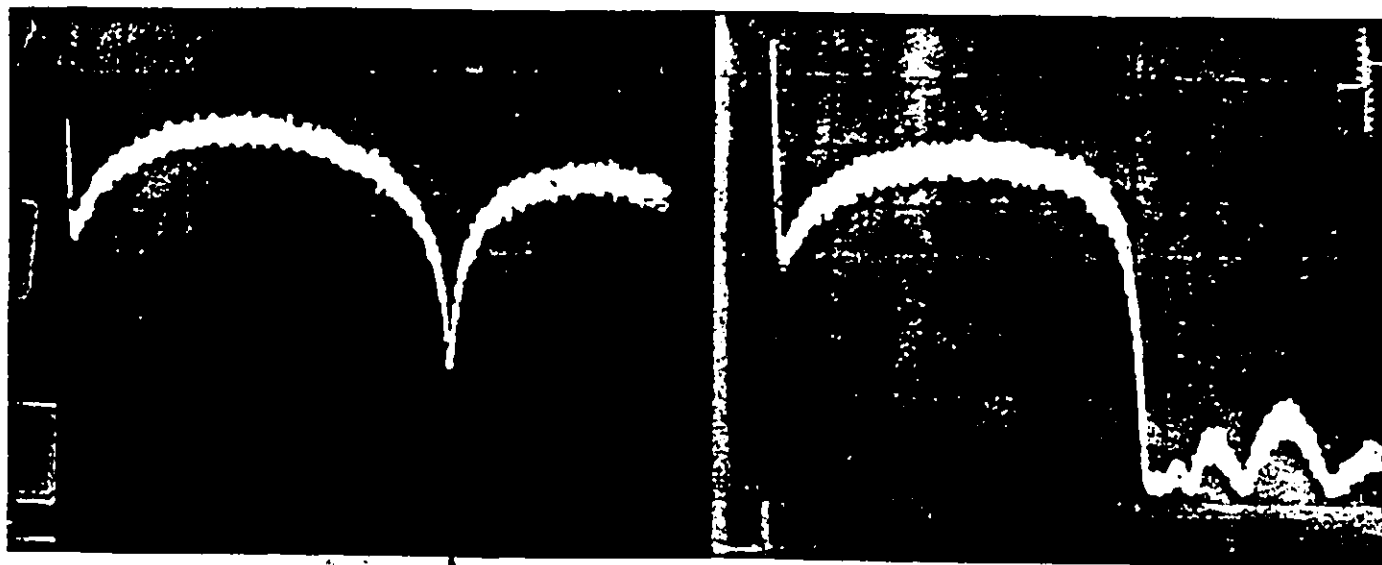
V: 200 mV/div

H: 685 ns/div

(c) The received eye diagram.

Fig.4.13 Measured PSD's and corresponding eye diagram of our 7-level class-IV PRS signal with $f_b = 506.2$ kb/s (an 8% increase above the Nyquist rate).

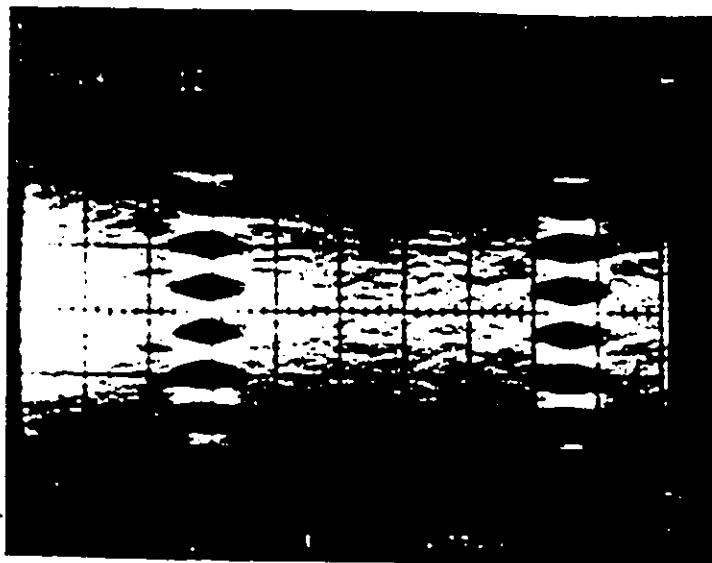
V: 10 dB/div
H: 20 kHz/div



131 kHz

(a) PSD before the lowpass filter.

(b) PSD after the lowpass filter.



V: 200 mV/div

H: 673 ns/div

(c) The received eye diagram.

Fig.4.14 Measured PSD's and corresponding eye diagram of our 7-level class-IV PRS signal with $f_b = 524$ kb/s (a 12% increase above the Nyquist rate).

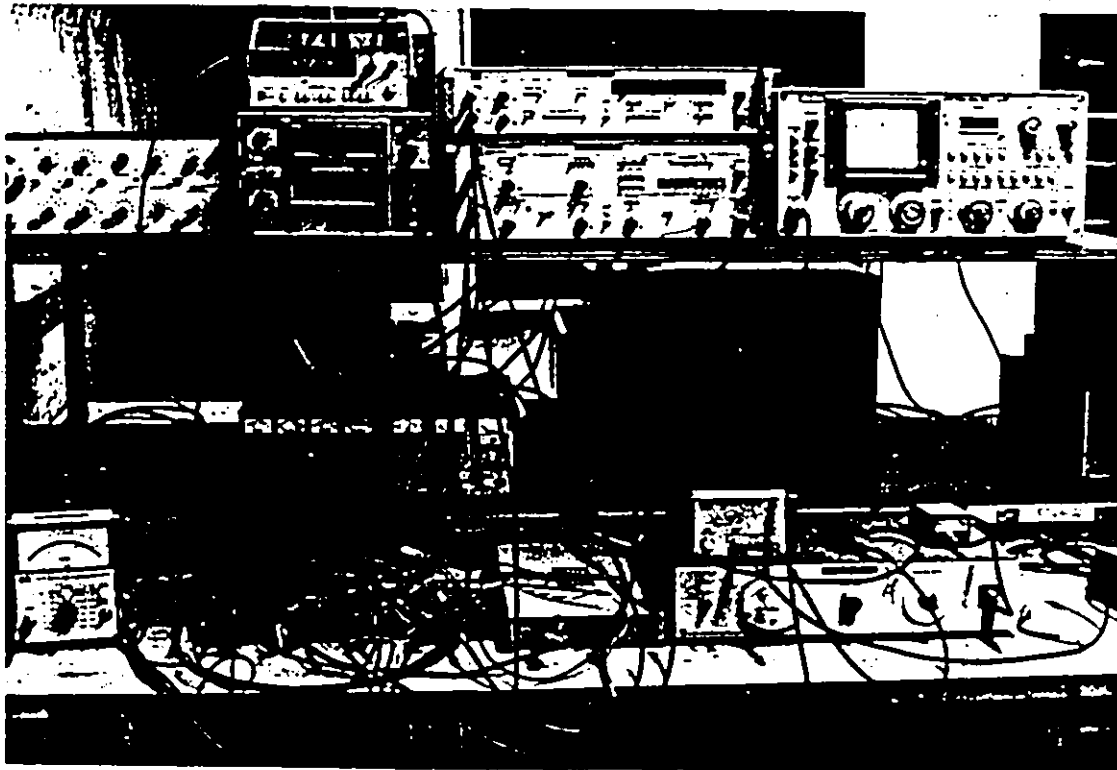


Fig.4.15 Photograph of the experimental set-up in the Digital Communications Laboratory, Department of Electrical Engineering, University of Ottawa.

4.4. CONCLUSIONS

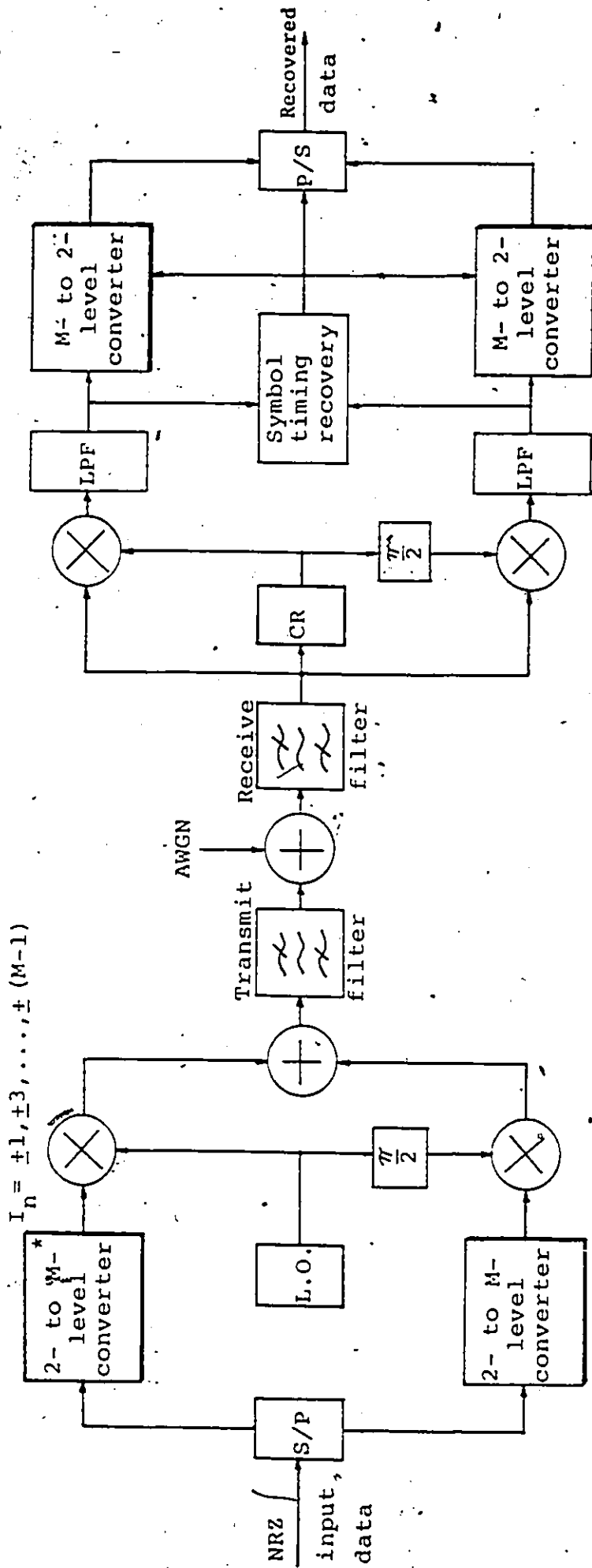
To verify the new concept previously presented for multi-level PRS above the Nyquist rate, a 7-level class-IV PRS baseband system has been designed and implemented. System design principles were highlighted and detailed circuit operation was described. Practical problems encountered during the experiment and the valuable experience learned from the measurement were also discussed. The measured BER performance of the improved efficiency 7-level PRS was confirmed to agree well with the simulated results.

Chapter V

256-QAM MODEM PERFORMANCE IN DISTORTED CHANNELS

In Chapter 1, after introducing the demand for highly spectrum-efficient modulation schemes, it was concluded that 256-QAM is one of the candidates. Essentially, 256-QAM is equivalent to a 16-level pulse-amplitude-modulation (PAM) in baseband. Multi-level signals are more sensitive to various impairments because the same impairment (e.g., filter imperfection) yields higher ISI in multi-level systems than in a binary system. As a result, filters specifications which are suitable for a binary system do not necessarily guarantee a satisfactory performance for a 16-level system. Thus it is important to investigate the effect of channel distortions [37], [38] and/or hardware imperfections on 256-QAM.

The objective of this chapter is to quantitatively evaluate the effects of group delay and amplitude distortions with linear, parabolic, or sinusoidal characteristic on the performance of a 256-QAM modem. The first part of this chapter will be devoted to a brief description of our simulation method. Simulated results for a 120 Mb/s system will then be presented. Finally, in order to efficiently apply the simulated results to systems with different bit rates, a simple scaling procedure will be described.



$Q_n = \pm 1, \pm 3, \dots, \pm (M-1)$ * $M = 16$ for 256 QAM
 $M = 8$ for 64 QAM

Fig. 5.1 256 and/or 64-QAM system block diagram.

5.1 DESCRIPTION OF COMPUTER SIMULATIONS

Fig.5.1 shows the block diagram of a 256-QAM system. The modulated 256-QAM signal can be represented by (5.1).

$$s(t) = \operatorname{Re} \left\{ \sum_{n=0}^{\infty} (I_n + jQ_n) g(t - nT_s) e^{j2\pi f_0 t} \right\} \quad (5.1)$$

where

$\operatorname{Re}\{ \}$ denotes real part of the complex-valued quantity in the brackets,

f_0 is the carrier frequency,

$1/T_s$ is the symbol rate; for 256-QAM $T_s = 8T_b$;

$1/T_b$ is the bit rate,

$g(t)$ is a pulse defined by

$$g(t) = \begin{cases} 1 & \text{for } 0 \leq t \leq T_s \\ 0 & \text{elsewhere.} \end{cases}$$

I_n and $Q_n = \pm 1, \pm 3, \dots, \pm 15$ are the sampled values of the in-phase and quadrature symbols.

The simulation is performed entirely in the complex baseband form as shown in Fig.5.2 for a system with a bit rate of 120 Mb/s, i.e., with a symbol rate of 15 MBaud. The choice of this Baud rate is for an easy comparison with the performance of 90 Mb/s 64-QAM systems which have the same Baud rate and were used in [8]. The results can be applied to another bit rate by appropriate scaling. In the simulation a perfect carrier and symbol timing is assumed. For filtering we use FFT techniques to alternate between the frequency and time domains. The assumed pseudo-random-binary-sequence (PRBS) sequence length is 16,384 bits and the number of samples per symbol is 32.

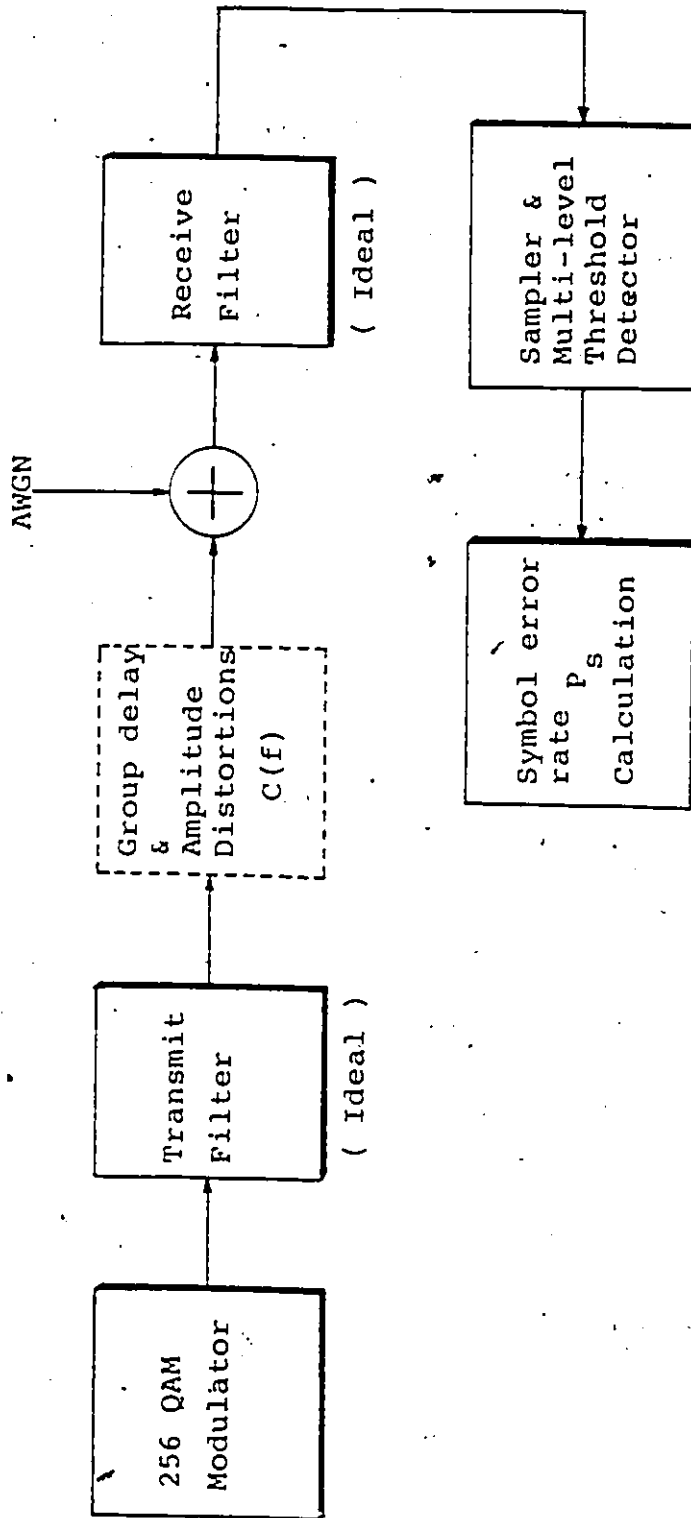


Fig.5.2 Computer simulation model.

The transmit and receive filters are assumed as ideal square root of raised-cosine filters with $x/\sin(x)$ equalization in the transmitter so that the whole system satisfies the Nyquist 1st criterion [14]. The resulting eye diagrams for $\alpha = 0.1$ and 0.4 are shown in Fig.5.3(a) and (b), where α denotes the roll-off factor, that is the ratio of the excess bandwidth to the Nyquist band. The eye diagram of an $\alpha = 0.2$ un-equalized channel, having a sinusoidal group delay distortion, is illustrated in Fig.5.3(c). Illustrative measurement results are shown in Fig.5.4.

Note that for ideal filters there is no ISI at the optimum sampling instants. However, data transition jitter is very significant, particularly in the $\alpha = 0.1$ case. This indicates a high-precision sampling clock would be required.

For a specified power of white Gaussian noise at the threshold detector input, the error probability of the i -th symbol with respect to the in-phase channel is calculated as follows:

$$P_{si}^I = \begin{cases} \frac{1}{2} \operatorname{erfc}\left(\frac{|\bar{S}_i - \text{THR1}_i|}{\sqrt{2}\sigma}\right), & \text{for } I_i = \pm 15 \\ \frac{1}{2} \operatorname{erfc}\left(\frac{|\bar{S}_i - \text{THR1}_i|}{\sqrt{2}\sigma}\right) + \frac{1}{2} \operatorname{erfc}\left(\frac{|\text{THR2}_i - \bar{S}_i|}{\sqrt{2}\sigma}\right), & \text{for } I_i = \pm 1, \pm 3, \dots, \pm 13. \end{cases} \quad (5.2)$$

where

I_i is the i -th transmitted symbol of the in-phase channel,

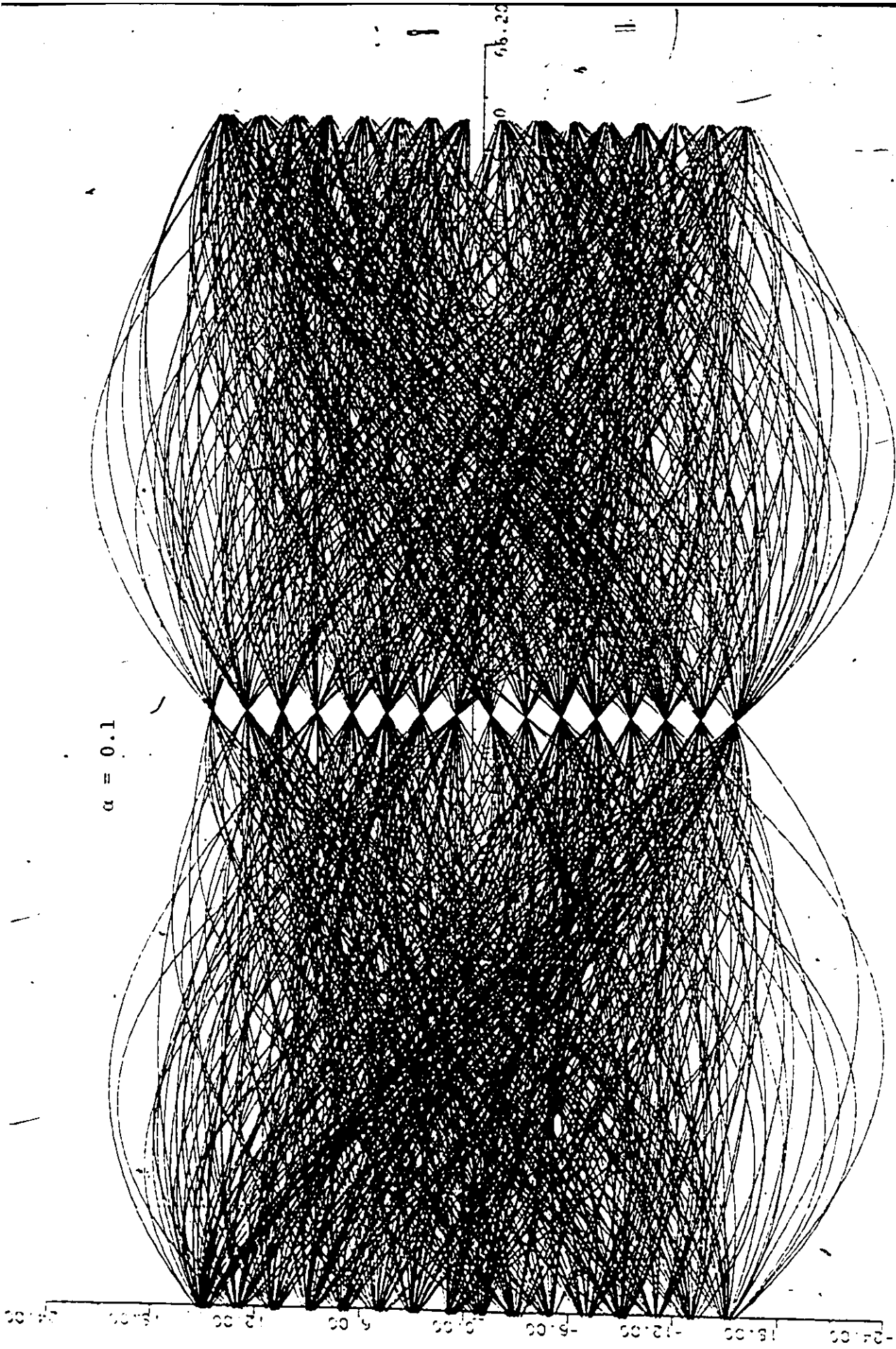


Fig. 5.3(a) Eye diagram of 256-QAM with $\alpha = 0.1$.

$\alpha = 0.4$

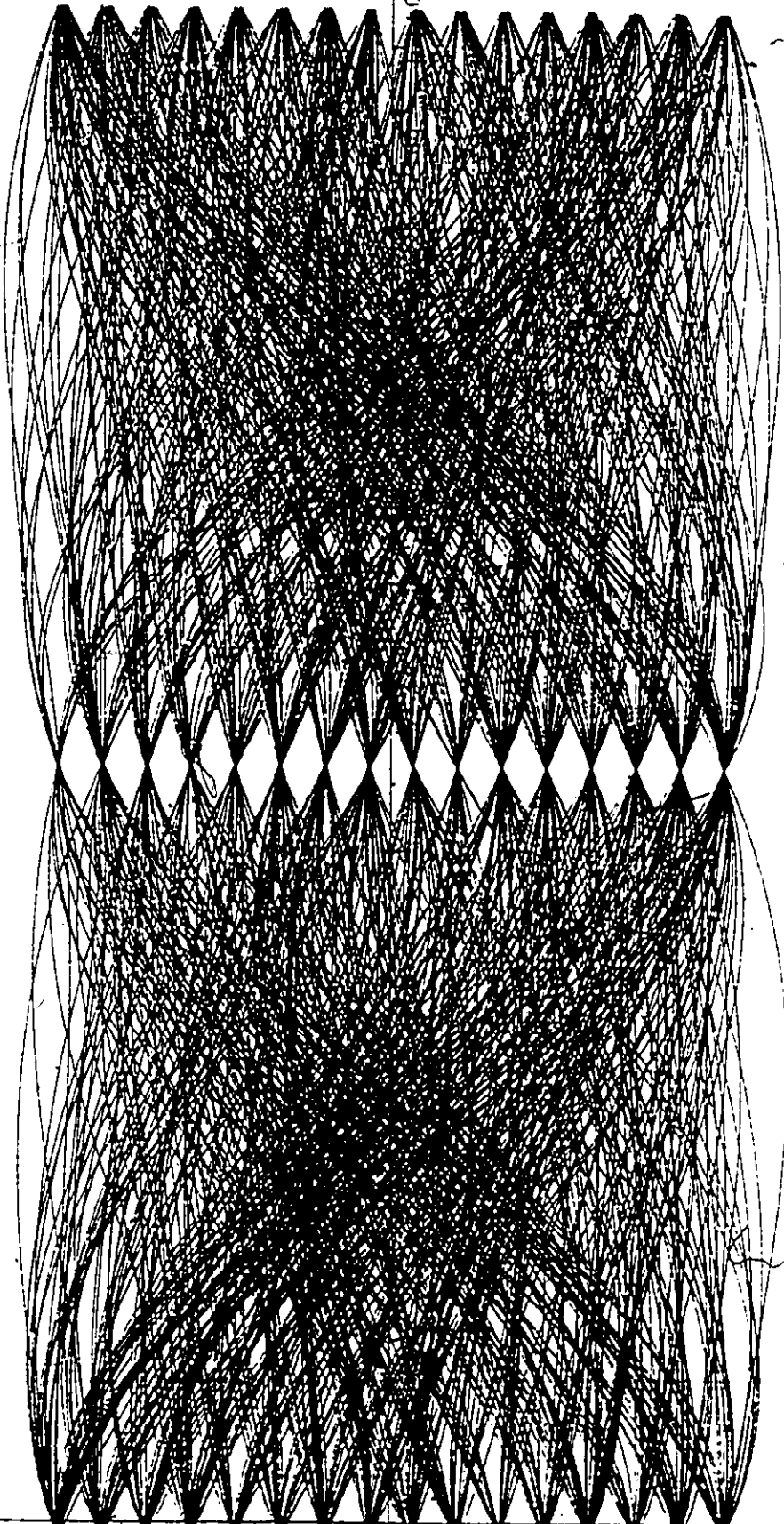


Fig. 5.3(b) Eye diagram of 256-QAM with $\alpha = 0.4$.

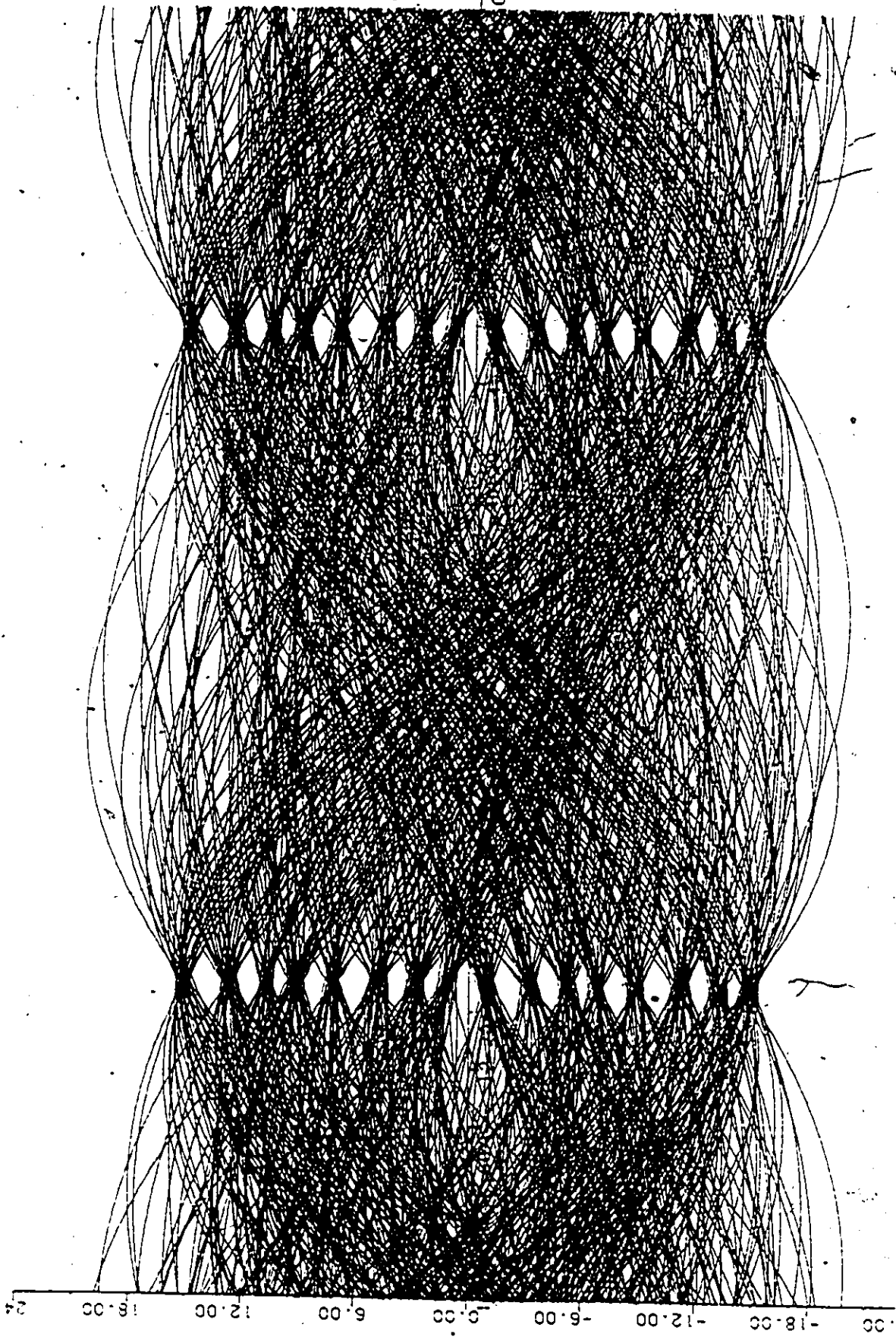
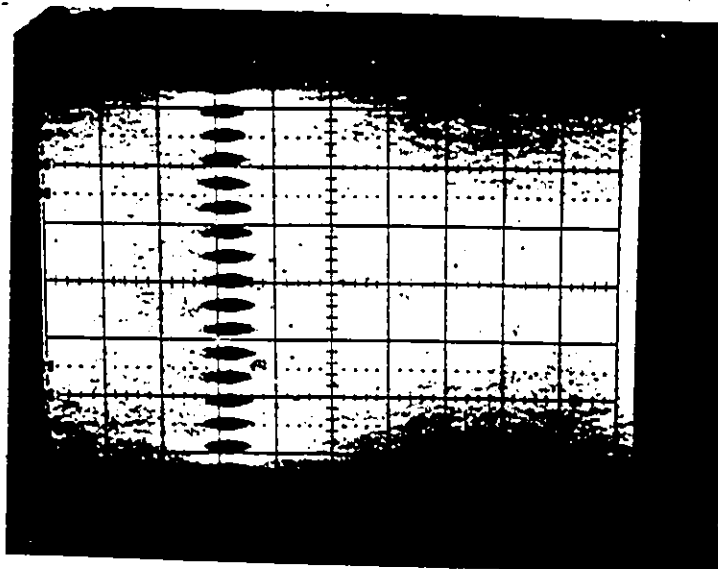
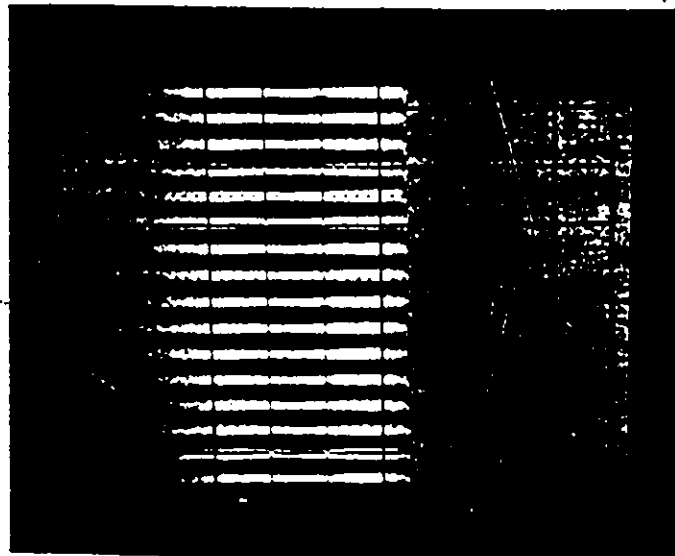


Fig. 5.3(c) Eye diagram of 256-QAM ($\alpha = 0.2$) with a sinusoidal group delay distortion, $D(f) = S_D \sin(2\pi Kf/2f_{BW})$, $S_D = 12$ ns and $K = 4$. Bit rate $f_b = 120$ Mb/s.



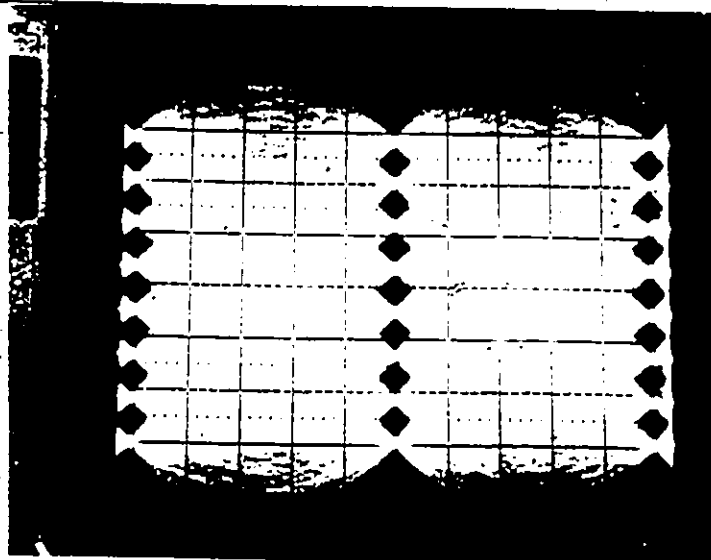
(a)

H: 500 ns/div
V: not
calibrated.



(b)

not calibrated.



(c)

H: 1 us/div
V: not calibrated.

Fig.5.4 Measured 16-level and 8-level PAM eye diagrams, which are the equivalent baseband signals of 256-QAM and 64-QAM, respectively. The symbol rate is 200 kBaud, which corresponds to bit rates of 800 kb/s (16-level PAM) and 600 kb/s (8-level PAM). Raised-cosine Nyquist channel filters ($f_N = 100$ kHz) having a roll-off factor $\alpha = 0.2$ and a 55 dB attenuation beyond 120 kHz, designed by Karkar Electronics, Inc., are used in this experiment. Photographs: (a) and (b) for 16-level PAM, (c) for 8-level PAM.

\bar{S}_i is the magnitude of the i -th received sample of the in-phase channel,

$$\text{THR1}_i = |\bar{I}_i| - 1; \text{THR2}_i = |\bar{I}_i| + 1;$$

$$\text{erfc}(x) = \frac{2}{\sqrt{\pi}} \int_x^{\infty} e^{-t^2} dt,$$

σ^2 is the received noise power at the threshold detector input.

The error probability P_{si}^Q with respect to the quadrature channel is obtained similarly from (5.2) and for a sequence of N symbols in each channel the average symbol error rate P_s is calculated as follows :

$$P_s = (1/N) \sum_{i=1}^N \frac{1}{2} (P_{si}^I + P_{si}^Q) \quad (5.3)$$

5.2 GROUP DELAY DISTORTIONS

To investigate the effects of selective fading and/or radio system hardware imperfections, we insert between the transmit and the receive filters a linear filter with the equivalent baseband transfer function $C(f)$, as shown in Fig.5.2. We may express the frequency response $C(f)$ as

$$C(f) = |C(f)| e^{j\theta(f)} \quad (5.4)$$

and

$$A(f) = |C(f)| \quad (5.5)$$

$$D(f) = (-1/2\pi) \frac{d\theta(f)}{df} \quad (5.6)$$

To simulate the group delay distortion we assume there is no amplitude distortion, i.e., $A(f) = 1$. The group delay distortions are defined as follows :

$$D(f) = \begin{cases} L_D f & \text{for linear group delay,} \\ P_D f^2 & \text{for parabolic group delay,} \\ S_D \sin(2\pi Kf/2f_{BW}) & \text{for sinusoidal group delay.} \end{cases} \quad (5.7)$$

where

$$f_{BW} = (1+\alpha)f_N \text{ and } f_N \text{ is the baseband Nyquist bandwidth.}$$

This $(1+\alpha)f_N$ bandwidth definition is more appropriate than f_N , as it includes the critical effect of the group delay at the edge of the filter attenuation band. In the case of sinusoidal group delay, we present only the results for $K = 4$. The symbol error rate P_S versus average C/N is computed. Typical results are shown in Fig.5.5. We define a maximum group delay, T_m , in the filter bandwidth ($2f_{BW}$) as follows :

$$\tau_m = \begin{cases} L_D(2f_{BW}) \text{ ns} & \text{for linear group delay,} \\ P_D(f_{BW})^2 \text{ ns} & \text{for parabolic group delay,} \\ S_D \text{ ns} & \text{for sinusoidal group delay.} \end{cases} \quad (5.8)$$

The degradation of C/N as a function of τ_m relative to the case with no distortion, for a P_S of 10^{-4} is shown in Fig.5.6. Note that here we simulate a 120 Mb/s system with $\alpha = 0.4$. We also include the performance of a 90 Mb/s 64 QAM system with $\alpha = 0.4$ in Fig.5.6, which is confirmed to be the same as in [8]. Again we notice that for a given

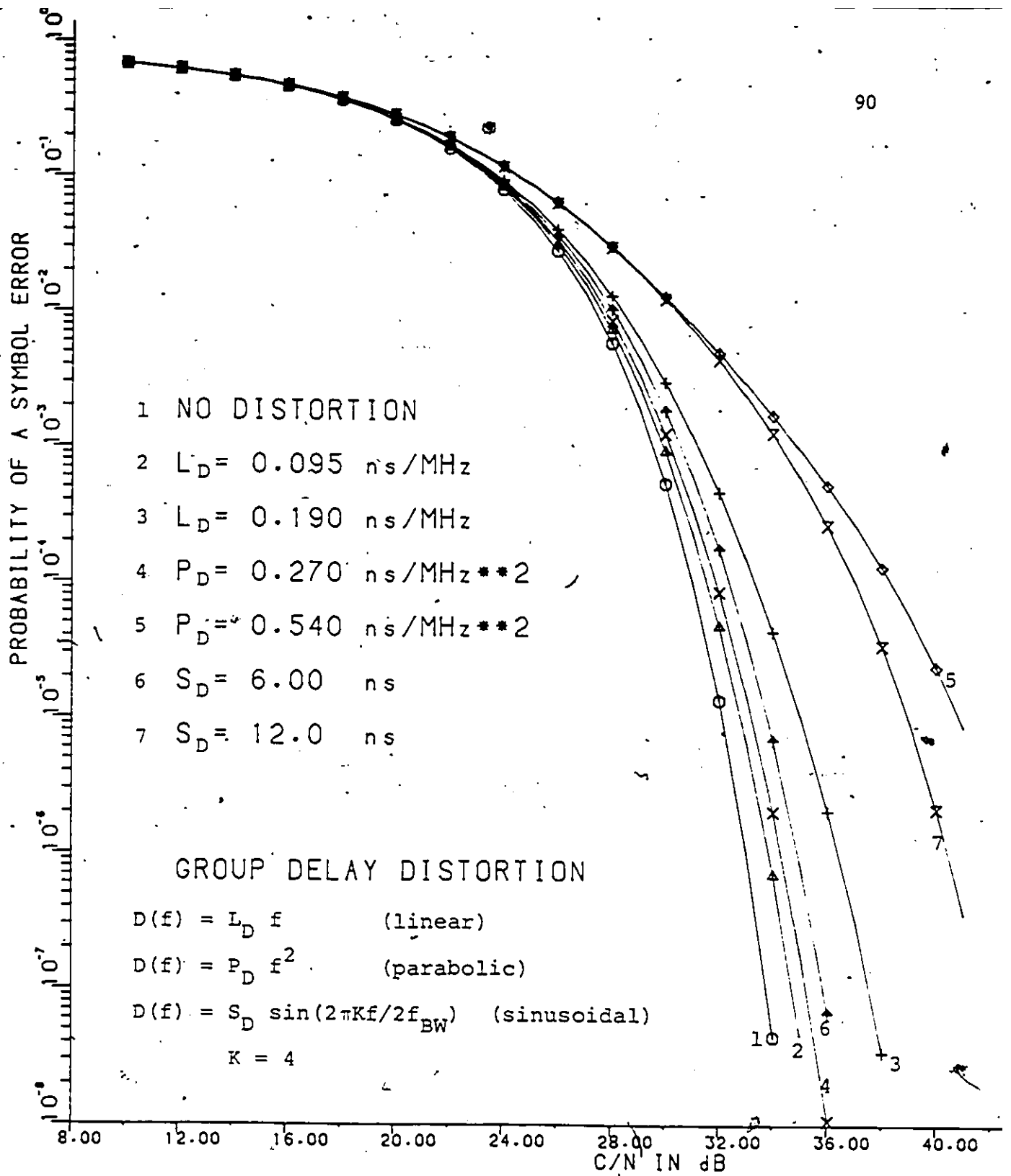


Fig.5.5 P_s versus C/N for linear, parabolic, and sinusoidal group delay distortions for 256-QAM with a bit rate of 120 Mb/s and $\alpha = 0.4$.

Noise is defined in the double-sided Nyquist bandwidth, i.e., the equivalent noise bandwidth is 15 MHz.

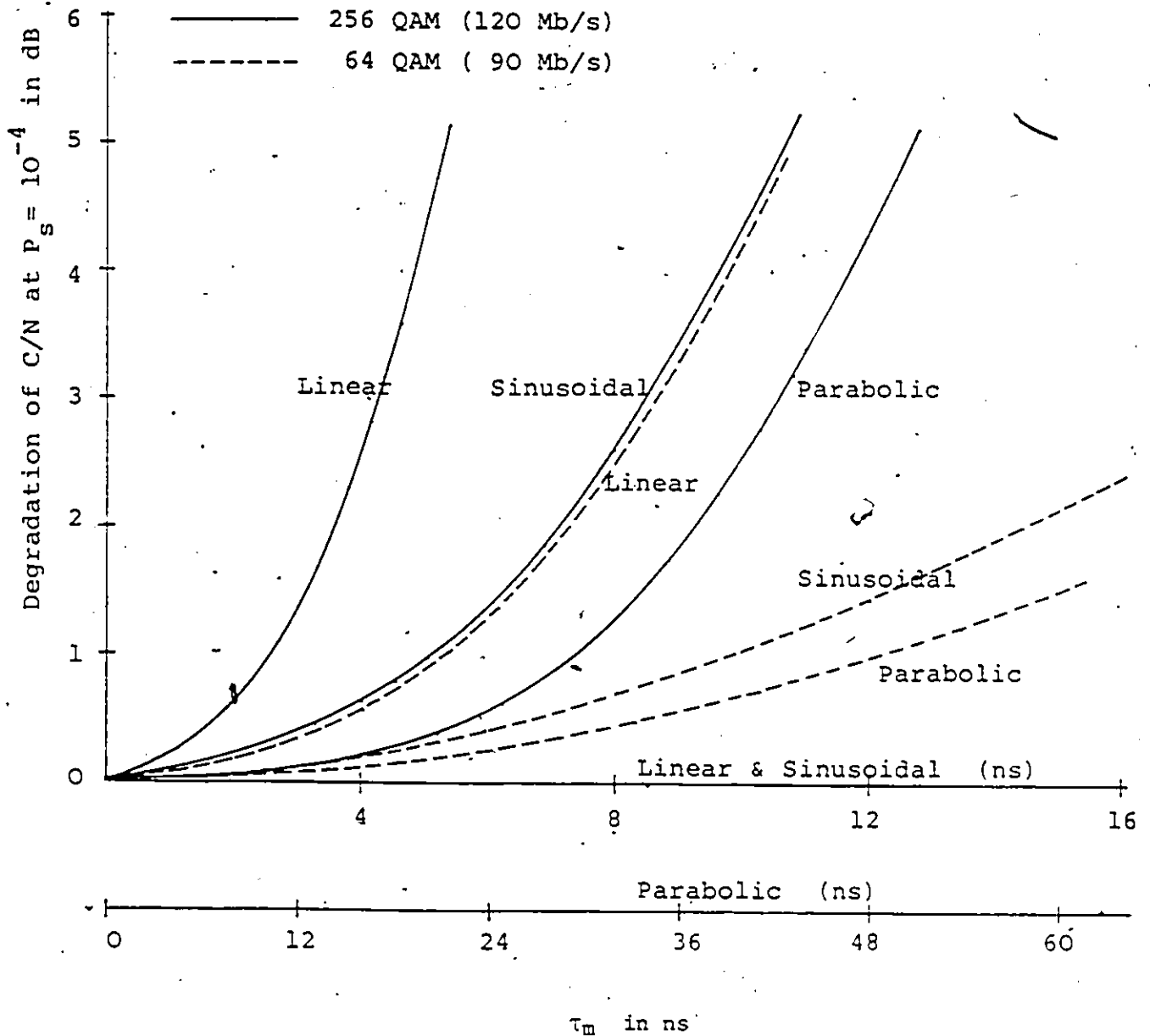


Fig.5.6 Degradation of C/N versus τ_m for linear, parabolic, and sinusoidal group delay distortions for 256-QAM and 64-QAM with a symbol rate of 15 MBaud and $\alpha = 0.4$ raised-cosine filters, where

$$\begin{aligned} \tau_m &= L_D(2f_{BW}) \quad \text{ns (linear)} \\ &= P_D(f_{BW})^2 \quad \text{ns (parabolic)} \\ &= S_D \quad \text{ns (sinusoidal)} \end{aligned}$$

$$f_{BW} = (1+\alpha)f_N = 1.4f_N = 10.5 \text{ MHz}$$

value of maximum group delay τ_m in the filter bandwidth, linear group delay distortion causes the most severe degradation to the system's performance as compared to parabolic or sinusoidal group delay distortions [8].

5.3 AMPLITUDE DISTORTIONS

For the simulation of the amplitude distortion, we assume the group delay distortion is equalized, i.e., $D(f)$ is equal to a constant. Three different characteristics for the amplitude distortion are defined as follows.

$$A(f) = \begin{cases} L_A f & \text{for linear amplitude distortion,} \\ P_A f^2 & \text{for parabolic amplitude distortion,} \\ S_A \sin(2\pi Kf/2f_{BW}) & \text{for sinusoidal amplitude distortion.} \end{cases} \quad (5.9)$$

The symbol error rate P_s versus C/N is computed. A typical result is shown in Fig.5.7. Degradations of C/N for 256-QAM and 64-QAM with 15 MBaud and $\alpha = 0.4$, versus maximum amplitude distortion, A_m , in the filter bandwidth, are plotted in Fig.5.8, where

$$A_m = \begin{cases} L_A (2f_{BW}) & \text{for linear amplitude distortion,} \\ P_A (f_{BW})^2 & \text{for parabolic amplitude distortion,} \\ S_A & \text{for sinusoidal amplitude distortion.} \end{cases} \quad (5.10)$$

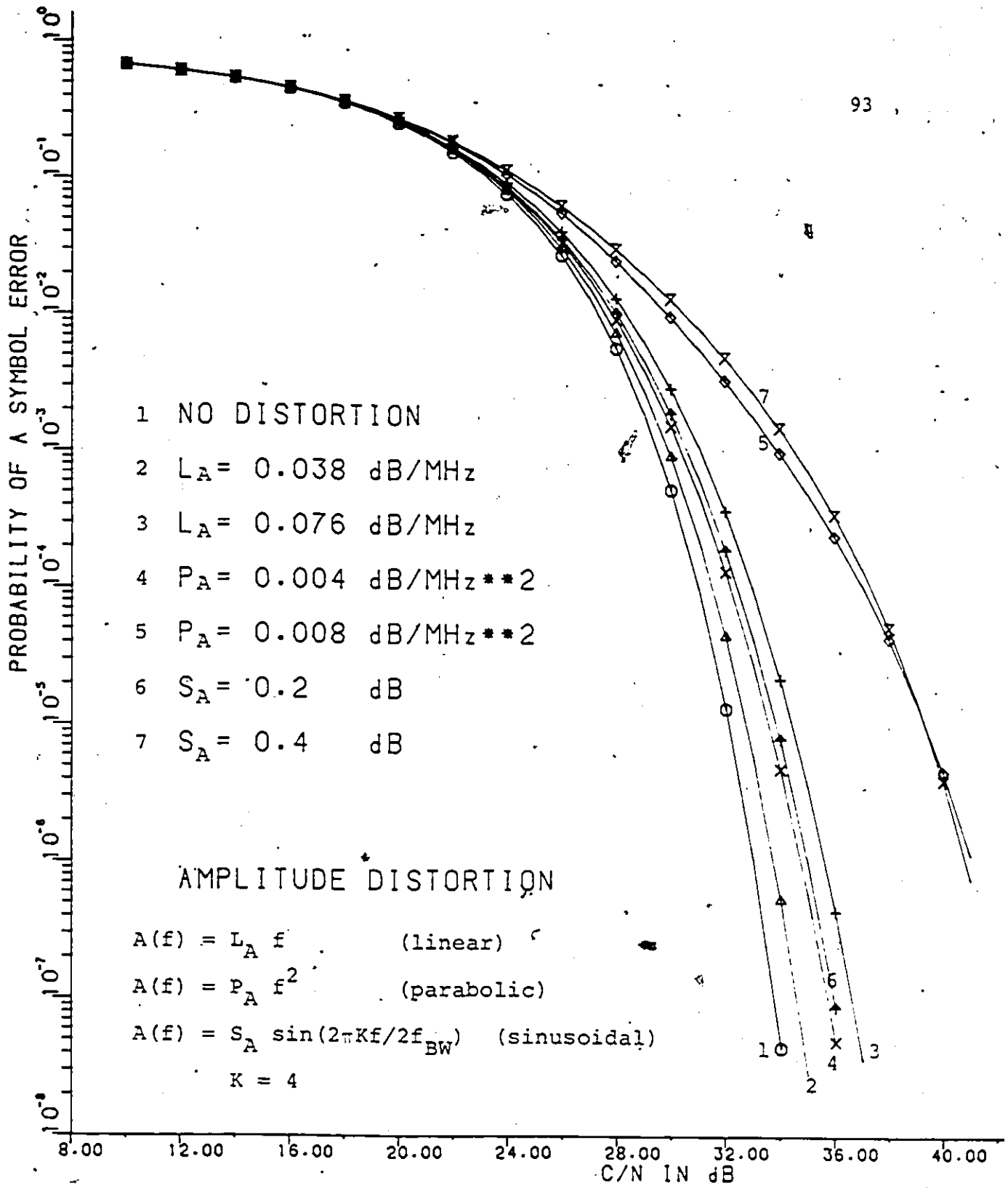


Fig.5.7 P_s versus C/N for linear, parabolic, and sinusoidal amplitude distortions for 256-QAM with a bit rate of 120 Mb/s, i.e., 15 MBaud and $\alpha = 0.4$.
 Noise is defined in the double-sided Nyquist bandwidth, i.e., the equivalent noise bandwidth is 15 MHz.

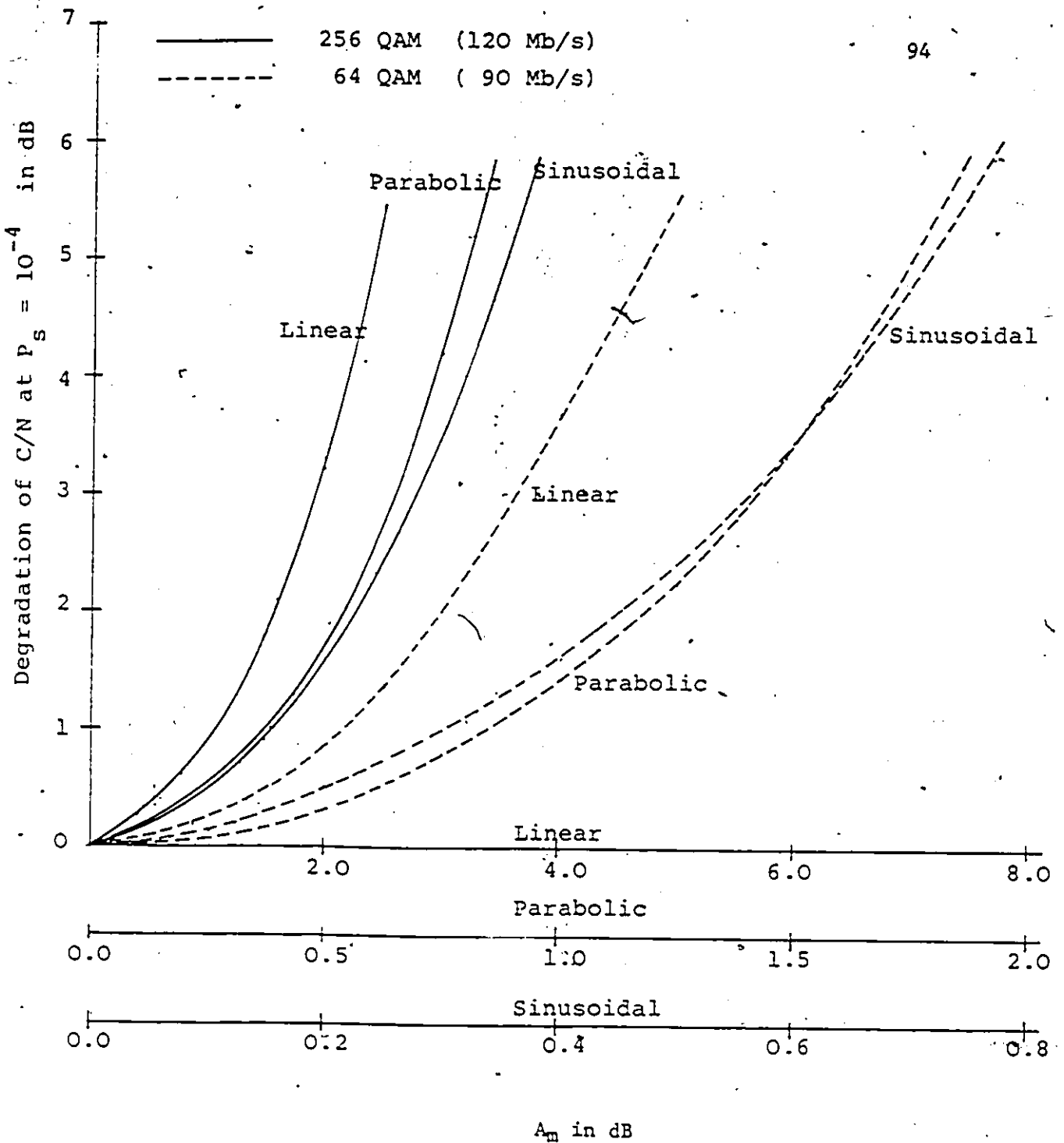


Fig.5.8 Degradation of C/N versus A_m for linear, parabolic, and sinusoidal amplitude distortions for 256-QAM and 64-QAM with a symbol rate of 15 MBaud and $\alpha = 0.4$ raised-cosine filters, where

$$\begin{aligned}
 A_m &= L_A(2f_{BW}) \text{ dB (linear)} \\
 &= P_A(f_{BW})^2 \text{ dB (parabolic)} \\
 &= S_A \text{ dB (sinusoidal)}
 \end{aligned}$$

$$f_{BW} = (1+\alpha)f_N = 1.4f_N = 10.5 \text{ MHz}$$

We note that for a given value of maximum amplitude distortion, A_m , linear amplitude distortion causes the least degradation, followed in order of increasing degradation by parabolic and sinusoidal amplitude distortions.

5.4 APPLYING THE SIMULATED RESULTS TO SYSTEMS WITH DIFFERENT BIT RATES

After presenting the simulated results for a 120 Mb/s system, we now want to show how these results can be applied to systems with different bit rates. This is important since in a number of applications where we might want to know the performance of a system in distorted channels which uses the same $\alpha = 0.4$ 256-QAM modulation format but has another bit rate. A simple scaling procedure to be described in this section will allow us to efficiently obtain the corresponding results without repeating similar computer simulation procedures, thereby saving a lot of computing time and efforts.

The key point lies in the fact that, in our computer simulation, all of the filtering processes are exactly related to the bit rate of a system and the modulation format. That is, assuming a fixed modulation format, once the bite is specified, the characteristics of filters are theoretically well defined. Consider two systems with bit rates f_{b1} and f_{b2} , suffering linear group delay distortions which are characterized by two parameters L_{D1} and L_{D2} , respectively. Let us define $\hat{\tau}_m$ to be the normalized maximum group delay with respect to symbol interval T_s , i.e.,

$$\hat{\tau}_m = \tau_m / T_s = \tau_m \cdot f_s \quad (5.11)$$

where

τ_m is the maximum group delay in the filter bandwidth, as defined in (5.8),

T_s is the symbol interval,

$$T_s = 1/f_s = 8T_b = 8/f_b \text{ for 256-QAM.}$$

It is obvious that, for systems having different bit rates, the group delay distortions which have the same characteristic and the same $\hat{\tau}_m$ will cause the same performance degradation. Thus for two linear group delay distortions causing the same degradation to the respective system a simple relation can easily be obtained from (5.11), i.e.,

$$\tau_{m1} f_{b1} = \tau_{m2} f_{b2} \quad (5.12)$$

or equivalently,

$$L_{D1} f_{b1}^2 = L_{D2} f_{b2}^2 \quad (5.13)$$

where (5.7) and (5.8) have been used. The following example will illustrate how (5.12) and (5.13) and the previous results for a 120 Mb/s system can be employed to predict the corresponding results for a 90 Mb/s system.

From Fig. 5.6, it is noted that in the case of linear group delay distortions, a τ_m of 2.5 ns causes a 1 dB degradation in C/N for a 120 Mb/s system. Substituting $f_{b1} = 120$ Mb/s, $f_{b2} = 90$ Mb/s, and $\tau_{m1} = 2.5$ ns into (5.12),

$$\tau_{m2} = 2.5 \cdot \frac{120}{90} = 3.1 \text{ ns}$$

This indicates that a τ_m of 3.1 ns will cause the same 1 dB degradation in C/N for a 90 Mb/s system. Furthermore, substituting $L_{D1} = 0.095$ ns/MHz, $f_{b1} = 120$ Mb/s, $f_{b2} = 90$ Mb/s, we find

$$L_{D2} = 0.095 \cdot \left(\frac{120}{90}\right)^2 = 0.126 \text{ ns/MHz}$$

This means that the P_s curve corresponding to $L_D = 0.095$ ns/MHz for a 120 Mb/s system also represents the P_e performance corresponding to $L_D = 0.126$ ns/MHz for a 90 Mb/s system.

On the other hand, consider the amplitude distortions case. It is obvious that the amplitude distortions which have the same characteristic and the same maximum amplitude distortion in the filter bandwidth will cause the same performance degradation to systems with different bit rates. Thus, for two linear amplitude distortions with parameters L_{A1} and L_{A2} which cause the same degradation to two systems with bit rates f_{b1} and f_{b2} , a simple relation can be drawn from (5.10) and the above argument as follows.

$$L_{A1} f_{b1} = L_{A2} f_{b2} \quad (5.14)$$

As a further illustration, the P_s curve corresponding to $L_A = 0.038$ dB/MHz for a 120 Mb/s represents also the P_e performance corresponding to $L_A = 0.038 \times 120/90 = 0.0507$ dB/MHz for a 90 Mb/s system. It is now clear that the results simulated for a 120 Mb/s system can easily be applied to systems with different bit rates. The equations which relate other distortion parameters to bit rates can be derived in the same way and are summarized in Table 5.1.

TABLE 5.1 RELATIONSHIP BETWEEN DISTORTION PARAMETERS AND BIT RATES FOR TWO SYSTEMS HAVING THE SAME MODULATION FORMAT AND PERFORMANCE BUT DIFFERENT BIT RATES.

	Group delay distortions	Amplitude distortions
Linear	$L_{D1} f_{b1}^2 = L_{D2} f_{b2}^2$	$L_{A1} f_{b1} = L_{A2} f_{b2}$
Parabolic	$P_{D1} f_{b1}^3 = P_{D2} f_{b2}^3$	$P_{A1} f_{b1}^2 = P_{A2} f_{b2}^2$
Sinusoidal	$S_{D1} f_{b1} = S_{D2} f_{b2}$	$S_{A1} = S_{A2}$

Note: L_{D1} and L_{D2} are the parameters of linear group delay distortions which cause the same performance to systems with bit rates f_{b1} and f_{b2} , respectively. Other parameters and notations follow similarly.

5.5 CONCLUSIONS

The effects of group delay and amplitude distortions on the error performance of a 256-QAM modem have been studied. Computer simulation results indicate that linear group delay distortion is the most critical group delay parameter. The simulated results could be useful for modem researchers and designers since it could indicate the tolerable imperfection in filters implementation which would not degrade system performance to below a specified value. Also presented is a simple scaling procedure which enables us to apply the simulated results for a bit rate of 120 Mb/s to any other bit rates without going through similar computation procedures.

Chapter VI

COMPARISON OF 256-QAM AND IMPROVED EFFICIENCY
225-QPRS IN DISTORTED CHANNELS

In Chapter 5 and [36], the performance of a 256-QAM modem in distorted channels was evaluated. An ideal 225-QPRS achieves an efficiency of 6 b/s/Hz, which is equivalent to that of 256-QAM with a roll-off factor $\alpha = 0.33$. However, at $P_e = 10^{-9}$ a 4 dB increase in C/N immunity can be obtained by using 225-QPRS instead of 256-QAM to achieve 6 b/s/Hz. Furthermore, an improved efficiency class-I 225-QPRS using our new Model-B has been described in Chapter 2. Therefore, it is important to study the performance of improved efficiency 225-QPRS in distorted channels.

In this chapter, we shall compare the performances of 256-QAM and improved efficiency 225-QPRS in distorted channels [39]. The comparison will be based on the same spectral efficiency of 6.3 b/s/Hz since the required C/N (dB) at $P_e = 10^{-9}$ is practically the same for these two modulation schemes to achieve this efficiency. The effects of group delay and amplitude distortions on the performance of these two modulation schemes will be evaluated and compared. The results could indicate the sensitivity of the two modulation schemes to different imperfections.

6.1 BACKGROUND FOR THE COMPARISON OF 256-QAM AND 225-QPRS

Fig.6.1 compares some of the results of class-I 225-QPRS using our new Model-B in Chapter 2 with the performance of 256-QAM. It is seen that at $P_e=10^{-9}$ the required C/N is about 35 dB for both 225-QPRS with a 5% increase above the Nyquist rate and 256-QAM. The spectral efficiency of 225-QPRS with a 5% increase above the Nyquist rate is 6.3 b/s/Hz, which can be achieved by 256-QAM with $\alpha = 0.27$. As mentioned in Chapter 1, this high spectral efficiency is required in many applications such as T1/SG. Therefore it is of interest to compare the sensitivity of these two modulation schemes to channel distortions. The comparison will be based on the same transmission rate in the same bandwidth to achieve 6.3 b/s/Hz. In the simulation, a bit rate of 120 Mb/s is used. However, following the scaling procedure described in Chapter 5, the results can be applied for another bit rate.

6.2 COMPUTER SIMULATION DESCRIPTIONS

The simulation is carried out entirely in the complex baseband form for a 120 Mb/s system i.e., with a symbol rate of 15 MBaud for 256-QAM and 20 MBaud for 225-QPRS, respectively. For 256-QAM, the transmit filter consists of an analog $x/\sin(x)$ shaped amplitude equalizer and an ideal square-root of $\alpha = 0.27$ raised-cosine filter, i.e., with a spectral efficiency of 6.3 b/s/Hz. The receive filter is an ideal square root of $\alpha = 0.27$ raised-cosine filter.

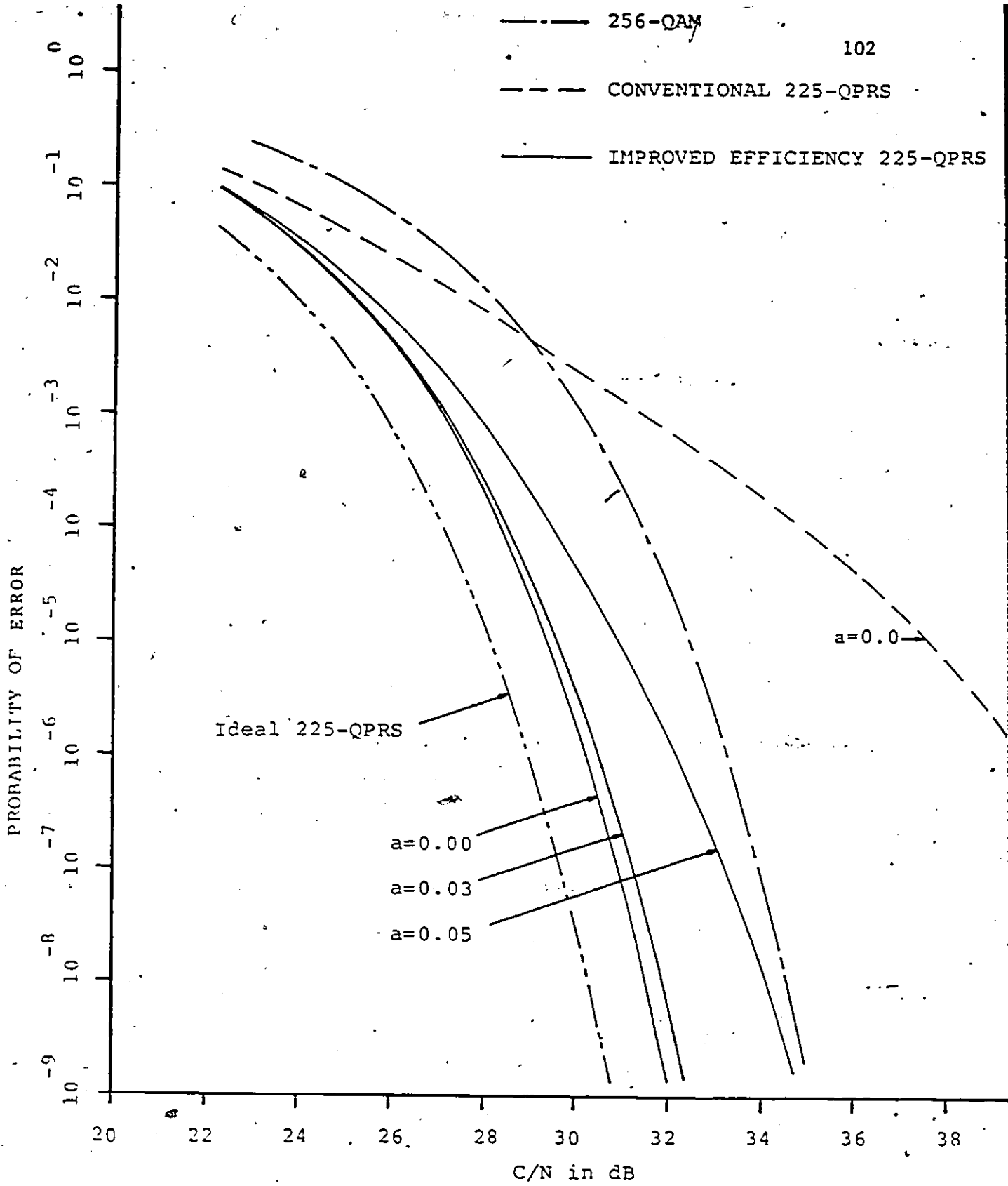


Fig.6.1 Probability of error of 256-QAM, conventional 225-QPRS, and improved efficiency 225-QPRS versus C/N.

For the improved efficiency class-I 225-QPRS, the transmitter consists of an analog $x/\sin(x)$ shaped amplitude equalizer, the duobinary filter and an ideal brick-wall filter with a cutoff frequency at $f_N/1.05$, where $f_N = 10$ MHz is the Nyquist frequency of the signal. Thus the spectral efficiency of this model is also 6.3 b/s/Hz. The receive filter simply bandlimits the channel noise.

We consider the effects of group delay and amplitude distortions with linear, parabolic, or sinusoidal characteristics on these two modulation techniques. The demodulated in-phase and quadrature signals are sampled and passed to the threshold comparators in the receiver. For a specified power of white Gaussian noise at the threshold detector input, the error probability of the i -th symbol with respect to the in-phase channel is calculated as follows:

$$P_{Si}^I = \begin{cases} \frac{1}{2} \operatorname{erfc}(|\bar{S}_i - \text{THR1}_i|/\sqrt{2}\sigma) & \text{for } I_i = \pm 15 \text{ (256-QAM)} \\ & = \pm 14 \text{ (225-QPRS)} \\ \frac{1}{2} \operatorname{erfc}(|\bar{S}_i - \text{THR1}_i|/\sqrt{2}\sigma) + \frac{1}{2} \operatorname{erfc}(|\text{THR2}_i - \bar{S}_i|/\sqrt{2}\sigma) & \text{for } I_i = \pm 1, \pm 3, \dots, \pm 13 \text{ (256-QAM)} \\ & = 0, \pm 2, \dots, \pm 12 \text{ (225-QPRS)} \end{cases} \quad (6.1)$$

where

I_i , \bar{S}_i , THR1_i , THR2_i , $\operatorname{erfc}(x)$, and σ are defined as in (5.2).

The error probability P_{Si}^Q with respect to the quadrature channel is obtained similarly from (6.1), and for a sequence of N symbols in each channel, the average symbol error P_s is calculated as (5.3).

We assume that the number of samples per symbol is 32 and the number of symbols is 2048 (which corresponds to a PRBS sequence

length of 16,348 bits). We average the probability of error over many symbol patterns. To confirm that the simulated results are meaningful, we investigated the uncertainty (which might be caused by an insufficient length of symbols) by increasing the simulated symbol length significantly. We found that the performance practically converges to that of a 2048 symbols length when the simulated length is longer than 2048 symbols.

6.3 256-QAM AND IMPROVED EFFICIENCY 225-QPRS WITH GROUP DELAY AND AMPLITUDE DISTORTIONS

We insert between the transmit and receive filters a linear filter with the equivalent baseband transfer function $C(f)$ expressed as (5.4)-(5.6). First, we assume that there is no amplitude distortion, i.e., $A(f) = 1$. The group delay distortions are defined as (5.7). The results are shown in Figs.6.2-6.4 for linear, parabolic and sinusoidal group delay distortions, respectively. The C/N degradation at $P_e = 10^{-4}$ of these modulation techniques for group delay distortions are compared in Table 6.1. It is found that 256-QAM is less sensitive to parabolic and sinusoidal group delay distortions than 225-QPRS. Next, we assume that the group delay distortion is equalized, i.e., $D(f) = k$ (k is a constant). The amplitude distortions are defined as (5.9).

The results are illustrated in Figs.6.5-6.7 for linear, parabolic and sinusoidal amplitude distortions, respectively. The C/N degradation at $P_e = 10^{-4}$ of these modulation techniques for amplitude distortions are compared in Table 6.1. It is found that 225-QPRS is less sensitive to parabolic and sinusoidal amplitude distortions.

PROBABILITY OF SYMBOL ERROR

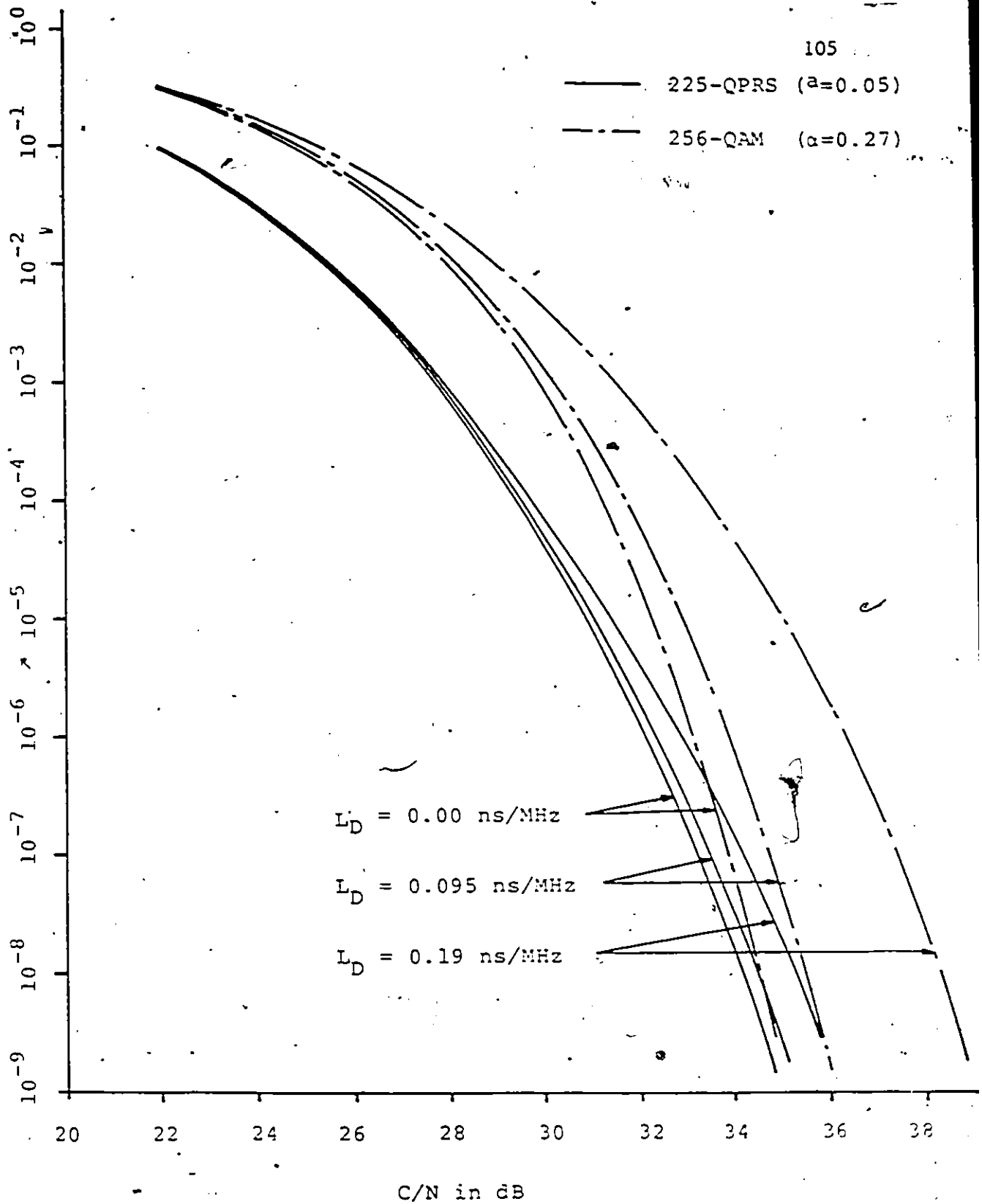


Fig.6.2 Probability of error of 225-QPRS above the Nyquist rate and 256-QAM for linear group delay distortions versus C/N.

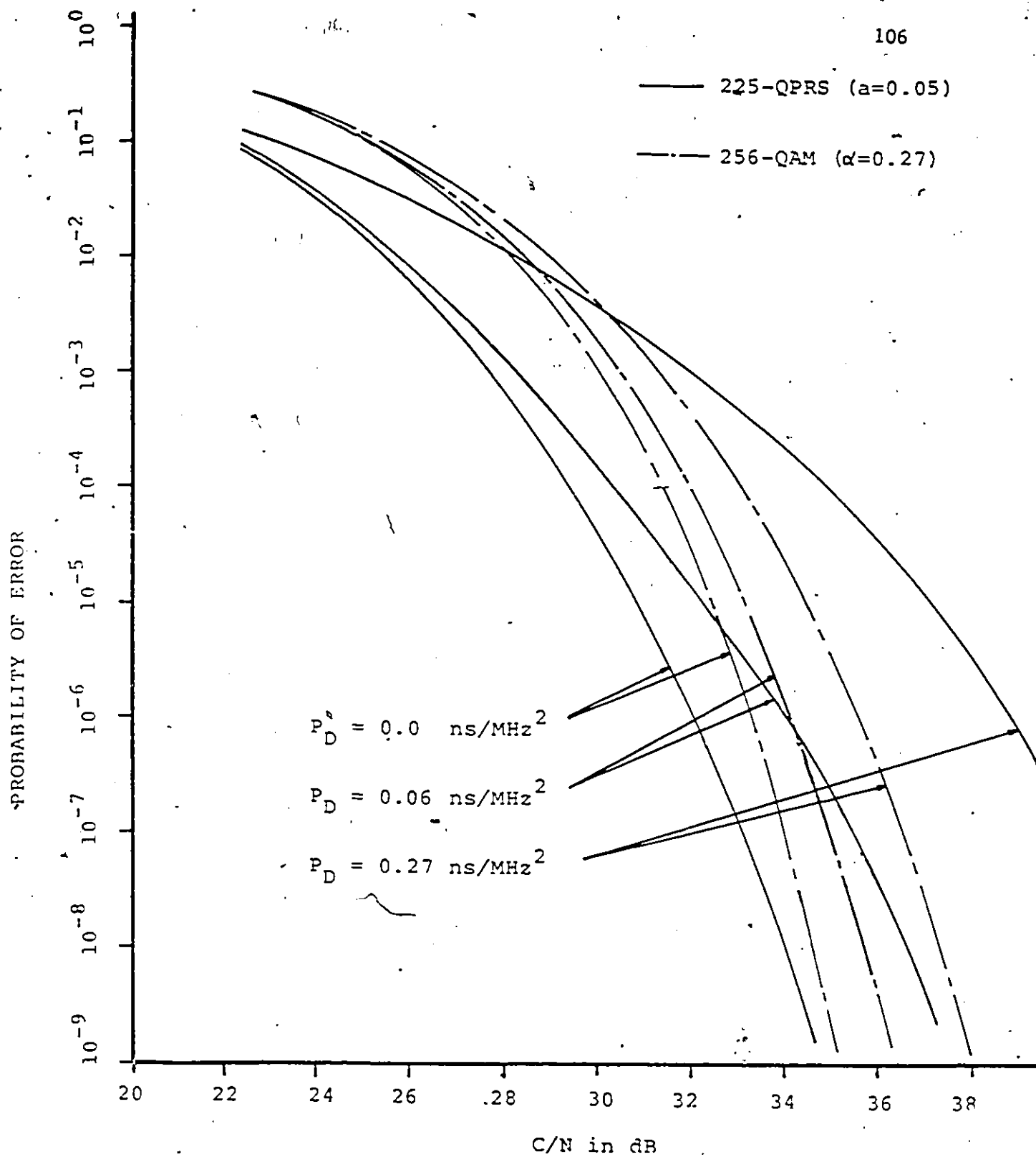


Fig.6.3 Probability of error of 225-QPRS above the Nyquist rate and 256-QAM for parabolic group delay distortions versus C/N.

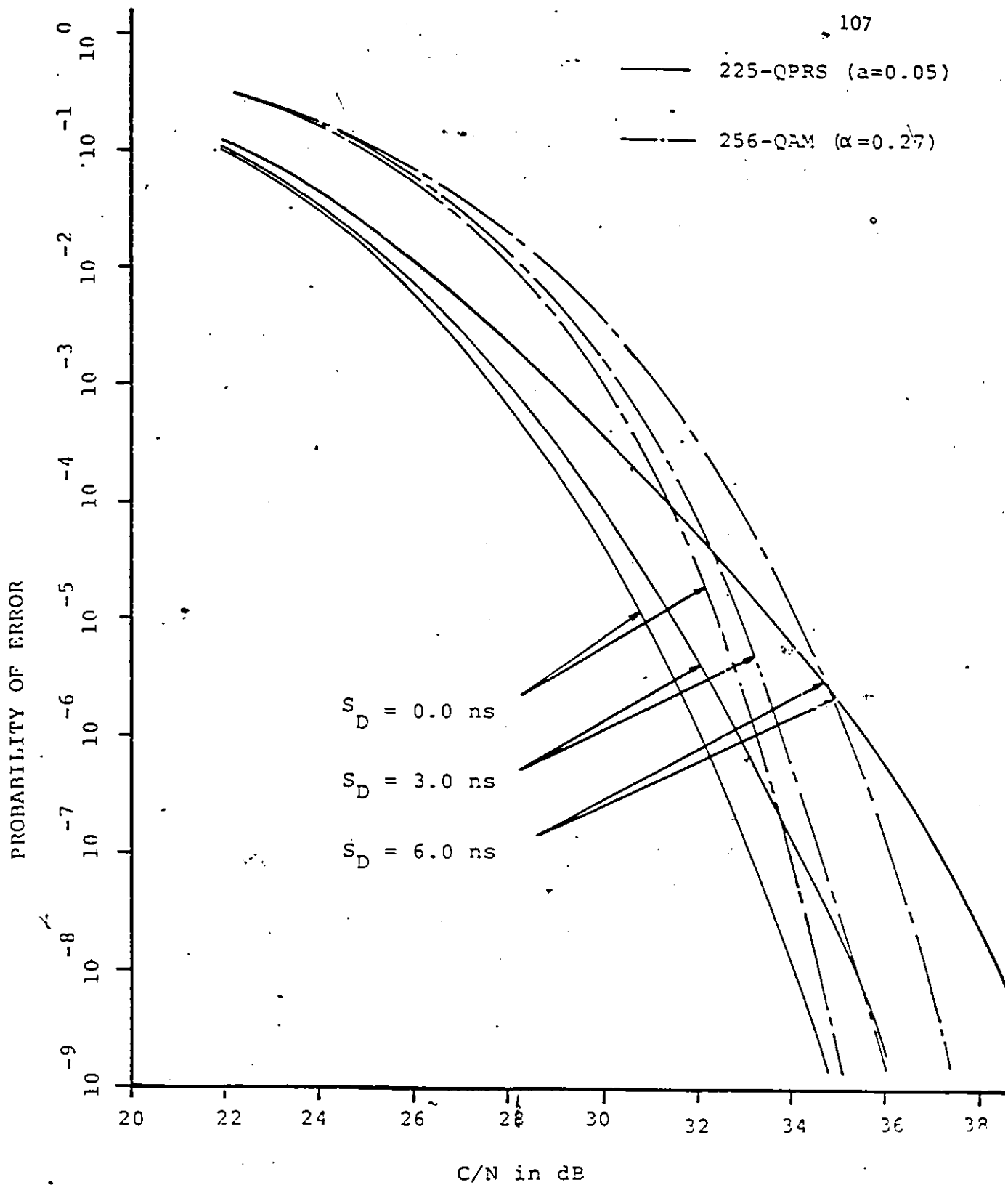


Fig.6.4 Probability of error of 225-QPRS above the Nyquist rate and 256-QAM for sinusoidal group delay distortions versus C/N.

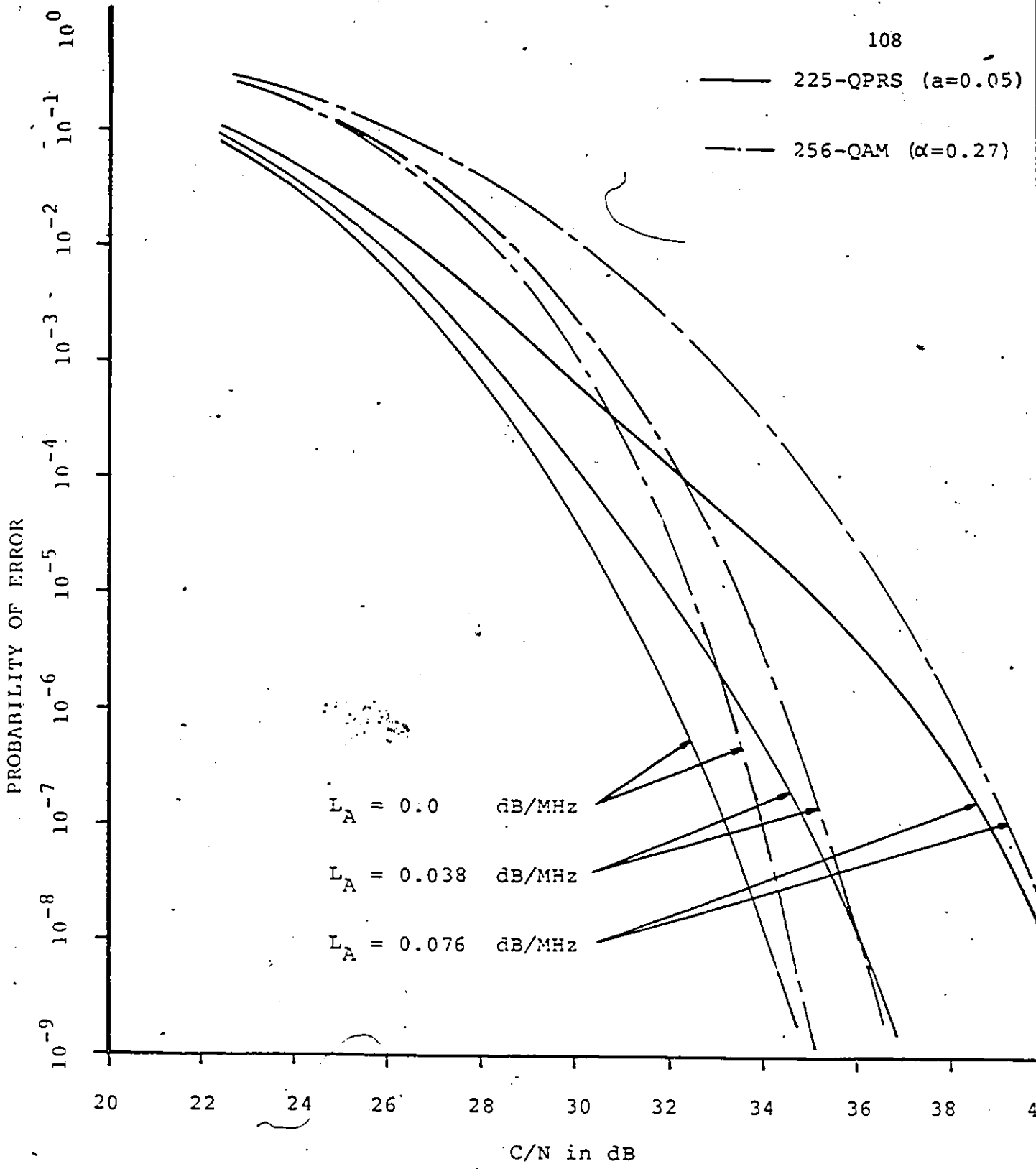


Fig.6.5 Probability of error of 225-QPRS above the Nyquist rate and 256-QAM for linear amplitude distortions versus C/N.

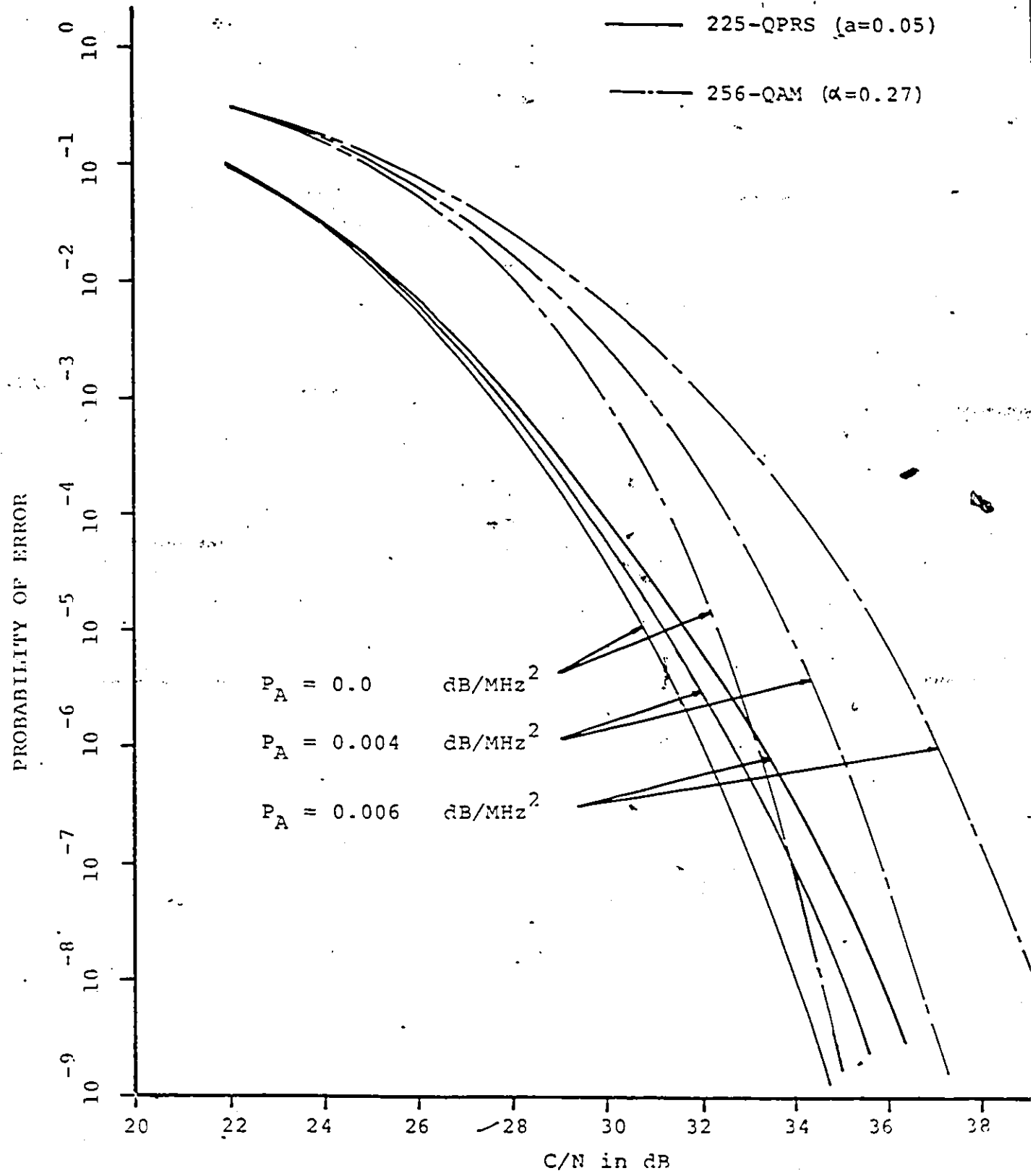


Fig.6.6 Probability of error of 225-QPRS above the Nyquist rate and 256-QAM for parabolic amplitude distortions versus C/N.

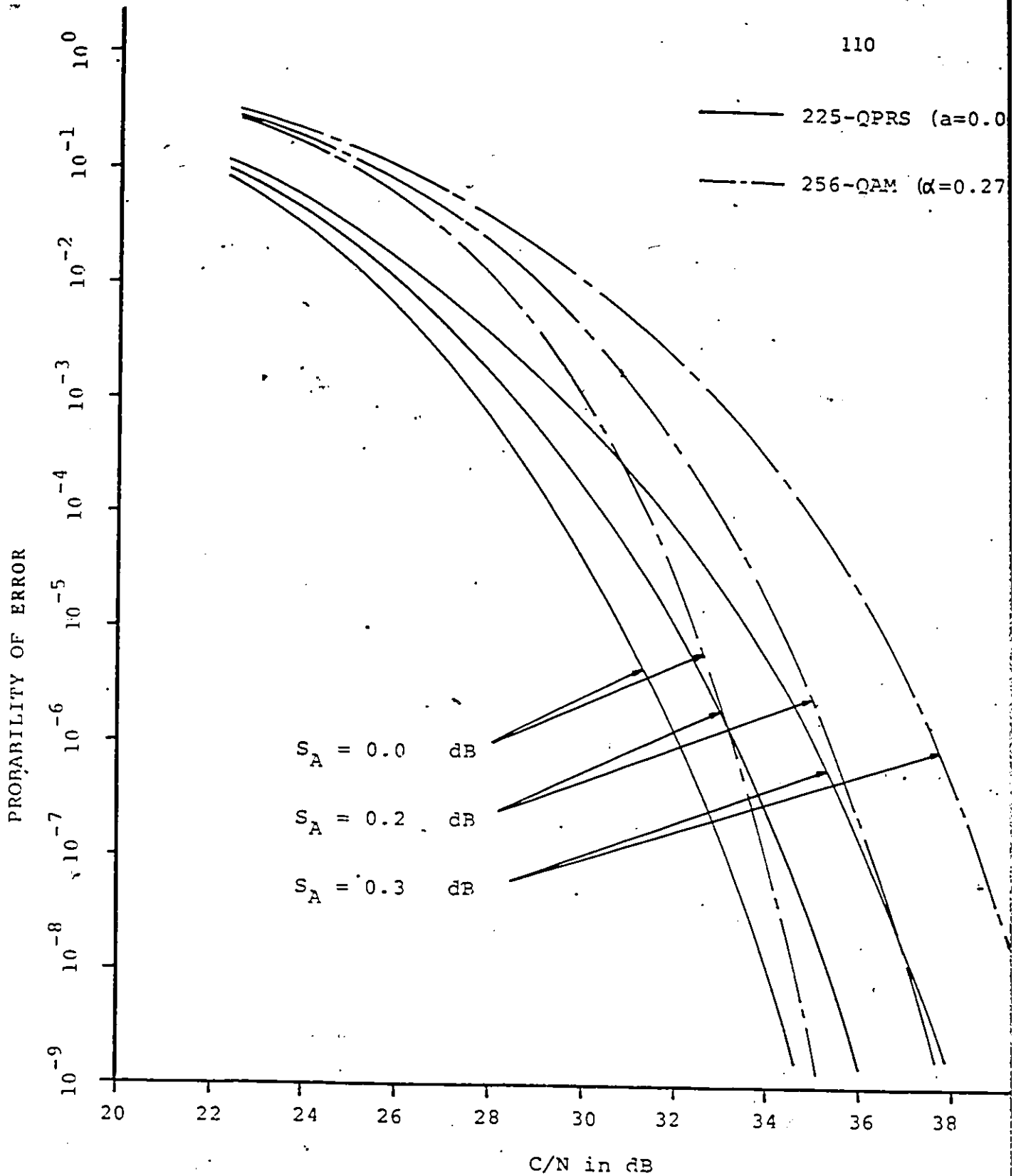


Fig.6.7 Probability of error of 225-QPRS above the Nyquist rate and 256-QAM for sinusoidal amplitude distortions versus C/N.

Group delay or amplitude distortions		C/N degradation at $P_e = 10^{-4}$ (dB)	
		225-QPRS (a=0.05)	256-QAM ($\alpha=0.27$)
linear group delay	$L_D = 0.095$ ns/MHz	0.1	0.6
	$L_D = 0.19$ ns/MHz	0.4	2.4
parabolic group delay	$P_D = 0.06$ ns/MHz ²	0.9	0.7
	$P_D = 0.27$ ns/MHz ²	5.5	1.8
sinusoidal group delay	$S_D = 3.0$ ns	0.5	0.5
	$S_D = 6.0$ ns	1.8	1.5
linear amplitude distortion	$L_A = 0.038$ dB/MHz	0.7	0.9
	$L_A = 0.076$ dB/MHz	2.8	3.6
parabolic amplitude distortion	$P_A = 0.004$ dB/MHz ²	0.3	1.3
	$P_A = 0.006$ dB/MHz ²	0.6	3.0
sinusoidal amplitude distortion	$S_A = 0.2$ dB	1.0	1.7
	$S_A = 0.3$ dB	2.3	3.6

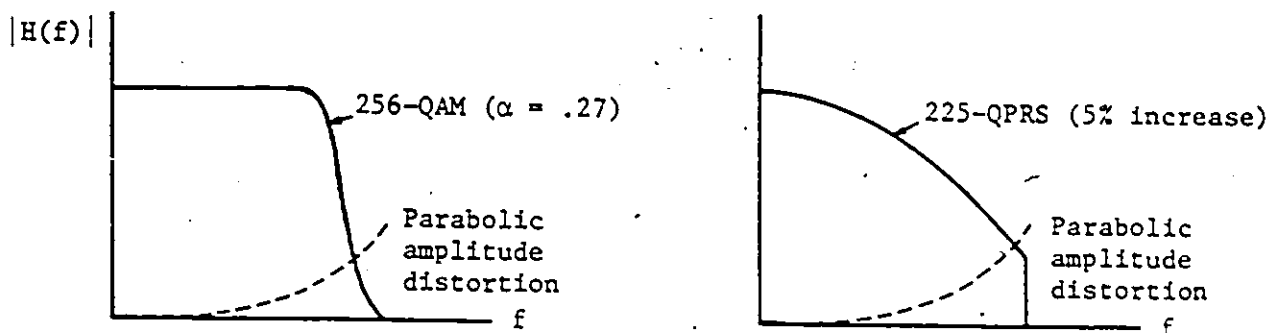
TABLE 6.1 C/N DEGRADATION OF 225-QPRS ABOVE THE NYQUIST RATE AND 256-QAM FOR GROUP DELAY AND AMPLITUDE DISTORTIONS AT $P_e = 10^{-4}$.

It is observed from the Figs. 6.4-6.6 that, while 225-QPRS is worse than 256-QAM for low enough error probabilities, the situation is reverse for high P_e values. The interpretation is the following. When C/N is small, Gaussian noise dominates the performance and ISI is negligible. Thus, the performance of 225-QPRS would be better than that of 256-QAM. On the other hand, when C/N is higher, ISI is more dominant than Gaussian noise. In our simulation, the ISI is due only to the channel distortions in the 256-QAM case, whereas in 225-QPRS, the "undesired" ISI exists due to not only the channel distortions but also the higher transmission rate than the Nyquist rate. Thus when C/N is high, the performance of 225-QPRS might be worse than that of 256-QAM in distorted channels with some specific group delay and amplitude distortions.

6.4 PHYSICAL INTERPRETATION OF THE RESULTS

Having presented the various simulated results, it is of importance to seek the physical reason why one of the two modulation schemes is more sensitive to certain distortions than the other. To begin with, let us consider amplitude distortions.

As illustrated in Fig. 6.8 for a parabolic amplitude distortion, we note that, in the case of 225-QPRS, most of the energy is concentrated around dc where the distortion is relatively small. On the other hand, for 256-QAM, a significant amount of energy is distributed in the region where the distortion is relatively large. This explains why 225-QPRS is less sensitive to parabolic amplitude distortions than 256-QAM, as already seen from the results in Fig. 6.6.



* $H(f)$ is the overall frequency response.

Fig.6.8 Frequency-domain comparison of 256-QAM ($\alpha = .27$) and 225-QPRS (5% increase) with a parabolic amplitude distortion.

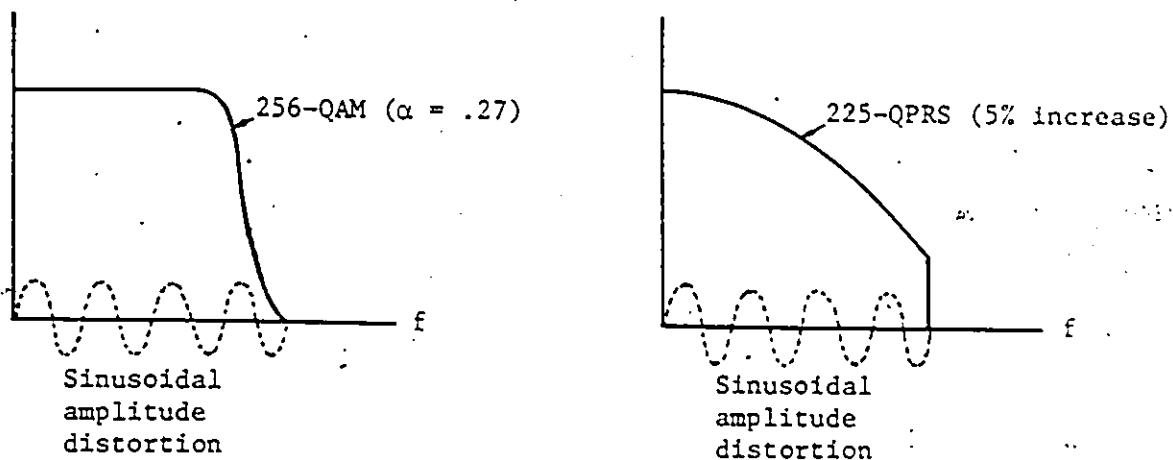


Fig.6.9 Frequency-domain comparison of 256-QAM ($\alpha = .27$) and 225-QPRS (5% increase) with a sinusoidal amplitude distortion.

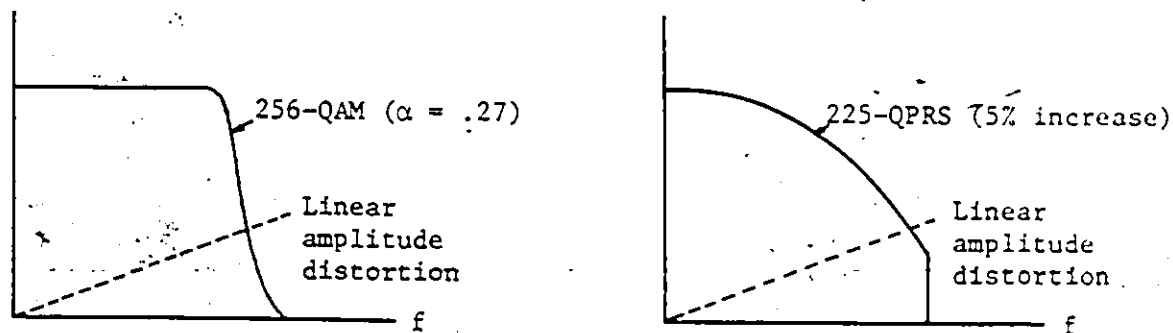


Fig.6.10 Frequency-domain comparison of 256-QAM ($\alpha = .27$) and 225-QPRS (5% increase) with a linear amplitude distortion.

For sinusoidal amplitude distortions, the frequency-domain comparison is shown in Fig.6.9. In both cases, all the frequency components suffer distortion. However, in the case of 225-QPRS, due to its cosine-shaped energy distribution, the effect of distortion in the average sense will be somewhat less than that on 256-QAM. Thus, we conclude that 225-QPRS is also less sensitive to sinusoidal amplitude distortions than 256-QAM, but the difference may not be as significant as in the parabolic case, as observed from Figs.6.6 and 6.7.

As to linear amplitude distortions, looking at Fig.6.10 for comparison, it is difficult to judge which scheme is more sensitive than the other. In fact, the results presented in Fig.6.5 indicate that 256-QAM and 225-QPRS have more or less the same sensitivity to linear amplitude distortions.

The effects of group delay distortions are more difficult to analyze. However, with efforts, we still can get some insight into it. Ideal filters/channels should have a linear phase characteristic, i.e., a constant group delay. In the case of linear group delay distortions which correspond to having a parabolic phase characteristic, there will be crosstalks between the in-phase (I) and quadrature (Q) channels. 256-QAM being a 16-level signal would have higher introduced crosstalk than 225-QPRS, which is a 15-level signal. Thus 225-QPRS, is less sensitive to linear group delay distortions than 256-QAM, as confirmed by the illustrative results in Fig.6.2.

For parabolic group delay distortions, there is no crosstalk. Thus, it is important to note the critical effect of the group delay at the band

edge where the parabolic group delay increases significantly. And it is there where the energy is truncated in the 225-QPRS case. So 225-QPRS has more energy than 256-QAM at the band edge, with the result of suffering more degradations. This leads to the conclusion that 256-QAM is less sensitive to parabolic group delay distortions, as illustrated in Fig.6.3.

Finally, coming to the case of sinusoidal group delay distortions, it is not fully understood yet. However, the results in Fig.6.4 show that 256-QAM is slightly less sensitive than 225-QPRS.

6.5 CONCLUSIONS

The effects of group delay and amplitude distortions on the performance of 256-QAM and improved efficiency 225-QPRS have been compared, based on the same spectral efficiency of 6.3 b/s/Hz . It is found that 256-QAM is less sensitive to parabolic and sinusoidal group delay distortions than 225-QPRS. And 225-QPRS is less sensitive to linear group delay distortions and parabolic and sinusoidal amplitude distortions.

Chapter VII

ERROR FLOORS IN DIGITAL TRANSMISSION SYSTEMS

In the study of multi-level PRS/QPRS systems operated above the Nyquist rate [22], it was found that error floors exist in these systems. Error floors are known in industry as one of the most severe problems of transmission systems. It is often noted that a practically measured BER curve tends to tail off at high S/N. That is, in some cases due to transmission impairments, a system cannot have a BER lower than a certain limit. The mechanism of error floors is still not well understood.

In this chapter, we introduce a new method to predict error floors caused by operating PRS systems above the Nyquist rate. Our method is, however, more general and could be used also in the study of other transmission systems. As an illustration, the evaluation of error floors for PAM systems with severe distortions will be described.

7.1 ERROR FLOORS IN MULTI-LEVEL PRS/QPRS SYSTEMS OPERATED ABOVE THE NYQUIST RATE

As mentioned in Chapter 2, PRS systems operate at the Nyquist rate by introducing deliberately a "controlled" or "desired" amount of ISI. When operated above the Nyquist rate, in addition to the "desired" ISI, there is, in general, introduced "undesired" ISI no matter which scheme

(the conventional Model-A or our new Model-B) is used. The following discussion concentrates on a noise-free system.

Referring to Figs. 2.2 and 2.3 and equations (2.1)-(2.5) for duobinary PRS, the parameter "a" indicates the system's spectral efficiency. For example, $a = 0$ means transmission at the Nyquist rate and a system with $a = 0.05$ would mean a 5% increase in spectral efficiency above the Nyquist rate. With $a = 0$ for the ideal duobinary PRS, the only two nonzero samples are at $t = -T_S/2$ and $T_S/2$, respectively. For m-ary inputs, i.e., the input symbols $\{x_n\}$ consist of the equally likely values of $\pm 1, \pm 3, \dots, \pm(m-3), \pm(m-1)$, the output $y(t)$ generally has $2m-1$ levels if $a=0$, i.e., at the Nyquist rate.

As one intends to increase the spectral efficiency above the Nyquist rate using Model-A or Model-B; i.e., with $a > 0$, the nominally zero pulse samples at $t = \pm(2n+1)T_S/2$, $n = 1, 2, 3, \dots$, are no longer zeros. These nonzero samples present "undesired" ISI to the system. The peak eye closure criterion [20], [40] is commonly used to determine the eye opening for a system in the presence of ISI. To apply this criterion, one must first evaluate the peak distortion D_p , which, for the present two models with m-ary inputs, can be expressed as follows:

$$D_p = 2(m-1) \sum_{n=1}^{\infty} \left| h\left(\frac{2n+1}{2} T_S\right) \right| \quad (7.1)$$

where $h(t)$ represents the overall impulse response of a system.

The impulse responses of the conventional Model-A and our new Model-B are given in eqs. (2.3) and (2.5).

The peak distortion represents the undesired ISI generated by an infinite number of interfering symbols under the worst-case combination. Neglecting all the undesired ISI for the moment, it is easy to see the output levels at the optimum sampling instants would be 0, $\pm 2h(T_s/2)$, $\pm 4h(T_s/2)$, ..., $\pm 2(m-2)h(T_s/2)$, $\pm 2(m-1)h(T_s/2)$ for m-ary inputs.

For example, if $x_0 = -1$, $x_1 = 1$ then $y(T_s/2) = 0$. If $x_0 = x_1 = 1$ then $y(T_s/2) = 2h(T_s/2)$. The decision thresholds can be set at $\pm h(T_s/2)$, $\pm 3h(T_s/2)$, ..., $\pm (2m-3)h(T_s/2)$, resulting in a decision distance of $h(T_s/2)$. According to the peak eye closure criterion if $D_p < h(T_s/2)$ the eye opening denoted by ρ , is

$$\rho = 2(h(T_s/2) - D_p) \quad (7.2)$$

And the eye is closed when the peak distortion is greater than the decision distance, i.e.,

$$D_p \geq h(T_s/2) \quad (7.3)$$

Our study [22] found that, for the worst case pulse sequence by using (7.1) and (7.2) to evaluate the eye opening, neither Model-A nor Model-B gives open eyes for m-ary inputs, if $m > 4$ and $a > 0.04$. This is because of inherently higher ISI in multi-level systems, as we note that a magnifying factor of $m-1$ appears in (7.1). However, this does not rule out the possibility of transmitting m-ary signals using Model-A or Model-B since the probability of occurrence of the worst sequence may be relatively low in some cases.

Instead of peak distortion, we introduce the concept of truncated peak distortion D_t defined by (7.4).

$$D_t = 2(m-1) \sum_{n=1}^N \left| h\left(\frac{2n+1}{2} T_s\right) \right| \quad (7.4)$$

The difference between (7.4) and (7.1) is that in (7.4) only a finite number of "undesired" ISI samples are considered.

The reason for limiting the number of interfering symbols to a finite value is that it leads to an error-floor concept which will be described in the following paragraphs. And it is true that the most significant ISI is practically due to finite symbols which are contiguous to the present symbol.

Now summing up the undesired ISI for N previous and N forthcoming symbols under the worst case, there might exist a minimum N , denoted by N_{\min} , such that

$$D_t \geq h(T_s/2) \quad \text{for } N \geq N_{\min} \quad (7.5)$$

When (7.3) is met, the eye is closed. We define

$$L = 2(N_{\min} + 1) \quad (7.6)$$

to be the shortest length of the worst data sequence which closes the eye. The probability of occurrence of this sequence is

$$E_f = 1/m^L \quad (7.7)$$

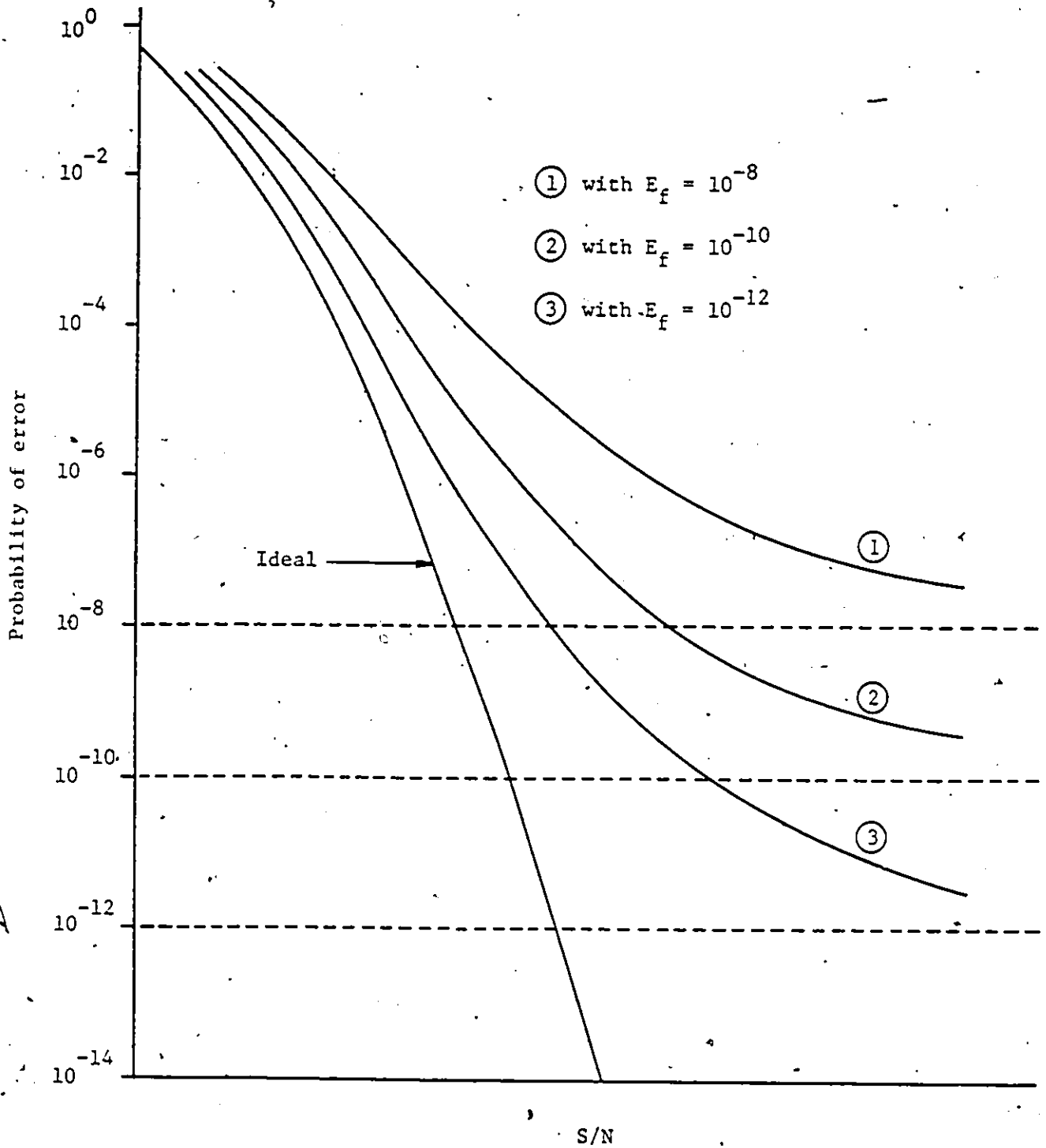


Fig.7:1 Illustrative P_e curves with error floors.

The probability E_f may be regarded as an error floor due to the shortest worst data sequence. This means, even without noise or practically with a very high S/N, the system cannot have a probability of error lower than E_f . To illustrate how error floors affect the P_e curves, a few examples are shown in Fig.7.1. The P_e curves tend to tail off at high S/N. E_f can serve as a means to predict how good a system would be. As a rule of thumb, a system with a lower error floor will be preferred.

The problem of finding L and the corresponding error floor, E_f , with 8-level inputs for Model-A and Model-B was programmed on a computer. The results, based on (7.4), (7.5) and (2.1)-(2.5), are summarized in Table 7.1.

From Table 7.1 we see that the error floors of our new Model-B are much lower than those of the conventional Model-A. For instance, for the same 5% increase above the Nyquist rate, the error floor caused by using our new Model-B is 8.2×10^{-84} whereas it is 6×10^{-8} by using the conventional Model-A. This indicates that our new scheme is better than the conventional method for a practical realization.

7.2 ERROR FLOORS IN PAM SYSTEMS UNDER SEVERE IMPAIRMENTS

Though the previous discussion was mainly to compare the error floors in PRS systems operated above the Nyquist rate using two different models, the concept and method could be extended to the study of other transmission systems. For instance, consider a PAM system under various impairments, such as channel distortions and hardware im-

TABLE 7.1 COMPARISON OF THE SHORTEST LENGTH OF THE WORST DATA SEQUENCE AND THE CORRESPONDING ERROR FLOORS FOR MODEL-A AND MODEL-B WITH 8-LEVEL INPUTS (15-LEVEL OUTPUTS)

%above Nyquist rate	Model-A (conventional model)		Model-B (new model)	
	L	$E_f = 1/8^L$	L	$E_f = 1/8^L$
3%	22	1.3×10^{-20}	686	≈ 0
4%	12	1.4×10^{-11}	206	≈ 0
5%	8	6×10^{-8}	92	8.2×10^{-84}
6%	6	3.8×10^{-6}	60	6.5×10^{-55}
7%	6	3.8×10^{-6}	34	1.9×10^{-31}
8%	6	3.9×10^{-6}	28	5.1×10^{-26}
9%	6	3.8×10^{-6}	22	1.3×10^{-20}

perfections, etc., which is modelled as Fig.7.2. We assume that the distortion is so severe that the system is regarded as failure by the peak eye closure criterion.

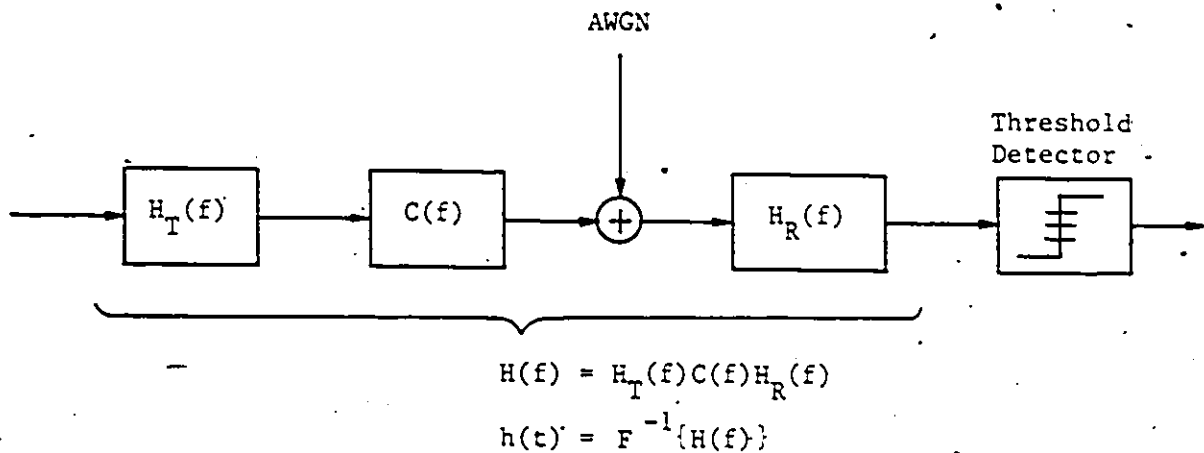


Fig.7.2 A PAM system model.

Let $h(t)$ denote the overall impulse response of the system shown in Fig.7.2, which comprises the transmit and receive filters and other impairments modelled as $C(f)$. Since $h(t)$ may not be always symmetric, it is necessary to modify the previous approach a little bit as the following. The input symbols are assumed to be equiprobable numbers $\pm 1, \pm 3, \dots, \pm(M-1)$. Thus, in the absence of ISI and noise, the signal levels before the threshold detector are $\pm h(0), \pm 3h(0), \dots, \pm(M-1)h(0)$, resulting in a decision distance of $h(0)$. Under the worst case, the ISI components are

$$(M-1) |h(nT_s)|, \quad \begin{matrix} n = -\infty \text{ to } \infty \\ n \neq 0 \end{matrix} \quad (7.8)$$

Let us form a sequence $\{S_i\}_{i=1,2,\dots}$ whose items are obtained by permuting all the ISI samples, shown in (7.8), in a non-decreasing order, i.e.,

$$S_i \geq S_{i+1} \quad \text{for } i = 1, 2, \dots \quad (7.9)$$

Define a distortion series D_N as follows.

$$D_N = \sum_{i=1}^N S_i \quad (7.10)$$

Note that the sequence $\{D_N\}_{N=1,2,\dots}$ is also non-decreasing and

$$\lim_{N \rightarrow \infty} D_N = D_p = (M - 1) \sum_{\substack{n=-\infty \\ n \neq 0}}^{\infty} |h(nT_s)| \quad (7.11)$$

In the event of severe distortions, there may exist a smallest integer number N_1 such that

$$D_{N_1} \geq h(0) \quad (7.12)$$

That is, N_1 is the smallest number of interfering symbols which may close the eye. The probability of occurrence of this particular sequence is M^{-N_1} which may be regarded as the error floor E_f of the system, i.e.,

$$E_f = M^{-N_1} \quad (7.13)$$

The above procedure has allowed us to evaluate error floors in PAM systems under sever distortions as long as we know the system's impulse response, which in general, can be measured practically.

7.3 CONCLUSIONS

A new method has been introduced to evaluate error floors in PRS systems operated above the Nyquist rate. The numerical results show that the error floors of our new Model-B are much lower than those of the conventional Model-A. This rigorously indicates that our new scheme is better than the conventional method for a practical realization.

The concept and method could be extended also to the study of other transmission systems, such as PAM systems with severe distortions. Stated briefly, a new concept has been introduced. That is, systems regarded as failure by the peak eye closure criterion are redefined as systems with error floors by the introduced truncated peak distortion. The error floors may be very small, depending on how severe the distortion is.

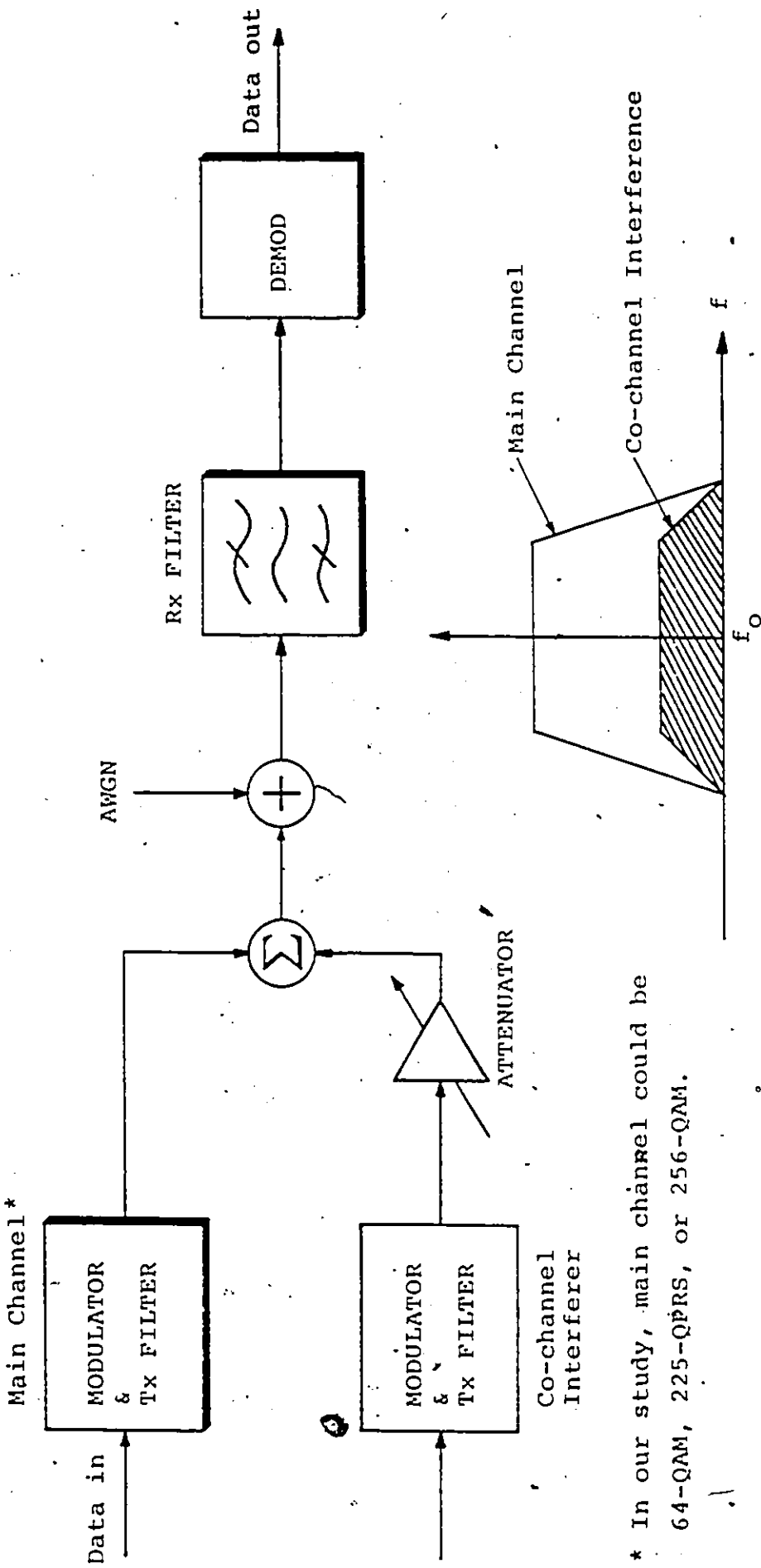
Chapter VIII

THE PERFORMANCE OF 64-QAM AND 225-QPRS AND 256-QAM IN A CO-CHANNEL INTERFERENCE ENVIRONMENT

One way to increase frequency utilization efficiency may be the use of dual polarization operation [42]. However, in a frequency-reuse communication system, co-channel interference (CCI) is one of the major sources of performance impairment [43]-[45]. In this chapter, we study the performance of 64-QAM, 225-QPRS, and 256-QAM in the presence of CCI so that their potential for radio systems could be assessed. Both constant-envelope (sinusoidal) and amplitude-modulated interferers are considered. In the simulation, coherent detection and perfect synchronization are assumed. Measured data for a 256-QAM modem in a CCI environment agree well with the simulated results.

8.1 SYSTEM PARAMETERS AND DESCRIPTION OF THE SIMULATION METHOD

A conceptual co-channel system block diagram is depicted in Fig.8.1 [46]. In this part of our study, we assume that only CCI and thermal noise cause degradation in the system. The main channel signal being considered may be 64-QAM, 225-QPRS, or 256-QAM in the presence of sinusoidal or amplitude-modulated interferers.



* In our study, main channel could be 64-QAM, 225-QPRS, or 256-QAM.

Illustrative frequency spectra of the desired and interfering signals

Fig.8.1 Block diagram of a conceptual co-channel system

For 64- and 256-QAM, the modulated signal without filtering can be represented by the general form:

$$s(t) = \text{Re}\left\{ \sum_n (I_n + jQ_n) g(t-nT_s) e^{j2\pi f_0 t} \right\} \quad (8.1)$$

where

f_0 is the carrier frequency,

$1/T_s$ is the symbol rate,

$g(t)$ is a rectangular pulse defined by

$$g(t) = \begin{cases} 1 & \text{if } 0 \leq t \leq T_s \\ 0 & \text{elsewhere} \end{cases}$$

I and Q are independent and identically distributed

random variables: $I_n, Q_n = \pm 1, \pm 3, \dots, \pm(2N-1)$.

$N = 4$ for 64-QAM; $N = 8$ for 256-QAM.

The transmit and receive filters are assumed as ideal square root of $\alpha = 0.2$ raised-cosine filters with $x/\sin(x)$ equalization in the transmitter so that the whole system satisfies the Nyquist 1st criterion [14].

If the main channel consists of 225-QPRS, the transmitted signal can be written as

$$s(t) = \text{Re}\left\{ \sum_n (I_n + jQ_n) h(t-nT_s) e^{j2\pi f_0 t} \right\} \quad (8.2)$$

where

the duobinary PRS shape $h(t)$ [20] is given by

$$h(t) = \frac{\sin(\pi t/T_s)}{\pi t/T_s} \cdot \frac{1}{1 - t/T_s} \quad (8.3)$$

Note that the center of the duobinary impulse response is at $T_s/2$.

We assume that all the pulse shaping is done at the transmitter, whereas the receive filter merely bandlimits the channel noise. This would result in approximately a 1 dB degradation in C/N, as explained in Appendix A.

Two types of CCI are considered. If the CCI consists of a single sinusoid, the total received signal $r(t)$ can be expressed as

$$r(t) = s_r(t) + K \cos(2\pi f_0 t + \phi) + n(t) \quad (8.4)$$

where

$K^2/2$ is the average power in the sinusoidal CCI,

ϕ is uniformly distributed in $(-\pi, \pi]$,

$s_r(t)$ is the received desired signal,

$n(t)$ is the additive white Gaussian noise.

If the CCI is a single amplitude-modulated signal, we assume that the interferer and the desired signal are of the same format but statistically independent of each other. In other words, we consider 64-QAM with a 64-QAM CCI, 225-QPRS with a 225-QPRS CCI, and the like. For 64-, and 256-QAM interferers, the transmitted interfering signal without filtering can be modelled

$$i(t) = K \operatorname{Re} \left\{ \sum_n (\tilde{I}_n + j\tilde{Q}_n) g(t - nT_s - \tau) e^{j(2\pi f_0 t + \phi)} \right\} \quad (8.5)$$

In the case of 225-QPRS interferer, the transmitted signal is

$$i(t) = K \operatorname{Re} \left\{ \sum_n (\tilde{I}_n + j\tilde{Q}_n) h(t - nT_s - \tau) e^{j(2\pi f_0 t + \phi)} \right\} \quad (8.6)$$

In (8.5) and (8.6), \tilde{I}_n , \tilde{Q}_n , $g(t)$, $h(t)$, T_s , and f_0 are defined as in (8.1) and (8.2). τ is the difference in symbol timing between the desired signal and interferer and is assumed to be uniformly distributed in $(0, T_s)$. ϕ is a random phase angle uniformly distributed in $(-\pi, \pi]$. $1/K^2$ is the carrier-to-interference ratio, C/I .

For a fixed C/I , the probability of error is calculated by computer simulations using the similar steps in [8], [36] and Chapter 5 for randomly selected ϕ and τ . To obtain a meaningful result, we average the probability of error for several sets of ϕ , τ , and data sequences.

8.2 SIMULATED RESULTS AND DISCUSSIONS.

The probability of error performances for 64-QAM, 225-QPRS, and 256-QAM with a single sinusoidal CCI are shown in Figs. 8.2-8.4, respectively. The parameter C/I is the ratio of the average power in the desired main channel signal to the average power in the CCI. The quantity C/N represents the ratio of the average power in the desired signal to the noise power. Since a system designer often wants to maintain a specified error rate even when there is interference, the increase in C/N required to maintain an error rate of 10^{-6} is plotted in Fig. 8.5.

The error probability of 64-QAM ($\alpha = 0.2$) with a 64-QAM ($\alpha = 0.2$) CCI is plotted in Fig. 8.6. For 225-QPRS with a 225-QPRS CCI, the error probability is shown in Fig. 8.7. In Fig. 8.8, we present the results for 256-QAM ($\alpha = 0.2$) with a 256-QAM ($\alpha = 0.2$) CCI. Fig. 8.9 compares the increase in C/N required to maintain an error rate of 10^{-6} for the three modulation schemes. The results in Figs. 8.5 and 8.9 are con-

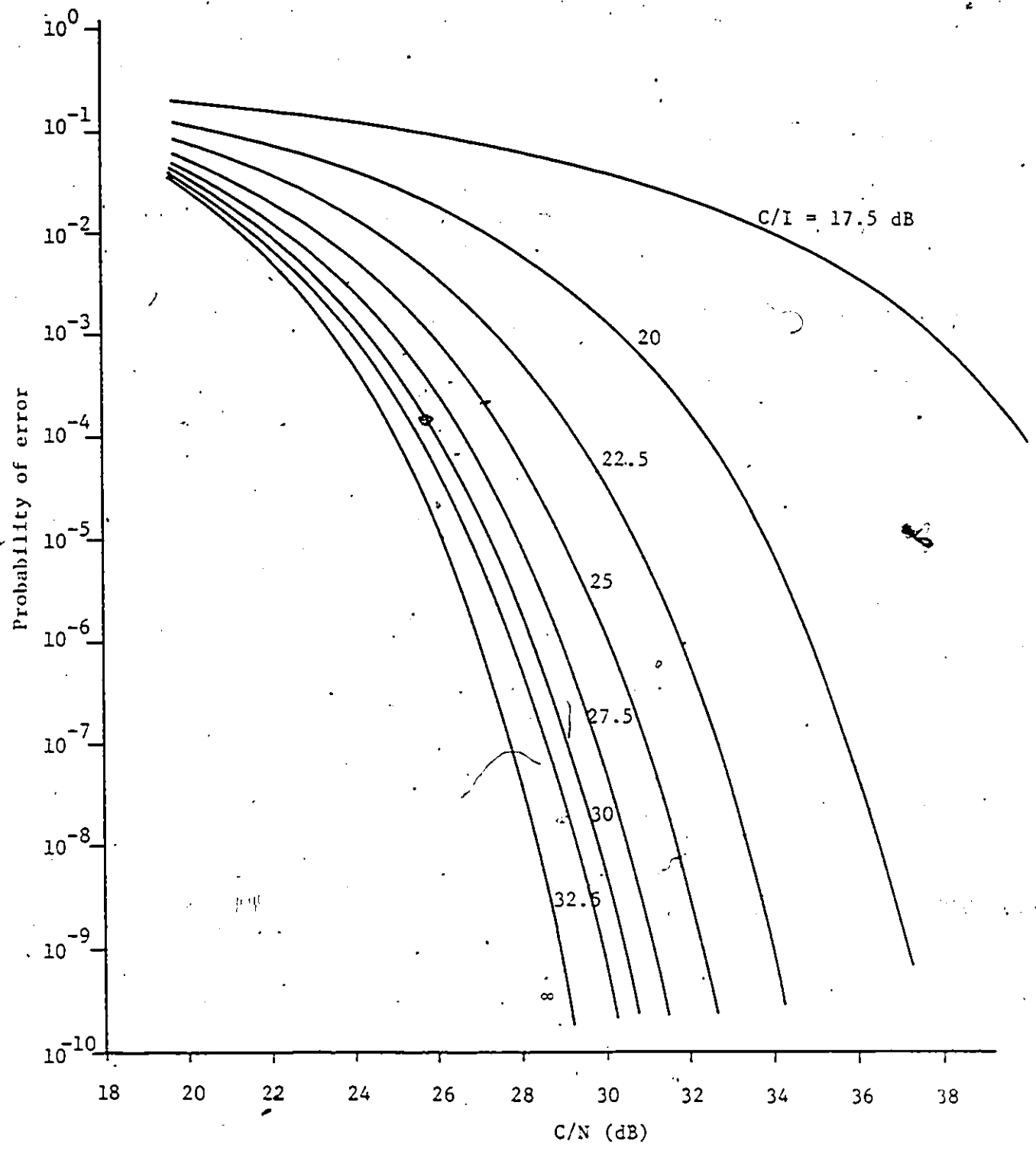


Fig. 8.2 Error probability of 64-QAM ($\alpha = 0.2$) with a single sinusoidal CCI. The parameter C/I is the ratio of the average carrier power to the average power in the interference. The quantity C/N represents the ratio of the average carrier power to the noise power.

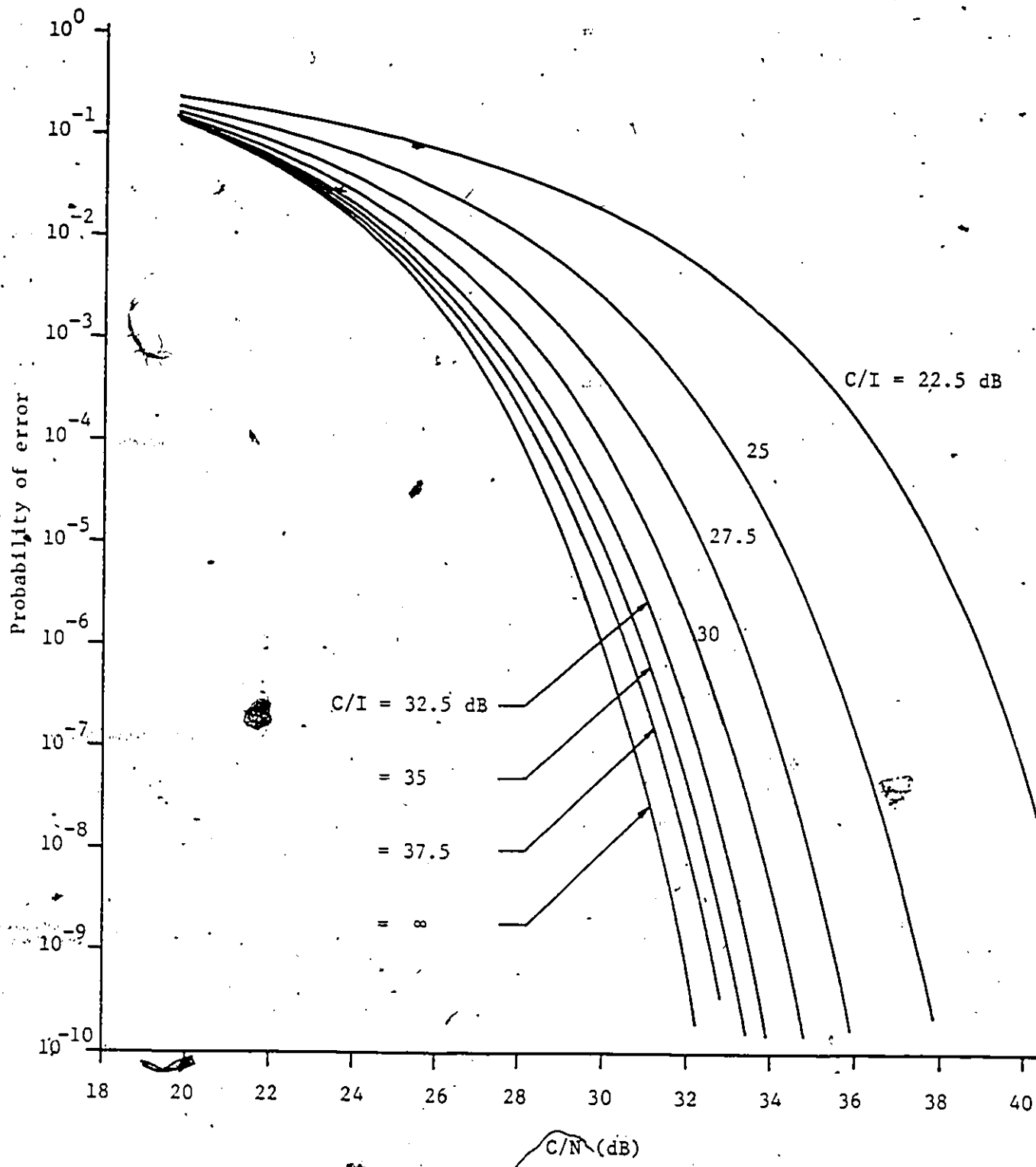


Fig.8.3 Error probability of 225-QPRS with a single sinusoidal CCI.

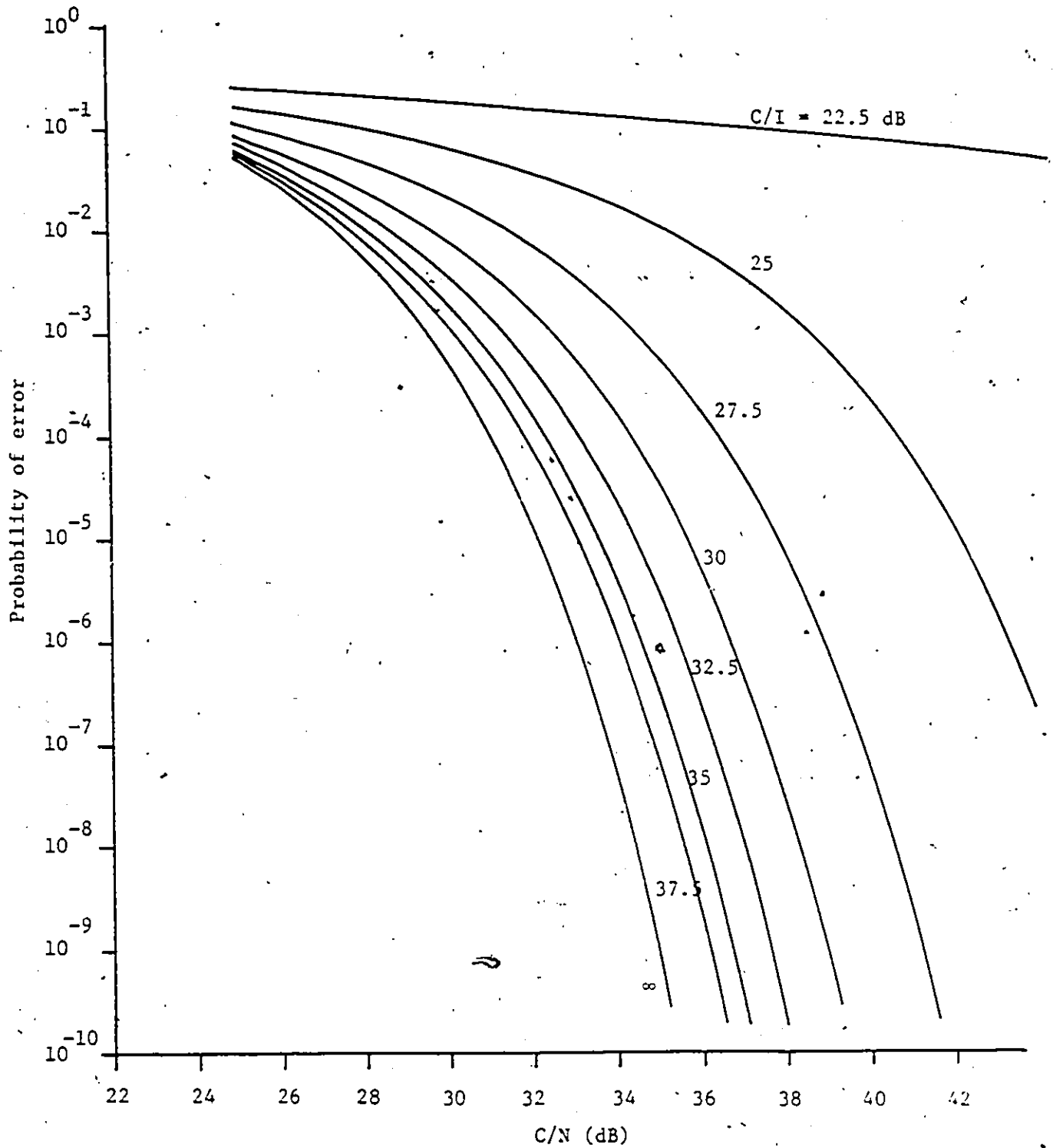


Fig.8.4 Error probability of 256-QAM ($\alpha = 0.2$) with a single sinusoidal co-channel interference.

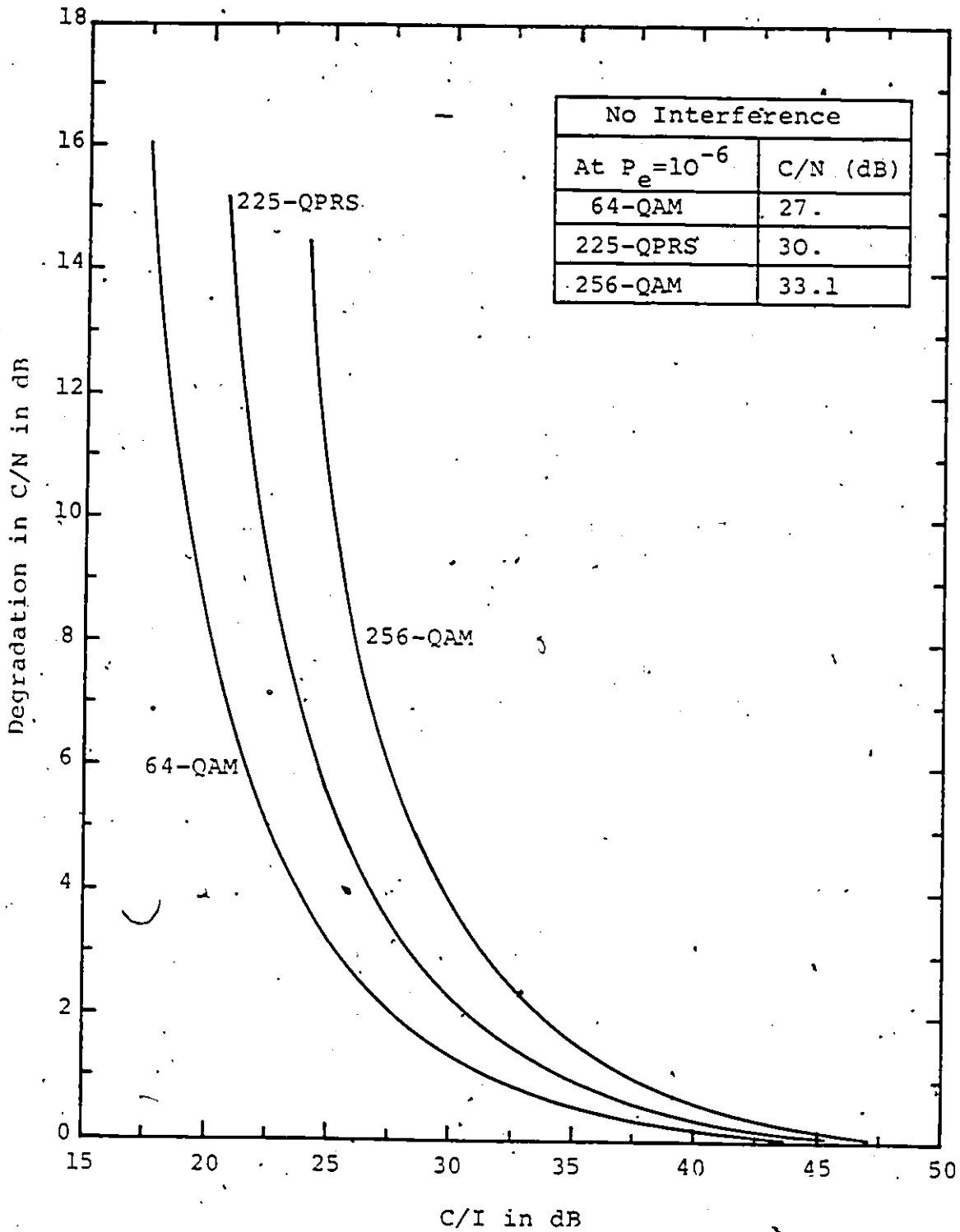


Fig.8.5 Degradation in C/N for 64-, 256-QAM ($\alpha = 0.2$), and 225-QPRS with a single sinusoidal CCI.

The ordinate represents the increase in C/N to maintain an error rate of 10^{-6} .

firmed to agree with those of Prabhu's [43] and of Borgne's [13] for 64-QAM.

Comparing Figs. 8.5 and 8.9, we observe that the amplitude-modulated CCI produces more degradation than the single sinusoidal CCI for the three modulation schemes considered. This can easily be perceived by comparing the peak value of the interference for the same power. For example, if $A^2/2$ is the average power in the interferer, the peak value for the single sinusoid is A ; for a QAM interferer (assume no filtering for simplicity) it is $A(2N-1)[3/(4N^2-1)]^{1/2}$ [44], where $N = 4$ for 64-QAM and $N = 8$ for 256-QAM. That is, the peak value for a 64-QAM CCI is $7/\sqrt{21} = 1.527$ times that of a sinusoidal CCI for the same power; and for 256-QAM CCI it is $15/\sqrt{85} = 1.627$ times. The peak amplitude of the CCI reduces the minimum half-distance of any two signal levels. Thus, the degradation with an amplitude-modulated CCI is higher than with a sinusoidal CCI.

8.3 EXPERIMENTAL RESULTS

To confirm the simulated results, the performance of a 256-QAM modem in the presence of CCI was experimentally measured [46]. The 256-QAM modem was designed to transmit a 1.6 Mb/s data stream in a 240 kHz SG band. Illustrative results are shown in Fig. 8.10. Note that the back-to-back modem through two SG filters has approximately a 1.3 dB degradation in C/N at $P_e = 10^{-6}$ with respect to the theoretical value when there is no CCI.

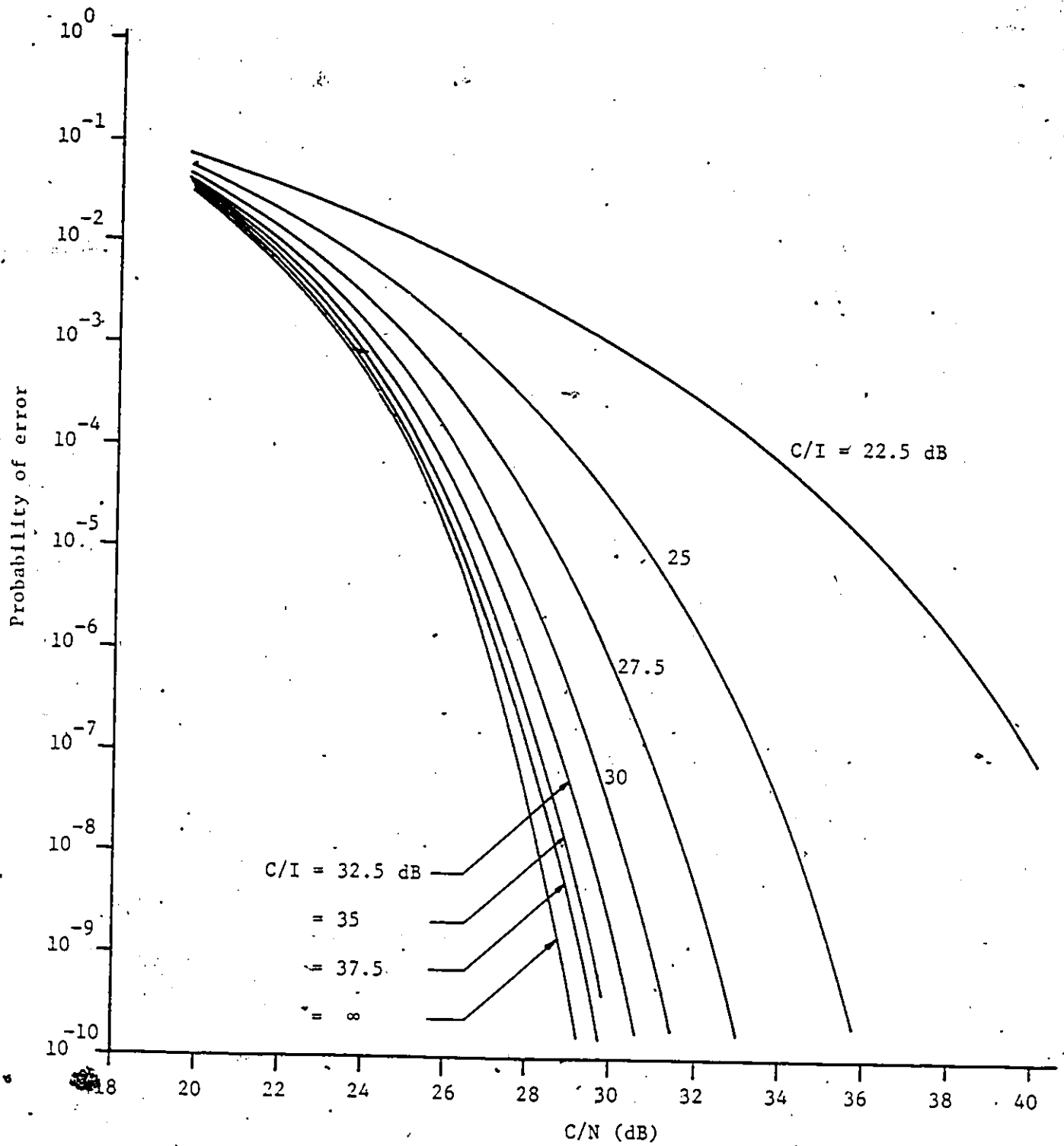


Fig.8.6 Error probability of 64-QAM ($\alpha = 0.2$) with a 64-QAM ($\alpha = 0.2$) CCI.

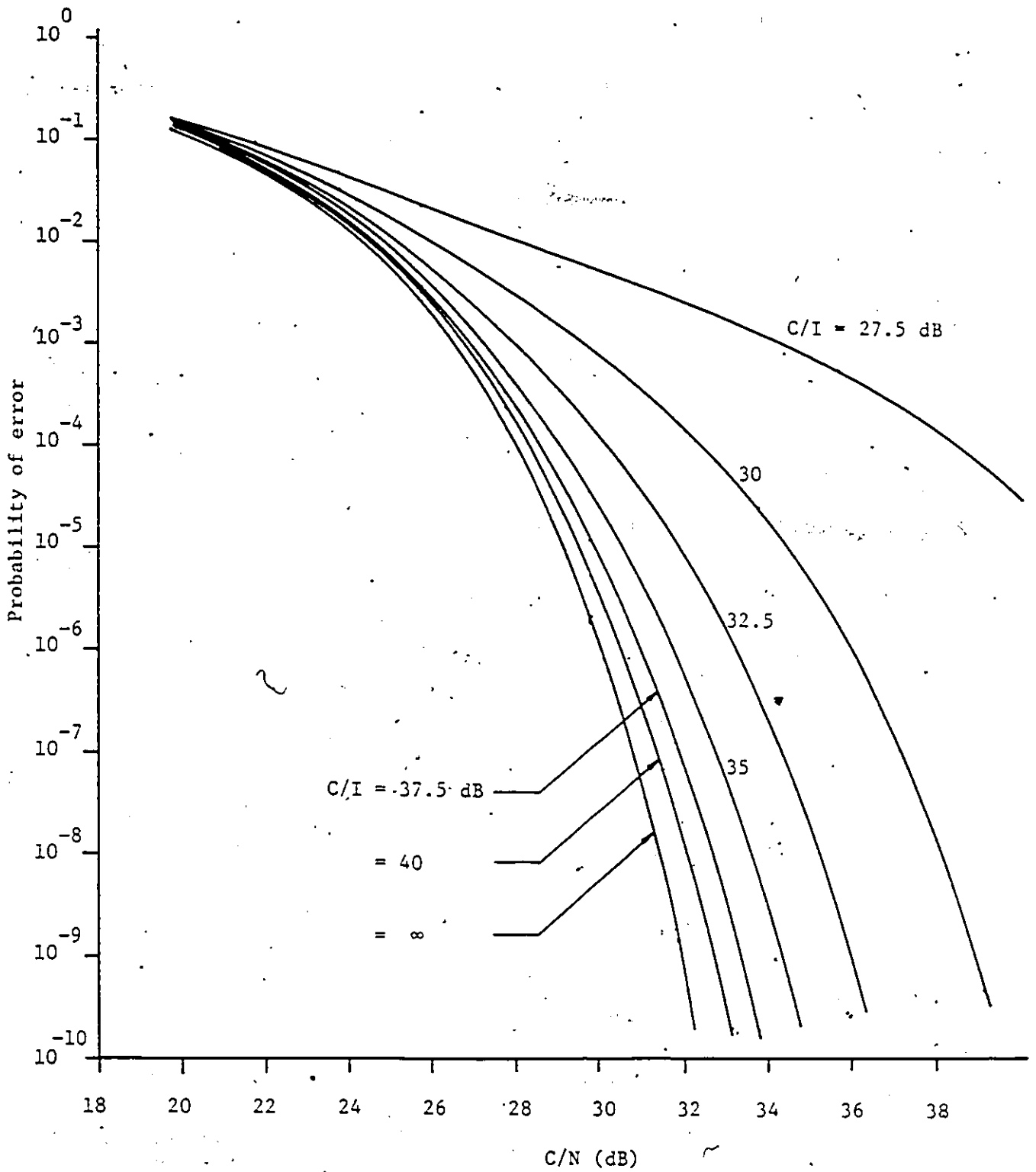


Fig.8.7 Error probability of 225-QPRS with a 225-QPRS CCI.

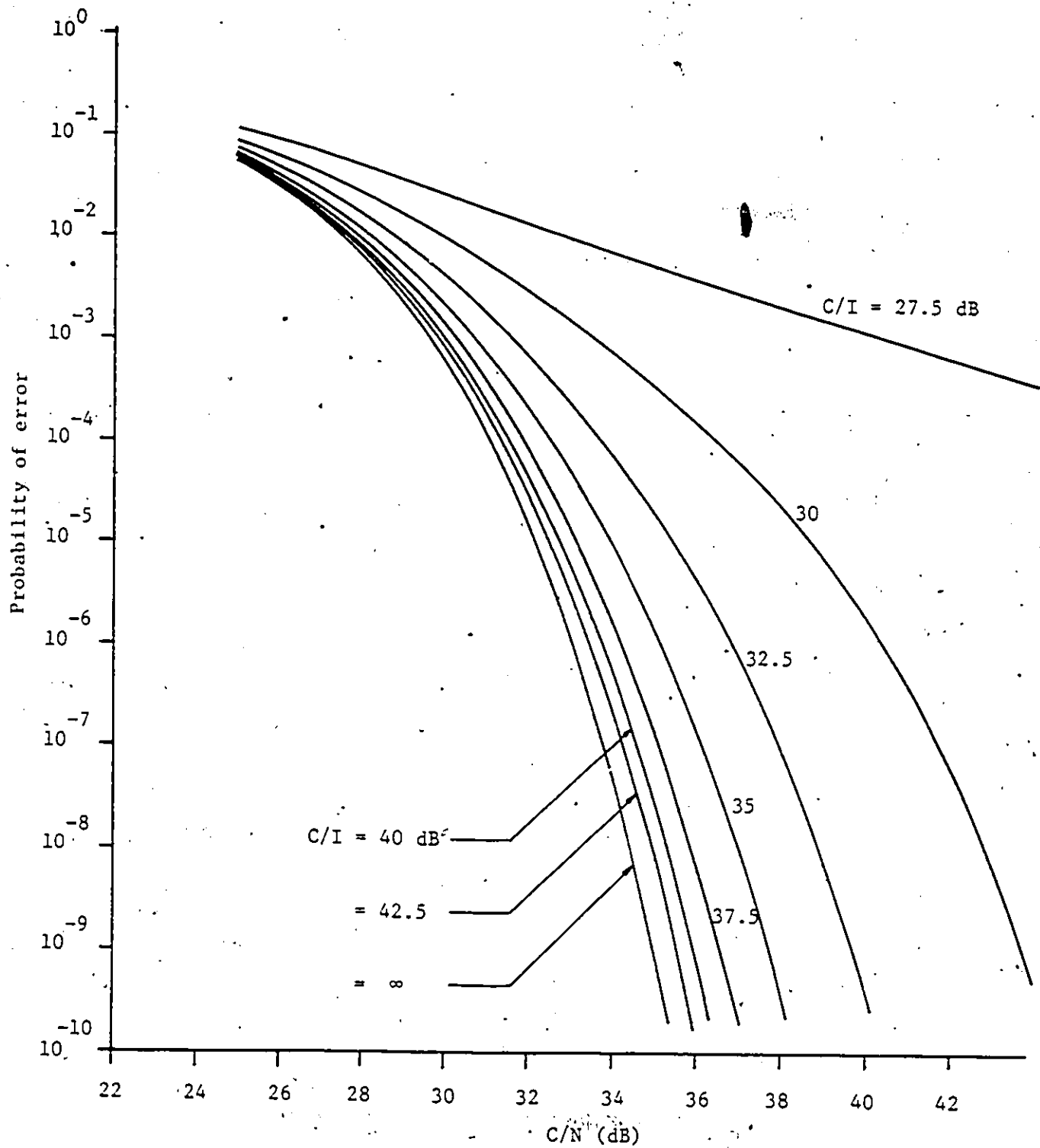


Fig.8.8 Error probability of 256-QAM ($\alpha = 0.2$) with a 256-QAM ($\alpha = 0.2$) CCI.

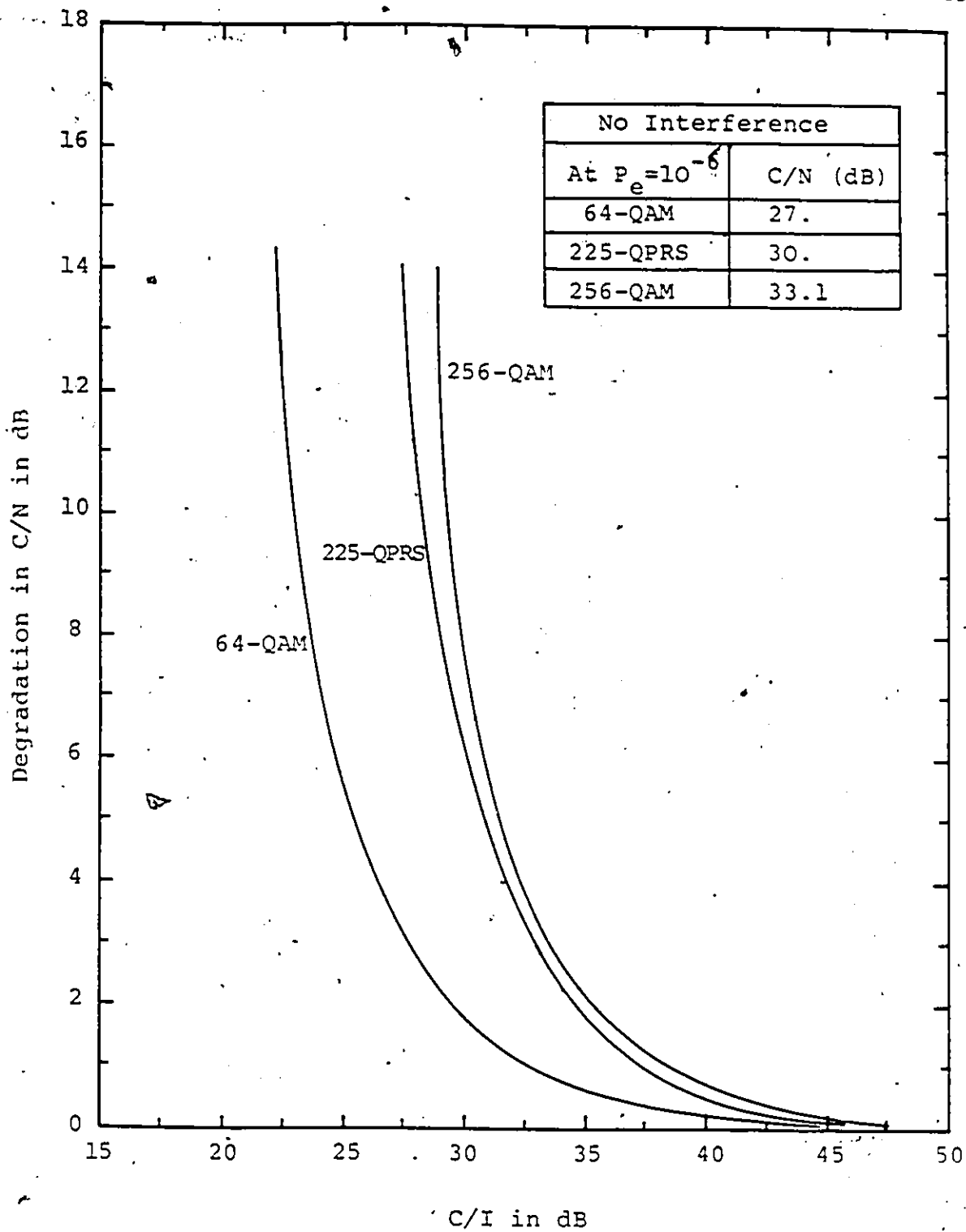


Fig.8.9 Degradation in C/N for 64-, 256-QAM ($\alpha = 0.2$), and 225-QPRS with an amplitude-modulated co-channel interference which has the same format as the desired signal, e.g., 64-QAM with a 64-QAM CCI, etc. The ordinate represents the increase in C/N to maintain an error rate of 10^{-6} .

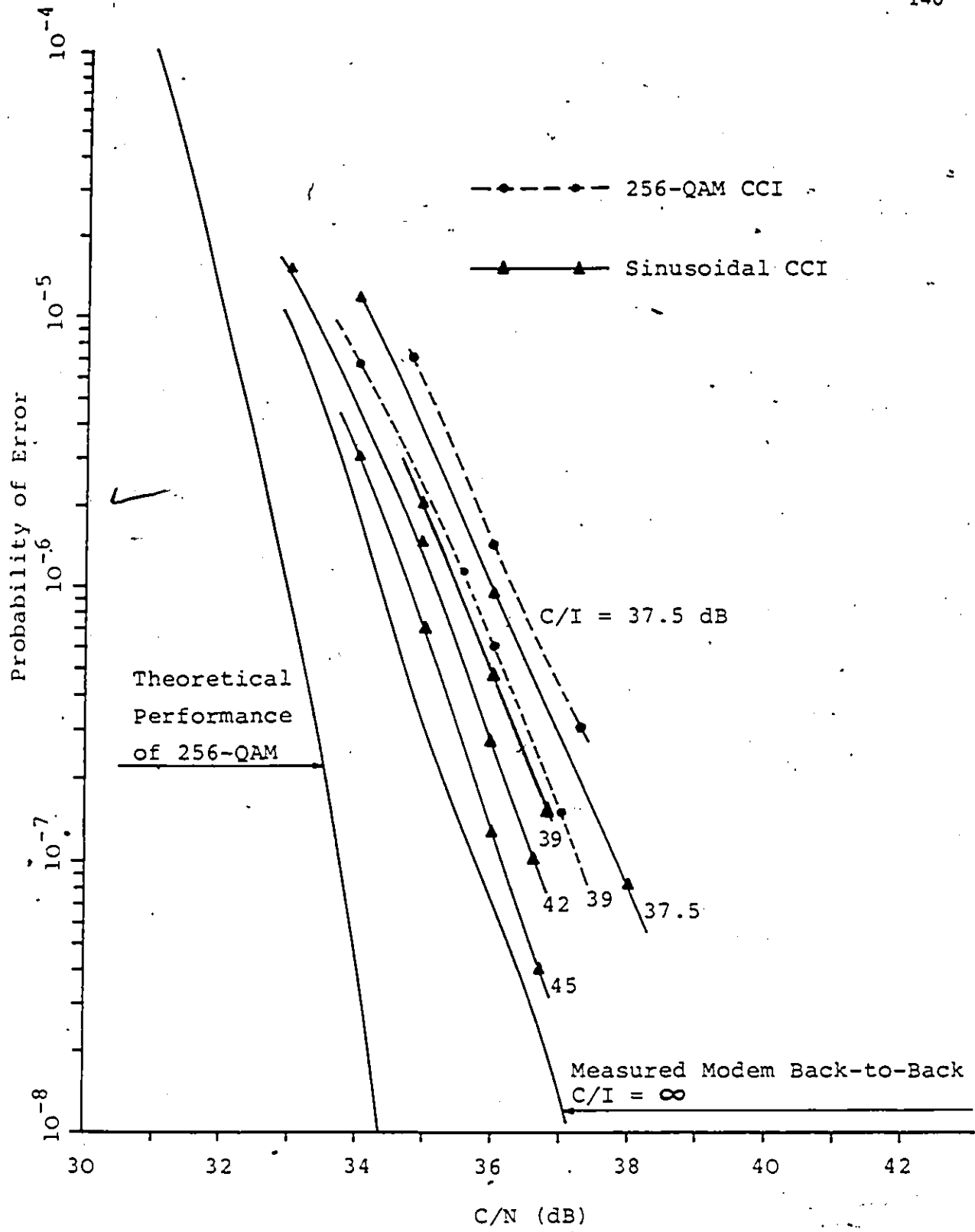


Fig.8.10 Measured performance of a 256-QAM modem in the presence of co-channel interference. The 256-QAM modem was designed to transmit 1.6 Mb/s data in a supergroup bandwidth of 240 kHz.

The measured data show more degradations than those in Figs. 8.4 and 8.8 in which an ideal modem was assumed. This is because that, due to hardware and filters imperfections, the 256-QAM signal itself contains ISI which reduces the minimum distance between adjacent signal levels and in turn causes the signal to be more susceptible to degradation caused by CCI. For example, for a sinusoidal CCI, at $P_e = 10^{-6}$ and $C/I = 37.5$ dB the required C/N is 36 dB from the measured data (Fig. 8.10), whereas it is 34 dB from Fig. 8.4. The difference of 2 dB in C/N is caused by hardware and filters imperfections. Therefore, the measured data generally show a good agreement with the simulated results.

8:4 CONCLUSIONS

For an error rate of 10^{-6} , the required C/N for 64-QAM, 225-QPRS and 256-QAM are 27, 30, and 33.1 dB, respectively when there is no interference. When there is an amplitude-modulated CCI with $C/I = 28.75$ dB, the degradation in C/N for 64-QAM, 225-QPRS, and 256-QAM are 2.3, 8.5, and 13 dB, respectively. In particular, degradations in 225-QPRS and 256-QAM increase dramatically when C/I becomes less than 40 dB. Measured data for a 256-QAM modem in a CCI environment are in good agreement with the simulated results. We conclude that to make dual polarization operation feasible for high-level modulation schemes, such as 225-QPRS and 256-QAM, a cross polarization discrimination of better than 40 dB is required since these systems are also sensitive to other impairments.

Chapter IX

AN ADAPTIVE BASEBAND EQUALIZER FOR 256-QAM
OVER DISTORTED CHANNELS

It is shown in Chapter 5 that 256-QAM is relatively sensitive to channel distortions. The design of filters must be made very carefully. However, in some cases, such as carrying digital data over existing analog cable and radio networks, the channel-protection filter cannot be removed [17]. Even if one could design a perfect modem, this channel filter will still cause performance degradation.

On the other hand, all digital radio systems, no matter what modulation method is used, suffer the variations of the propagation medium characteristics which occur during selective fading. Usually, in the design of the transmission channel, no ISI is the major aim. The desired amplitude and phase characteristics of the channel are obtained by means of filters in the transmitter and receiver, whose synthesis is made with reference to normal propagation conditions, i.e., only one ray from the transmitting antenna to the receiving one. In the presence of multiple paths, during selective fading, the behavior of the propagation medium shows notable variations which produce ISI in the signal. This ISI, in some propagation conditions, can cause system unavailability. Under these circumstances, adaptive equalizers [47]-[52] can be used to meet design objectives.

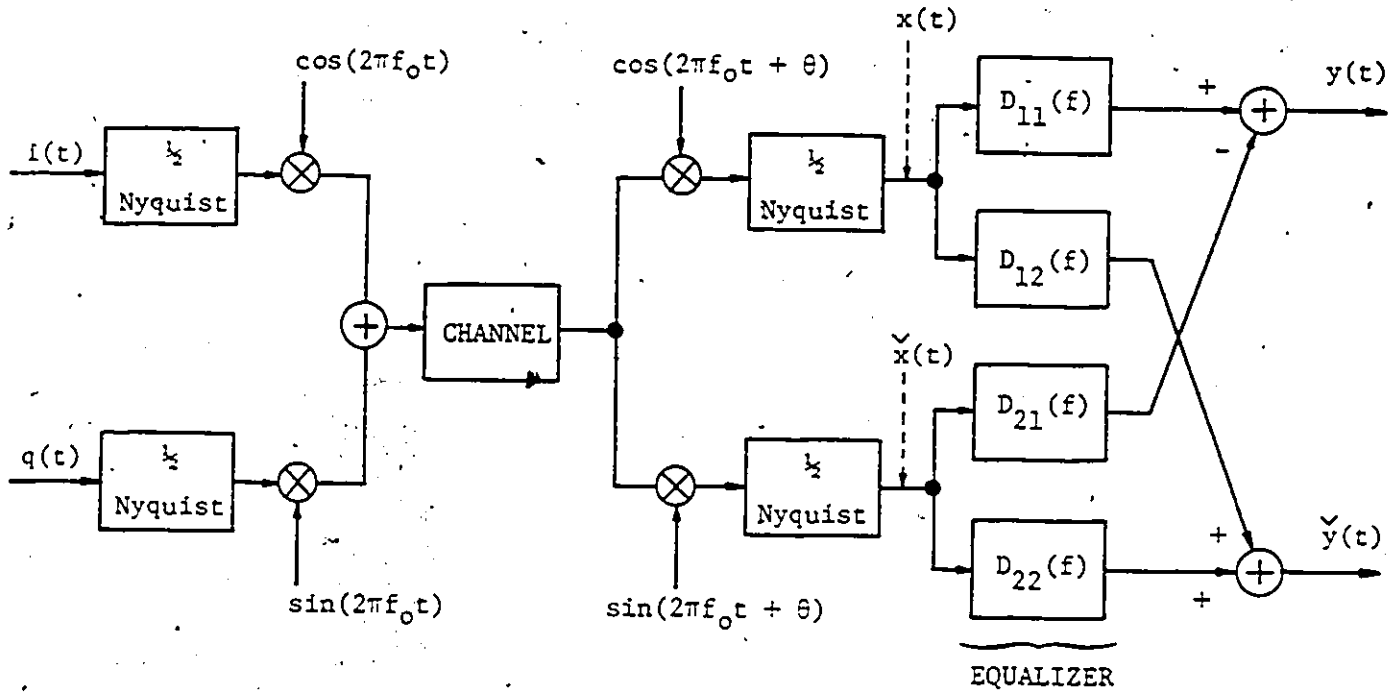
In this chapter, we shall study the possibility of using a baseband complex adaptive equalizer for 256-QAM to combat channel distortions. The function and structure of the equalizer will be described first. Then the computer simulated results for certain distortion conditions will be presented.

9.1 FUNCTIONAL DESCRIPTION OF THE EQUALIZER

The equalizer structure employed for 256-QAM is similar to that described in [47] for 16-QAM. Fig.9.1 depicts the block diagram of a 256-QAM system with $\alpha = 0.2$ raised-cosine filters equally split between the transmitter and receiver. First, it is important to see how the equalizer structure is constructed. It is convenient to represent the in-phase (I) and quadrature (Q) channel lowpass filter output signals in Fig.9.1 by $x(t)$ and $\check{x}(t)$ as the real and imaginary parts of a complex-value signal. (Note that the signals are real, but it will be convenient to use complex notation.) The baseband equalizer with a complex transfer function $D(f) = D_1(f) + j D_2(f)$ produces a complex equalized signal $y(t) + j \check{y}(t)$ as shown in Fig.9.2.

The function of the equalizer is the multiplication of $[X(f) + j \check{X}(f)]$ and $[D_1(f) + j D_2(f)]$, i.e.,

$$\begin{aligned}
 & \{X(f) + j\check{X}(f)\} \{D_1(f) + jD_2(f)\} \\
 &= X(f)D_1(f) - \check{X}(f)D_2(f) + j\{\check{X}(f)D_1(f) + X(f)D_2(f)\} \\
 &= Y(f) + j\check{Y}(f) = \mathcal{F}\{y(t) + j\check{y}(t)\} \quad (9.1)
 \end{aligned}$$



$$i(t) = \sum_n I_n \delta(t - nT_s)$$

$$q(t) = \sum_n Q_n \delta(t - nT_s)$$

$$I_n \text{ and } Q_n \in \{ \pm 1, \pm 3, \dots, \pm 15 \}$$

Fig.9-1 Block diagram of a 256-QAM system with a complex baseband equalizer.

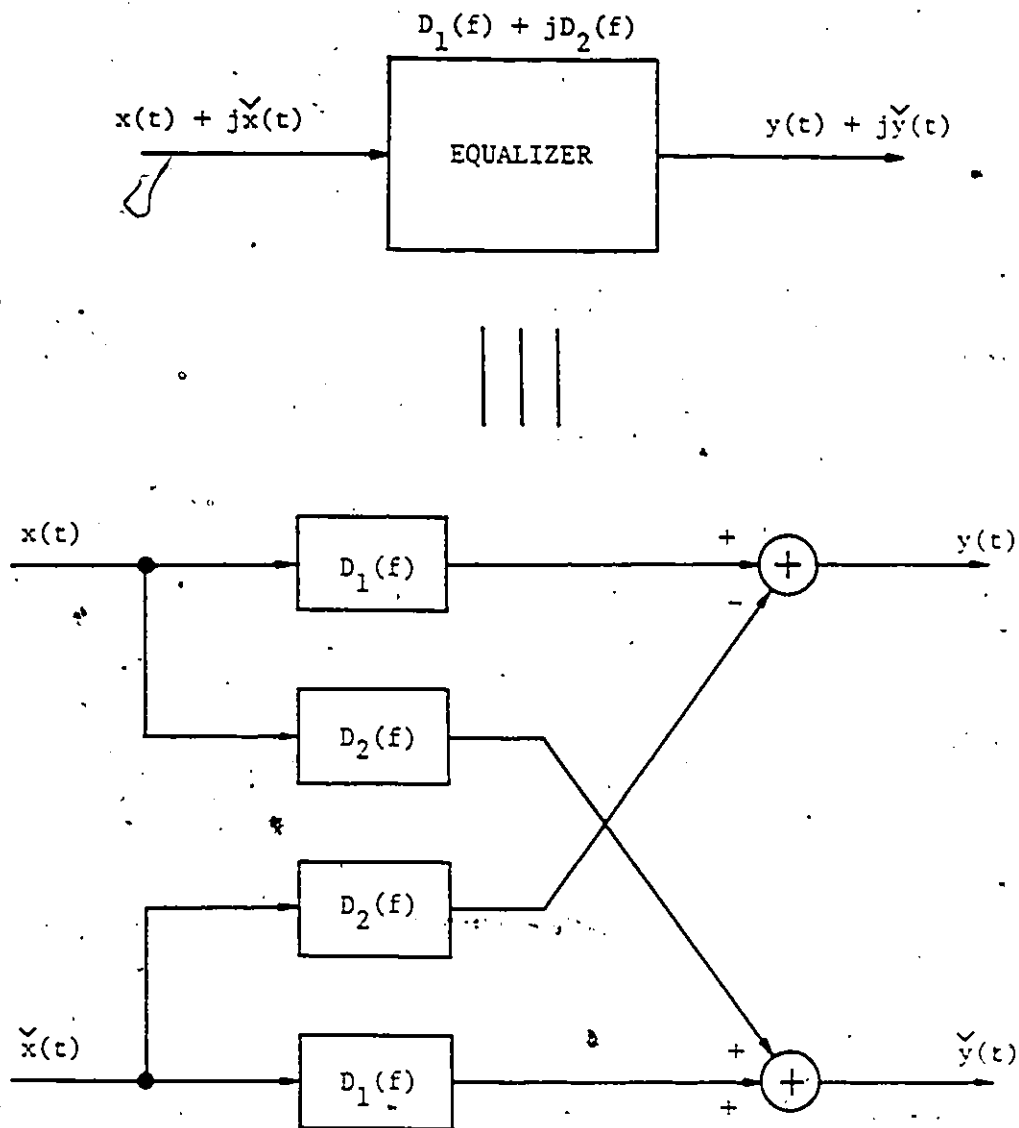


Fig.9.2 Complex transversal equalizer for QAM modems.

where

$y(t)$ and $\tilde{y}(t)$ are the equalized I and Q-channel signals.

Fig.9.2 and eq.(9.1) illustrate more concretely the concept of a complex equalizer as a set of four real baseband filters (with cross-coupling) for two inputs and two outputs. In practice, due to hardware imperfection, the combination of the receive filter and the equalizer in the I-channel may not be exactly identical to that in the Q-channel. Moreover, the channel distortion may not be always symmetric about the carrier frequency. In both cases, the introduced crosstalk from I-channel to Q-channel is not the same as that from Q-channel to I-channel. This suggests that it is better to have four different baseband equalizers in order to have a better control in reducing the ISI and crosstalk. This also explains the use of notations $D_{11}(f)$, $D_{12}(f)$, $D_{21}(f)$, and $D_{22}(f)$ in Fig.9.1. What is more, the implementation of the structure shown in Fig.9.1 is not more complicated than that of Fig.9.2. Because of hardware simplicity, the equalizer chosen is a linear tapped-delay-line transversal structure described by

$$D_{11}(f) = \sum_i c_{i,I} e^{-j2\pi n f T_s} \quad (9.2)$$

$$D_{12}(f) = \sum_i d_{i,I} e^{-j2\pi n f T_s} \quad (9.3)$$

$$D_{21}(f) = \sum_i d_{i,Q} e^{-j2\pi n f T_s} \quad (9.4)$$

$$D_{22}(f) = \sum_i c_{i,Q} e^{-j2\pi n f T_s} \quad (9.5)$$

A 5-tap adaptive transversal equalizer is depicted in Fig.9.3 for illustration. The number of taps can easily be changed in the simulation.

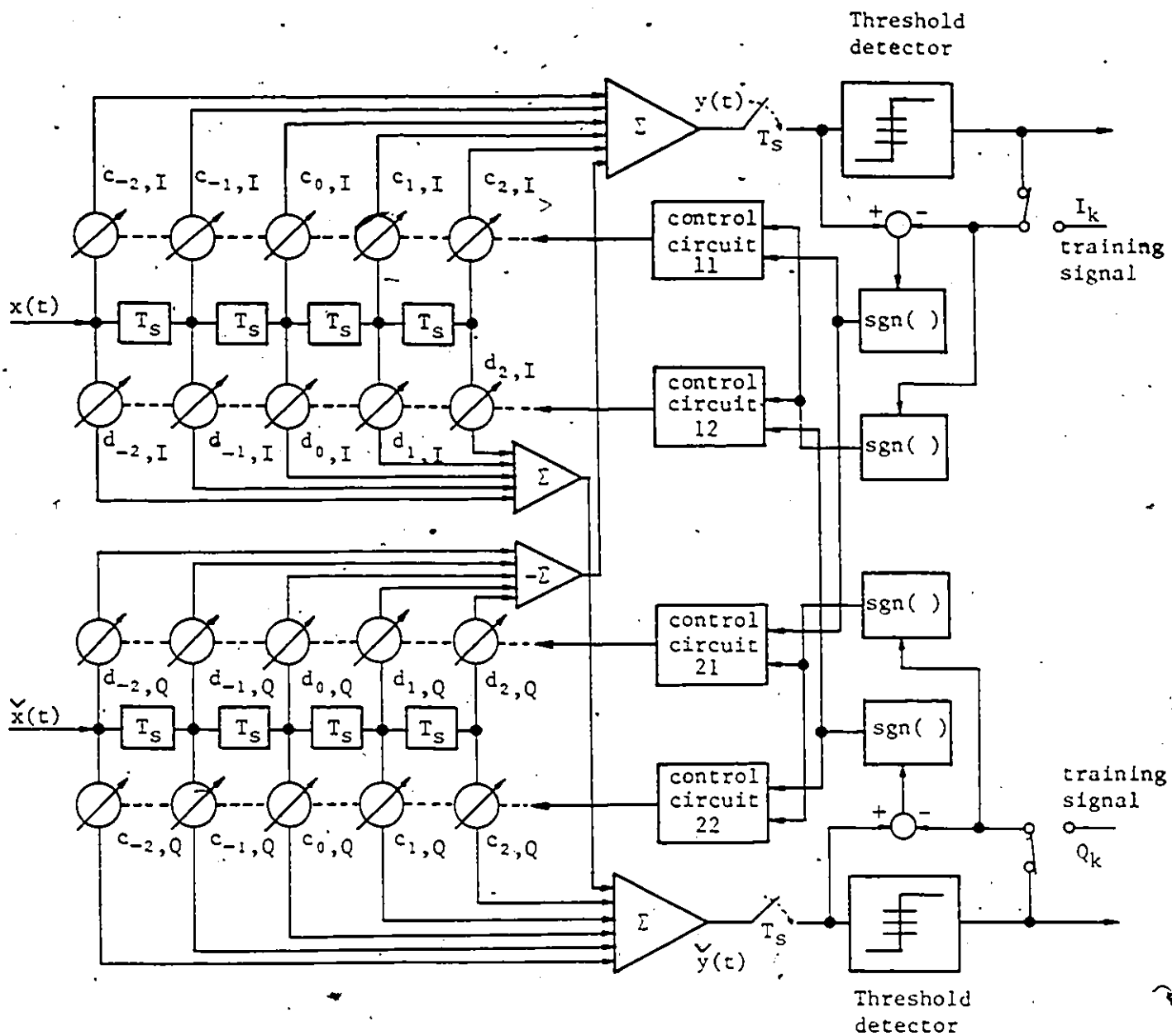


Fig.9.3 An illustrative structure of a 5-tap complex baseband adaptive equalizer for QAM systems.

In Figs. 9.1 and 9.3, let y_k and \check{y}_k be the samples of the output of the equalizer for the I- and Q-channel signals, respectively. The tap-weight adjustment algorithm is governed by the following equations (for the i -th tap-weight at the k -th symbol interval):

$$c_{i,I}^{(k+1)} = c_{i,I}^{(k)} - \Delta \text{sgn}(e_k) \text{sgn}(y_{k-i}) \quad (9.6)$$

$$c_{i,Q}^{(k+1)} = c_{i,Q}^{(k)} - \Delta \text{sgn}(\check{e}_k) \text{sgn}(\check{y}_{k-i}) \quad (9.7)$$

$$d_{i,I}^{(k+1)} = d_{i,I}^{(k)} - \Delta \text{sgn}(\check{e}_k) \text{sgn}(y_{k-i}) \quad (9.8)$$

$$d_{i,Q}^{(k+1)} = d_{i,Q}^{(k)} - \Delta \text{sgn}(e_k) \text{sgn}(\check{y}_{k-i}) \quad (9.9)$$

where $\{c_{i,I}, d_{i,I}\}$ are tap-weights associated with the I-channel tapped delay line and $\{c_{i,Q}, d_{i,Q}\}$ are with the Q-channel tapped delay line. Δ is the tap-weight incremental step size, and $e_k = y_k - I_k$, $\check{e}_k = \check{y}_k - Q_k$ represent the errors between the equalized and the transmitted samples for the I- and Q-channels, respectively. Implementation of (9.6)-(9.9) makes possible not only the minimization of the ISI but also the suppression of the crosstalks between the I and Q channels.

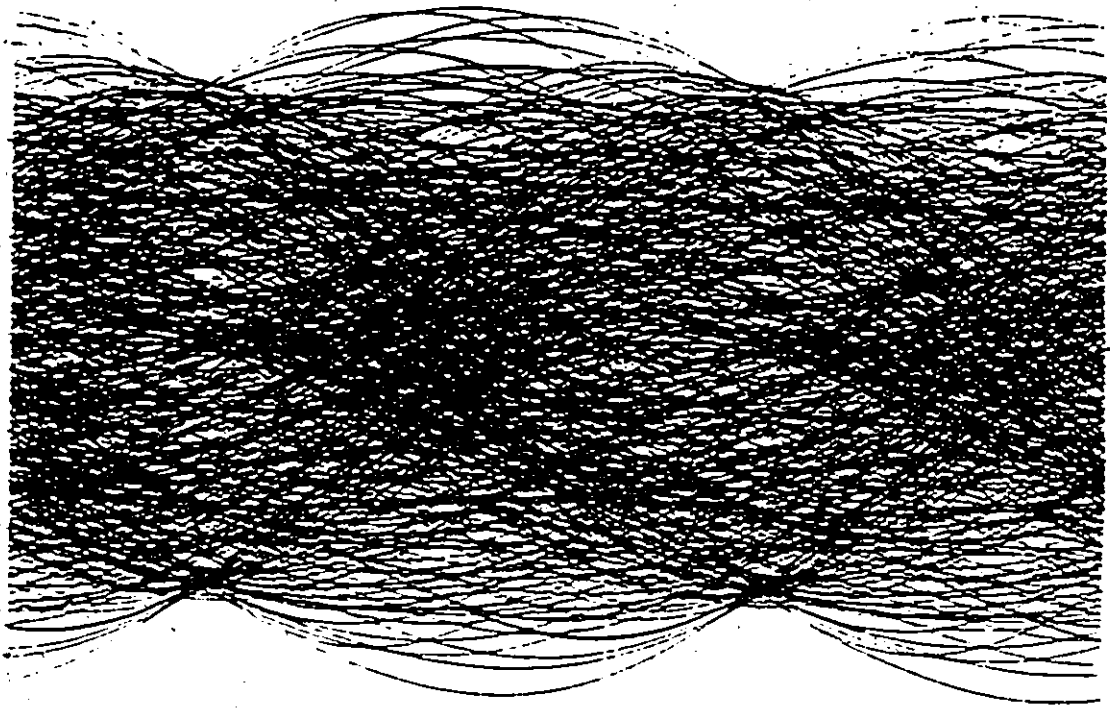
9.2 EQUALIZER PERFORMANCE

In this section, the equalizer performance is demonstrated by some typical results obtained by computer simulations. A bit rate of 120 Mb/s, which is equivalent to a symbol rate of 15-MBaud, is used in the simulation. The results can be applied to another bit rate by appropriate scaling, as previously described in Chapter 5. A training procedure

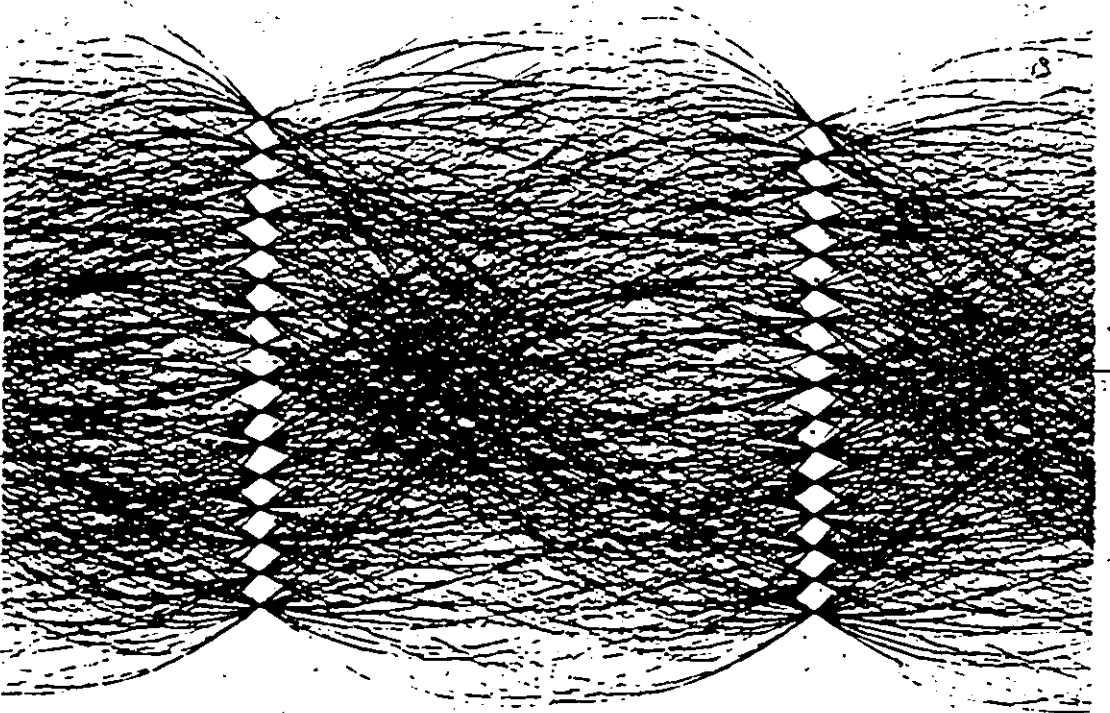
is used for fast convergence of the equalizer's tap coefficients and it is found that a training sequence of 2048 symbols is sufficient for ensuring convergence. A step size of 0.0001 was used in obtaining all the results presented in this section. This value was found to be most favorable after trying several different values for the step size.

First, we present a few eye diagrams which illustrate the powerfulness of the equalizer. For a channel distortion network which introduces a parabolic group delay distortion described by (5.7) with $P_D = 0.81$ ns/MHz², the eye diagrams before and after the equalizer are shown in Fig.9.4(a) and (b), respectively. We see that the equalizer opens the multi-level eyes which were completely closed before the equalizer. Fig.9.5 compares the eye diagrams before and after the equalizer for 256-QAM ($\alpha = 0.2$) with a sinusoidal group delay channel distortion described by (5.7) with $S_D = 12$ ns and $K = 4$.

We notice that significant ISI exists in the eye diagram before the equalizer and the equalizer effectively eliminates the ISI caused by the channel distortion. The error rate performance for a parabolic group delay distortion with $P_D = 0.81$ ns/MHz² is shown in Fig.9.6. Without the equalizer, the received signal cannot be decoded. The equalizer brings back the result (curve A) pretty close to the ideal curve. The small degradation is due to the finite taps of the equalizer which in turn yields a residual ISI. It is found that, in this case, a 31-tap adaptive equalizer is needed for 256-QAM to combat the channel distortion. Also shown in Fig.9.6 is curve B for a 15-tap equalizer in which the residual ISI is higher so that the performance is worse than curve



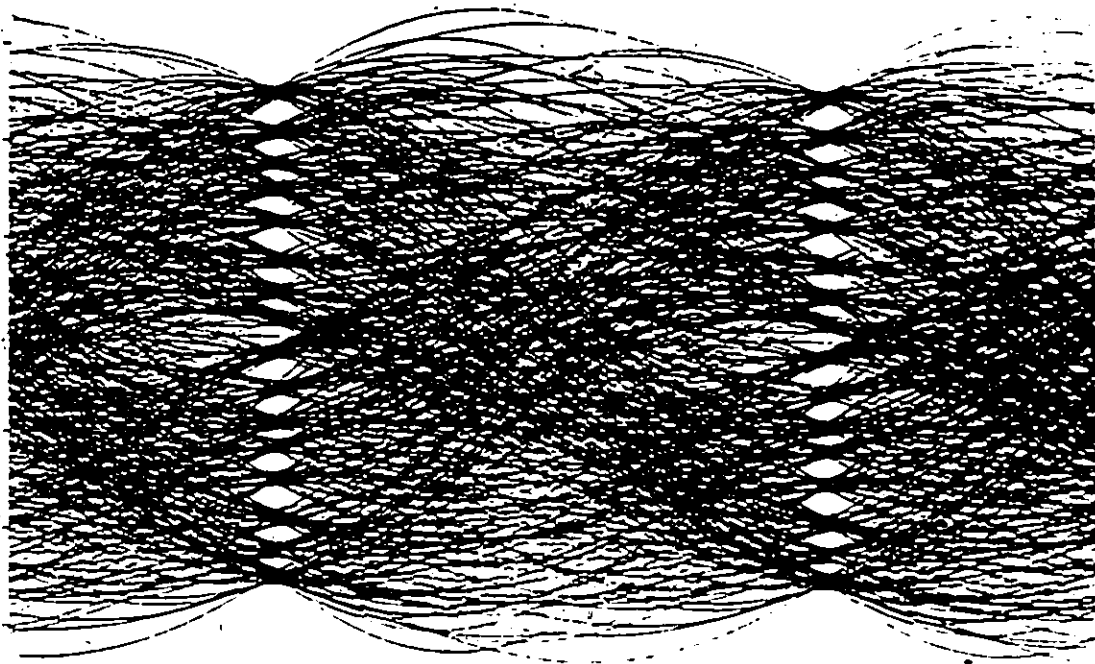
(a) Before equalization.



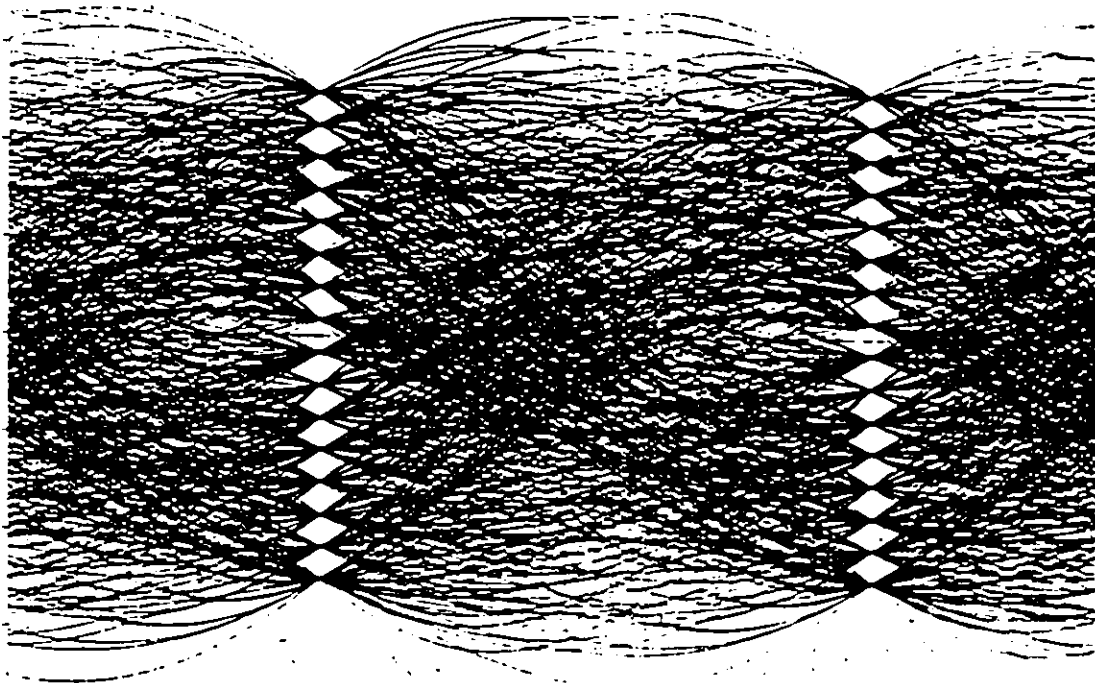
(b) After equalization..

Fig.9.4 Eye diagrams of 256-QAM ($\alpha = 0.2$) with a parabolic group delay distortion, $P_D = 0.81 \text{ ns/MHz}^2$. Bit rate = 120 Mb/s.

(a) Before equalization, (b) After equalization.



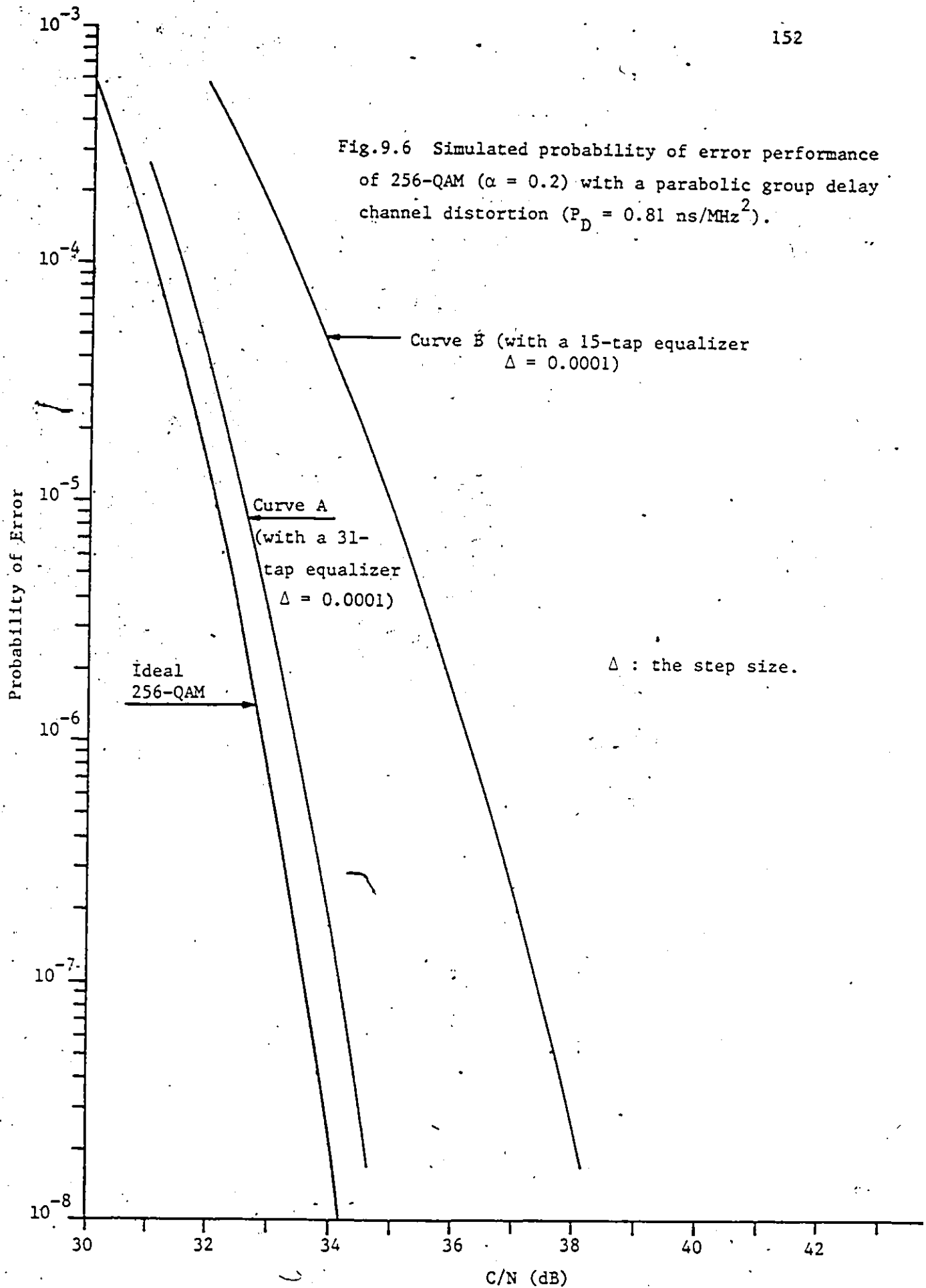
(a) Before equalization.

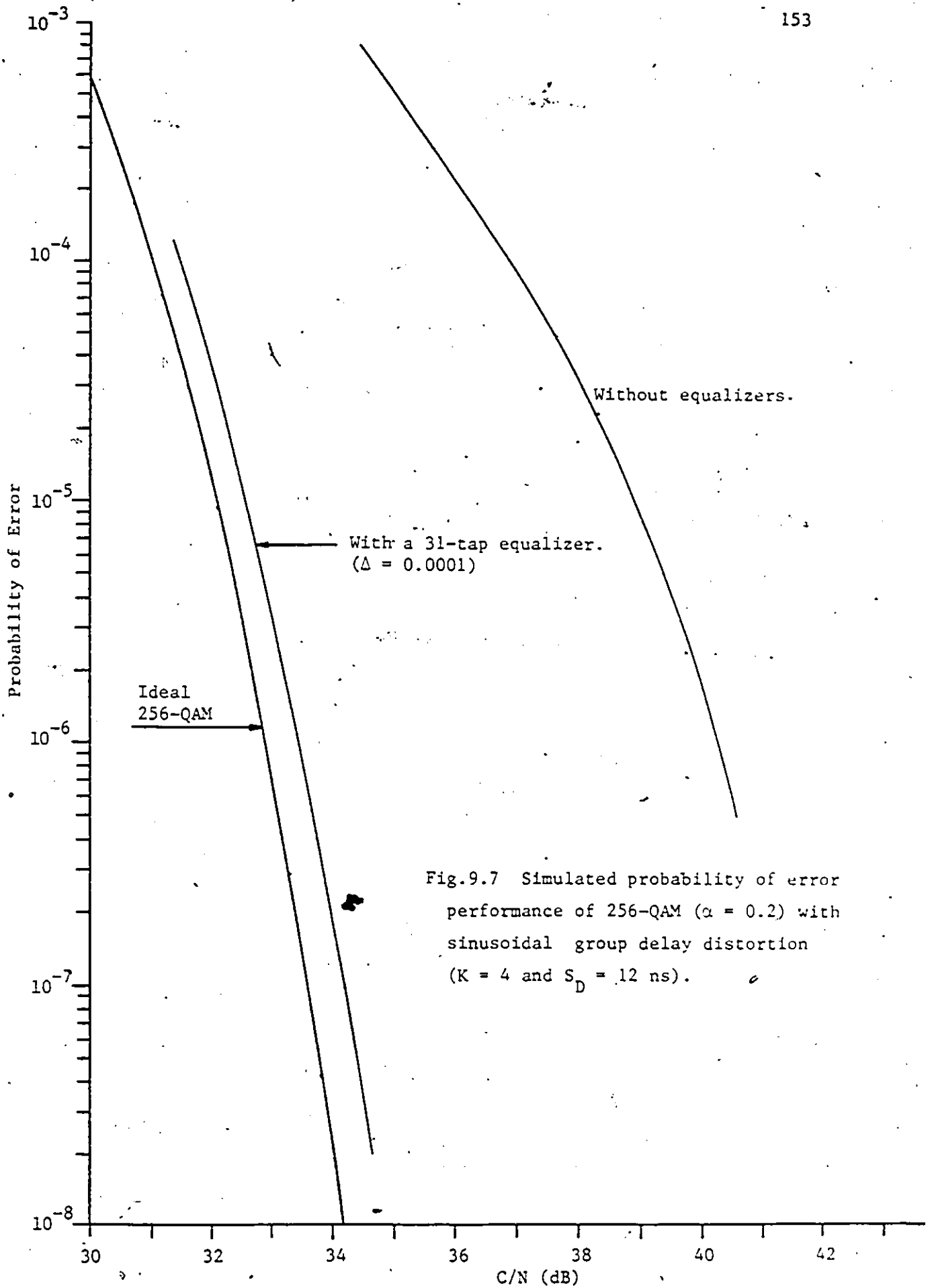


(b) After equalization.

Fig.9.5 Eye diagrams of 256-QAM ($\alpha = 0.2$) with a sinusoidal group delay distortion $D(f) = S_D \sin(2\pi Kf/2f_{BW})$, $S_D = 12$ ns and $K = 4$.
Bit rate = 120 b/s/Hz.

Fig.9.6 Simulated probability of error performance of 256-QAM ($\alpha = 0.2$) with a parabolic group delay channel distortion ($P_D = 0.81 \text{ ns/MHz}^2$).





A. For the sinusoidal group delay distortion, the probability of error performance is given in Fig.9.7. Again we see that the equalizer works very well in significantly reducing the residual ISI to a negligible amount.

9.3 CONCLUSIONS

A baseband tapped delay line adaptive equalizer for a 256-QAM system over distorted channels has been described and simulated. The results show that the adaptive equalizer easily compensates for transmission impairments and in turn improves the error rate performance significantly. It has to be mentioned that, in collaboration with Karkar Electronics, Inc., San Francisco, we credited permission to use and modify their adaptive equalizer simulation programs for thesis. However, these programs are not to be listed in the thesis.

Chapter X

CONCLUSION AND RECOMMENDED FURTHER RESEARCH

10.1 SUMMARY

Motivated by the increasing need for efficient utilization of spectrum in the digital radio world and in hybrid analog and digital channels, such as the transmission of a T1 carrier in a standard analog SG band, we have investigated two potential modulation schemes, i.e., 256-QAM and 225-QPRS. In order to achieve a spectral efficiency of more than 6 b/s/Hz by means of 225-QPRS, it is essential to operate it above the Nyquist rate, leading to the study of multi-level PRS/QPRS above the Nyquist rate. We found that the conventional method for multi-level PRS/QPRS above the Nyquist rate is inappropriate since it introduces too much "undesired" ISI, resulting in serious performance degradations. Therefore, we proposed an improved efficiency PRS/QPRS data filtering strategy ("chopping technique"), which enables a higher transmission rate than feasible with conventional PRS/QPRS systems. We demonstrated that, with the use of our new method, an increase of 5% above the Nyquist rate for class-I 225-QPRS, i.e., a spectral efficiency of 6.3 b/s/Hz can be achieved with a small degradation.

We also demonstrated that our new chopping technique can be applied to class-IV PRS systems which are useful in applications where reduced low-frequency components in the spectrum are required. The

advantages of combining class-IV PRS with our new technique are that a small bandwidth around dc can be carved out for accommodating a service channel and that a higher increase in spectral efficiency can be obtained in an FDM SSB system.

To confirm the concept of our new chopping technique for PRS above the Nyquist rate and the accuracy of computer simulations, an experimental 7-level class-IV PRS system was designed and implemented. System design principles and detailed description of circuit operations were presented. Measured BER performance was shown to agree well with the simulated results.

In order to enable one to select a suitable modulation scheme which is less sensitive to certain distortions, a quantitative evaluation of the effect of channel group delay and amplitude distortions with a linear, parabolic or sinusoidal characteristic on the performance of 256-QAM and 225-QPRS was performed with the aid of computer simulations. The numerical results could be useful for modem designers and researchers since it could indicate how flat and how linear their filter amplitude and phase responses should be.

In Chapter 7, we introduced a method to predict error floors in digital transmission systems. We compared the error floors caused by signalling above the Nyquist rate for duobinary PRS using the conventional method and our new scheme. The results show that the error floors caused by using our new scheme are much much lower than those by the conventional method. This rigorously verifies that our new scheme is better than the conventional method for multi-level PRS/QPRS above

the Nyquist rate for a practical realization. The method could be extended to the study of other transmission systems, as illustrated by an example which can evaluate error floors for PAM systems under severe distortions.

Since co-channel interference (CCI) is one of the major sources of performance impairments, we also evaluated the performance degradation caused by CCI for 64-QAM, 225-QPRS, and 256-QAM. Both sinusoidal and amplitude modulated CCI's were considered. The results indicate that, to make dual polarization operation feasible for high level modulation schemes, such as 225-QPRS and 256-QAM, a cross polarization discrimination of better than 40 dB is required since these systems are also sensitive to other impairments.

Finally, in order to improve the performance of a 256-QAM modem degraded by channel distortions as previously investigated, the use of an adaptive baseband transversal equalizer has been described and simulated. Illustrative eye diagrams and probability of error performance show that the adaptive equalizer easily compensates for transmission impairments and thus improve the error rate performance significantly.

10.2 SUGGESTIONS FOR FURTHER RESEARCH

In this final section, a few interesting research topics, which are related to our study, will be presented for further research. A brief description of these topics follows.

10.2.1 Carrier and Symbol Timing Recovery for 256-QAM and 225-QPRS

A perfect synchronization information was assumed to be available in the receiver in this thesis for the analysis and simulation of QAM and QPRS systems in an additive white Gaussian noise environment. High-level modulation schemes, such as 256-QAM and 225-QPRS require precise synchronization. Thus, it is important to study performance degradations caused by imperfect synchronization and methods to precisely recover the carrier and symbol timing.

10.2.2 Effects of Nonlinear Amplifiers on the Performance of 256-QAM and 225-QPRS

In this thesis, only linear distortions were considered. In a practical system, it is necessary to use power amplifiers, e.g., TWT or GaAs FET, at the output stage. These amplifiers exhibit a certain amount of nonlinearity [55], thus degrading the system's performance. The effect of nonlinearity on the performance of 256-QAM and 225-QPRS should be evaluated. Also the linearization of these power amplifiers could be another interesting and important topic [56].

10.2.3 The Performance of 256-QAM and 225-QPRS in an Adjacent Channel Interference (ACI) Environment

The performance of 256-QAM and 225-QPRS in a CCI environment has been evaluated in this thesis. In a multi-channel environment, ACI is also one of the major sources of performance impairment. Performance degradations caused by ACI on 256-QAM and 225-QPRS are thus worth studying.

10.2.4 Tailing Off BER Curves in QAM and QPRS Systems

It is often noted that a practically measured BER curve shows tailing off at high S/N. We have introduced in Chapter 7 a method to predict error floors for PRS systems operated above the Nyquist rate. A method very similar to ours has been presented in [41] at the same time to estimate the signature of QAM systems. This approach could be explored more and extended to investigate the tailing-off problems for QAM and QPRS systems caused by other impairments.

10.2.5 The Performance of 256-QAM and 225-QPRS in a Multipath Fading Environment

In the T1/SG DIV application example, as mentioned in Chapter 1, due to the narrow bandwidth, selective fading presents no problem. However, for high-speed digital radio applications, the effect of multipath (selective) fading should be considered [57]. Thus it is of interest to investigate the performance of 256-QAM and 225-QPRS in a multipath fading environment. This would in turn allow the outage of a system to be accurately estimated [58]. And it is of even more importance to study how equalization techniques can be employed to reduce the outage of these systems under selective fading [59], [60].

Appendix A

DERIVATION OF THE P_e PERFORMANCE OF CLASS-I AND CLASS-IV PRS SYSTEMS

The performance in terms of the probability of error of class-I and class-IV PRS systems over a white Gaussian noise channel will be evaluated. A symbol-by-symbol detection procedure is assumed. The model of the communications system is shown in Fig.A.1.

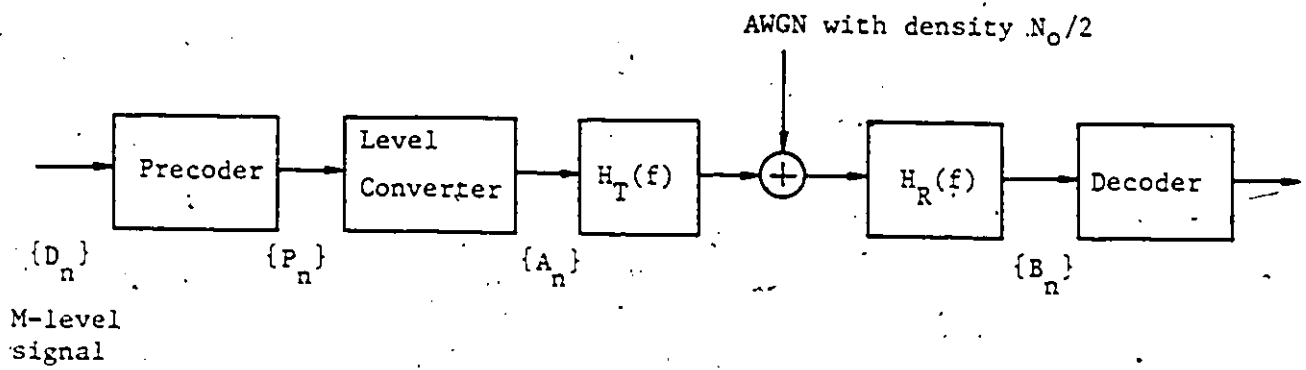


Fig.A.1 Block diagram of PRS systems.

Let $\{D_n\}$ denote the M-level input data sequence consisting of the equally likely numbers $0, 1, 2, \dots, M-1$, and let $\{P_n\}$ denote the output of the precoder which is used to prevent error propagation. The relationship between $\{P_n\}$ and $\{D_n\}$ is

$$P_n = (D_n - P_{n-1}) \text{ Mod } M \quad \text{for class-I PRS} \quad (A.1)$$

and

$$P_n = (D_n + P_{n-2}) \text{ Mod } M \quad \text{for class-IV PRS} \quad (\text{A.2})$$

where Mod M represents the modulo M arithmetic operation. e.g., $(-3) \text{ Mod } 4 = 1$, $7 \text{ Mod } 4 = 3$, etc.

The precoded symbol P_n is converted into the transmitted amplitude level A_n according to following relation.

$$A_n = 2P_n - (M-1) \quad (\text{A.3})$$

The transmit filter with transfer function $H_T(f)$ is excited at the Nyquist rate by impulses having as areas the sequence of amplitudes $\{A_n\}$:

We shall first concentrate on class-I PRS. For class-I PRS, the overall transfer function $X(f)$ is expressed as (A.4).

$$X(f) = H_T(f)H_R(f) = \begin{cases} 2T_s \cos(\pi f T_s) & \text{for } |f| \leq 1/2T_s \\ 0 & \text{elsewhere.} \end{cases} \quad (\text{A.4})$$

where T_s is the duration of a signaling interval. The Nyquist frequency is defined as

$$f_N = 1/2T_s \quad (\text{A.5})$$

In the absence of noise, due to the class-I PRS operation, the received signal just before the decoder at the optimum sampling instants can be expressed as

$$B_n = A_n + A_{n-1} \quad (\text{A.6})$$

The rule for converting the received sequence $\{B_n\}$ into the original data sequence $\{D_n\}$ is obtained as follows.

$$B_n = 2(P_n + P_{n-1} - (M-1)) \quad (\text{A.7})$$

$$\text{But } D_n = (P_n + P_{n-1}) \text{ Mod } M \quad (\text{A.8})$$

$$\text{Hence } D_n = (B_n/2 + (M-1)) \text{ Mod } M \quad (\text{A.9})$$

Since the input symbols are assumed to be equally probable, $\{A_n\}$ thus has a uniform probability distribution, i.e.,

$$\Pr\{A_n = k\} = 1/M, \quad k = -(M-1), -(M-3), \dots, -1, 1, \dots, (M-3), (M-1). \quad (\text{A.10})$$

From (A.6), we see that the probability density function (pdf) of B_n is the convolution of the two identical uniform pdf's shown as (A.10). Thus, it is easily shown that in the absence of noise, the output levels have a triangular probability distribution, i.e.,

$$\Pr(B_n = 2ld) = \frac{M - |l|}{M^2} \quad l = -(M-1), -(M-2), \dots, 0, 1, 2, \dots, M-1. \quad (\text{A.11})$$

where B_n denotes the received level in the n -th signaling interval and $2d$ is the distance between any two adjacent received levels.

The actual received sample (signal plus noise), call it y , is Gaussian with mean $E(y) = B_n = 2ld$ and variance σ^2 ,

$$\text{where } \sigma^2 = \frac{N_0}{2} \int_{-\infty}^{\infty} |H_R(f)|^2 df \quad (\text{A.12})$$

Thus a tight bound on the average probability of a symbol error, denoted by P_M , can be derived as follows.

$$\begin{aligned}
 P_M &\leq \sum_{l=-(M-2)}^{M-2} \Pr(|y - 2ld| > d | B_n = 2ld) \cdot \Pr(B_n = 2ld) \\
 &\quad + 2 \Pr(|y + 2(M-1)d| > d | B_n = -2(M-1)d) \cdot \Pr[B_n = -2(M-1)d] \\
 &= \Pr(|y| > d | B_n = 0) \left\{ 2 \sum_{l=0}^{M-1} \Pr(B_n = 2ld) - \Pr(B_n = 0) \right. \\
 &\quad \left. - \Pr[B_n = -2(M-1)d] \right\} \\
 &= \left(1 - \frac{1}{M^2}\right) \Pr(|y| > d | B_n = 0) \tag{A.13}
 \end{aligned}$$

But

$$\Pr(|y| > d | B_n = 0) = \frac{2}{\sqrt{2\pi}\sigma} \int_d^{\infty} e^{-x^2/2\sigma^2} dx = 2Q(d/\sigma), \tag{A.14}$$

where

$$Q(x) = \frac{1}{\sqrt{2\pi}} \int_x^{\infty} \exp(-t^2/2) dt$$

Hence, substituting (A.14) into (A.13), we obtain

$$P_M \leq 2(1 - 1/M^2) Q(d/\sigma) \tag{A.15}$$

That the sign "<" appears in the above equations is because of the "Mod M" decoding (see (A.9)). For example, let $M = 4$ and suppose due to noise a level of +3 has been driven to -1. Note that $(-1) \text{ Mod } 4 = 3$, i.e., in this case no error is observed. However due to the nature of Gaussian noise, such cases occur at relatively low probability. Thus (A.14) is a tight bound.

It is necessary to express P_M in terms of the average S/N at the input of the receiver measured in the Nyquist bandwidth ($\frac{1}{2T_s}$). To do so, the distribution of filters is important and must be clarified.

A.1 OPTIMALLY SPLIT FILTERS

Optimum refers to splitting the overall class-I PRS shaping equally between the transmitter and the receiver, i.e.,

$$H_T(f) = H_R(f) = \begin{cases} (2T_s \cos \pi f T_s)^{1/2} & |f| \leq 1/2T_s, \\ 0 & \text{elsewhere.} \end{cases} \quad (\text{A.16})$$

In this case, the received noise power σ^2 is

$$\begin{aligned} \sigma^2 &= \frac{N_0}{2} \int_{-\infty}^{\infty} |H_R(f)|^2 df \\ &= N_0 T_s \int_{-1/2T_s}^{1/2T_s} \cos^2(\pi f T_s) df = 2N_0/\pi^2 \end{aligned} \quad (\text{A.17})$$

Denote by N the noise power at the input of the receiver measured in the Nyquist bandwidth ($\frac{1}{2T_s}$).

$$N = \int_{-1/2T_s}^{1/2T_s} \frac{N_0}{2} df = N_0/2T_s = \pi \sigma^2/(4T_s) \quad (\text{A.18})$$

The transmitted power, denoted by S , is calculated as follows.

$$S = \frac{\overline{k^2}}{T_s} \int_{-1/2T_s}^{1/2T_s} |H_T(f)|^2 df = 4 \overline{k^2}/(\pi T_s) \quad (\text{A.19})$$

where $\overline{k^2}$ is the mean-square value of the transmitted levels. For the case of equally likely transmitted levels with the adjacent levels separated by a distance of $2d$,

$$\overline{k^2} = d^2 (M^2 - 1)/3 \quad (\text{A.20})$$

Substituting (A.18) - (A.20) into (A.15), we obtain P_M in terms of S/N . That is

$$P_M \leq 2(1 - 1/M^2)Q\left(\sqrt{\frac{3}{M^2 - 1}} \left(\frac{\pi}{4}\right)^2 \frac{S}{N}\right) \quad (\text{A.21})$$

Instead of the "Q" function, it is often seen in the literature that some authors used the "erfc" function. Thus (A.21) can be expressed also as

$$P_M \leq (1 - 1/M^2) \operatorname{erfc}\left(\sqrt{\frac{3}{2(M^2 - 1)}} \left(\frac{\pi}{4}\right)^2 \frac{S}{N}\right) \quad (\text{A.22})$$

where the relation $\operatorname{erfc}(y) = 2Q(\sqrt{2}y)$ has been used.

A.2 . SUBOPTIMUM DISTRIBUTION OF FILTERS

By suboptimum, we mean that the class-I PRS shaping is fully at the transmitter, whereas the receiver simply bandlimits the noise. That is

$$H_T(f) = \begin{cases} 2 T_s \cos(\pi f T_s) & |f| \leq 1/2T_s \\ 0 & \text{elsewhere.} \end{cases} \quad (\text{A.23})$$

and

$$H_R(f) = \begin{cases} 1 & |f| \leq 1/2T_s \\ 0 & \text{elsewhere.} \end{cases}$$

The transmitted power S is

$$S = \frac{k^2}{T_s} \int_{-\infty}^{\infty} |H_T(f)|^2 df$$

$$\begin{aligned}
 S &= 8T_s \overline{k^2} \int_0^{1/2T_s} \cos(\pi f T_s)^2 df \\
 &= 2 \overline{k^2} = 2 d^2 (M^2 - 1)/3
 \end{aligned} \tag{A.24}$$

In this case, the noise power at the input of the receiver measured in the Nyquist bandwidth is the same as that of the output of the receive filter, i.e.,

$$N = \sigma^2 = \int_{-1/2T_s}^{1/2T_s} \frac{N_0}{2} df = N_0/2T_s \tag{A.25}$$

Substituting (A.24) and (A.25) into (A.15), the following expression can be derived:

$$P_M \leq 2 (1 - 1/M^2) Q \left(\sqrt{\frac{3}{M^2 - 1} \frac{1}{2} \frac{S}{N}} \right) \tag{A.26}$$

or equivalently,

$$P_M \leq (1 - 1/M^2) \operatorname{erfc} \left(\sqrt{\frac{3}{M^2 - 1} \frac{1}{4} \frac{S}{N}} \right) \tag{A.27}$$

Comparing the arguments of the "Q" functions in (A.26) and (A.21), we note that the suboptimum distribution of filters results in a loss of approximately

$$10 \log_{10} \frac{(\pi/4)^2}{1/2} = 0.91 \text{ dB} \tag{A.28}$$

in S/N relative to the case of optimally split filters.

It has to be noted that if the S/N is measured at the output of the receive filter, i.e., just before the decoder, the two filters distribution strategies (optimum and suboptimum) result in the same P_M expression as (A.26).

P_M for class-IV PRS can be derived similarly. For the class-IV PRS shaping,

$$X(f) = H_T(f)H_R(f) = \begin{cases} j2T_s \sin(2\pi fT_s), & |f| \leq 1/2T_s \\ 0 & \text{elsewhere.} \end{cases} \quad (\text{A.29})$$

In the absence of noise, the received signal at the optimum sampling instants can be represented as

$$B_n = A_n - A_{n-2} \quad (\text{A.30})$$

To obtain the rule for converting the received sequence $\{B_n\}$ into the data sequence $\{D_n\}$ we substitute for A_n .

$$\text{Thus, } B_n = 2(P_n - P_{n-2}) \quad (\text{A.31})$$

$$\text{But } D_n = (P_n - P_{n-2}) \text{ Mod } M \quad (\text{A.32})$$

$$\text{Hence, } D_n = (B_n/2) \text{ Mod } M \quad (\text{A.33})$$

Following the above procedures, it is very straightforward to obtain the P_M for class-IV PRS and the results are found to be exactly identical to (A.21) and (A.26). This can be understood by noting that the areas under class-I and class-IV PRS shapes are the same. That is

$$\int_{-1/2T_s}^{1/2T_s} |2T_s \cos(\pi f T_s)|^2 df \quad (\text{Area under class-I PRS shape})$$

$$= \int_{-1/2T_s}^{1/2T_s} |j2T_s \sin(2\pi f T_s)|^2 df \quad (\dots \text{class-IV PRS} \dots)$$

$$= 4/\pi.$$

(A.34)

Appendix B

SIMULATION PROGRAMS FOR QAM AND QPRS SYSTEMS.

The simulation programs listed in this appendix were used to simulate various performances of QAM and QPRS systems, such as the performance of QPRS above the Nyquist rate, QAM and QPRS systems performances in distorted channels, the impact of CCI on QAM and QPRS systems, etc. The author of this thesis used, modified, and extended numerous subroutines and programs which were developed by the Digital Communications Research Group, Department of Electrical Engineering, University of Ottawa.

FILE: DIGIMP FORTRAN A UNIV D'OF OTTAWA

```

C*****
C FILE NAME : DIGIMP FORTRAN
C DRAWS THE DISCRETE IMPULSE RESPONSE OF PRS ABOVE THE
C NYQUIST RATE USING MODEL-A OR B.
C ONLY THE ABSOLUTE VALUES OF IMPULSE RESPONSE SAMPLES
C ARE PLOTTED.
C
C PARAMETERS: MODEL=1 FOR CONVENTIONAL MODEL-A.
C MODEL=2 FOR OUR NEW MODEL-B.
C B IS THE PERCENTAGE INCREASE.
C FOR EXAMPLE, B=.05 MEANS A 5% INCREASE.
C*****
C DIMENSION XA(153),YA(153)
C MODEL=2
C B=0.05
C A=1./(1.+B)
C X=-50.5
C PI=3.1415926
C GO TO (1,2), MODEL
C 1 DO 100 I=1,101
C Y=PI*(A*X+0.5)
C Z=PI*(A*X-0.5)
C IF((Z*Y).EQ.0.) GO TO 33
C HX=SIN(Y)/Y+SIN(Z)/Z
C GO TO 55
C 33 HX=1.
C 55 YA(I)=HX
C XA(I)=X
C X=X+1.0
C 100 CONTINUE
C GO TO 300
C 2 DO 200 I=1,101
C Y=PI*A*(X+0.5)
C Z=PI*A*(X-0.5)
C IF(Y.EQ.0.) HX=A+A*SIN(Z)/Z
C IF(Z.EQ.0.) HX=A*SIN(Y)/Y+A
C IF((Y*Z).EQ.0.) GO TO 45
C HX=A*SIN(Y)/Y+A*SIN(Z)/Z
C 45 YA(I)=HX
C XA(I)=X
C X=X+1.0
C 200 CONTINUE
C 300 WRITE(6,80) MODEL,A
C 80 FORMAT(10X,'MODEL',I2,' A=',F8.4,/)
C WRITE(6,85)
C 85 FORMAT(13X,' I ',13X,' X ',15X,' IMPULSE SAMPLES H(X)',/)
C WRITE(6,90) (I,XA(I),YA(I),I=1,101)
C 90 FORMAT(10X,15,10X,F10.5,10X,F10.5)
C CALL DRAW(XA,YA)
C STOP
C END
C SUBROUTINE DRAW(XA,YA)
C DIMENSION X(4),Y(4),YA(1),XA(1)
C ESTABLISH THE SURFACE AREA.
C CALL PLOTS(30.0,27.5)

```

DIG00010
DIG00020
DIG00030
DIG00040
DIG00050
DIG00060
DIG00070
DIG00080
DIG00090
DIG00100
DIG00110
DIG00120
DIG00130
DIG00140
DIG00150
DIG00160
DIG00170
DIG00180
DIG00190
DIG00200
DIG00210
DIG00220
DIG00230
DIG00240
DIG00250
DIG00260
DIG00270
DIG00280
DIG00290
DIG00300
DIG00310
DIG00320
DIG00330
DIG00340
DIG00350
DIG00360
DIG00370
DIG00380
DIG00390
DIG00400
DIG00410
DIG00420
DIG00430
DIG00440
DIG00450
DIG00460
DIG00470
DIG00480
DIG00490
DIG00500
DIG00510
DIG00520
DIG00530
DIG00540
DIG00550

FILE: DIGIMP FORTRAN A UNIV D'OF OTTAWA

C	CALL FACTOR(0.75)	DIG00560
C	ESTABLISH THE ORIGIN.	DIG00570
C	CALL PLOT(3.0,6.0,-3)	DIG00580
C	WRITE THE TITLE OF THE GRAPH.	DIG00590
C	CALL SYMBOL(10.0,17.0,0.49,16HQPRS EYE DIAGRAM,0.0,16)	DIG00600
C	DRAW THE TIME AXIS.	DIG00610
C	CALL AXIS(0.0,0.0,1H,-1,21.,0.0,-50.5,5.0)	DIG00620
C	DRAW THE AMPLITUDE AXIS.	DIG00630
	DIV=0.05/15.	DIG00640
C	DIV=0.1/15. FOR B=0.10	DIG00650
C	CALL AXIS(0.0,0.0,1H,1,16.,90.0,0.0,DIV)	DIG00660
C	PLOT THE DATA.	DIG00670
	JJ=2	DIG00680
	Y(JJ+1)=0.0	DIG00690
	Y(JJ+2)=DIV	DIG00700
	X(JJ+1)=-50.5	DIG00710
	X(JJ+2)=5.0	DIG00720
	DO 100 I=1,101	DIG00730
	X(1)=XA(1)	DIG00740
	X(2)=X(1)	DIG00750
	Y(1)=0.	DIG00760
	Y(2)=YA(-1)/YA(51)	DIG00770
	Y(2)=ABS(Y(2))	DIG00780
C	IF(Y(2).GT.0.1) Y(2)=0.1 FOR B=0.10	DIG00790
	IF(Y(2).GT.0.05) Y(2)=0.05.	DIG00800
	CALL LINE(X,Y,JJ,1,0,0)	DIG00810
100	CONTINUE	DIG00820
	CALL PLOT(0.0,0.0,999)	DIG00830
	RETURN	DIG00840
	END	DIG00850

FILE: 256GD FORTRAN A UNIV D'/OF OTTAWA

```

C*****
C PROGRAM FOR SIMULATING 256-QAM IN LINEAR CHANNEL WITH LINEAR,
C PARABOLIC, AND SIN/COSINE RIPPLE FILTER DISTORTIONS.
C FILE NAME: 256GD
C FOR AMPLITUDE DISTORTIONS, SET ID=1 AND USE SUB. AMPD.
C FOR GD DISTORTIONS, SET ID=2 AND USE SUB. DLYD.
C SOME PARAMETERS IN SUB. DRAWCN MUST BE MODIFIED IN
C ACCORDANCE WITH THOSE IN SUB. AMPD OR DLYD.
C THE NOMINAL BIT RATE IS 120 MB/S, BUT IT CAN BE
C CHANGED TO ANOTHER BIT RATE BY CHANGING THE PARAMETER BR.
C*****
C COMPLEX DATA(65536), TF(65536)
C DIMENSION PEI(32), EBNO(32), NI(2048), NQ(2048)
C DIMENSION XARRAY(32), YARRAY(32)
C INITIALIZATION
C COMMON /NUMB1/ FBW, ALPHA, LDIM, IOFF, LSAMPL
C COMMON /NUMB2/ NSNR, NSYMB, BAUD
C ALPHA=0.4
C LDIM=65536
C IOFF=0
C LSAMPL=32
C NSNR=32
C NSYMB=2047
C BR=120.
C WRITE(6,19) BR
C 19 FORMAT(10X, 'BIT RATE =', F8.3, ' MB/S')
C BAUD=15.*(BR/120.)
C FBW=BAUD/2.
C ISIN=1
C NFILTR=2
C NRUNS=7
C WRITE(6,666) ALPHA
C 666 FORMAT(10X, 'ALPHA=', F8.4)
C=====
C ID=1 FOR AMPLITUDE DISTORTIONS
C ID=2 FOR GD DISTORTIONS
C ID WILL BE USED IN SUB. DRAWCN
C-----
C ID=1
C END OF INITIALIZATION.
C START OF COMPUTATIONS.
C DO 100 NR=1, NRUNS
C=====
C CALL LD256(DATA, NI, NQ)
C CALL LOAD64(DATA, NI, NQ)
C DO 43 I=1, LDIM
C 43 DATA(I)=2.*DATA(I)
C-----
C CALL RCOSTX(TF)
C=====
C GO TO (31,32), ID
C 31 CALL AMPD(NR, TF, ISIN)
C GO TO 33
C 32 CALL -DLYD(NR, TF, ISIN)

```

25600010
25600020
25600030
25600040
25600050
25600060
25600070
25600080
25600090
25600100
25600110
25600120
25600130
25600140
25600150
25600160
25600170
25600180
25600190
25600200
25600210
25600220
25600230
25600240
25600250
25600260
25600270
25600280
25600290
25600300
25600310
25600320
25600330
25600340
25600350
25600360
25600370
25600380
25600390
25600400
25600410
25600420
25600430
25600440
25600450
25600460
25600470
25600480
25600490
25600500
25600510
25600520
25600530
25600540
25600550

FILE: 256GD FORTRAN A UNIV D'/OF OTTAWA

```

C-----
33 CALL FILTER(DATA,TF)
CALL ENERGY(DATA,EB)
C
C   END OF TRANSMITTER
C
CALL RCOSRX(TF)
CALL HHGG(TF,PNOISE)
CALL FILTER(DATA,TF)
CALL SYNCRO(DATA,PNOISE,NI,NQ,MI,MQ,EB)
CALL DECODE(DATA,PNOISE,MI,MQ,NI,NQ,
#EBNO,PEI,EB)
C
C   CALL THE DRAWING ROUTINE
C
DO 99 I=1,NSNR
XARRAY(I)=EBNO(I)
99 YARRAY(I)=PEI(I)
CALL DRAWCN(ID,XARRAY,YARRAY,NR,NRUNS)
C
C   CALL THE EYE DIAGRAM ROUTINE
C
CALL EYEQ(DATA)
100 CONTINUE
STOP
END
C*****
C   THIS SUBROUTINE IS TO SIMULATE GROUP DELAY DISTORTIONS
C   I/P : NR
C         ISIN
C         TF
C   O/P : TF
C*****
SUBROUTINE DLYD(NR,TF,ISIN)
COMMON /NUMB2/ NSNR,NSYMB,BAUD
COMPLEX TF(1)
GO TO (84,2,3,4,5,6,7),NR
2 B=.095*(15./BAUD)**2
GO TO 10
3 B=.19*(15./BAUD)**2
10 WRITE (6,11) B
11 FORMAT (10X,'LINEAR GROUP DELAY IN NS/MHZ=',F8.5)
CALL LINGD(B,TF)
GO TO 84
4 S=0.27*(15./BAUD)**3
GO TO 20
5 S=0.54*(15./BAUD)**3
20 WRITE (6,12) S
12 FORMAT (10X,'PARABOLIC GROUP DELAY IN NS/MHZ**2=',F8.5)
CALL PARGD(S,TF)
GO TO 84
6 C=6.00*(15./BAUD)
GO TO 30
7 C=12.0*(15./BAUD)
30 K=4

```

25600560
25600570
25600580
25600590
25600600
25600610
25600620
25600630
25600640
25600650
25600660
25600670
25600680
25600690
25600700
25600710
25600720
25600730
25600740
25600750
25600760
25600770
25600780
25600790
25600800
25600810
25600820
25600830
25600840
25600850
25600860
25600870
25600880
25600890
25600900
25600910
25600920
25600930
25600940
25600950
25600960
25600970
25600980
25600990
25601000
25601010
25601020
25601030
25601040
25601050
25601060
25601070
25601080
25601090
25601100

FILE: 256GD .FORTRAN A UNIV D'OF OTTAWA

```

WRITE (6,17) K,C
17 FORMAT (5X,'# OF RIPPLES=',13,'SINE AMPLITUDE GROUP DELAY=',
#F8.5,/)
CALL SINCGD(ISIN,C,K,TF)
84 RETURN
END
C*****
C THIS SUBROUTINE IS TO SIMULATE AMPLITUDE DISTORTIONS
C I/P : NR
C ISIN
C TF
C O/P : TF
C*****
SUBROUTINE AMPD(NR,TF,ISIN)
COMMON /NUMB2/ NSNR,NSYMB,BAUD
COMPLEX TF(1)
GO TO (74,2,3,4,5,6,7),NR
2 Z=.038*(15./BAUD)
GO TO 10
3 Z=0.076*(15./BAUD)
10 WRITE (6,8) Z
8 FORMAT (10X,'LINEAR AMPLITUDE SLOPE IN DB/MGZ=',F8.5,/)
CALL LINAMP(Z,TF)
GO TO 74
4 P=.00400*(15./BAUD)**2
GO TO 20
5 P=.00800*(15./BAUD)**2
20 WRITE(6,9) P
9 FORMAT(10X,'PARABOLIC AMPLITUDE DIST. IN DB/MHX**2=',F8.5,/)
CALL PARAMP(P,TF)
GO TO 74
6 D=0.2
GO TO 30
7 D=.4
30 K=4
WRITE(6,77) K,D
77 FORMAT(5X,'# OF RIPPLES=',13,'SINE AMPLITUDE DIST. IN DB=',
#F8.5,/)
CALL SINAMP(ISIN,D,K,TF)
74 RETURN
END
C*****
C RAISED COSINE FILTER WITH ARBITRARY ALPHA AND X/SINX
C*****
SUBROUTINE RCSTX(TF)
COMPLEX TF(65536)
COMMON /NUMB1/ FBW,ALPHA,LDIM,IOFF,LSAMPL
COMMON /NUMB2/ NSNR,NSYMB,BAUD
SBANDW=BAUD*LSAMPL
NO=LDIM/2
NO1=NO+1
IF (ALPHA.EQ.0) ALPHA=0.0001
FN=LDIM*(FBW/SBANDW)
F1=(1.-ALPHA)*FN
F2=(1.+ALPHA)*FN

```

25601110
25601120
25601130
25601140
25601150
25601160
25601170
25601180
25601190
25601200
25601210
25601220
25601230
25601240
25601250
25601260
25601270
25601280
25601290
25601300
25601310
25601320
25601330
25601340
25601350
25601360
25601370
25601380
25601390
25601400
25601410
25601420
25601430
25601440
25601450
25601460
25601470
25601480
25601490
25601500
25601510
25601520
25601530
25601540
25601550
25601560
25601570
25601580
25601590
25601600
25601610
25601620
25601630
25601640
25601650

FILE: 256GD FORTRAN A UNIV D'YOF OTTAWA

```

C      AMPLITUDE CHARACTERISTIC
C
      A1=3.141592/(2.*FLOAT(IFN))
      DO 8 I=2,IF1
      TF(I)=CMPLX(1.0,0.0)
      J=I-1
      TF(I)=CMPLX(1.,0.0)
8     CONTINUE
      JK=IF1+1
      DO 9 J=JK,IF2
      I=J-1
C
C      ROOT OF RAISED COSINE
C
      A=(3.141592/(2.0*ALPHA))*((FLOAT(I)/FLOAT(IFN))-1.)
      TF(J)=CMPLX(SQRT(0.5*(1.0-SIN(A))),0.0)
9     CONTINUE
      JH=IF2+1
      DO 10 I=JH,NO1
      TF(I)=CMPLX(0.0,0.0)
10    CONTINUE
      NO2=NO1+1
      DO 5 I=NO2,LDIM
      TF(I)=CONJG(TF(LDIM+2-I))
5     CONTINUE
      RETURN
      END
C*****
C      THE FOLLOWING SUBROUTINE PERFORMS THE FILTERING
C      PROCESS ON THE DATA SEQUENCE.
C*****
      SUBROUTINE FILTER(DATA,TF)
      COMPLEX DATA(1),TF(1)
      DIMENSION IWK(17)
      COMMON /NUMB1/ FBW,ALPHA,LDIM,IOFF,LSAMPL
      CALL FFT2C(DATA,16,IWK)
      DO 1 I=1,LDIM
1     DATA(I)=CONJG(DATA(I)*TF(I))
      CALL FFT2C(DATA,16,IWK)
      DO 2 I=1,LDIM
2     DATA(I)=CONJG(DATA(I))/FLOAT(LDIM)
      RETURN
      END
C*****
C      THIS SUBROUTINE COMPUTES THE EFFECTIVE NOISE (PNOISE)
C      AT THE OUTPUT OF THE RECEIVE FILTER
C*****
      SUBROUTINE HHGG(TF,PNOISE)
      COMPLEX TF(1)
      COMMON /NUMB1/ FBW,ALPHA,LDIM,IOFF,LSAMPL
      COMMON /NUMB2/ NSNR,NSYMB,BAUD
      SUM=0.0
      SBANDW=BAUD*LSAMPL
      DO 1 L=1,LDIM
      HH=(CABS(TF(L)))**2

```

25602210
25602220
25602230
25602240
25602250
25602260
25602270
25602280
25602290
25602300
25602310
25602320
25602330
25602340
25602350
25602360
25602370
25602380
25602390
25602400
25602410
25602420
25602430
25602440
25602450
25602460
25602470
25602480
25602490
25602500
25602510
25602520
25602530
25602540
25602550
25602560
25602570
25602580
25602590
25602600
25602610
25602620
25602630
25602640
25602650
25602660
25602670
25602680
25602690
25602700
25602710
25602720
25602730
25602740
25602750

FILE: 256GD FORTRAN A UNIV D' / OF OTTAWA

```

K3=3
K4=4
K5=5
K6=6
K7=7
K8=8
DO 2 I=1, KKK
  IF (K1.EQ.KKK) K1=1
  IF (K2.EQ.KKK) K2=1
  IF (K3.EQ.KKK) K3=1
  IF (K4.EQ.KKK) K4=1
  IF (K5.EQ.KKK) K5=1
  IF (K6.EQ.KKK) K6=1
  IF (K7.EQ.KKK) K7=1
  IF (K8.EQ.KKK) K8=1
  NI(1)=NX(K1)+NX(K3)*2+NX(K5)*4+NX(K7)*8
  NQ(1)=NX(K2)+NX(K4)*2+NX(K6)*4+NX(K8)*8
C
C   LOAD INTO SAMPLE ARRAY, 16 SAMPLES PER SYMBOL
  J1=(1-1)*LSAMPL+1
  J2=1*LSAMPL
  DO 3 J3=J1,J2
3   DATA(J3)=CMPLX(FLOAT(NI(1)),FLOAT(NQ(1)))
    K1=K1+1
    K2=K2+1
    K3=K3+1
    K4=K4+1
    K5=K5+1
    K6=K6+1
    K7=K7+1
    K8=K8+1
  2   CONTINUE
    IF(10FF.EQ.0) RETURN
    LL=LDIM-1
    DO 4 I=1,10FF
    XX=AIMAG(DATA(1))
    DO 5 K=1,LL
5   DATA(K)=CMPLX(REAL(DATA(K)),AIMAG(DATA(K+1)))
4   DATA(LDIM)=CMPLX(REAL(DATA(LDIM)),XX)
    RETURN
    END
C*****
C   THE FOLLOWING SUBROUTINE SYNCHRONIZES THE RECEIVED DATA.
C*****
SUBROUTINE SYNCRO(DATA,PNOISE,NI,NQ,MI,MQ,EB)
  INTEGER Q7FLAG
  COMPLEX DATA(1),AMP
  DIMENSION NI(1),NQ(1)
  COMMON /NUMB1/ FBW,ALPHA,LDIM,10FF,LSAMPL
  COMMON /NUMB2/ NSNR,NSYMB,BAUD
  NERROR=0
  IF (10FF.EQ.0) GO TO 111
  DO 6 K=1,10FF
  XX=AIMAG(DATA(LDIM))
  DO 7 KK=2,LDIM

```

25603310
25603320
25603330
25603340
25603350
25603360
25603370
25603380
25603390
25603400
25603410
25603420
25603430
25603440
25603450
25603460
25603470
25603480
25603490
25603500
25603510
25603520
25603530
25603540
25603550
25603560
25603570
25603580
25603590
25603600
25603610
25603620
25603630
25603640
25603650
25603660
25603670
25603680
25603690
25603700
25603710
25603720
25603730
25603740
25603750
25603760
25603770
25603780
25603790
25603800
25603810
25603820
25603830
25603840
25603850

FILE: 256GD FORTRAN A UNIV D' / OF OTTAWA

```

7   DATA(KK)=CMPLX(REAL(DATA(KK)),AIMAG(DATA(KK-1)))
6   DATA(1)=CMPLX(REAL(DATA(1)),XX)
C
C   SYNCHRONIZE THE RECEIVED DATA
C
111  NOLD=0
      NOF=0
      K=1
300  CONTINUE
      NEW=0
      DO 200 J=1, NSYMB
      J1=K+(J-1)*LSAMPL
      IF(J1.GT.LDIM) J1=J1-LDIM
      AXBAR=REAL(DATA(J1))
      AYBAR=AIMAG(DATA(J1))
      SS=AXBAR*NI(J)
      IF(SS.GT.0.) NEW=NEW+1
      SS=AYBAR*NQ(J)
      IF(SS.GT.0.) NEW=NEW+1
200  CONTINUE
      IF(NOLD.GE.NEW) GO TO 399
      NOLD=NEW
      NOF=K
399  K=K+1
      LFU=2*NSYMB
C
C   SHIFT RECEIVED DATA LEFT UNTIL ALL SYMBOLS ARE LINED UP
C
C-----
      NSFT=LSAMPL*3
      IF(NOLD.LT.LFU.AND.K.LE.NSFT) GO TO 300
      NOF=NOF-1
      WRITE(6,56) NOLD,K
56  FORMAT(1X,'NO OF CORRECT SYMBOLS = ',16,5X,'NO OF
      *SHIFT IN SAMPLES = ',16,/)
      IF(NOF.EQ.0) GO TO 230
      LO=LDIM-1
      DO 250 I=1,NOF
      AMP=DATA(1)
      DO 240 J=1,LO
      DATA(J)=DATA(J+1)
240  CONTINUE
      DATA(LDIM)=AMP
250  CONTINUE
C
C   OPTIMIZE THE SAMPLING INSTANT
C
230  MI=1
      MQ=1
      EO1=FLOAT(NSYMB) + 1.
      EOQ=FLOAT(NSYMB) + 1.
      M=22
      VARIAN=PNOISE*EB*(10.**(-0.1*FLOAT(M)))
      SIGMA=SQRT(VARIAN)
      DO 80 J=1,LSAMPL

```

25603860
25603870
25603880
25603890
25603900
25603910
25603920
25603930
25603940
25603950
25603960
25603970
25603980
25603990
25604000
25604010
25604020
25604030
25604040
25604050
25604060
25604070
25604080
25604090
25604100
25604110
25604120
25604130
25604140
25604150
25604160
25604170
25604180
25604190
25604200
25604210
25604220
25604230
25604240
25604250
25604260
25604270
25604280
25604290
25604300
25604310
25604320
25604330
25604340
25604350
25604360
25604370
25604380
25604390
25604400

FILE: 256GD FORTRAN A UNIV D'OF OTTAWA

```

E1=0.
EQ=0.
DO 70 K=1, NSYMB.
C VERIFY THAT NO SAMPLED SYMBOL IS IN ERROR
J1=(K-1)*LSAMPL+J
AXBAR=(REAL(DATA(J1))+REAL(DATA(J1+1)))/2.
AYBAR=(AIMAG(DATA(J1))+AIMAG(DATA(J1+1)))/2.
INDEXI=0
SS=FLOAT(NI(K))*AXBAR
IF (SS .LT. 0.) INDEXI=1
AMPX=ABS(AXBAR)
AMPI=ABS(FLOAT(NI(K)))
THR1I=AMPI - 1.0
THR2I=AMPI + 1.0
I7FLAG=0
IF (AMPI.EQ. 15.) GO TO 30
IF (( AMPX.GE.THR2I).OR.(AMPX.LE.THR1I)) INDEXI=1
GO TO 40
30 IF(AMPX.LE.THR1I) INDEXI=1
I7FLAG=1
40 CONTINUE
INDEXQ=0
SS=FLOAT(NQ(K))*AYBAR
IF (SS .LT. 0.) INDEXQ=1
AMPY=ABS(AYBAR)
AMPQ=ABS(FLOAT(NQ(K)))
THR1Q=AMPQ - 1.0
THR2Q=AMPQ + 1.0
Q7FLAG=0
IF (AMPQ.EQ. 15.) GO TO 50
IF (( AMPY.GE.THR2Q).OR.(AMPY.LE.THR1Q)) INDEXQ=1
GO TO 60
50 IF(AMPY.LE.THR1Q) INDEXQ=1
Q7FLAG=1
60 CONTINUE
IF (INDEXI.EQ.1) E1=E1 + 1.
IF (INDEXQ.EQ.1) EQ=EQ + 1.
C
C COMPUTE THE PROBABILITY OF ERROR FOR THIS SYMBOL AT EB/NO=22dB
C
D1=ABS(AMPX-THR1I)
ARG=D1/(SIGMA*SQRT(2.))
C CHECK IF ARG IS LARGE INWHICH CASE PE IS INSIGNIFICANT
C
IF (ARG.GT.12.) ARG=12.
E1=E1 + ERFC(ARG)/2.
IF (I7FLAG .EQ. 1) GO TO 65
D2=ABS(THR2I-AMPX)
ARG=D2/(SIGMA*SQRT(2.))
IF (ARG.GT.12.) ARG=12.
E1=E1 + ERFC(ARG)/2.
65 D1=ABS(AMPY-THR1Q)
ARG=D1/(SIGMA*SQRT(2.))
IF (ARG.GT.12.) ARG=12.
EQ=EQ + ERFC(ARG)/2.

```

25604410
25604420
25604430
25604440
25604450
25604460
25604470
25604480
25604490
25604500
25604510
25604520
25604530
25604540
25604550
25604560
25604570
25604580
25604590
25604600
25604610
25604620
25604630
25604640
25604650
25604660
25604670
25604680
25604690
25604700
25604710
25604720
25604730
25604740
25604750
25604760
25604770
25604780
25604790
25604800
25604810
25604820
25604830
25604840
25604850
25604860
25604870
25604880
25604890
25604900
25604910
25604920
25604930
25604940
25604950

FILE: 256GD FORTRAN A UNIV. D' OF OTTAWA

```

      IF (Q7FLAG .EQ. 1) GO TO 70
      D2=ABS(THR2Q-AMPY)
      ARG=D2/(SIGMA*SQRT(2.))
      IF (ARG.GT.12.) ARG=12.
      EQ=EQ + ERFC(ARG)/2.
70  CONTINUE
      IF (EO1.LE.E1) GO TO 75
      EO1=E1
      MI=J
75  CONTINUE
      IF (EQ.LE.EQ) GO TO 80
      EQ=EQ
      MQ=J
80  MOFF=IABS(MI-MQ)
      IF(MOFF.NE.0) WRITE(6,90) MOFF
      OFF=(FLOAT(MI) + FLOAT(MQ))/FLOAT(LSAMPL)
90  FORMAT(5X, 'SAMPLING POINTS FOR I AND Q CHANNELS DIFFER BY',
      #12, ' SIXTEENTHS OF THE SYMBOL INTERVAL',/)
      WRITE(6,95) OFF
95  FORMAT(5X, 'RECEIVED DATA IS DELAYED BY ',F7.3, ' SYMBOLS',/)
      RETURN
      END
C*****
C THE FOLLOWING SUBROUTINE DECODES THE RECEIVED DATA.
C*****
      SUBROUTINE DECODE(DATA, PNOISE, MI, MQ, NI, NQ, EBNO, PE, EB)
      INTEGER Q7FLAG
      COMPLEX DATA(1), AMP
      DIMENSION EBNO(1), PE(1), NI(1), NQ(1)
      COMMON /NUMB1/ FBW, ALPHA, LDIM, IOFF, LSAMPL
      COMMON /NUMB2/ NSNR, NSYMB, BAUD
      NERROR=0
      DO 1 I=1, NSNR
1    PE(I)=0.
C CHECK FOR AN ERROR AT THE SAMPLING INSTANT, ONLY THOSE
C ERRORS IN ADJACENT LEVELS ARE CONSIDERED
3    DO 2 K=1, NSYMB
      J1=(K-1)*LSAMPL+MI
      J2=(K-1)*LSAMPL + MQ
      AXBAR=(REAL(DATA(J1))+REAL(DATA(J1+1)))/2.
      AYBAR=(AIMAG(DATA(J2))+AIMAG(DATA(J2+1)))/2.
      INDEXI=0
      SS=FLOAT(NI(K))*AXBAR
      IF (SS .LT. 0.) INDEXI=1
      AMPX=ABS(AXBAR)
      AMPI=ABS(FLOAT(NI(K)))
      THR1=AMPI - 1.0
      THR2=AMPI + 1.0
      I7FLAG=0
      IF (AMPI.EQ. 15.) GO TO 30
      IF (( AMPX.GE.THR2).OR.(AMPX.LE.THR1)) INDEXI=1
      GO TO 40
30  IF(AMPX.LE.THR1) INDEXI=1
      I7FLAG=1
40  CONTINUE

```

25604960
25604970
25604980
25604990
25605000
25605010
25605020
25605030
25605040
25605050
25605060
25605070
25605080
25605090
25605100
25605110
25605120
25605130
25605140
25605150
25605160
25605170
25605180
25605190
25605200
25605210
25605220
25605230
25605240
25605250
25605260
25605270
25605280
25605290
25605300
25605310
25605320
25605330
25605340
25605350
25605360
25605370
25605380
25605390
25605400
25605410
25605420
25605430
25605440
25605450
25605460
25605470
25605480
25605490
25605500

FILE: 256GD FORTRAN A UNIV D'OF OTTAWA

```

INDEXQ=0
SS=FLOAT(NQ(K))*AYBAR
IF(SS.LT.0.)INDEXQ=1
AMPY=ABS(AYBAR)
AMPQ=ABS(FLOAT(NQ(K)))
THR1Q=AMPQ-1.0
THR2Q=AMPQ+1.0
Q7FLAG=0
IF(AMPQ.EQ.15.)GO TO 50
IF((AMPY.GE.THR2Q).OR.(AMPY.LE.THR1Q))INDEXQ=1
GO TO 60
50 IF(AMPY.LE.THR1Q)INDEXQ=1
Q7FLAG=1
60 CONTINUE
IF((INDEX1.EQ.1).OR.(INDEXQ.EQ.1))NERROR=NERROR+1
C
C COMPUTE THE PROBABILITY OF ERROR FOR THIS SYMBOL.
C THE VARIABLES ARE AS FOLLOWS: M IS EB/NO IN dB; PNOISE IS
C 1/2*INTERGAL (H(F)**2 DF); AND VARIAN = NO*PNOISE.
C FOR THE END POINTS (7FLAG=1) THE PE=1/2*ERFC(D1/(SIGMA*SQRT(2)))
C AND FOR THE INNER POINTS THE PE=1/2*ERFC(D1/(SIGMA*SQRT(2))) +
C 1/2*ERFC(D2/(SIGMA*SQRT(2))).
C
DO 4 M=1,NSNR
VARIAN=PNOISE*EB*(10.**(-0.1*FLOAT(M)))
SIGMA=SQRT(VARIAN)
D1=ABS(AMPX-THR1)
ARG=D1/(SIGMA*SQRT(2.))
CHECK IF ARG IS LARGE INWHICH CASE PE IS INSIGNIFICANT
CHECK IF SYMBOL IS IN ERROR. IF IT IS TERMINATE RUN
C
C IF (INDEX1.EQ.1) GO TO 153
C IF (ARG.GT.12.) ARG=12.
C PE1=ERFC(ARG)/2.
C IF (7FLAG.EQ.1) GO TO 100
C D2=ABS(THR21-AMPX)
C ARG=D2/(SIGMA*SQRT(2.))
C IF (ARG.GT.12.) ARG=12.
C PE1=PE1+ERFC(ARG)/2.
100 D1=ABS(AMPY-THR1Q)
ARG=D1/(SIGMA*SQRT(2.))
IF (INDEXQ.EQ.1) GO TO 153
IF (ARG.GT.12.) ARG=12.
PEQ=ERFC(ARG)/2.
IF (Q7FLAG.EQ.1) GO TO 110
D2=ABS(THR2Q-AMPY)
ARG=D2/(SIGMA*SQRT(2.))
IF (ARG.GT.12.) ARG=12.
PEQ=PEQ+ERFC(ARG)/2.
110 IF(PE1.LT.1.E-15) PE1=0.
IF(PEQ.LT.1.E-15) PEQ=0.
4 PE(M)=PE(M)+(PE1+PEQ)/2.
2 CONTINUE
DO 5 I=1,NSNR
PE(I)=PE(I)/FLOAT(NSYMB)
25605510
25605520
25605530
25605540
25605550
25605560
25605570
25605580
25605590
25605600
25605610
25605620
25605630
25605640
25605650
25605660
25605670
25605680
25605690
25605700
25605710
25605720
25605730
25605740
25605750
25605760
25605770
25605780
25605790
25605800
25605810
25605820
25605830
25605840
25605850
25605860
25605870
25605880
25605890
25605900
25605910
25605920
25605930
25605940
25605950
25605960
25605970
25605980
25605990
25606000
25606010
25606020
25606030
25606040
25606050

```

FILE: 256GD FORTRAN A UNIV D'OF OTTAWA

```

5  EBNO(1)=FLOAT(1)
   PRINT 150
150 FORMAT(5X,'EB/NO',10X,'PROB. OF ERROR',/)
   WRITE (6,151) (EBNO(1),PE(1),I=1,NSNR)
151 FORMAT(5X,F5.1,10X,E13.6)
   WRITE (6,152) NERROR
152 FORMAT(/5X,'ERRORS=',15,/)
   GO TO 155
153 PRINT 154
154 FORMAT (10X,'SYMBOL WAS IN ERROR, RUN WAS TERMINATED',/)
155 CONTINUE
   RETURN
   END
C*****
C   THIS SUBROUTINE DRAWS PROBABILITY OF ERROR CURVES FOR
C   P(E) AS LOW AS 1.0E-8 AND A C/N RATIO AS HIGH AS 35 dB.
C   I/P : ID=1 FOR AMPLITUDE DISTORTIONS
C         ID=2 FOR GD DISTORTIONS
C*****
SUBROUTINE DRAWCN (ID,XARRAY,YARRAY,JCURV,JLAST)
DIMENSION XARRAY(34),YARRAY(34),X(29),Y(29)
COMMON /NUMB1/ FBW,ALPHA,LDIM,IOFF,LSAMPL
COMMON /NUMB2/ NSNR,NSYMB,BAUD
M=NSNR
CF=8.
DO 1 K=1,NSNR
XARRAY(K)=XARRAY(K) + 10*(ALOG10(CF))
IF(YARRAY(K).GE.1.0) YARRAY(K)=1.0
IF(YARRAY(K).LE.1.0E-8) GOTO 3
GOTO 1
3  M=K-1
   GOTO 4
1  CONTINUE
4  CONTINUE
   I=M+1
   II=I+1
   XARRAY(II)=8.0
   XARRAY(II)=2.0
   YARRAY(II)=1.E-8
   YARRAY(II)=0.4
   IF(JCURV.GT.1) GOTO 2
C
C   ESTABLISH THE SURFACE AREA.
C
C   CALL PLOTS(30.0,27.5)
C   CALL FACTOR(.8)
C
C   ESTABLISH THE ORIGIN.
C
C   CALL PLOT(3.0,1.5,-3)
C
C   DRAW THE LOGARITHMIC Y-AXIS.
C
C   CALL LGAXS(0.0,0.0,29HPROBABILITY OF A SYMBOL ERROR,29,25.,
+90.,1.0E-8,.4)

```

25606060
25606070
25606080
25606090
25606100
25606110
25606120
25606130
25606140
25606150
25606160
25606170
25606180
25606190
25606200
25606210
25606220
25606230
25606240
25606250
25606260
25606270
25606280
25606290
25606300
25606310
25606320
25606330
25606340
25606350
25606360
25606370
25606380
25606390
25606400
25606410
25606420
25606430
25606440
25606450
25606460
25606470
25606480
25606490
25606500
25606510
25606520
25606530
25606540
25606550
25606560
25606570
25606580
25606590
25606600

FILE: 256GD FORTRAN A UNIV D'/OF OTTAWA

```

C
C   DRAW THE LINEAR X-AXIS.                                25606610
C   CALL AXIS(0.0,0.0,9HC/N IN dB,-9,                      25606620
+22.0,0.0,8.0,2.0)                                       25606630
C   WRITE THE TITLE OF THE GRAPH.                          25606640
C   CALL SYMBOL(6.,23.,.35,'PARABOLIC AMPLITUDE DISTORTION',0.,30) 25606650
C   PLOT LEGEND                                            25606660
C*****                                                    25606670
C   GO TO (11,22), 1D                                      25606680
22 CALL SYMBOL(2.,13.,.35,'NO DISTORTION',0.,13)          25606690
   CALL SYMBOL(2.,12.,.35,'L = 0.095 ns/MHZ',0.,16)      25606700
   CALL SYMBOL(2.,11.,.35,'L = 0.190 ns/MHZ',0.,16)      25606710
   CALL SYMBOL(2.,10.,.35,'P = 0.270 ns/MHZ**2',0.,19)   25606720
   CALL SYMBOL(2.,9.,.35,'P = 0.540 ns/MHZ**2',0.,19)   25606730
   CALL SYMBOL(2.,8.,.35,'S = 6.00 ns',0.,12)            25606740
   CALL SYMBOL(2.,7.,.35,'S = 12.0 ns',0.,12)            25606750
   CALL SYMBOL(2.,4.5,.35,22HGROUP DELAY DISTORTION,0.,22) 25606760
   GO TO 2                                                 25606770
C*****                                                    25606780
11 CALL SYMBOL(2.,13.,.35,'NO DISTORTION',0.,13)          25606790
   CALL SYMBOL(2.,12.,.35,'L = 0.038 dB/MHZ',0.,16)      25606800
   CALL SYMBOL(2.,11.,.35,'L = 0.076 dB/MHZ',0.,16)      25606810
   CALL SYMBOL(2.,10.,.35,'P = 0.004 dB/MHZ**2',0.,19)   25606820
   CALL SYMBOL(2.,9.,.35,'P = 0.008 dB/MHZ**2',0.,19)   25606830
   CALL SYMBOL(2.,8.,.35,'S = 0.2 dB',0.,12)              25606840
   CALL SYMBOL(2.,7.,.35,'S = 0.4 dB',0.,12)              25606850
   CALL SYMBOL(2.,4.5,.35,20HAMPLITUDE DISTORTION,0.,20) 25606860
2   CONTINUE                                              25606870
C   YPAGE=6.5 - (JCURV-1)                                  25606880
C   YPGE=YPAGE-.1                                         25606890
C   CALL SYMBOL(2.,YPAGE,.2,JCURV,0.,-1)                  25606900
C   CALL SYMBOL(2.5,YPGE,.28,2HZ=.0.,2)                   25606910
C   CALL SYMBOL (5.0,YPAGE,.28,'IN dB/MHZ**2',0.,12)      25606920
C   PLOT THE DATA IN LOG-LINEAR MODE.                     25606930
C   CALL LGLIN(XARRAY,YARRAY,M,1,2,JCURV,1)               25606940
C   IF(JCURV.EQ.JLAST) CALL PLOT(0.0,0.0,999)             25606950
C   RETURN                                                 25606960
C   END                                                    25606970
C*****                                                    25606980
C   THIS SUBROUTINE DRAWS THE EYE DIAGRAM FOR A           25606990
C   SYMBOL DURATION.                                       25607000
C*****                                                    25607010
C   SUBROUTINE EYEQ(DATA)                                   25607020
C   DIMENSION DATA2(64),DATA3(64)                       25607030
C   COMPLEX DATA(1)                                       25607040
C   COMMON /NUMB1/ FBW,ALPHA,LDIM,IOFF,LSAMPL             25607050
C   COMMON /NUMB2/ NSNR,NSYMB,BAUD                       25607060
C   ESTABLISH THE SURFACE AREA.                            25607070
C   CALL PLOTS(35.0,27.5)                                  25607080

```

FILE: 256GD FORTRAN A UNIV D'OF OTTAWA

```

C      ESTABLISH THE ORIGIN.
      CALL PLOT(3.0,13.0,-3)
C      WRITE THE TITLE OF THE GRAPH.
      CALL SYMBOL(10.0,12.0,0.49,16HQPSK EYE DIAGRAM,0.0,16)
C      DRAW THE TIME AXIS.
      CALL AXIS(0.0,0.0,1H,-1,31.,0.0,1.0,1.0)
C      DRAW THE AMPLITUDE AXIS.
      CALL AXIS(0.0,-12.0,1H,1,26.0,90.0,-3.0,0.25)
C-     PLOT THE DATA.
      JJ=2*LSAMPL
      DATA2(JJ+1)=0.0
      DATA2(JJ+2)=0.25
      DATA3(JJ+1)=1.0
      DATA3(JJ+2)=1.0
      M2=NSYMB/2
      DO 4 KK=1,M2
      DO 2 I=1,JJ
      I1=(KK-1)*2*LSAMPL+I
      DATA2(I)=REAL(DATA(I1))
      DATA3(I)=FLOAT(I1)
2     CALL LINE(DATA3,DATA2,JJ,1,0,0)
4     CONTINUE
      CALL PLOT(0.0,0.0,999)
      RETURN
      END
C*****
C      THIS SUBROUTINE COMPUTES THE POWER SPECTRUM
C*****
      SUBROUTINE SPECT(SIGNAL,PO)
      COMPLEX SIGNAL(1)
      COMPLEX CWK(130)
      DIMENSION X(4096),PO(1),IWK(7),WK(64),TPD(65)
      COMMON /NUMB1/ FBW,ALPHA,LDIM,IOFF,LSAMPL
      S=0.
      DO 10 I=1,LDIM
      L=I-IOFF
      IF(L.LE.0) L=L+LDIM
      X(I)=REAL(SIGNAL(I))
      X(I+LDIM)=AIMAG(SIGNAL(L))
10     S=S+X(I)+X(I+LDIM)
      S=S/FLOAT(4096)
      DO 20 I=1,4096
      X(I)=X(I)-S
20     CALL FTGPS(X,Y,4096,4096,0,PO,PSY,XPS,IWK,WK,CWK,IER)
      PMAX=PO(1)
      DO 30 I=1,65
      TPO(I)=-10.*ALOG10(PO(I)/PMAX)
      WRITE(6,1) (TPO(I),I=1,65)
      TPO(65)=PO(65)
      DO 40 I=1,63
      TPO(65-I)=TPO(66-I)+2.*PO(65-I)
      TPO(1)=TPO(2)+PO(1)
      TPMAX=TPO(1)
      DO 50 I=1,65
      PO(I)=-10.*ALOG10(PO(I)/TPMAX)
50

```

25607160
25607170
25607180
25607190
25607200
25607210
25607220
25607230
25607240
25607250
25607260
25607270
25607280
25607290
25607300
25607310
25607320
25607330
25607340
25607350
25607360
25607370
25607380
25607390
25607400
25607410
25607420
25607430
25607440
25607450
25607460
25607470
25607480
25607490
25607500
25607510
25607520
25607530
25607540
25607550
25607560
25607570
25607580
25607590
25607600
25607610
25607620
25607630
25607640
25607650
25607660
25607670
25607680
25607690
25607700

FILE: 256GD FORTRAN A UNIV D'/OF OTTAWA

```

WRITE(6,2) (PO(I),I=1,65)
2   FORMAT(2X,'NORM. POWER SPECTRUM WITH TOTAL POWER=1'/
      &,10(2X,F6.1))
1   FORMAT(2X,'POWER SPECTRUM'/,10(2X,F6.1))
RETURN
END
C*****
C THIS SUBROUTINE SIMULATES A HARD LIMITER
C*****
SUBROUTINE HLIM(DATA)
COMPLEX DATA(1)
COMMON /NUMB1/ FBW, ALPHA, LDIM, IOFF, LSAMPL
DO 10 I=1, LDIM
10  DATA(I)=DATA(I)/CABS(DATA(I))
RETURN
END
C*****
C          PARABOLIC GROUP DELAY
C          GROUP DELAY IN NANOSECONDS = S*F*F
C*****
SUBROUTINE PARGD(S,TF)
COMMON /NUMB1/ FBW, ALPHA, LDIM, IOFF, LSAMPL
COMMON /NUMB2/ NSNR, NSYMB, BAUD
COMPLEX TF(1)
SBANDW=FLOAT(LSAMPL)*BAUD
NO1=LDIM/2 + 1
NO2=NO1 + 1
DO 20 I=1, NO1
A1=FLOAT(I-1)*SBANDW/FLOAT(LDIM)
PHI=2.*3.141592/3.*(1S*(A1**3.))/(10.**3.)
TF(I)=TF(I)*CPLX(COS(PHI),-SIN(PHI))
20  CONTINUE
DO 21 I=NO2, LDIM
TF(I)=CONJG(TF(LDIM+2-I))
21  CONTINUE
RETURN
END
C*****
C          SINE OR COSINE GROUP DELAY WITH ARBITRARY AMPLITUDE
C          AND NUMBER OF RIPPLES
C          GROUP DELAY IN NANOSECONDS = C*COS(2*PIE*K*F/FNYQ +ISIN*PIE/2)
C*****
SUBROUTINE SINCGD(ISIN,C,K,TF)
COMMON /NUMB1/ FBW, ALPHA, LDIM, IOFF, LSAMPL
COMMON /NUMB2/ NSNR, NSYMB, BAUD
COMPLEX TF(1)
SBANDW=FLOAT(LSAMPL)*BAUD
NO1=LDIM/2 + 1
NO2=NO1 + 1
C1=(1.+ALPHA)*BAUD/K
IF (ISIN.EQ.1) GO TO 50
DO 10 I=1, NO1
A1=FLOAT(I-1)*SBANDW/FLOAT(LDIM)
PHI=(C*C1/(10.**3.))*SIN(2.*3.141592*A1/CT)
TF(I)=TF(I)*CPLX(COS(PHI),-SIN(PHI))

```

25607710
25607720
25607730
25607740
25607750
25607760
25607770
25607780
25607790
25607800
25607810
25607820
25607830
25607840
25607850
25607860
25607870
25607880
25607890
25607900
25607910
25607920
25607930
25607940
25607950
25607960
25607970
25607980
25607990
25608000
25608010
25608020
25608030
25608040
25608050
25608060
25608070
25608080
25608090
25608100
25608110
25608120
25608130
25608140
25608150
25608160
25608170
25608180
25608190
25608200
25608210
25608220
25608230
25608240
25608250

FILE: 256GD FORTRAN. A UNIV D'OF OTTAWA

```

10 CONTINUE
DO 11 I=NO2,LDIM
TF(I)=CONJG(TF(LDIM+2-I))
11 CONTINUE
GO TO 60
50 DO 12 I=1,NO1
AI=FLOAT(I-1)*SBANDW/FLOAT(LDIM)
PHI=(C*C1/(10.**3.))*COS(2.*3.141592*AI/C1)
TF(I)=TF(I)*CMPLX(COS(PHI),SIN(PHI))
12 CONTINUE
DO 13 I=NO2,LDIM
TF(I)=TF(LDIM+2-I)
13 CONTINUE
60 RETURN
END
C*****
C LINEAR GROUP DELAY
C GROUP DELAY IN NANOSECONDS = B*F
C*****
SUBROUTINE LINGD(B,TF)
COMMON /NUMB1/ FBW,ALPHA,LDIM,IOFF,LSAMPL
COMMON /NUMB2/ NSNR,NSYMB,BAUD
COMPLEX TF(1)
SBANDW=FLOAT(LSAMPL)*BAUD
NO1=LDIM/2 + 1
NO2=NO1 + 1
DO 10 I=1,NO1
AI=FLOAT(I-1)*SBANDW/FLOAT(LDIM)
PHI=3.141592*(B/(10.**3.))*(AI**2.)
TF(I)=TF(I)*CMPLX(COS(PHI),-SIN(PHI))
10 CONTINUE
DO 20 I=NO2,LDIM
TF(I)=TF(LDIM+2-I)
20 CONTINUE
RETURN
END
C*****
C LINEAR AMPLITUDE DISTORTION
C*****
SUBROUTINE LINAMP(Z,TF)
COMMON /NUMB1/ FBW,ALPHA,LDIM,IOFF,LSAMPL
COMMON /NUMB2/ NSNR,NSYMB,BAUD
COMPLEX TF(1)
SBANDW=FLOAT(LSAMPL)*BAUD
NO1=LDIM/2 + 1
NO2=NO1 + 1
AI=Z*SBANDW/FLOAT(LDIM)
DO 10 I=1,NO1
AJ=(I-1)*AI/20.
TF(I)=TF(I)*(10.**AJ)
10 CONTINUE
DO 20 I=NO2,LDIM
AZ=(LDIM+2-I)*AI/20.
TF(I)=TF(I)/(10.**AZ)
20 CONTINUE

```

FILE: 256GD FORTRAN A UNIV D' OF OTTAWA

```

RETURN
END
C*****
C PARABOLIC AMPLITUDE DISTORTION
C*****
SUBROUTINE PARAMP(P,TF)
COMMON /NUMB1/ FBW,ALPHA,LDIM,IOFF,LSAMPL
COMMON /NUMB2/ NSNR,NSYMB,BAUD
COMPLEX TF(1)
SBANDW=FLOAT(LSAMPL)*BAUD
NO1=LDIM/2 + 1
NO2=NO1 + 1
A1=P*((SBANDW/FLOAT(LDIM))**2.)
DO 10 I=1,NO1
AJ=((I-1)**2.)*A1/20.
TF(I)=TF(I)*(10.**AJ)
10 CONTINUE
DO 11 I=NO2,LDIM
TF(I)=TF(LDIM+2-I)
11 CONTINUE
RETURN
END
C*****
C SINE OR COSINE RIPPLE FOR AMPLITUDE DISTORTION
C*****
SUBROUTINE SINAMP(ISIN,D,K,TF)
COMMON /NUMB1/ FBW,ALPHA,LDIM,IOFF,LSAMPL
COMMON /NUMB2/ NSNR,NSYMB,BAUD
COMPLEX TF(1)
SBANDW=FLOAT(LSAMPL)*BAUD
NO1=LDIM/2 + 1
NO2=NO1 + 1
AJ=SBANDW/FLOAT(LDIM)
C1=(1.+ALPHA)*BAUD/K
IF(ISIN.EQ.1) GO TO 50
DO 10 I=1,NO1
AZ=D*COS(2.*3.141592*AJ*(FLOAT(I)-1.)/C1)/20.
TF(I)=TF(I)*(10.**AZ)
10 CONTINUE
DO 20 I=NO2,LDIM
TF(I)=TF(LDIM+2-I)
20 CONTINUE
RETURN
50 DO 30 I=1,NO1
AZ=D*SIN(2.*3.141592*AJ*(FLOAT(I)-1.)/C1)/20.
TF(I)=TF(I)*(10.**AZ)
30 CONTINUE
DO 40 I=NO2,LDIM
AZ=D*SIN(2.*3.141592*AJ*(FLOAT(LDIM+2-I)-1.)/C1)/20.
TF(I)=TF(I)/(10.**AZ)
40 CONTINUE
RETURN
END
25608810
25608820
25608830
25608840
25608850
25608860
25608870
25608880
25608890
25608900
25608910
25608920
25608930
25608940
25608950
25608960
25608970
25608980
25608990
25609000
25609010
25609020
25609030
25609040
25609050
25609060
25609070
25609080
25609090
25609100
25609110
25609120
25609130
25609140
25609150
25609160
25609170
25609180
25609190
25609200
25609210
25609220
25609230
25609240
25609250
25609260
25609270
25609280
25609290
25609300
25609310
25609320
25609330

```


FILE: 225Q FORTRAN A UNIV D' OF OTTAWA

```

IS=2
IBAUD=BAUD/A
CALL PR1(TF, IBAUD, IS)
CALL MHGG(TF, PNOISE)
CALL FILTER(DATA, TF)
C
CALL PRCODE(NI, NIP, NSYMB)
CALL PRCODE(NQ, NQP, NSYMB)
CALL SYNCRO(DATA, PNOISE, NIP, NQP, MI, MQ, EB)
CALL DECODE(NERROR, DATA, PNOISE, MI, MQ, NIP, NQP, EBNO, PEI, EB)
IF((NERROR.NE.0).AND.(NR.EQ.NRUNS)) CALL PLOT(0.0,0.0,999)
IF(NERROR.NE.0) GO TO 100
DO, 99 I=1, NSNR
XARRAY(I)=EBNO(I)
99 YARRAY(I)=PEI(I)
-A=1.
CALL DRAWCN(XARRAY, YARRAY, NR, NRUNS, A)
111 CALL EYEQ(DATA)
100 CONTINUE
STOP
END
C*****
C PARTIAL RESPONSE ENCODER (1+D)
C B: I/P SYMBOL SEQUENCE
C C: O/P SYMBOL SEQUENCE
C C(I)=B(I)+B(I-1)
C*****
SUBROUTINE PRCODE(B, C, NSYMB)
INTEGER B(1), C(1)
C(1)=B(1)+B(NSYMB)
DO 10 I=2, NSYMB
C(I)=B(I)+B(I-1)
10 CONTINUE
RETURN
END
C*****
C FORMS A COMPLEX BASEBAND SIGNAL
C NI : I-CHANNEL SYMBOL SEQ
C NQ : Q-CHANNEL SYMBOL SEQ
C DATA : O/P SIGNAL
C*****
SUBROUTINE SIGNAL(DATA, NI, NQ)
COMPLEX DATA(1)
DIMENSION NI(1), NQ(1)
COMMON /NUMB1/ FBW, ALPHA, LDIM, IOFF, LSAMPL, SBANDW
COMMON /NUMB2/ NSNR, NSYMB, BAUD, NO1, NO2
DO 2 I=1, NSYMB
LOAD INTO SAMPLE ARRAY, 16 SAMPLES PER SYMBOL
J1=(I-1)*LSAMPL+1
J2=I*LSAMPL
DO 3 J3=J1, J2
3 DATA(J3)=CMPLX(FLOAT(NI(I)), FLOAT(NQ(I)))
2 CONTINUE
RETURN
END

```

22500560
22500570
22500580
22500590
22500600
22500610
22500620
22500630
22500640
22500650
22500660
22500670
22500680
22500690
22500700
22500710
22500720
22500730
22500740
22500750
22500760
22500770
22500780
22500790
22500800
22500810
22500820
22500830
22500840
22500850
22500860
22500870
22500880
22500890
22500900
22500910
22500920
22500930
22500940
22500950
22500960
22500970
22500980
22500990
22501000
22501010
22501020
22501030
22501040
22501050
22501060
22501070
22501080
22501090
22501100

FILE: 225Q FORTRAN A UNIV D'OF OTTAWA

```

SUBROUTINE LOAD64(DATA,NI,NQ)
COMPLEX DATA(1)
DIMENSION NY(11),NI(1),NQ(1),NX(2048)
COMMON /NUMB1/ FBW,ALPHA,LDIM,IOFF,LSAMPL
C DATA NX(1),NX(2),NX(3),NX(4),NX(5),NX(6),NX(7),NX(8),NX(9),
C #NX(10),NX(11),NX(12)/-1,-1,-1,-1,-1,-1,-1,-1,-1,-1,-1,-1/
DATA NY(1),NY(2),NY(3),NY(4),NY(5),NY(6),NY(7),NY(8),NY(9),
#NY(10),NY(11)/-1,-1,1,1,1,-1,-1,-1,-1,-1,-1/
DATA JLAST,JTAP/11,1/
KKK=2**JLAST
KK=KKK-(1+JLAST)
DO 6 I=1,JLAST
NX(I)=NY(I)
6 CONTINUE
C GENERATE 2**JLAST -1 LENGTH SEQUENCE USING GIVEN DATA AND
C GENERATOR POLYNOMIAL.
DO 1 J=1,KK
I=J+JLAST
NX(I)=NX(J)*NX(J+2)
NX(I)=0-NX(I)
1 CONTINUE
C
C GENERATE 6 CYCLICALLY SHIFTED VERSIONS OF ORIGINAL
C SEQUENCE OF LENGTH 2**JLAST.
C
K1=1
K2=2
K3=3
K4=4
K5=5
K6=6
DO 2 I=1,KKK
IF (K1.EQ.KKK) K1=1
IF (K2.EQ.KKK) K2=1
IF (K3.EQ.KKK) K3=1
IF (K4.EQ.KKK) K4=1
IF (K5.EQ.KKK) K5=1
IF (K6.EQ.KKK) K6=1
NI(I)=(NX(K1)*4) + (NX(K3)*2) + NX(K5)
NQ(I)=(NX(K2)*4) + (NX(K4)*2) + NX(K6)
C
C LOAD INTO SAMPLE ARRAY, 16 SAMPLES PER SYMBOL
J1=(I-1)*LSAMPL+1
J2=1*LSAMPL
DO 3 J3=J1,J2
3 DATA(J3)=CMPLX(FLOAT(NI(I)),FLOAT(NQ(I)))
K1=K1+1
K2=K2+1
K3=K3+1
K4=K4+1
K5=K5+1
K6=K6+1
2 CONTINUE
IF (IOFF.EQ.0) RETURN
LL=LDIM-1

```

22501660
22501670
22501680
22501690
22501700
22501710
22501720
22501730
22501740
22501750
22501760
22501770
22501780
22501790
22501800
22501810
22501820
22501830
22501840
22501850
22501860
22501870
22501880
22501890
22501900
22501910
22501920
22501930
22501940
22501950
22501960
22501970
22501980
22501990
22502000
22502010
22502020
22502030
22502040
22502050
22502060
22502070
22502080
22502090
22502100
22502110
22502120
22502130
22502140
22502150
22502160
22502170
22502180
22502190
22502200

FILE: 225Q FORTRAN A UNIV D' / OF OTTAWA

```

DO 4 I=1, IOFF
  XX=AIMAG(DATA(1))
DO 5 K=1, LL
5 DATA(K)=CMPLX(REAL(DATA(K)), AIMAG(DATA(K+1)))
4 DATA(LDIM)=CMPLX(REAL(DATA(LDIM)), XX)
  RETURN
  END
C*****
C RAISED COSINE FILTER WITH ARBITRARY ALPHA AND X/SINX
C*****
SUBROUTINE RCOSTX(TF)
  COMPLEX TF(65536)
  COMMON /NUMB1/ FBW, ALPHA, LDIM, IOFF, LSAMPL
  COMMON /NUMB2/ NSNR, NSYMB, BAUD
  SBANDW=BAUD*LSAMPL
  NO=LDIM/2
  NO1=NO+1
  IF (ALPHA.EQ.0) ALPHA=0.0001
  FN=LDIM*(FBW/SBANDW)
  F1=(1.-ALPHA)*FN
  F2=(1.+ALPHA)*FN
  IFN=IFX(FN)
  IF1=IFX(F1)+1
  IF2=IFX(F2)+1
C
C THE AMPLITUDE CHARACTERISTICS
C
  A1=3.1415926/(2.*FLOAT(IFN))
  DO 8 I=2, IF1
  TF(I)=CMPLX(1.0,0.0)
  J=I-1
C
C X/SIN(X) EQUALIZATION
C
  A2=(FLOAT(J)*A1)/(SIN(FLOAT(J)*A1))
  TF(I)=CMPLX(A2,0.0)
8 CONTINUE
  JK=IF1+1
  DO 9 J=JK, IF2
  I=J-1
C
C ROOT OF RAISED COSINE
C
  A3=(FLOAT(I)*A1)/(SIN(FLOAT(I)*A1))
  A=(3.1415926/(2.0*ALPHA))*((FLOAT(I)/FLOAT(IFN))-1.)
  TF(J)=CMPLX(SQRT(0.5*(1.0-SIN(A))),0.0)
  TF(J)=TF(J)*CMPLX(A3,0.0)
9 CONTINUE
  JH=IF2+1
  DO 10 I=JH, NO1
  TF(I)=CMPLX(0.0,0.0)
10 CONTINUE
  NO2=NO1+1
  DO 5 I=NO2, LDIM
  TF(I)=CONJG(TF(LDIM+2-I))

```

22502210
22502220
22502230
22502240
22502250
22502260
22502270
22502280
22502290
22502300
22502310
22502320
22502330
22502340
22502350
22502360
22502370
22502380
22502390
22502400
22502410
22502420
22502430
22502440
22502450
22502460
22502470
22502480
22502490
22502500
22502510
22502520
22502530
22502540
22502550
22502560
22502570
22502580
22502590
22502600
22502610
22502620
22502630
22502640
22502650
22502660
22502670
22502680
22502690
22502700
22502710
22502720
22502730
22502740
22502750

FILE: 225Q FORTRAN A UNIV D'OF OTTAWA

```

5 CONTINUE
  RETURN
  END
C*****
C RAISED COSINE FILTER WITH ARBITRARY ALPHA
C*****
  SUBROUTINE RCOSRX(TF)
    COMPLEX TF(65536)
    COMMON /NUMB1/ FBW,ALPHA,LDIM,IOFF,LSAMPL
    COMMON /NUMB2/ NSNR,NSYMB,BAUD
    SBANDW=BAUD*LSAMPL
    NO=LDIM/2
    NO1=NO+1
    IF (ALPHA.EQ.0) ALPHA=0.0001
    FN=LDIM*(FBW/SBANDW)
    F1=(1.-ALPHA)*FN
    F2=(1.+ALPHA)*FN
    IFN=IFIX(FN)
    IF1=IFIX(F1)+1
    IF2=IFIX(F2)+1
C
C   AMPLITUDE CHARACTERISTIC
C
    A1=3.141592/(2.*FLOAT(IFN))
    DO 8 I=2,IF1
      TF(I)=CMPLX(1.0,0.0)
      J=I-1
      TF(J)=CMPLX(1.,0.0)
    8 CONTINUE
    JK=IF1+1
    DO 9 J=JK,IF2
      I=J-1
C
C   ROOT OF RAISED COSINE
C
    A=(3.141592/(2.0*ALPHA))*((FLOAT(I)/FLOAT(IFN))-1.)
    TF(J)=CMPLX(SQRT(0.5*(1.0~SIN(A))),0.0)
    9 CONTINUE
    JH=IF2+1
    DO 10 I=JH,NO1
      TF(I)=CMPLX(0.0,0.0)
    10 CONTINUE
    NO2=NO1+1
    DO 5 I=NO2,LDIM
      TF(I)=CONJG(TF(LDIM+2-I))
    5 CONTINUE
    RETURN
    END
C*****
C X/SIN(X) EQUALIZER
C FBX : NYQUIST FREQ FOR THIS EQUALIZER
C*****
  SUBROUTINE XSINX(TF,FBX)
    COMPLEX TF(65536)
    COMMON /NUMB1/ FBW,ALPHA,LDIM,IOFF,LSAMPL

```

22502760
22502770
22502780
22502790
22502800
22502810
22502820
22502830
22502840
22502850
22502860
22502870
22502880
22502890
22502900
22502910
22502920
22502930
22502940
22502950
22502960
22502970
22502980
22502990
22503000
22503010
22503020
22503030
22503040
22503050
22503060
22503070
22503080
22503090
22503100
22503110
22503120
22503130
22503140
22503150
22503160
22503170
22503180
22503190
22503200
22503210
22503220
22503230
22503240
22503250
22503260
22503270
22503280
22503290
22503300

FILE: 225Q FORTRAN A UNIV D'OF OTTAWA

```

COMMON /NUMB2/ NSNR, NSYMB, BAUD
SBANDW=BAUD*LSAMPL
NO=LDIM/2
NO1=NO+1
IF (ALPHA.EQ.0) ALPHA=0.0001
FN=LDIM*(FBX/SBANDW)
F1=(1.-ALPHA)*FN
F2=(1.+ALPHA)*FN
IFN=IFIX(FN)
IF1=IFIX(F1)+1
IF2=IFIX(F2)+1
C
C
C THE AMPLITUDE CHARACTERISTICS
A1=3.1415926/(2.*FLOAT(IFN))
TF(1)=CMPLX(1.0,0.0)
DO 8 I=2,IF1
J=I-1
C
C
C X/SIN(X) EQUALIZATION
A2=(FLOAT(J)*A1)/(SIN(FLOAT(J)*A1))
TF(1)=CMPLX(A2,0.0)
8 CONTINUE
JK=IF1+1
DO 9 J=JK,IF2
I=J-1
C
C
C ROOT OF RAISED COSINE
A3=(FLOAT(I)*A1)/(SIN(FLOAT(I)*A1))
TF(J)=CMPLX(A3,0.0)
9 CONTINUE
JH=IF2+1
DO 10 I=JH,NO1
TF(I)=CMPLX(0.0,0.0)
10 CONTINUE
NO2=NO1+1
DO 5 I=NO2,LDIM
TF(I)=CONJG(TF(LDIM+2-I))
5 CONTINUE
RETURN
END
C*****
C THE FOLLOWING SUBROUTINE PERFORMS THE FILTERING
C PROCESS ON THE DATA SEQUENCE.
C*****
SUBROUTINE FILTER(DATA,TF)
COMPLEX DATA(1),TF(1)
DIMENSION IWK(17)
COMMON /NUMB1/ FBW,ALPHA,LDIM,IOFF,LSAMPL
CALL FFT2C(DATA,16,IWK)
DO 1 I=1,LDIM
1 DATA(I)=CONJG(DATA(I)*TF(I))
CALL FFT2C(DATA,16,IWK)

```

22503310
22503320
22503330
22503340
22503350
22503360
22503370
22503380
22503390
22503400
22503410
22503420
22503430
22503440
22503450
22503460
22503470
22503480
22503490
22503500
22503510
22503520
22503530
22503540
22503550
22503560
22503570
22503580
22503590
22503600
22503610
22503620
22503630
22503640
22503650
22503660
22503670
22503680
22503690
22503700
22503710
22503720
22503730
22503740
22503750
22503760
22503770
22503780
22503790
22503800
22503810
22503820
22503830
22503840
22503850

FILE: 225Q FORTRAN A UNIV D' / OF OTTAWA

```

      DO 2 I=1,LDIM
2     DATA(1)=CONJG(DATA(1))/FLOAT(LDIM)
      RETURN
      END
C*****
C     THIS SUBROUTINE COMPUTES THE EFFECTIVE NOISE (PNOISE)
C     AT THE OUTPUT OF THE RECEIVE FILTER
C*****
      SUBROUTINE HHGG(TF,PNOISE)
      COMPLEX TF(1)
      COMMON /NUMB1/ FBW,ALPHA,LDIM,IOFF,LSAMPL
      COMMON /NUMB2/ NSNR,NSYMB,BAUD
      SUM=0.0
      SBANDW=BAUD*LSAMPL
      DO 1 L=1,LDIM
      HH=(CABS(TF(L)))**2
1     SUM=SUM+HH
      PNOISE=SUM*SBANDW/FLOAT(LDIM)/2.
      WRITE (6,2) PNOISE
2     FORMAT(5X,'PNOISE=',F7.3,/)
      RETURN
      END
C*****
C CALCULATE EB
C*****
      SUBROUTINE ENERGY(DATA,EB)
      COMPLEX DATA(1)
      WATTS=0.
      COMMON /NUMB2/ NSNR,NSYMB,BAUD
      COMMON /NUMB1/ FBW,ALPHA,LDIM,IOFF,LSAMPL
      DO 1 I=1,LDIM
      WATTS=WATTS+((CABS(DATA(I)))**2.)
1     CONTINUE
      WATTS=WATTS/(FLOAT(LDIM))
      EB=WATTS/(6.*BAUD)
      WRITE (6,40) WATTS,EB
40    FORMAT(10X,'C=',F15.6,5X,'EB=',E15.8)
      RETURN
      END
C*****
C     THE FOLLOWING SUBROUTINE SYNCHRONIZES THE RECEIVED DATA.
C*****
      SUBROUTINE SYNCRO(DATA,PNOISE,NI,NQ,MI,MQ,EB)
      INTEGER QL14
      COMPLEX DATA(1),AMP
      DIMENSION NI(1),NQ(1)
      COMMON /NUMB1/ FBW,ALPHA,LDIM,IOFF,LSAMPL
      COMMON /NUMB2/ NSNR,NSYMB,BAUD
      NERROR=0
      IF (IOFF.EQ.0) GO TO 111
      DO 6 K=1,IOFF
      XX=AIMAG(DATA(LDIM))
      DO 7 KK=2,LDIM
7     DATA(KK)=CMPLX(REAL(DATA(KK)),AIMAG(DATA(KK-1)))
6     DATA(1)=CMPLX(REAL(DATA(1)),XX)

```

22503860
22503870
22503880
22503890
22503900
22503910
22503920
22503930
22503940
22503950
22503960
22503970
22503980
22503990
22504000
22504010
22504020
22504030
22504040
22504050
22504060
22504070
22504080
22504090
22504100
22504110
22504120
22504130
22504140
22504150
22504160
22504170
22504180
22504190
22504200
22504210
22504220
22504230
22504240
22504250
22504260
22504270
22504280
22504290
22504300
22504310
22504320
22504330
22504340
22504350
22504360
22504370
22504380
22504390
22504400

FILE: 225Q FORTRAN A UNIV D'/OF OTTAWA

```

DATA(LDIM)=AMP
250 CONTINUE
C
C   OPTIMIZE THE SAMPLING INSTANT
C
230 M1=1
    MQ=1
    EO1=FLOAT(NSYMB) + 1.
    EQ=FLOAT(NSYMB) + 1.
    M=22
    VARIAN=PNOISE*EB*(10.**(-0.1*FLOAT(M)))
    SIGMA=SQRT(VARIAN)
    MOS=LSAMPL/4
    DO 80 J=1,MOS
        EI=0.
        EQ=0.
        IERX=0
        IERY=0
        DO 70 K=1,NSYMB
            VERIFY THAT NO SAMPLED SYMBOL IS IN ERROR
            J1=(K-1)*LSAMPL+J
            AXBAR=(REAL(DATA(J1))+REAL(DATA(J1+1)))/2.
            AYBAR=(AIMAG(DATA(J1))+AIMAG(DATA(J1+1)))/2.
            INDEXI=0
            AMPX=ABS(AXBAR)
            AMPI=ABS(FLOAT(NI(K)))
            THR1I=AMPI - 1.0
            THR2I=AMPI + 1.0
            IL14=0
            IF (AMPI.EQ. 14.) GO TO 30
            IF (( AMPX.GE.THR2I).OR.(AMPX.LE.THR1I)) INDEXI=1
            GO TO 40
        30 IF(AMPX.LE.THR1I) INDEXI=1
            IL14=1
        40 CONTINUE
            INDEXQ=0
            AMPY=ABS(AYBAR)
            AMPQ=ABS(FLOAT(NQ(K)))
            THR1Q=AMPQ - 1.0
            THR2Q=AMPQ + 1.0
            QL14=0
            IF (AMPQ.EQ. 14.) GO TO 50
            IF (( AMPY.GE.THR2Q).OR.(AMPY.LE.THR1Q)) INDEXQ=1
            GO TO 60
        50 IF(AMPY.LE.THR1Q) INDEXQ=1
            QL14=1
        60 CONTINUE
            IF(INDEXI.EQ.1) EI=EI + 1.
            IF(INDEXQ.EQ.1) EQ=EQ + 1.
C
C   COMPUTE THE PROBABILITY OF ERROR FOR THIS SYMBOL AT EB/NO=22dB
C
D1=ABS(AMPX-THR1I)
ARG=D1/(SIGMA*SQRT(2.))
C   CHECK IF ARG IS LARGE INWHICH CASE PE IS INSIGNIFICANT

```

22504960
22504970
22504980
22504990
22505000
22505010
22505020
22505030
22505040
22505050
22505060
22505070
22505080
22505090
22505100
22505110
22505120
22505130
22505140
22505150
22505160
22505170
22505180
22505190
22505200
22505210
22505220
22505230
22505240
22505250
22505260
22505270
22505280
22505290
22505300
22505310
22505320
22505330
22505340
22505350
22505360
22505370
22505380
22505390
22505400
22505410
22505420
22505430
22505440
22505450
22505460
22505470
22505480
22505490
22505500

FILE: 225Q .FORTRAN A UNIV D' /OF OTTAWA

```

C
  IF (ARG.GT.12.) ARG=12.
  E1=E1 + ERFC(ARG)/2.
  IF (IL14 .EQ. 1) GO TO 65
  D2=ABS(THR21-AMPX)
  ARG=D2/(SIGMA*SQRT(2.))
  IF (ARG.GT.12.) ARG=12.
  E1=E1 + ERFC(ARG)/2.
65 D1=ABS(AMPY-THR1Q)
  ARG=D1/(SIGMA*SQRT(2.))
  IF (ARG.GT.12.) ARG=12.
  EQ=EQ + ERFC(ARG)/2.
  IF (QL14 .EQ. 1) GO TO 70
  D2=ABS(THR2Q-AMPY)
  ARG=D2/(SIGMA*SQRT(2.))
  IF (ARG.GT.12.) ARG=12.
  EQ=EQ + ERFC(ARG)/2.
  IERX=IERX+INDEXI
  IERY=IERY+INDEXQ
70 CONTINUE
  WRITE(6,81) IERX, IERY
81 FORMAT(5X, 'IERX=', 15, 5X, 'IERY=', 15)
  IF (EO1.LE.E1) GO TO 75
  EO1=E1
  MI=J
75 CONTINUE
  IF (EQQ.LE.EQ) GO TO 80
  EQQ=EQ
  MQ=J
80 MOFF=ABS(MI-MQ)
  WRITE(6,91) MI, MQ
91 FORMAT(5X, 'MI=', 13, 5X, 'MQ=', 13)
  IF (MOFF.NE.0) WRITE(6,90) MOFF
  OFF=(FLOAT(MI) + FLOAT(MQ))/FLOAT(LSAMPL)
90 FORMAT(5X, 'SAMPLING POINTS FOR I AND Q CHANNELS DIFFER BY',
#12, ' SIXTEENTHS OF THE SYMBOL INTERVAL', /)
  WRITE(6,95) OFF
95 FORMAT(5X, 'RECEIVED DATA IS DELAYED BY ', F7.3, ' SYMBOLS', /)
  RETURN
  END
C*****
C THE FOLLOWING SUBROUTINE DECODES THE RECEIVED DATA.
C*****
  SUBROUTINE DECODE(NERROR, DATA, PNOISE, MI, MQ, NI, NQ, EBNO, PE, EB)
  INTEGER QL14
  COMPLEX DATA(1), AMP
  DIMENSION EBNO(1), PE(1), NI(1), NQ(1)
  COMMON /NUMB1/ FBW, ALPHA, LDIM, IOFF, LSAMPL
  COMMON /NUMB2/ NSNR, NSYMB, BAUD
  NERROR=0
  DO 1 I=1, NSNR
  PE(I)=0.
1 CHECK FOR AN ERROR AT THE SAMPLING INSTANT, ONLY THOSE
C ERRORS IN ADJACENT LEVELS ARE CONSIDERED
C
3 DO 2 K=1, NSYMB

```

```

22505510
22505520
22505530
22505540
22505550
22505560
22505570
22505580
22505590
22505600
22505610
22505620
22505630
22505640
22505650
22505660
22505670
22505680
22505690
22505700
22505710
22505720
22505730
22505740
22505750
22505760
22505770
22505780
22505790
22505800
22505810
22505820
22505830
22505840
22505850
22505860
22505870
22505880
22505890
22505900
22505910
22505920
22505930
22505940
22505950
22505960
22505970
22505980
22505990
22506000
22506010
22506020
22506030
22506040
22506050

```


FILE: 225Q FORTRAN A UNIV D' /OF OTTAWA

```

100 D1=ABS(AMPY-THR1Q)
    ARG=D1/(SIGMA*SQRT(2.))
    IF (INDEXQ.EQ.1) GO TO 153
    IF (ARG.GT.12.) ARG=12.
    PEQ=ERFC(ARG)/2.
    IF (QL14 .EQ. 1) GO TO 110
    D2=ABS(THR2Q-AMPY)
    ARG=D2/(SIGMA*SQRT(2.))
    IF (ARG.GT.12.) ARG=12.
    PEQ=PEQ + ERFC(ARG)/2.
110 IF (PE1.LT.1.E-15) PE1=0.
    IF (PEQ.LT.1.E-15) PEQ=0.
    4 PE(M)=PE(M)+(PE1+PEQ)/2.
    2 CONTINUE
    DO 5 I=1, NSNR
    5 PE(I)=PE(I)/FLOAT(NSYMB)
    PRINT 150
150 FORMAT(5X, 'EB/NO', 10X, 'PROB. OF ERROR', /)
    WRITE (6, 151) (EBNO(I), PE(I), I=1, NSNR)
151 FORMAT(5X, F5.1, 10X, E10.2)
    WRITE (6, 152) NERROR
152 FORMAT(/5X, 'ERRORS=', 15, /)
    GO TO 155
153 PRINT 154
154 FORMAT (10X, 'SYMBOL WAS IN ERROR, RUN WAS TERMINATED', /)
    WRITE(6, 157) NERI
157 FORMAT(5X, 'NERI=', 15)
155 CONTINUE
    RETURN
    END
C*****
C THIS SUBROUTINE DRAWS PROBABILITY OF ERROR CURVES FOR
C P(E) AS LOW AS 1.0E-10 AND A C/N RATIO AS HIGH AS 42 dB.
C*****
SUBROUTINE DRAWCN(XARRAY, YARRAY, JCURV, JLAST, A)
DIMENSION XARRAY(1), YARRAY(1)
COMMON /NUMB2/ NSNR, NSYMB, BAUD
M=NSNR
BR=2.*3.*BAUD
NBW=BAUD/A
CF=BR/NBW
DO 1 K=1, NSNR
XARRAY(K)=XARRAY(K) + 10*(ALOG10(CF))
IF(YARRAY(K).LE.1.0E-10) GOTO 3
GOTO 1
3 M=M-1
GOTO 4
1 CONTINUE
4 CONTINUE
I=M+1
II=I+1
XARRAY(II)=22.
XARRAY(II)=1.0
YARRAY(II)=1.E-10
YARRAY(II)=0.4

```

22506610
22506620
22506630
22506640
22506650
22506660
22506670
22506680
22506690
22506700
22506710
22506720
22506730
22506740
22506750
22506760
22506770
22506780
22506790
22506800
22506810
22506820
22506830
22506840
22506850
22506860
22506870
22506880
22506890
22506900
22506910
22506920
22506930
22506940
22506950
22506960
22506970
22506980
22506990
22507000
22507010
22507020
22507030
22507040
22507050
22507060
22507070
22507080
22507090
22507100
22507110
22507120
22507130
22507140
22507150

FILE: 225Q FORTRAN A UNIV D'OF OTTAWA

```

C      IF(JCURV.GT.1) GOTO 2
C      ESTABLISH THE SURFACE AREA.
C      CALL PLOTS(30.0,27.5)
C      CALL FACTOR(0.85)
C      ESTABLISH THE ORIGIN.
C      CALL PLOT(3.0,1.5,-3)
C      DRAW THE LOGARITHMIC Y-AXIS.
C      CALL LGAXS(0.0,0.0,20HPROBABILITY OF ERROR,20,25.,
C      +90.,1.0E-10,.4)
C      DRAW THE LINEAR X-AXIS.
C      CALL AXIS(0.0,0.0,9HC/N IN dB,-9,
C      +22.0,0.0,22.,1.0)
C      WRITE THE TITLE OF THE GRAPH.
C      CALL SYMBOL(6.,23.,.35,'PARABOLIC AMPLITUDE DISTORTION',0.,30)
C      PLOT LEGEND
C      *****
C      GO TO 2
C      41 CALL SYMBOL(2.,13.,.35,'NO DISTORTION',0.,13)
C      CALL SYMBOL(2.,12.,.35,'B=0.095 ns/MHZ',0.,14)
C      CALL SYMBOL(2.,11.,.35,'B=0.190 ns/MHZ',0.,14)
C      CALL SYMBOL(2.,10.,.35,'S=0.270 ns/MHZ**2',0.,17)
C      CALL SYMBOL(2.,9.,.35,'S=0.540 ns/MHZ**2',0.,17)
C      CALL SYMBOL(2.,8.,.35,'C=12.0 ns',0.,9)
C      CALL SYMBOL(2.,7.,.35,'C=24.0 ns',0.,9)
C      CALL SYMBOL(2.,4.5,.35,22HGROUP DELAY DISTORTION,0.,22)
C      CALL SYMBOL(2.0,3.5,.35,'T(f)=B*f',0.,8)
C      CALL SYMBOL(2.0,2.5,.35,'T(f)=S*f*f',0.,11)
C      CALL SYMBOL(2.0,1.5,.35,'T(f)=C*sin(4 f/f)',0.,18)
C      CALL SYMBOL(2.0,1.3,.35,'f',0.,18)
C      *****
C      CALL SYMBOL(2.,13.,.35,'NO DISTORTION',0.,13)
C      CALL SYMBOL(2.,12.,.35,'Z=0.076 dB/MHZ',0.,14)
C      CALL SYMBOL(2.,11.,.35,'Z=0.152 dB/MHZ',0.,14)
C      CALL SYMBOL(2.,10.,.35,'P=0.00725 dB/MHZ**2',0.,19)
C      CALL SYMBOL(2.,9.,.35,'P=0.0145 dB/MHZ**2',0.,18)
C      CALL SYMBOL(2.,8.,.35,'D=0.4 dB',0.,8)
C      CALL SYMBOL(2.,7.,.35,'D=0.8 dB',0.,8)
C      CALL SYMBOL(2.,4.5,.35,20HAMPLITUDE DISTORTION,0.,20)
C      CALL SYMBOL(2.0,3.5,.35,'A(f)=Z*f',0.,8)
C      CALL SYMBOL(2.0,2.5,.35,'A(f)=P*f*f',0.,11)
C      CALL SYMBOL(2.0,1.5,.35,'A(f)=D*sin(4 f/f)',0.,18)
C      CALL SYMBOL(2.0,1.3,.35,'f',0.,18)
C      2 CONTINUE
C      YPAGE=6.5 - (JCURV-1)

```

22507160
22507170
22507180
22507190
22507200
22507210
22507220
22507230
22507240
22507250
22507260
22507270
22507280
22507290
22507300
22507310
22507320
22507330
22507340
22507350
22507360
22507370
22507380
22507390
22507400
22507410
22507420
22507430
22507440
22507450
22507460
22507470
22507480
22507490
22507500
22507510
22507520
22507530
22507540
22507550
22507560
22507570
22507580
22507590
22507600
22507610
22507620
22507630
22507640
22507650
22507660
22507670
22507680
22507690
22507700

FILE: 225Q FORTRAN A UNIV D' / OF OTTAWA

```

C      YPGE=YPAGE-.1
C      CALL SYMBOL(2.,YPAGE,.2,JCURV,0.,-1)
C      CALL SYMBOL(2.5,YPGE,.28,2HZ=,0.,2)
C      CALL SYMBOL(5:0,YPAGE,.28,'IN dB/MHZ**2',0.,12)
C
C      PLOT THE DATA IN LOG-LINEAR MODE.
C
C      CALL LGLIN(XARRAY,YARRAY,M,1;4,JCURV,1)
C      IF(JCURV.EQ.JLAST) CALL PLOT(0.0,0.0,999)
C      RETURN
C      END
C*****
C      THIS SUBROUTINE DRAWS THE EYE DIAGRAM FOR A
C      SYMBOL DURATION.
C*****
C      SUBROUTINE EYEQ(DATA)
C      DIMENSION DATA2(66),DATA3(66)
C      COMPLEX DATA(1)
C      COMMON /NUMB1/ FBW,ALPHA,LDIM,IOFF,LSAMPL
C      COMMON /NUMB2/ NSNR,NSYMB,BAUD
C      ESTABLISH THE SURFACE AREA.
C      CALL PLOTS(37.0,27.5)
C      ESTABLISH THE ORIGIN.
C      CALL PLOT(3.0,13.0,-3)
C      WRITE THE TITLE OF THE GRAPH.
C      CALL SYMBOL(10.0,12.0,0.49,16HQPSK EYE DIAGRAM,0.0,16)
C      DRAW THE TIME AXIS.
C      CALL AXIS(0.0,0.0,1H,-1,24.,0.0,1.0,2.8)
C      DRAW THE AMPLITUDE AXIS.
C      CALL AXIS(0.0,-8.00,1H,1,16.0,90.0,-24.,3.0)
C      PLOT THE DATA.
C      JJ=2*LSAMPL
C      DATA2(JJ+1)=0.0
C      DATA2(JJ+2)=3.0
C      DATA3(JJ+1)=1.0
C      DATA3(JJ+2)=2.8
C      M2=NSYMB/4
C      M3=3*M2+1
C      M4=4*M2-1
C      DO 4 KK=1,M2
C      DO 2 I=1,JJ
C      II=(KK-1)*LSAMPL+I
C      IF(II.GT.LDIM) II=II-(II/LDIM)*LDIM
C      DATA2(I)=REAL(DATA(II))
C      DATA3(I)=FLOAT(I)
C      CALL LINE(DATA3,DATA2,JJ,1,0,0)
C      CONTINUE
C      CALL PLOT(0.0,0.0,999)
C      RETURN
C      END
C*****
C      PARABOLIC GROUP DELAY
C      GROUP DELAY IN NANoseconds = S*F*F
C      F IN KHZ
C*****

```

22507710
22507720
22507730
22507740
22507750
22507760
22507770
22507780
22507790
22507800
22507810
22507820
22507830
22507840
22507850
22507860
22507870
22507880
22507890
22507900
22507910
22507920
22507930
22507940
22507950
22507960
22507970
22507980
22507990
22508000
22508010
22508020
22508030
22508040
22508050
22508060
22508070
22508080
22508090
22508100
22508110
22508120
22508130
22508140
22508150
22508160
22508170
22508180
22508190
22508200
22508210
22508220
22508230
22508240
22508250

FILE: 225Q FORTRAN A UNIV D'OF OTTAWA

```

SUBROUTINE PARGD(S,TF)
COMMON /NUMB1/ FBW,ALPHA,LDIM,IOFF,LSAMPL
COMMON /NUMB2/ NSNR,NSYMB,BAUD
COMPLEX TF(1)
SBANDW=FLOAT(LSAMPL)*BAUD
NO1=LDIM/2 + 1
NO2=NO1 + 1
DO 20 I=1,NO1
A1=FLOAT(I-1)*SBANDW/FLOAT(LDIM)
PHI=2.*3.141592/3.*((S*(A1**3.)))/(10.**6.)
TF(I)=TF(I)*CMPLX(COS(PHI),-SIN(PHI))
CONTINUE
20 DO 21 I=NO2,LDIM
TF(I)=CONJG(TF(LDIM+2-I))
21 CONTINUE
RETURN
END
C*****
C SINE OR COSINE GROUP DELAY WITH ARBITRARY AMPLITUDE
C AND NUMBER OF RIPPLES
C GROUP DELAY IN NANoseconds = C*COS(2*PIE*K*F/FNYQ +ISIN*PIE/2)
C F IN KHZ
C*****
SUBROUTINE SINCGD(ISIN,C,K,TF)
COMMON /NUMB1/ FBW,ALPHA,LDIM,IOFF,LSAMPL
COMMON /NUMB2/ NSNR,NSYMB,BAUD
COMPLEX TF(1)
SBANDW=FLOAT(LSAMPL)*BAUD
NO1=LDIM/2 + 1
NO2=NO1 + 1
C1=2.*(1.+ALPHA)*FBW/K
IF (ISIN.EQ.1) GO TO 50
DO 10 I=1,NO1
A1=FLOAT(I-1)*SBANDW/FLOAT(LDIM)
PHI=(C*C1/(10.**6.))*SIN(2.*3.141592*A1/C1)
TF(I)=TF(I)*CMPLX(COS(PHI),-SIN(PHI))
10 CONTINUE
DO 11 I=NO2,LDIM
TF(I)=CONJG(TF(LDIM+2-I))
11 CONTINUE
GO TO 60
50 DO 12 I=1,NO1
A1=FLOAT(I-1)*SBANDW/FLOAT(LDIM)
PHI=(C*C1/(10.**6.))*COS(2.*3.141592*A1/C1)
TF(I)=TF(I)*CMPLX(COS(PHI),SIN(PHI))
12 CONTINUE
DO 13 I=NO2,LDIM
TF(I)=TF(LDIM+2-I)
13 CONTINUE
60 RETURN
END
C*****
C LINEAR GROUP DELAY
C GROUP DELAY IN NANoseconds = B*F
C B : ns/KHZ

```

FILE: 225Q FORTRAN, A UNIV D'/OF OTTAWA

```

C      DISCRETE FREQ SPACING =SBANDW/LDIM KHZ
C*****
C      SUBROUTINE LINGD(B,TF)
COMMON /NUMB1/ FBW,ALPHA,LDIM,IOFF,LSAMPL
COMMON /NUMB2/ NSNR,NSYMB,BAUD
COMPLEX TF(1)
SBANDW=FLOAT(LSAMPL)*BAUD
NO1=LDIM/2 + 1
NO2=NO1 + 1
DO 10 I=1,NO1
AI=FLOAT(I-1)*SBANDW/FLOAT(LDIM)
PHI=3.141592*(B/(10.**6.))*AI**2.
TF(I)=TF(I)*CPLX(COS(PHI),-SIN(PHI))
10 CONTINUE
DO 20 I=NO2,LDIM
TF(I)=TF(LDIM+2-I)
20 CONTINUE
RETURN
END
C*****
C      LINEAR AMPLITUDE DISTORTION
C*****
C      SUBROUTINE LINAMP(Z,TF)
COMMON /NUMB1/ FBW,ALPHA,LDIM,IOFF,LSAMPL
COMMON /NUMB2/ NSNR,NSYMB,BAUD
COMPLEX TF(1)
SBANDW=FLOAT(LSAMPL)*BAUD
NO1=LDIM/2 + 1
NO2=NO1 + 1
AI=Z*SBANDW/FLOAT(LDIM)
DO 10 I=1,NO1
AJ=(I-1)*AI/20.
TF(I)=TF(I)*(10.**AJ)
10 CONTINUE
DO 20 I=NO2,LDIM
AZ=(LDIM+2-I)*AI/20.
TF(I)=TF(I)/(10.**AZ)
20 CONTINUE
RETURN
END
C*****
C      PARABOLIC AMPLITUDE DISTORTION
C*****
C      SUBROUTINE PARAMP(P,TF)
COMMON /NUMB1/ FBW,ALPHA,LDIM,IOFF,LSAMPL
COMMON /NUMB2/ NSNR,NSYMB,BAUD
COMPLEX TF(1)
SBANDW=FLOAT(LSAMPL)*BAUD
NO1=LDIM/2 + 1
NO2=NO1 + 1
AI=P*((SBANDW/FLOAT(LDIM))**2.)
DO 10 I=1,NO1
AJ=((I-1)**2.)*AI/20.
TF(I)=TF(I)*(10.**AJ)
10 CONTINUE

```

22508810
22508820
22508830
22508840
22508850
22508860
22508870
22508880
22508890
22508900
22508910
22508920
22508930
22508940
22508950
22508960
22508970
22508980
22508990
22509000
22509010
22509020
22509030
22509040
22509050
22509060
22509070
22509080
22509090
22509100
22509110
22509120
22509130
22509140
22509150
22509160
22509170
22509180
22509190
22509200
22509210
22509220
22509230
22509240
22509250
22509260
22509270
22509280
22509290
22509300
22509310
22509320
22509330
22509340
22509350

FILE: 225Q FORTRAN A UNIV D'/OF OTTAWA

```

DO 11 I=NO2,LDIM
  TF(I)=TF(LDIM+2-I)
11 CONTINUE
  RETURN
  END
C*****
C SINE OR COSINE RIPPLE FOR AMPLITUDE DISTORTION
C*****
SUBROUTINE SINAMP(ISIN,D,K,TF)
COMMON /NUMB1/ FBW,ALPHA,LDIM,IOFF,LSAMPL
COMMON /NUMB2/ NSNR,NSYMB,BAUD
COMPLEX TF(1)
SBANDW=FLOAT(LSAMPL)*BAUD
NO1=LDIM/2 + 1
NO2=NO1 + 1
AJ=SBANDW/FLOAT(LDIM)
C1=BAUD/K
IF (ISIN.EQ.1) GO TO 50
DO 10 I=1,NO1
  AZ=D*COS(2.*3.141592*AJ*(FLOAT(I)-1.)/C1)/20.
  TF(I)=TF(I)*(10.**AZ)
10 CONTINUE
DO 20 I=NO2,LDIM
  TF(I)=TF(LDIM+2-I)
20 CONTINUE
  RETURN
50 DO 30 I=1,NO1
  AZ=D*SIN(2.*3.141592*AJ*(FLOAT(I)-1.)/C1)/20.
  TF(I)=TF(I)*(10.**AZ)
30 CONTINUE
DO 40 I=NO2,LDIM
  AZ=D*SIN(2.*3.141592*AJ*(FLOAT(LDIM+2-I)-1.)/C1)/20.
  TF(I)=TF(I)/(10.**AZ)
40 CONTINUE
  RETURN
  END
C*****
C RANDOM NUMBER GENERATOR
C*****
SUBROUTINE RAND(IR)
INTEGER IR(256)
REAL R(256)
DOUBLE PRECISION DSEED
DSEED=123457.DO
N=256
DO 300 I=1,N
  R(I)=GCUBFS(DSEED)
  IR(I)=IFIX(R(I)*2040.)
300 CONTINUE
WRITE(6,10) IR
10 FORMAT(10X,15)
RETURN
END

```

REFERENCES

1. Y. Tan, S. Shinmyo, M. Murakami, and M. Tsunokuni, "2 GHz band digital radio equipment employing 8-level PSK with cosine roll-off spectrum shaping," Proc. of the IEEE-ICC'78, pp. 33.3.1-33.3.5.
2. S.G. Barber and C.W. Anderson, "Modulation considerations for the DRS-8 91 Mb/s digital radio," Proc. of the IEEE-ICC'77, pp. 5.6-111-5.6-115.
3. G.R. McMillen, M. Shafi, and D.P. Taylor, "Simultaneous adaptive estimation of carrier phase, symbol timing and data for a 49-QPRS DFE radio receiver," IEEE Trans. Commun., Vol. COM-32, pp. 429-443, April 1984.
4. H. Yamamoto, "Advanced 16-QAM techniques for digital microwave radio," IEEE Trans. Commun., COM-19, pp.36-45, 1981.
5. I. Horikawa, T. Murase, and Y. Saito, "Design and performance of a 200 Mb/s 16-QAM digital radio system," IEEE Trans. Commun., Vol. COM-2, pp. 1953-1958, 1979.
6. Y. Saito, K. Morita, and H. Yamamoto, "5L-D1 digital radio system," Proc. of the IEEE-ICC'82, pp. 2B.1.1-2B.1.7.
7. P. Dupuis, M. Joindot, and D. Soufflet, "16-QAM modulation for high capacity digital radio system," IEEE Trans. Commun., Vol. COM-27, pp. 1771-1782, 1979.
8. T. Hill and K. Feher, "A performance study of NLA 64-state QAM," IEEE Trans. Commun., Vol. COM-31, pp. 821-826, June 1983.
9. B.T. Bynum and E.W. Allen, "135 Mb/s-6 GHz transmission system design considerations," Proc. of the IEEE-ICC'83, pp. F2.5.1-F2.5.6.
10. T. Noguchi, et al., "6 GHz 135 MBPS digital radio system with 64-QAM modulation," Proc. of the IEEE-ICC'83, pp. F2.4:1-F2.4.6.
11. P.R. Hartmann and J.A. Crossett, "135 MBS-6GHz Transmission system using 64-QAM modulation," Proc. of the IEEE-ICC'83, pp. F2.6.1-F2.6.7.

12. J.D. McNicol, S.G. Barber, and F. Rivest, "Design and application of the RD-4A and RD-6A 64-QAM digital radio systems," Proc. of the IEEE-ICC'84, pp. 646-652.
13. M. Borgne, "Comparison of 16, 32, 64 and 128 QAM modulation schemes for digital radio systems," Proc. of the IEEE-GLOBECOM'83, pp.1.7.1-1.7.5.
14. K. Feher, "Digital Communications : Satellite/Earth Station Engineering," Englewood cliffs, NJ : Prentice-Hall, 1983, Chapter 5.
15. K. Feher, "Digital Communications : Microwave Applications," Englewood Cliffs, NJ : Prentice-Hall, 1981, Chapter 8.
16. R.L. Freeman, "Telecommunication System Engineering : Analog and Digital Design," John Wiley & Sons, New York, 1980, Chapter 4.
17. K. Feher, E.M. Karkar, and J.C.Y. Huang, "On 6.67 b/s/Hz - 256-QAM and 225-QPRS modems for T1/SG data-invoice (DIV) applications," Proc. of the IEEE-ICC'85, pp. 453-459, June 1985.
18. W.R. Bennett and J.R. Davey, "Data Transmission," New York : McGraw-Hill, 1965, Chapter 7.
19. E.R. Kretzmer, "Generalization of a technique for binary data communication," IEEE Trans. Commun., Vol. COM-14, pp.67-68 Feb. 1966.
20. P. Kabal and S. Pasupathy, "Partial-response signalling," IEEE Trans. Commun., Vol. COM-23, pp. 921-934, Sept. 1975.
21. A. Lender, "Correlative (Partial response) techniques and applications to digital radio systems," Published as Chapter 7 in K. Feher, "Digital Communications : Microwave Applications," Englewood Cliffs, NJ : Prentice-Hall, 1981.
22. K.T. Wu and K. Feher, "Multi-level PRS/QPRS above the Nyquist rate," IEEE Trans. Commun., Vol. COM-33, pp. 735-739., July 1985.
23. J.E. Mazo, "Faster than Nyquist signaling," Bell Syst. Tech. J., Vol. 54, pp. 1451-1462, Oct. 1976.
24. G.J. Foschini, "Contrasting performance of faster binary signaling with QAM," Bell Syst. Tech. J., Vol. 63, pp.1419-1445, Oct. 1984.

25. A. Fihel and H. Sari, "Reduced-bandwidth 16-QAM : A power and bandwidth efficient modulation technique for digital microwave radio systems," Proc. of the IEEE ICC'85, Chicago, pp.15.6.1-15.6.5, June 1985.
26. M.D. Eggers and J.H. Painter, "Optimal symbol by symbol detection for duobinary signaling," IEEE Trans. Commun. Vol. COM-31, pp. 1077-1085 Sept. 1983.
27. G.D. Forney, Jr., "Maximum-likelihood sequence estimation of digital sequences in the presence of intersymbol interference," IEEE Trans. Inform. Theory, Vol. IT-18, pp. 363-378, May 1972.
28. C.A. Belfiore and J.H. Park, Jr., "Decision feedback equalization," Proc. IEEE, Aug. 1979, pp. 1143-1156.
29. D.D. Falconer and F.R. Magee, Jr., "Evaluation of decision feedback equalization and Viterbi detection for voiceband data transmission-part I," IEEE Trans. Commun. Vol. COM-24, pp. 1130-1139, Oct. 1976.
30. D.D. Falconer and F.R. Magee, Jr., "Evaluation of decision feedback and viterbi algorithm detection for voiceband data transmission-part II," IEEE Trans. Commun., Vol. COM-24, pp. 1238-1245, Nov. 1976.
31. D.D. Falconer, "Application of passband decision feedback equalization in two-dimension data communication systems," IEEE Trans. Commun., Vol. COM-24, pp. 1159-1166, Oct. 1976.
32. D.D. Falconer and G.J. Foschini, "Theory of minimum mean-square-error QAM systems employing decision feedback equalization," Bell Syst. Tech. J., Vol. 52, pp. 1821-1849, Dec. 1973.
33. K. Feher, K.T. Wu, J.C.Y. Huang, and D.E. MacNally, "Improved efficiency data transmission technique," U.S. and Canadian patent disclosure, University of Ottawa and Pascal Associate, No. 256-8148-1, Oct 1, 1984.
34. A. Lender, R. Rogers, and H. Olszanski, "4 Bits/Hz correlative single-sideband digital radio at 2 GHz," Proc. of the IEEE-ICC'79 pp.5.2.1-5.2.5.
35. K.T. Wu, I. Sasase, and K. Feher, "Improved efficiency 15-level modified duobinary PRS above the Nyquist rate," Proc. of the IEEE-ICC'85, pp. 31.3.1-31.3.5, June 1985.
36. K.T. Wu and K. Feher, "256-QAM modem performance in distorted channels," IEEE Trans. Commun. Vol. COM-33, pp. 487-491, May 1985.

37. M. Subramanian, K.C. O'Brien, and P.J. Puglis, "Phase dispersion characteristics during fade in a microwave line-of-sight radio channel," *Bell Syst. Tech. J.*, Vol. 52, Dec. 1973.
38. G.M. Babler, "Selectively faded nondiversity and space diversity narrowband microwave radio channels," *Bell Syst. Tech. J.*, Vol. 52, Feb. 1973.
39. I. Sasase, K.T. Wu, and K. Feher, "Comparison of improved efficiency 225-QPRS and 256-QAM in distorted channels," *Proc. of the IEEE-ICC'85*, pp. 15.3.1-15.3.5, June 1985.
40. R.W. Lucky, J. Salz, and E.J. Weldon, Jr., "Principles of Data Communication," New York : McGraw-Hill, 1968, Chapter 4.
41. G. Bianconi and L. Calandrino, "Adaptive baseband equalization in digital M-QAM radio systems in presence of multipath propagation," *Proc. of the IEEE-ICC'85*, Chicago, pp. 15.7.1-15.7.8, June 1985.
42. Y. Saito, S. Komaki, and M. Murotani, "Feasibility considerations of high-level multi-carrier system," *Proc. of the IEEE-ICC'84*, pp. 656-671.
43. V.K. Prabhu, "Co-channel interference immunity of high capacity QAM," *Proc. of the IEEE-ICC'81*, pp. 68.8.1-68.8.4.
44. V.K. Prabhu, "The detection efficiency of 16-ray QAM," *Bell Syst. Tech. J.*, Vol. 59, pp. 639-656, April 1980.
45. J.J. Spilker, Jr., "Digital Communications by Satellite," Englewood Cliffs, NJ : Prentice-Hall, 1977, Chapter 11.
46. K.T. Wu and K. Feher, "Error rate considerations for 64-, 256-QAM and 225-QPRS with co-channel interference," *Proc. of the IEEE ELECTRONICOM'85*, pp. 662-665, Toronto, Oct. 1985.
47. Y.L. Kuo and T.J. Aprille, "A baseband equalizer for a 16-state QAM digital system over mastergroup band analog networks," *Proc. of the IEEE-GLOBECOM'82*, pp. F3.6.1-F3.6.5.
48. D.E. MacNally and J.C.Y. Huang, "Propagation protection techniques for high capacity digital radio systems," *Proc. of the IEEE-ICC'84*, pp. 1007-1010.

49. K. Aoki, et al., "The adaptive transversal equalizer for 90 MBPS 64-QAM radio relay system," Proc. of the IEEE-ICC'84, pp.1003-1006.
50. R.W. Lucky, "Survey of communication theory literature : 1968-1973," IEEE Trans. Inform. Theory, pp.725-739, 1973.
51. R.W. Lucky, "Techniques for adaptive equalization of digital communication systems," Bell Syst. Tech. J., Vol. 45, No.2, pp. 255-286, Feb. 1966.
52. D. Hirsch and W.J. Wolf, "A simple adaptive equalizer for efficient data transmission," IEEE Trans. Commun. Tech. Vol. COM-18, pp. 5-11, Feb. 1970.
53. J. Proakis, "Digital Communications," New York : McGraw-Hill, 1983, Chapter 6.
54. G.L. Fenderson, et al., "Adaptive transversal equalization of multipath propagation for 16-QAM, 90 Mb/s digital radio," Bell Syst. Tech. J., Vol. 63, pp. 1447-1463 Oct. 1984.
55. A.A.M. Saleh, "Frequency-independent and frequency-dependent nonlinear models of TWT amplifiers," IEEE Trans. Commun., Vol. COM-29, pp. 1715-1720, Nov. 1981.
56. A.A.M. Saleh and J. Salz, "Adaptive linearization of power amplifiers in digital radio systems," Proc. of the IEEE-ICC'83, pp. C8.4.1-C8.4.5, 1983.
57. W.D. Rummler, "A new selective fading model : application to propagation data," Bell Syst. Tech. J., Vol. 58, pp. 1037-1071, May-June 1979.
58. W.D. Rummler, "Digital radio outage due to selective fading-observation vs prediction from laboratory simulation," Bell Syst. Tech. J., Vol. 58, pp. 1073-1110, May-June, 1979.
59. G.J. Foschini and J. Salz, "Digital communications over fading radio channels," Proc. of the IEEE-ICC'83, pp. C8.1.1-C8.1.7.
60. N. Amitay and L.J. Greenstein, "Multipath outage performance of digital radio receivers using finite-tap adaptive equalizers," IEEE Trans. Commun., Vol. COM-32, pp. 597-608, May 1984.